IMR – Ion-Molecule Reactions

$$I^+ + AB \rightarrow C^+ + D$$

$$O^+ + H_2 \rightarrow OH^+ + H$$

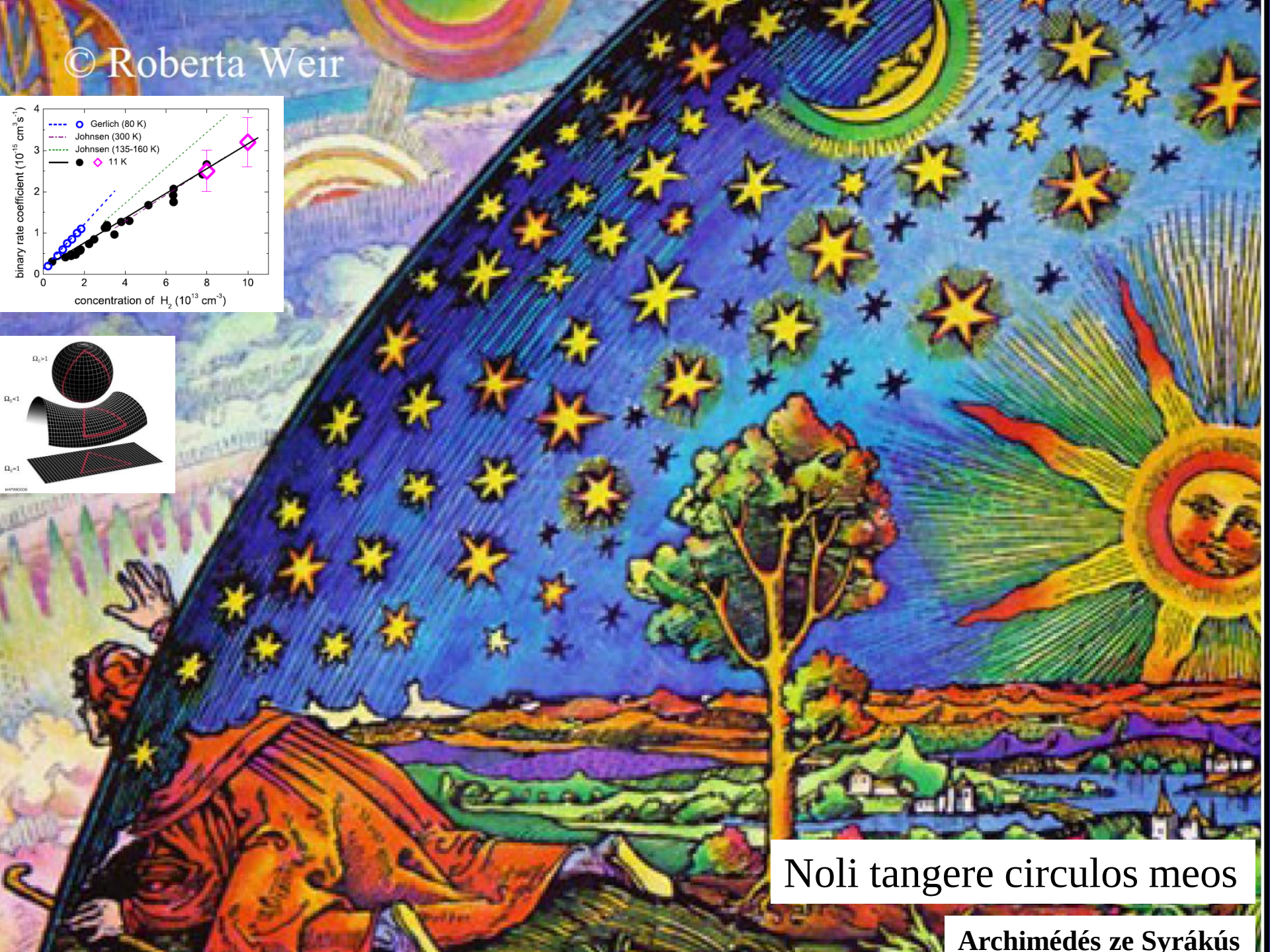
© Roberta Weir
Gerlich (80 K)
Johnsen (300 K)
Johnsen (135-160 K)
11 K
binary rate coefficient (10^{-15} cm^{3}s^{-1})
concentration of H_2 (10^{13} cm^{-3})
0
1
2
3
4
0
2
4
6
8
10
$\Omega_0>1$
$\Omega_0<1$
$\Omega_0=1$
Noli tangere circulos meos
Archimédés ze Syrákús

When we were still Barbarians

Paesto Italy

Keď my sme ešte boli Barbari
Paestum

When we were still Barbarians

Keď my sme ešte boli Barbari

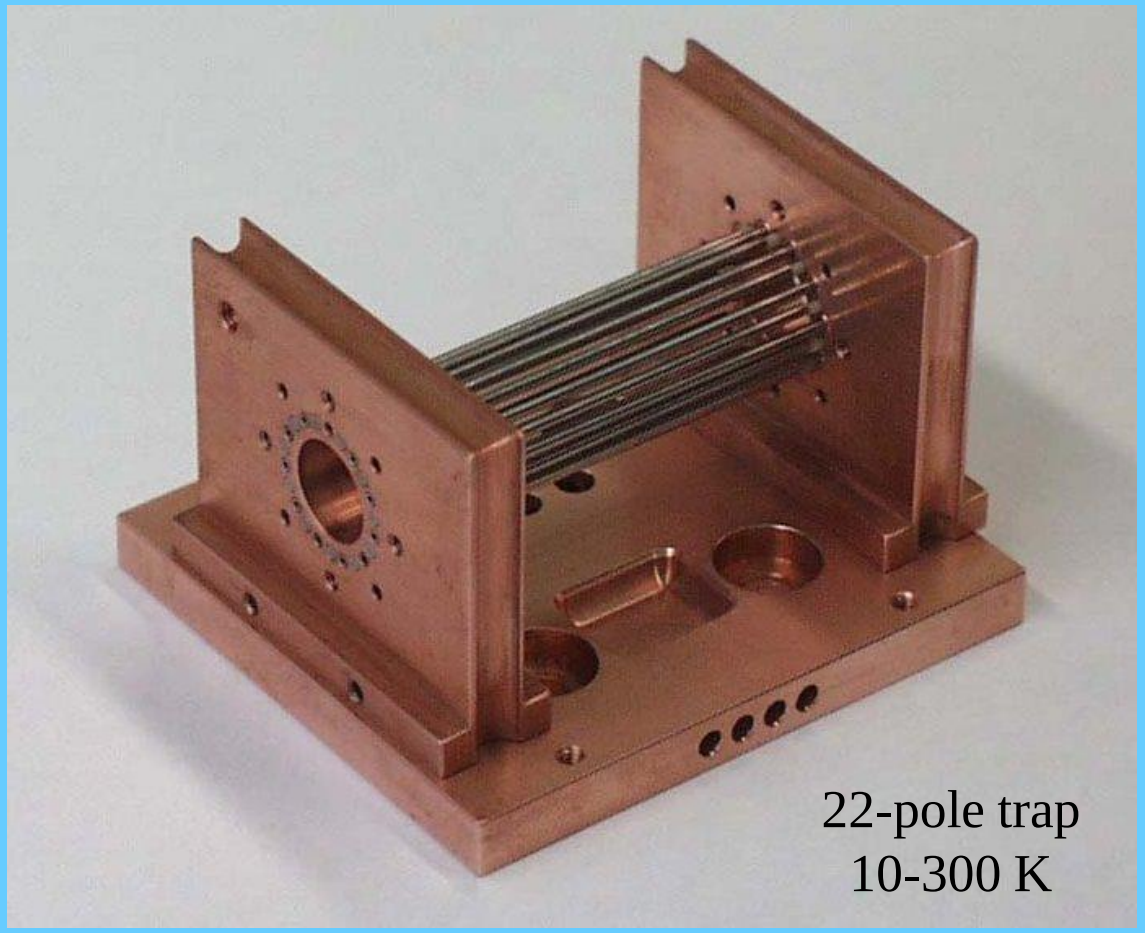

14th August 2002

Our LAB

FACULTY OF MATHEMATICS AND PHYSICS

TROJA, Praha 8

Interactions of electron
Rotational and vibrational excitation

Rutherford atom

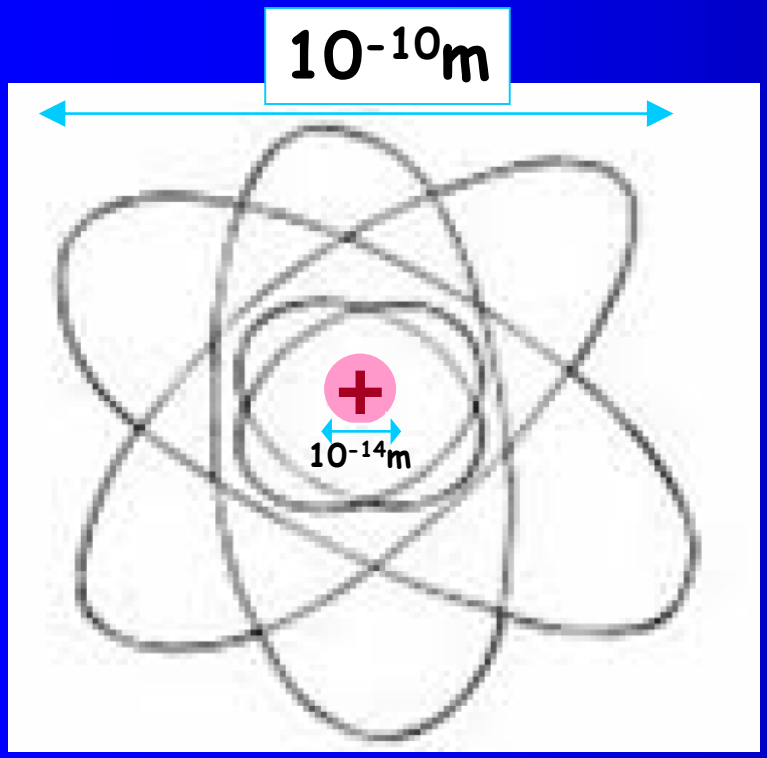

Excitation energies

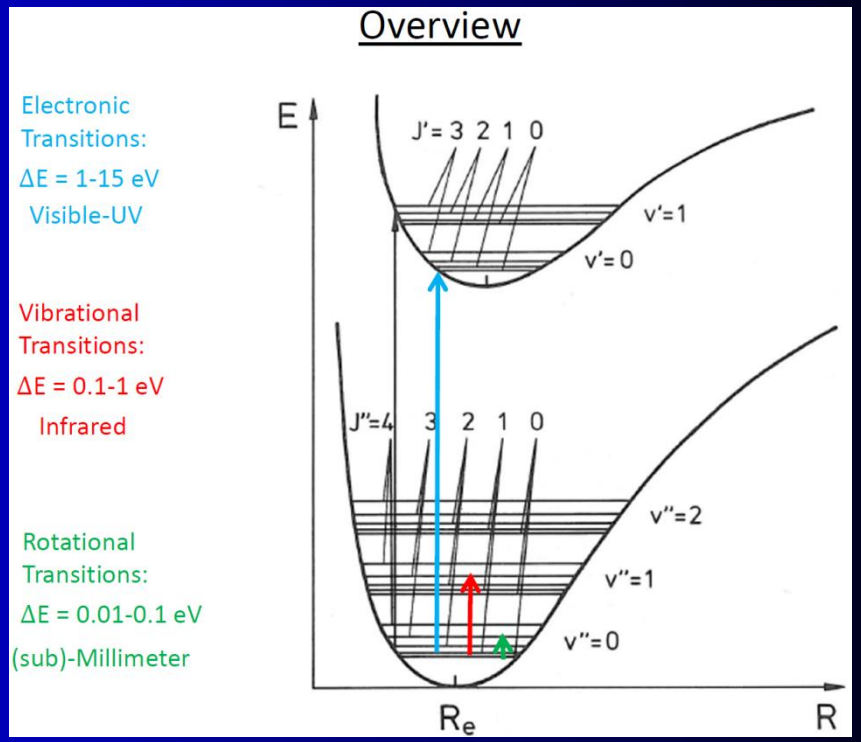

A **shape resonance** is a metastable state in which an electron is trapped due the shape of a potential barrier.

Unimolecular reactions

$A \rightarrow P$

$(A \rightarrow B+C)$

Binary reactions

$A + B \rightarrow P$

$2\,A \rightarrow P$

Ternary reactions

$A + B + C \rightarrow P$

$(A + B + He \rightarrow AB + He)$

$2\,A + B \rightarrow P$

$3\,A \rightarrow P$

Introduction

1A 25. 02. 2025

IMR – Ion-Molecule Reactions

$$A^+ + B \rightarrow C^+ + D$$

$$O^+ + H_2 \rightarrow OH^+ + H$$

Ion-Molecule Reactions

$$A^+ + B \rightarrow C^+ + D$$

- Experimental evidence down to a few K
- Rate coefficients explained by classical "capture" models in most but not all instances.
- ion-non polar (Langevin case)

$$k_L = 2\pi e\sqrt{\frac{\alpha}{\mu}} \approx 2\times 10^{-9} \quad \text{cm}^3\ \text{s}^{-1}$$

- ERIC HERBST
- DEPARTMENTS OF PHYSICS, CHEMISTRY AND ASTRONOMY
- THE OHIO STATE UNIVERSITY

Ion-mol. r. (cont)

- Ion-polar

$$k_{TS} = k_L[0.62 + 0.4767x]$$

$$k_{LD} = k_L[1 + \frac{2}{\pi^{1/2}}x] \rightarrow 10^{-7} cm^3 s^{-1}$$

$$x = \frac{\mu_D}{\sqrt{2\alpha k_B T}} \propto T^{-1/2}$$

+ more complex state-specific models

Ion Molecule Reactions

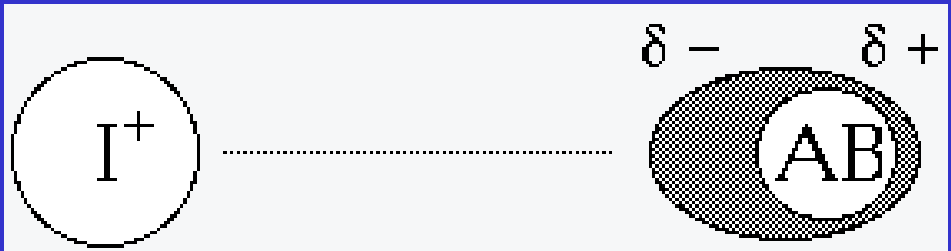

Binary reactions of cations

$$CH_4^+ + CH_4 \rightarrow CH_5^+ + CH_3$$

$$CH_4^+ + H_2 \rightarrow CH_5^+ + H$$

$$H_3^+ + CH_4 \rightarrow CH_5^+ + H_2$$

$$H_5^+ + H_2 \rightarrow H_3^+ + H_2 + H_2$$

$$H_2^+ + Ar \Rightarrow ArH^+ + H$$

$$H_3^+ + HD \Leftrightarrow H_2D^+ + H_2$$

$$H_2D^+ + HD \Leftrightarrow HD_2^+ + H_2$$

$$HD_2^+ + HD \Leftrightarrow D_3^+ + H_2$$

Unimolecular reactions

Ternary reactions

Efficient Low T Gas-Phase Reactions

1. Ion-molecule reactions
2. Radiative association reactions
3. Dissociative recombination reactions
4. Radical-radical reactions
5. Radical-stable reactions

$E_a = 0$

Exothermic

Endothermic

In areas of star formation, reactions with barriers occur.

Radiative Association

$$A^+ + B \Leftrightarrow AB^{+*} \rightarrow AB^+ + h\nu$$

$$k_{ra} = \frac{k_1}{k_{-1}} k_r = K(T) k_r ; k_r \approx 10^2 s^{-1}$$

$$K(T) \propto T^{-(r_A + r_B)/2}$$, size, bond engy

Few ion trap measurements by Gerlich, Dunn down to 10 K

By now many more IMR…..

What is the 0 K limit?

What about competitive channels?

Dissociative Recombination Reactions

$$AB^{+} + e \rightarrow A + B$$

Studied in storage rings down to “zero” relative energy; products measured for approx.10 systems

Stationary and Flowing Afterglow plasma

$$k(T) = A(T/300)^{-n}$$ n=0.5, 1.5

$$A \approx 10^{-7} cm^{3} s^{-1}$$

Some systems studied: H_3^+, HN_2^+, $HCNH^+$, H_3O^+, NH_4^+, CH_5^+ ,$C_nH_m^+$

HeH+, Ar+…..

Attachment

$$e + A \rightarrow A^{-} + h\nu$$

$$\boxed{\mathbf{O_2 + e^- \rightarrow O_2^-}}$$

Anions formation

Some Conclusions

- 1) Low-temperature chemistry in interstellar clouds (both gas-phase and surface) partially understood only.
- 2) Chemistry gives us many insights into the current state and history of sources
- 3) More work on “cold chemistry” is clearly needed to make our mirror into the cosmos more transparent.

Kinetics of elementary process

Parameters of reactions….

reaction cross section

reaction rate coefficient

Single collision

$$H_2^+ + Ar \Rightarrow ArH^+ + H$$

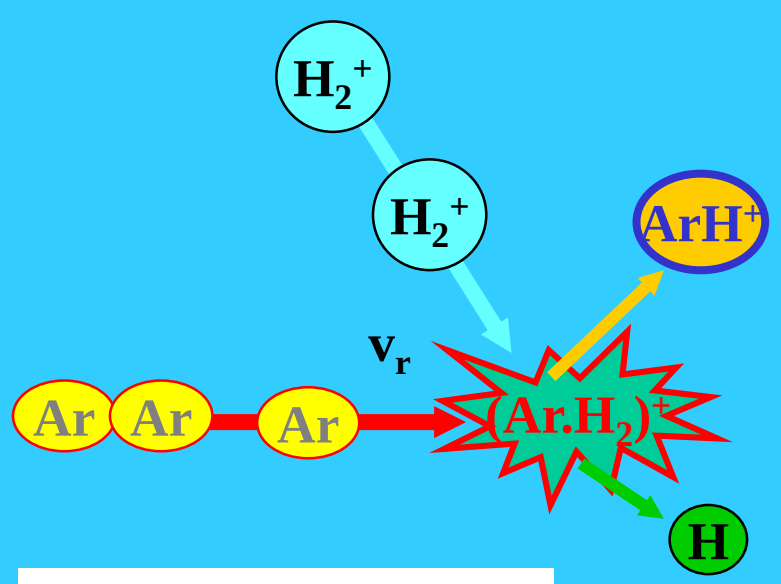

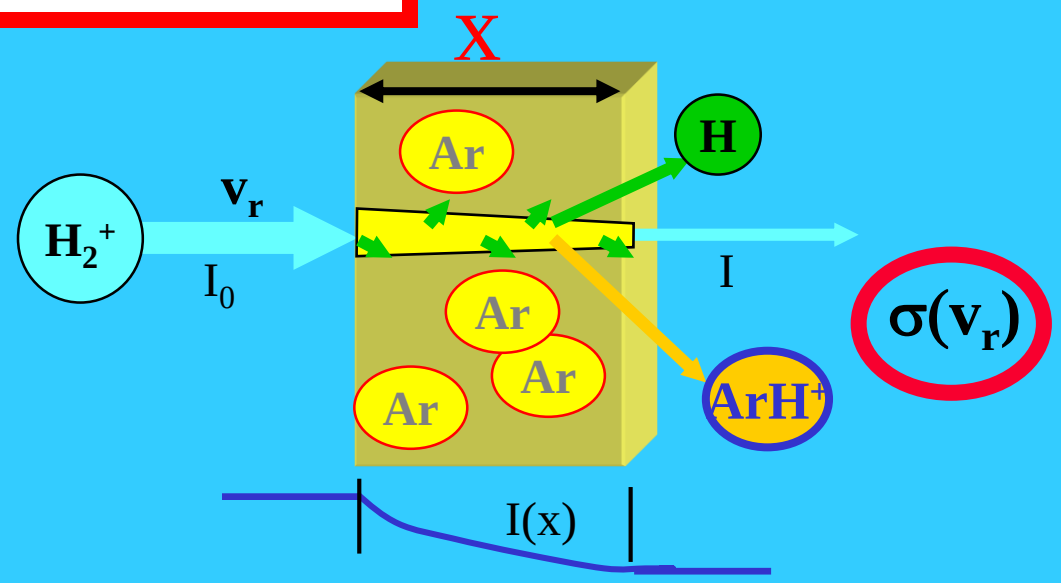

reaction cross section

$$I=I_0\exp(-\sigma n_{Ar} x)$$

$$\nu_{coll} = +nV_{rel} = +n\nu S = +n\nu\pi\delta^2 = +n\nu\sigma$$

Collisional cross section

$$\frac{dI}{dt} = -\frac{I}{\tau_{coll}} = -I\nu_{coll}$$

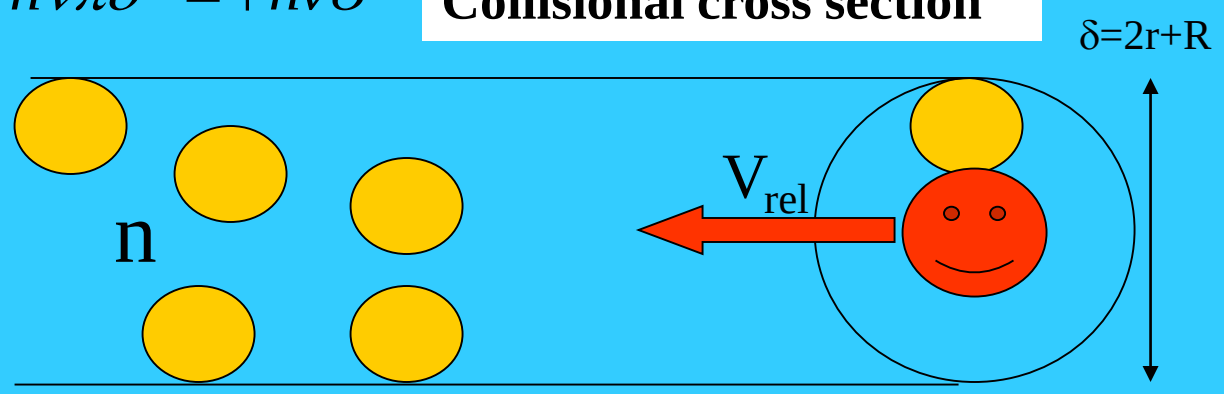

$$I(t) = I_0 \exp(-\nu_{coll} t) = I_0 \exp(-\sigma n \nu_{rel} t)$$

$$I=I_0\exp(-\sigma n_{Ar} x)$$

Kinetics of elementary process

$$H_2^+ + Ar \Rightarrow ArH^+ + H$$

Single collision

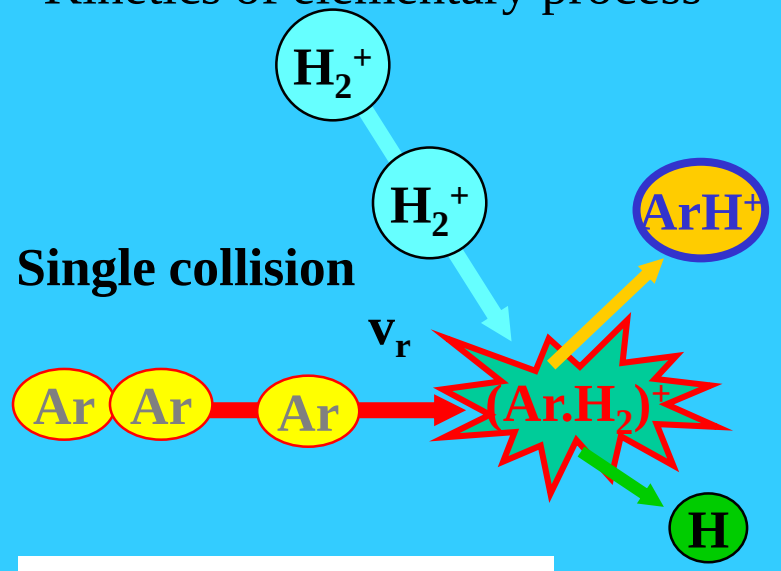

reaction cross section

$$I=I_0\exp(-\sigma n_{Ar}x)$$

$\sigma(v_r)$

$k(T)=\langle v\sigma\rangle$

$k(T)$

Multiple collision

@ T

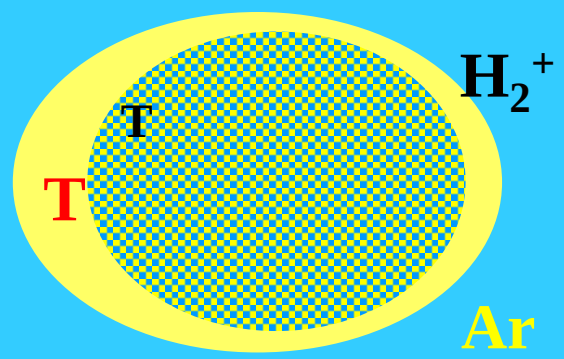

reaction rate coefficient

$$d(n_{H2^+})/dt=-k\, n_{H2^+}.\, n_{Ar}$$

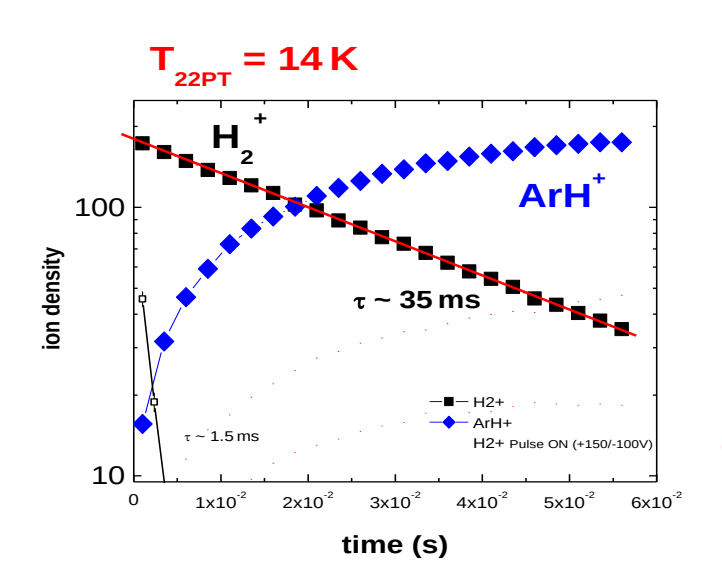

$$n_{H2^+}.=(n_{H2^+}).{}_0\exp(-kn_{Ar}t)$$

Kinetics of elementary process

$$H_2^+ + Ar \Rightarrow ArH^+ + H$$

$$A^+ + B \rightarrow C^+ + D$$

Simple description using symbols A+….
for number densities….

$$\frac{dA^+}{dt} = -k_{BIN} A^+ B$$

[B]>>[A+]

$$\frac{d[A^+]}{dt} = -k_{BIN}[A^+][B]$$

$$[A^+]_t = [A^+]_{t=0} \cdot e^{-k[B]t}$$

Multiple collision

@ T

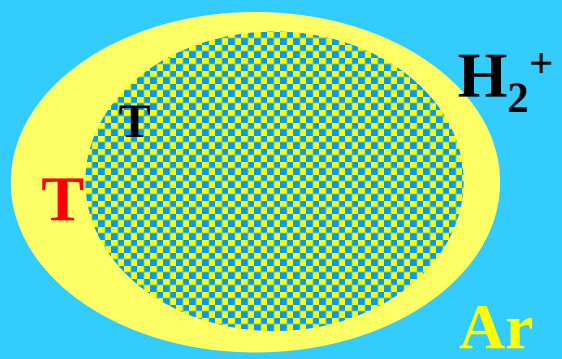

reaction rate coefficient

$$d(n_{H2^+})/dt = -k\, n_{H2^+} \cdot n_{Ar}$$

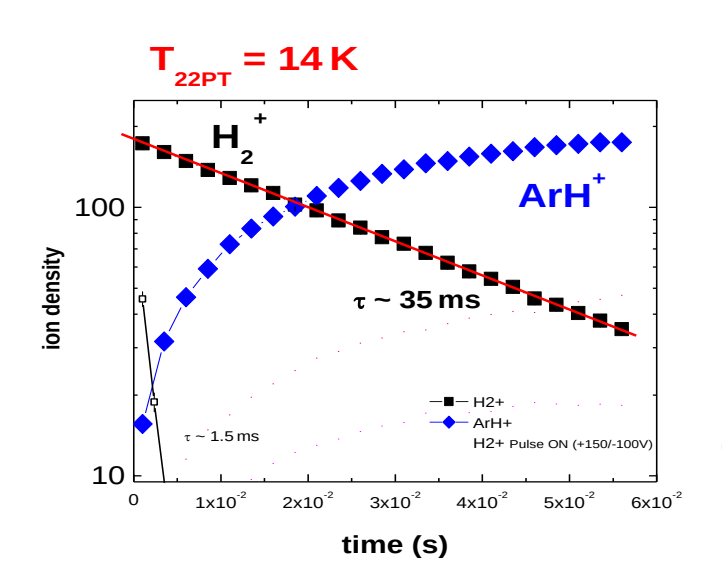

k(T)

$$n_{H2^+} = (n_{H2^+})_0 \exp(-k n_{Ar} t)$$

Binary reactions Reaction rate coefficient

$$A^+ + B \rightarrow C^+ + D$$

$$[k_{BIN}] = cm^3 s^{-1}$$

$$\frac{d[A^+]}{dt} = -k_{BIN}[A^+][B]$$

Often it is written in simpler form using A^+ instead of $[A^+]$

$$\frac{dA^+}{dt} = -k_{BIN}A^+B$$

$$A^+ + B \rightarrow C^+ + D$$

$$\sigma(v_r)$$

$$k_{BIN} = k_{BIN}(T)$$

$$\mathbf{k(T)=<v_r\sigma(v_r)>}$$

$$k = \int_v f_T(v).v.\sigma(v)dv = k(T)$$

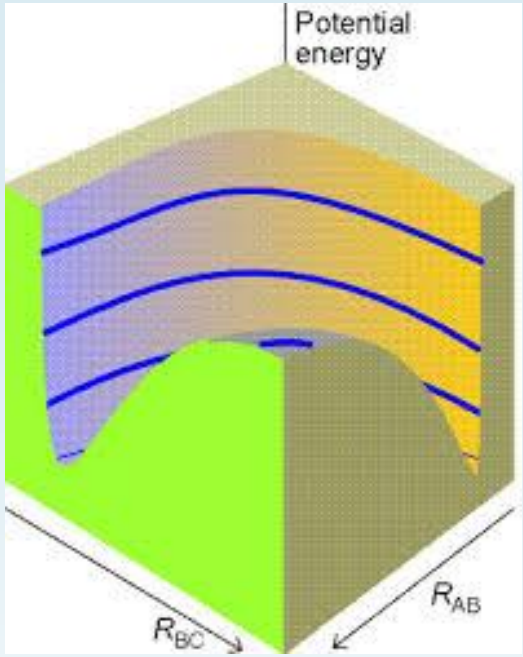

H-C + D ➔ H—C / D ➔ H + C-D

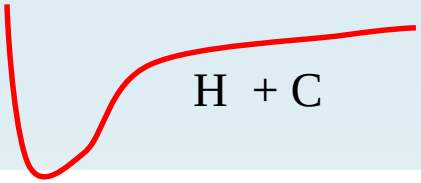

H⇔C

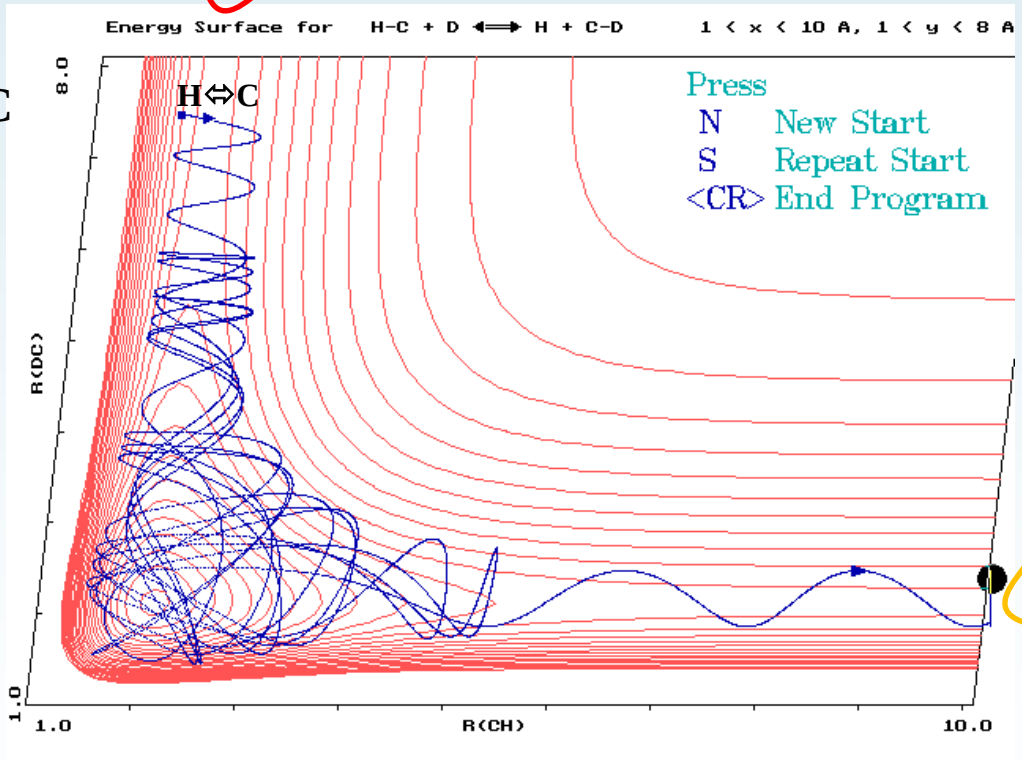

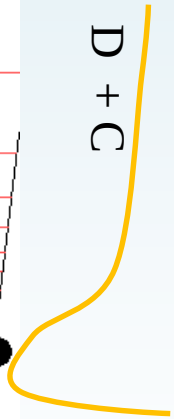

D

H

C⇔D

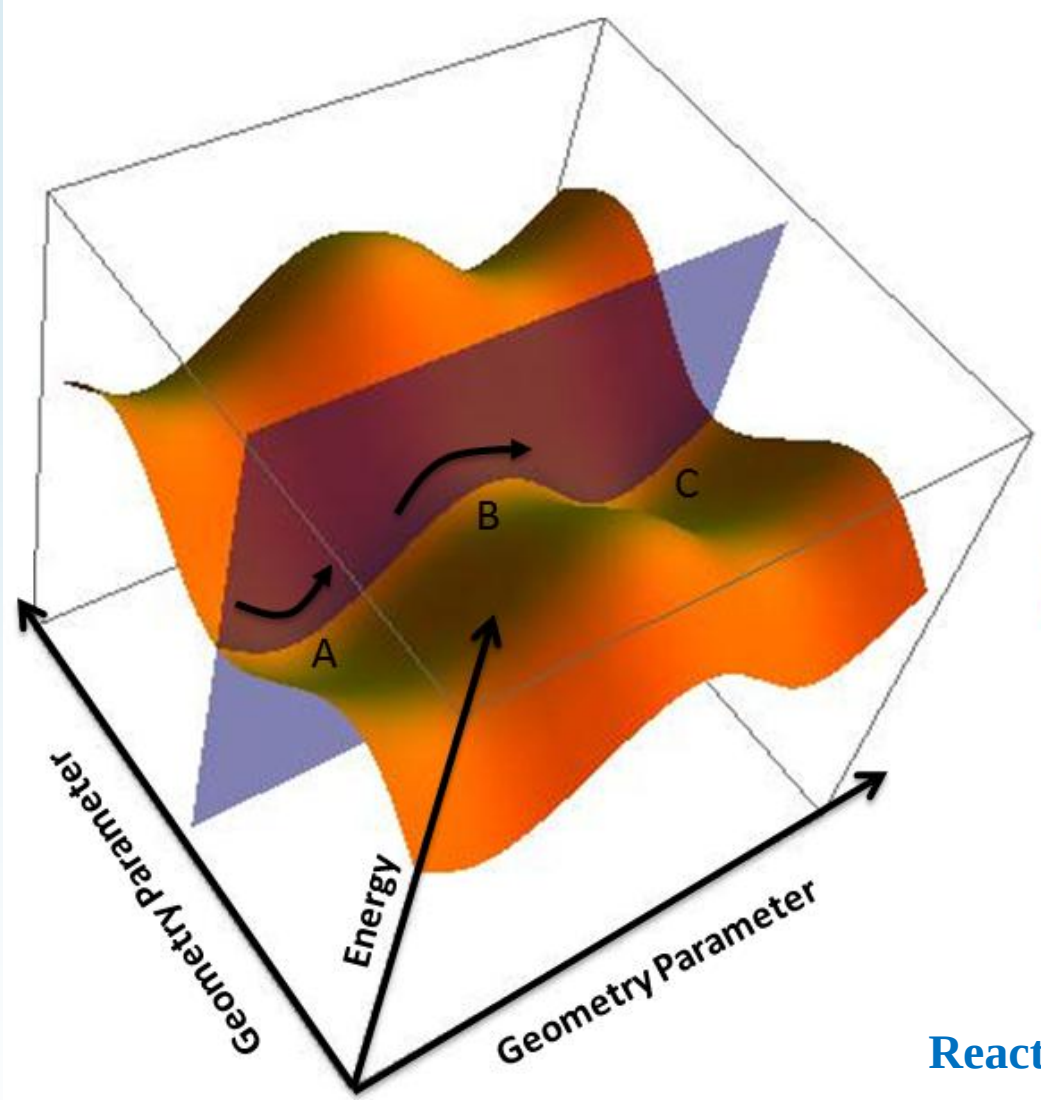

Reaction coordinate

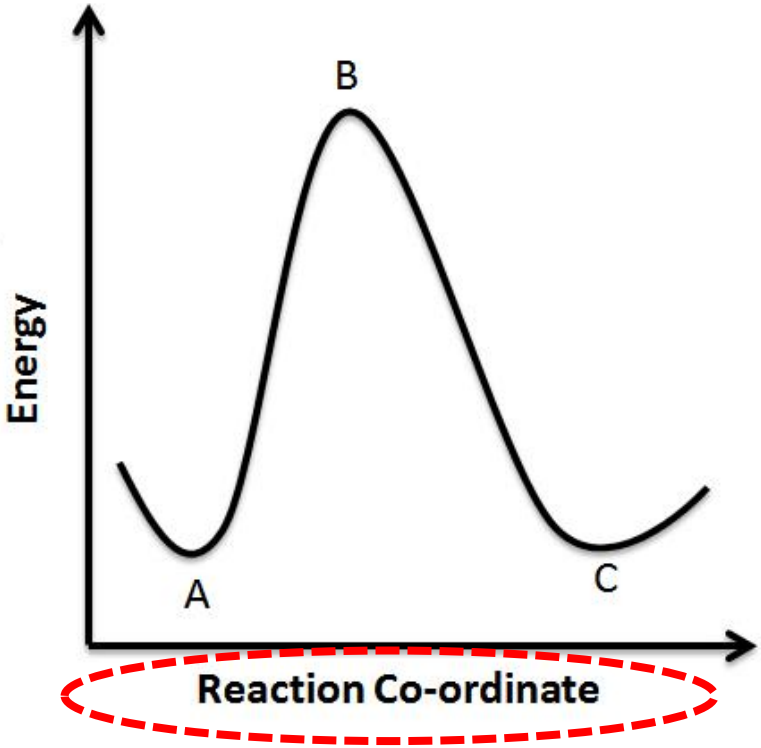

Reaction Coordinate

"…..In chemistry, a reaction coordinate is an abstract one-dimensional coordinate which represents progress along a reaction pathway. It is usually a geometric parameter that changes during the conversion of one or more molecular entities. In molecular dynamics simulations, a reaction coordinate is called collective variable. …..."

$$A + H_2 \rightarrow \ldots \rightarrow C + \ldots$$

The ion chemistry of the lower atmosphere

Binary reactions

Ternary reactions

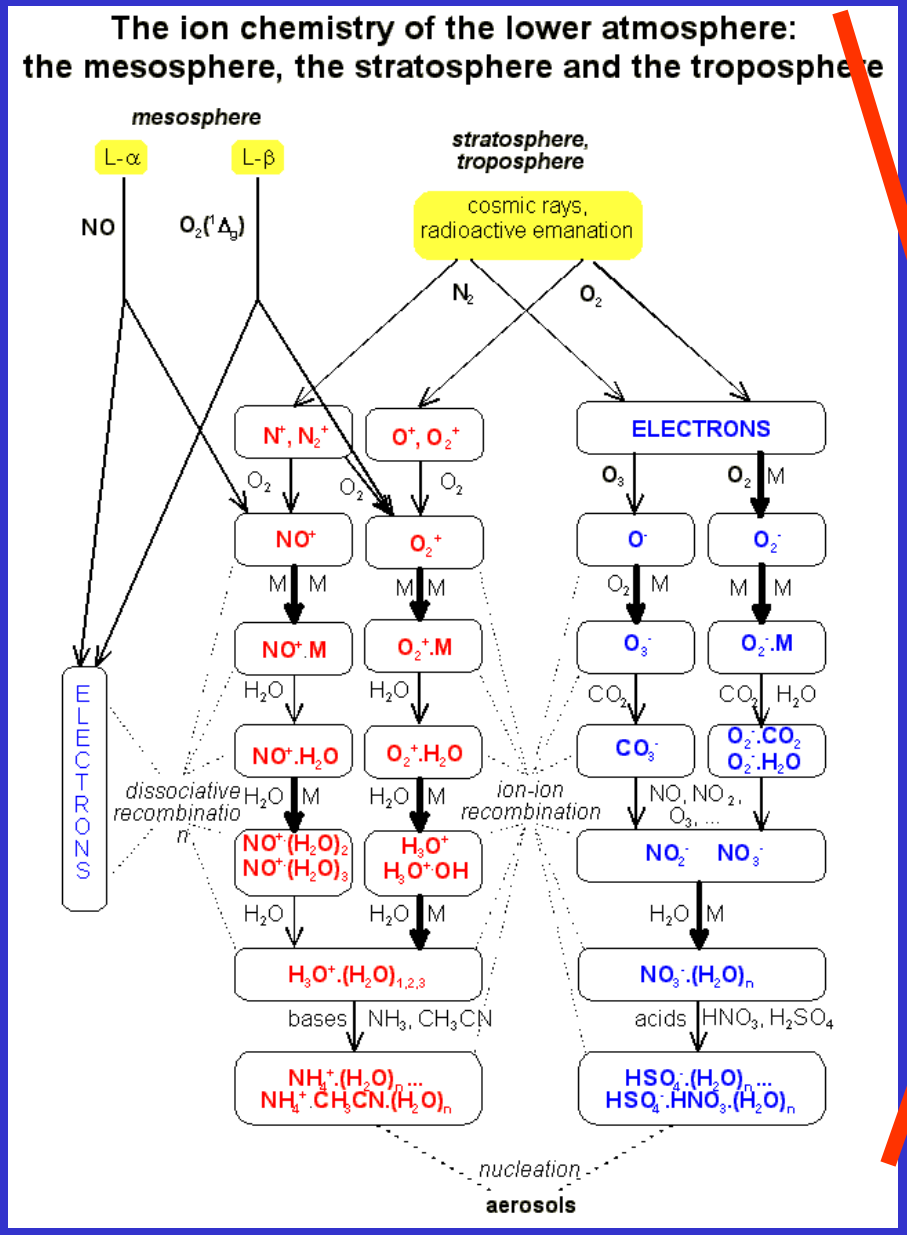

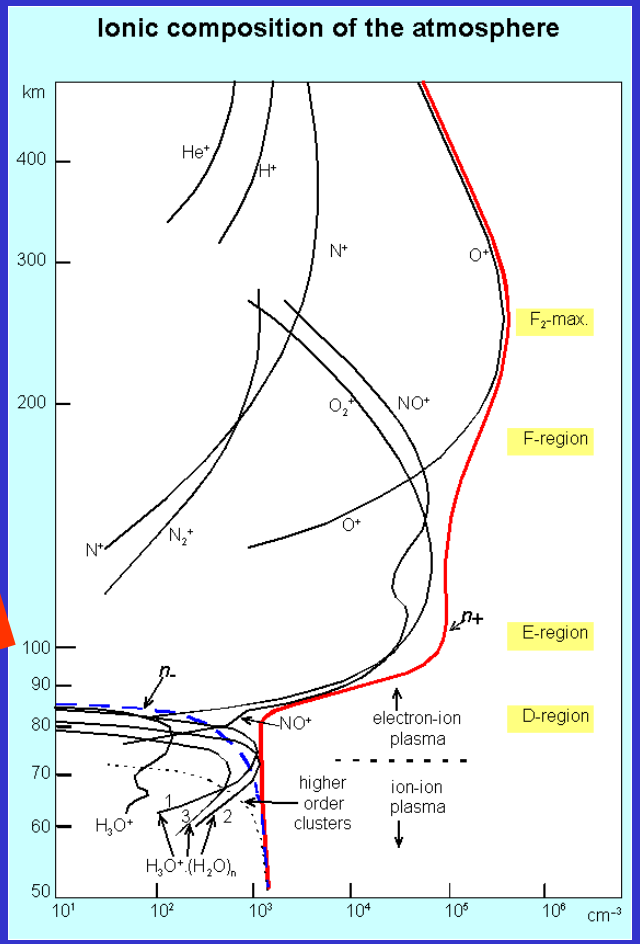

……probability of reactive collision

Collision rate coefficient - Langevin rate coefficient

$k(T)=\langle v_r \sigma(v_r)\rangle$

Reaction rate coefficient

Temperature Dependence of Ion-Molecule Reactions

$k_L \sim 10^{-9} cm^3 s^{-1}$

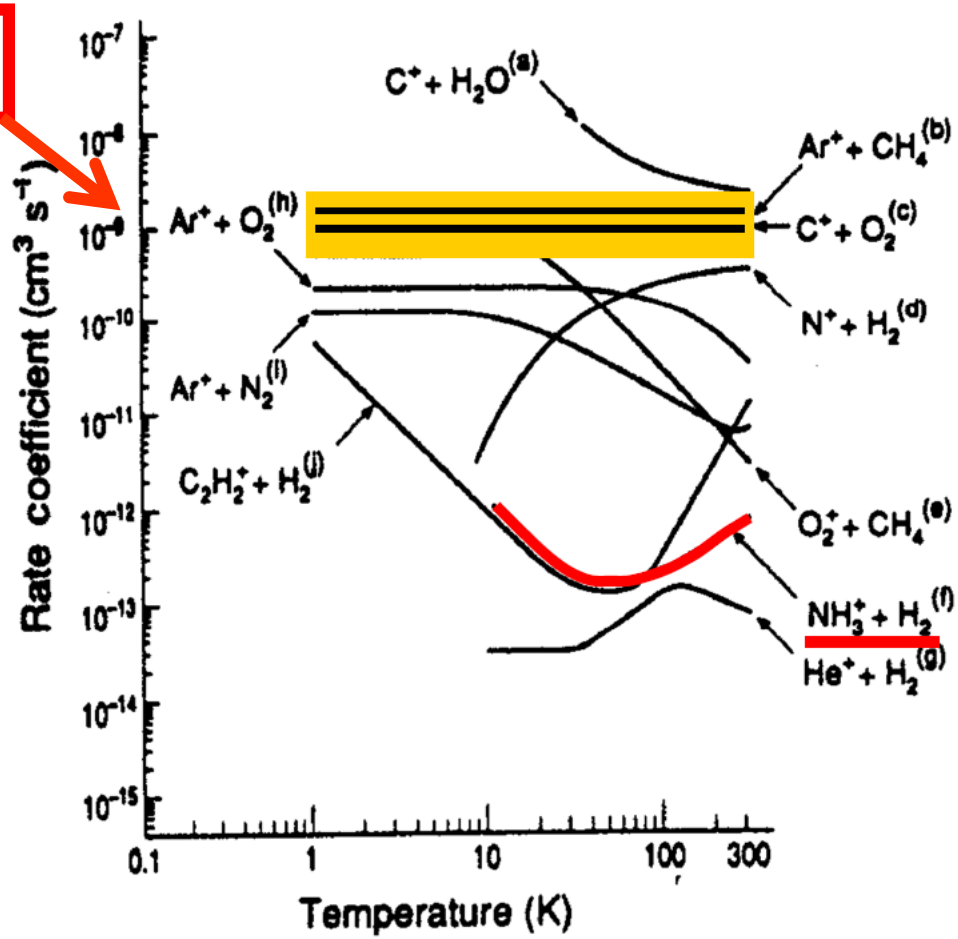

Langevin Rate Coefficient:

$$k_L = q\sqrt{\frac{\pi\alpha}{\mu\varepsilon_0}}$$

M.A. Smith (1994)

Dense Interstellar Cloud Cores

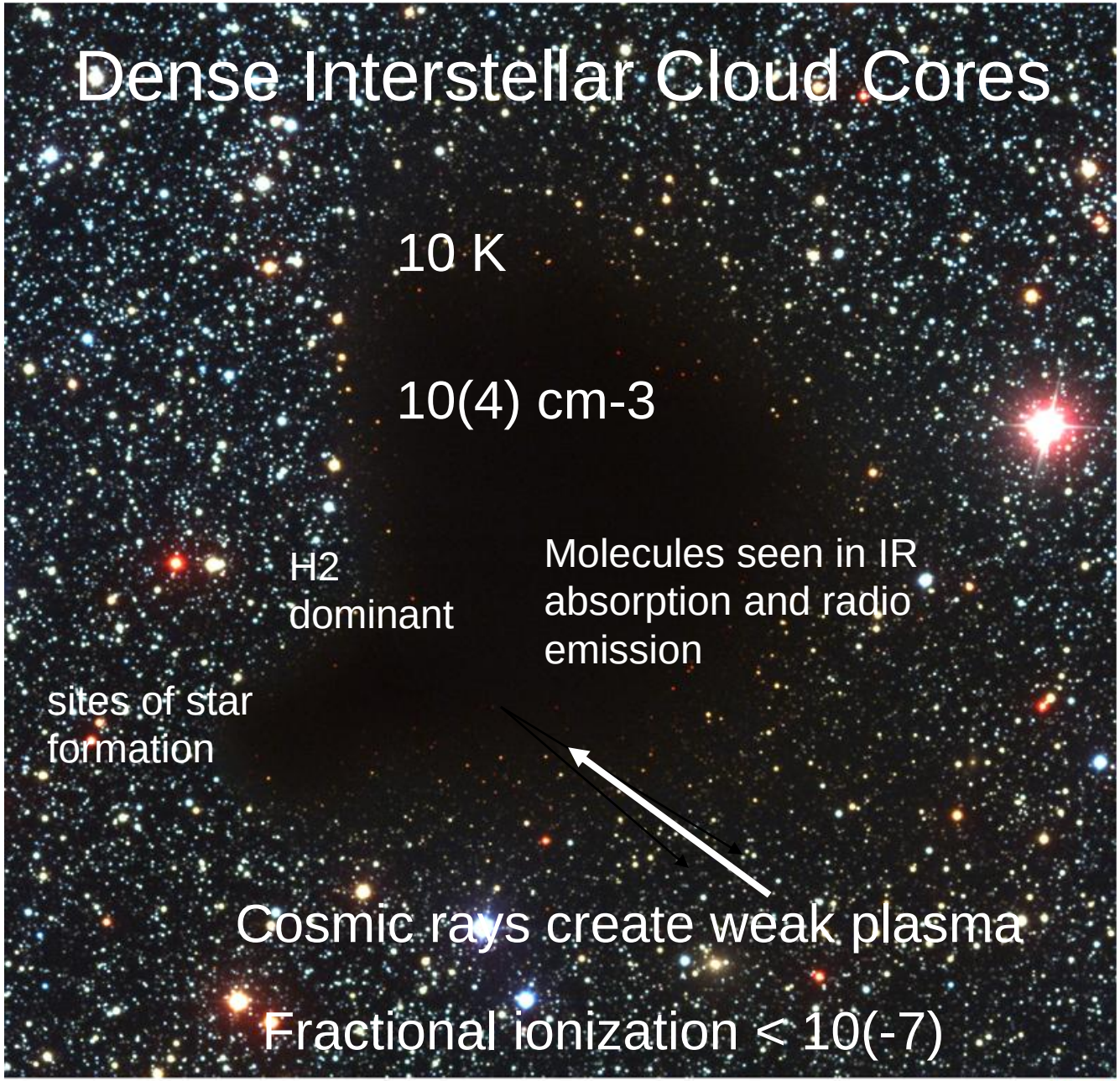

ESO PR Photo 20a/99 (30 April 1999)

The "Black Cloud" B68
(VLT ANTU + FORS1)

Cosmic Elemental Abundances

- H = 1
- He = 6.3(-2)
- O = 7.4(-4) 1.8(-4)
- C = 4.0(-4) 7.3(-5)
- N = 9.3(-5) 2.1(-5)
- S = 2.6(-5) 8.0(-8)
- Si = 3.5(-5) 8.0(-9)
- Fe = 3.2(-5) 3.0(-9)

- Dust/gas = 1% by mass
- Gas-phase abundances of heavy elements in clouds reduced.

GAS PHASE INTERSTELLAR/CIRCUMSTELLAR MOLECULES - HIGH RESOLUTION (12/03)

H_2	KCl	HNC	NH_3	C_3S	C_5	C_6H
			CH_3			HC_4CN
CH	AlCl	HCO	H_3O^+	CH_4	CH_3OH	C_7H, C_6H_2
						C_8H
CH^+	AlF	HCO^+	H_2CO	SiH_4	CH_3SH	$HCOOCH_3$
						CH_3COOH
NH	PN	HOC^+	H_2CS	CH_2NH	C_2H_4	CH_3C_2CN
						H_2C_6(lin)
OH	SiN	HN_2^+	HCCH	H_2C_3(lin)	CH_3CN	C_6H_2
						$H_2COHCHO$
C_2	SiO	HNO	$HCNH^+$	c-C_3H_2	CH_3NC	C_2H_5OH
						$(CH_3)_2O$
CN	SiS	HCS^+	H_2CN	CH_2CN	HC_2CHO	C_2H_5CN
CO	CO^+	C_3	C_3H(lin)	NH_2CN	NH_2CHO	CH_3C_4H
CSi	SO^+	C_2O	c-C_3H	CH_2CO	HC_3NH^+	HC_6CN
		CO_2			C_4H_2	$(CH_2OH)_2$
CP	H_3^+	C_2S	HCCN	HCOOH	H_2C_4(lin)	$(CH_3)_2CO$
		AlNC				
CS	CH_2	SiC_2	HNCO	C_4H	C_5H	CH_3C_4CN?
HF		SiCN	SiC_3		C_5N	
NO	NH_2	SO_2	$HOCO^+$	HC_2CN	CH_3NH_2	NH_2CH_2COOH?
		NaCN			CH_2CHOH	
NS	H_2O	OCS	HNCS	HCCNC	CH_3CCH	HC_8CN
SO	H_2S	MgNC	C_2CN	HNCCC	CH_3CHO	c-C_6H_6
HCl	C_2H	MgCN	C_3O	C_4Si	CH_2CHCN	$HC_{10}CN$
NaCl	HCN	N_2O	NaCN	H_2COH^+	c-CH_2OCH_2	+ *ISOTOPOMERS*
					c-CH_2SCH_2	

Some Fractional Abundances in TMC-1

- CO 1(-4)
- HCN 2(-8)
- C4H 9(-8)
- HCO+ 8(-9)
- c-C3H2 1(-8)
- HC9N 5(-10)
- OH 2(-7)
- NH3 2(-8)
- HC3N 2(-8)
- N2H+ 4(-10)
- HNC 2(-8)
- O2 < 8(-8)

IMR – Ion-Molecule Reactions

Introduction

THE ASTROPHYSICAL JOURNAL, 787:44 (10pp), 2014 May 20

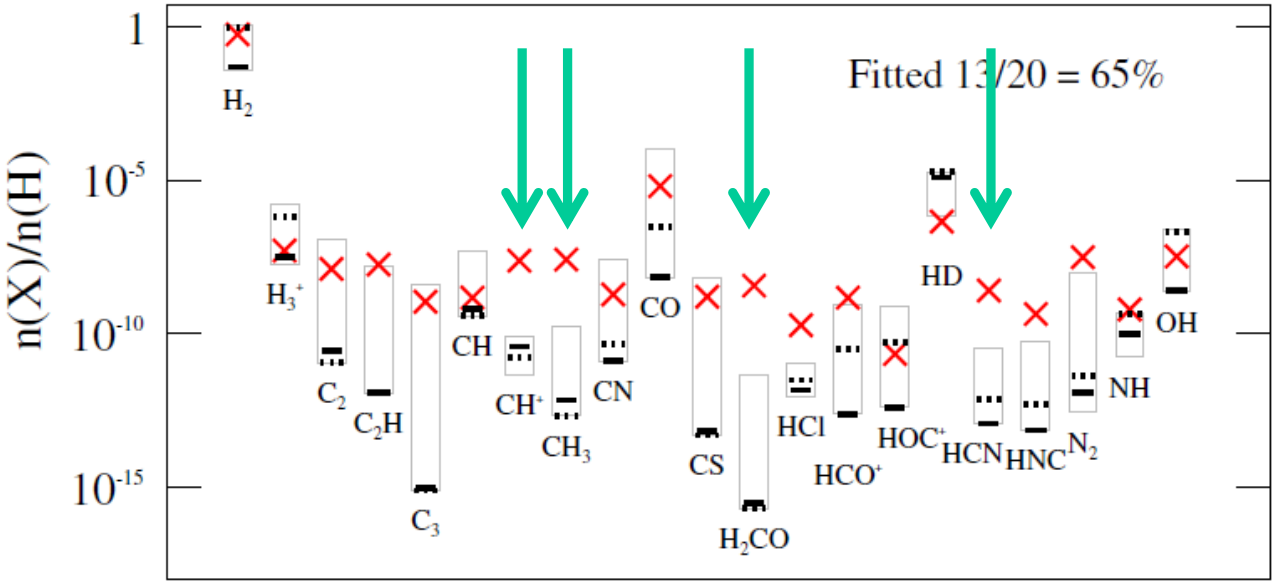

Figure 6. Comparison of observed abundances (red crosses) to modeled values of key species in diffuse clouds. Gray boxes show the range of abundances calculated from the considered models (Table 2) and black lines show abundances from the best-fit model "2X+C15" (30 K, solid line, and 90 K, dotted line).

THE ASTROPHYSICAL JOURNAL, 787:44 (10pp), 2014 May 20 doi:10.1088/0004-637X/

FIRST TIME-DEPENDENT STUDY OF H_2 AND H_3^+ *ORTHO–PARA* CHEMISTRY IN THE DIFFUSE INTERSTELLAR MEDIUM: OBSERVATIONS MEET THEORETICAL PREDICTIONS*

T. ALBERTSSON[1], N. INDRIOLO[2], H. KRECKEL[3], D. SEMENOV[1], K. N. CRABTREE[4], AND TH. HENNING[1]

Energies experiments

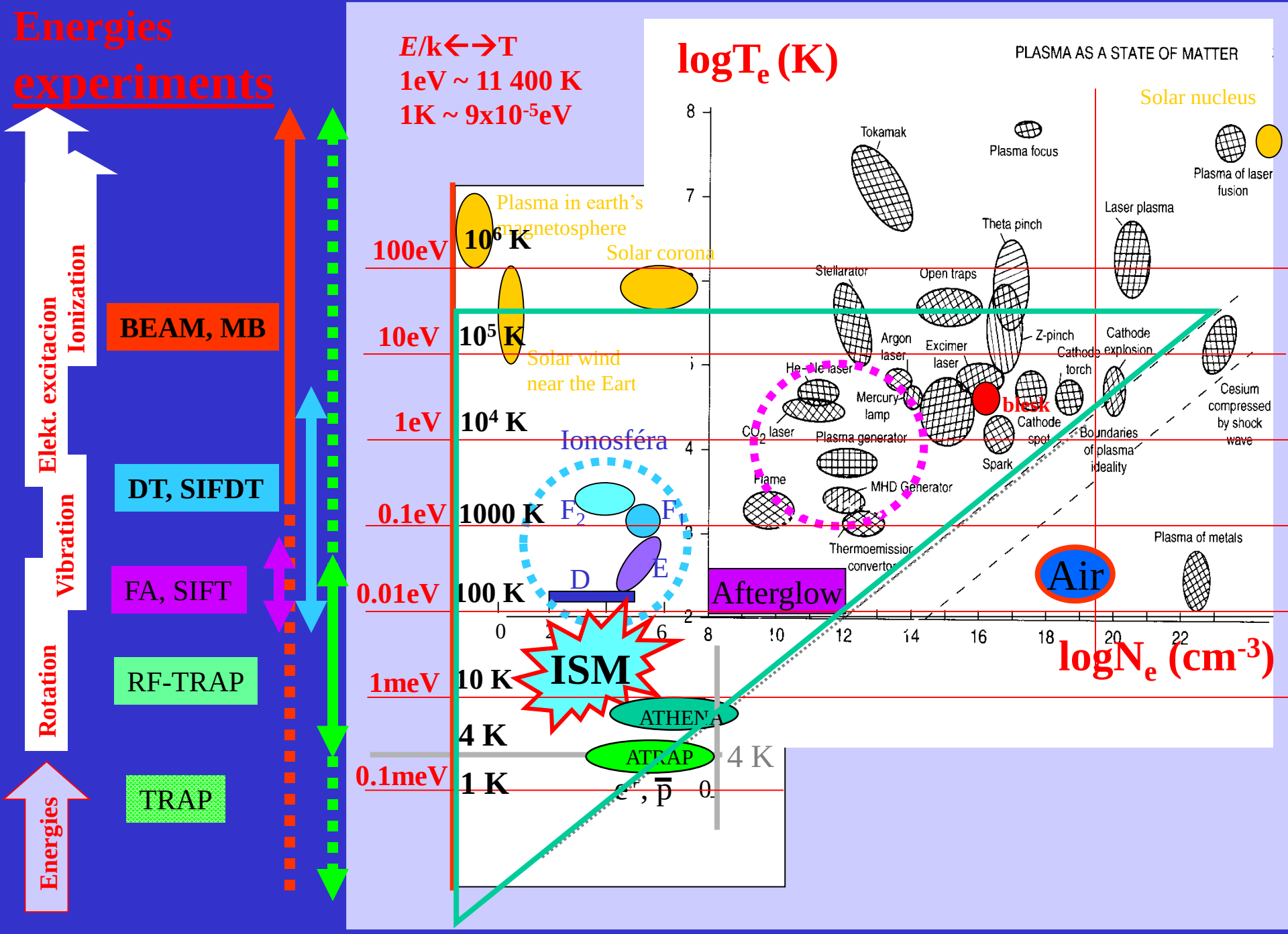

First-order reaction

A ➔ B + C

<u>Unimolecular</u> reactions

$$A^+ \rightarrow product$$

$$A^+ \rightarrow B^+$$

$$k_{UNI} = 1/\tau_{UNI}$$

$$\frac{d[A^+]}{dt} = -k_{UNI}[A^+] = -[A^+]/\tau_{UNI}$$

$$[k_{UNI}] = s^{-1}$$

$$A^+ \rightarrow B^+$$

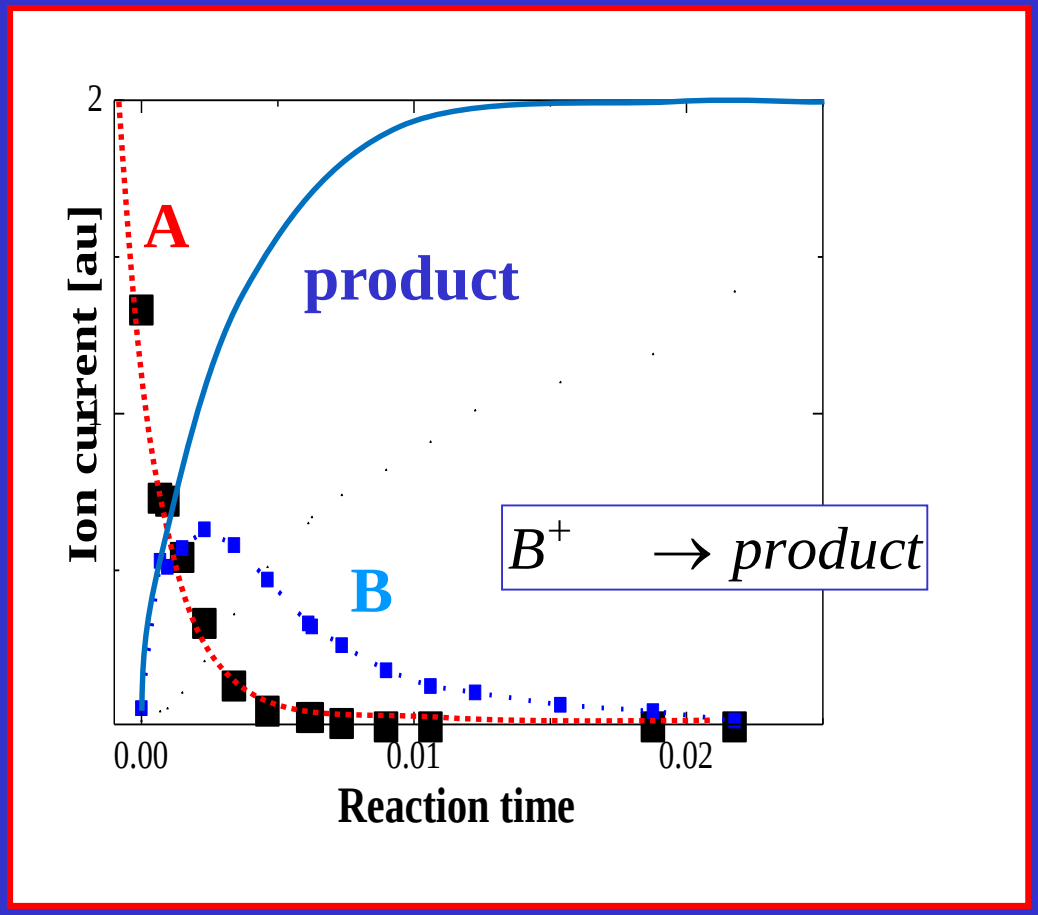

$$A^+ \rightarrow product$$

$$\frac{d[A^+]}{dt} = -k_{UNI}[A^+] = -[A^+]/\tau_{UNI}$$

$$k_{UNI} = 1/\tau_{UNI}$$

$$[k_{UNI}] = s^{-1}$$

$$[A^+]_t = [A^+]_{t=0} \cdot e^{-k_{UNI}t} = [A^+]_{t=0} \cdot e^{-t/\tau_{UNI}}$$

$$A^+ \rightarrow B^+$$

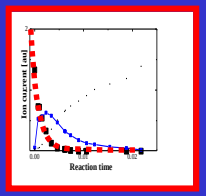

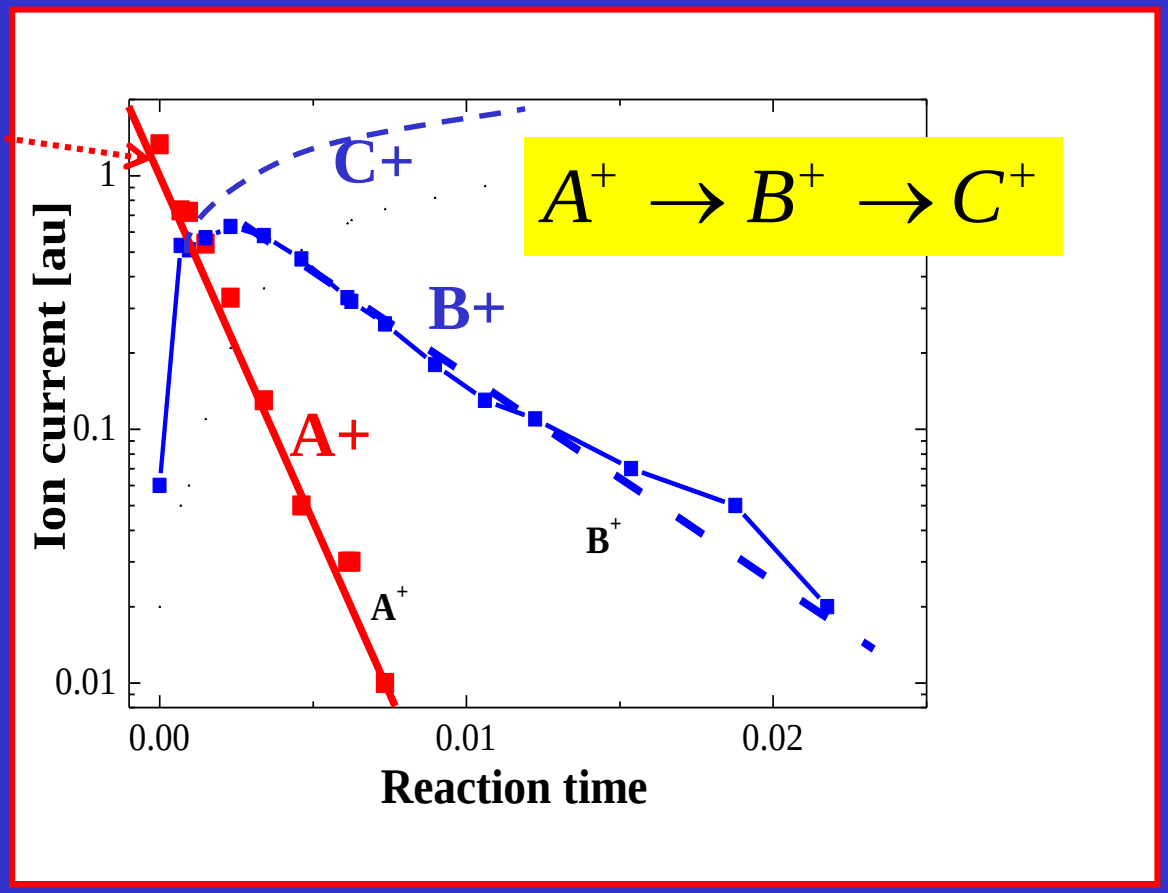

First-Order Reactions

$$\frac{d[A^+]}{dt} = -k_{UNI}[A^+] = -[A^+]/\tau_{UNI}$$

$$[A] = [A]_o e^{-k_A t}$$

$$\ln[A] = \ln[A]_o - k_A t$$

$$\frac{[A]}{[A]_o} = e^{-k_A t}$$

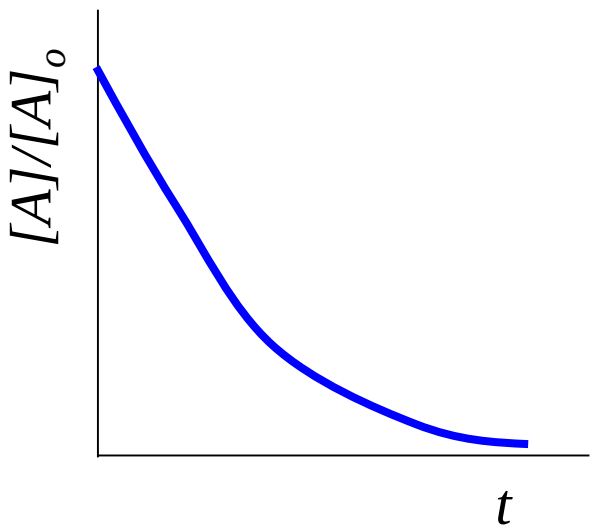

First-order reaction: $[A]/[A]_o$ vs t

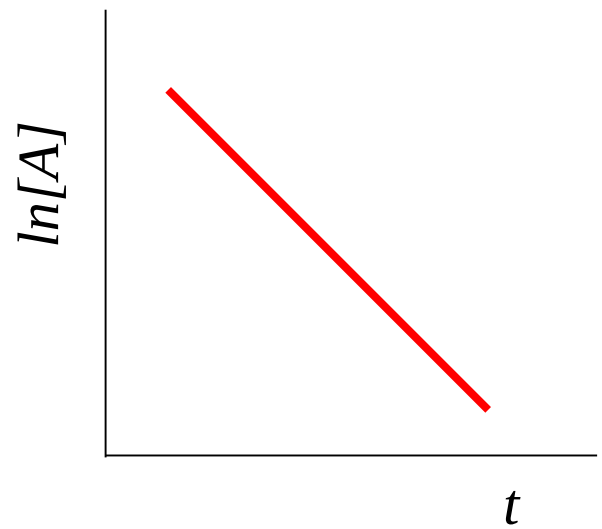

First-order reaction: $ln[A]$ vs t

Unimolecular reactions

$$A^+ \rightarrow product$$

$$A^+ \rightarrow B^+ \rightarrow C^+$$

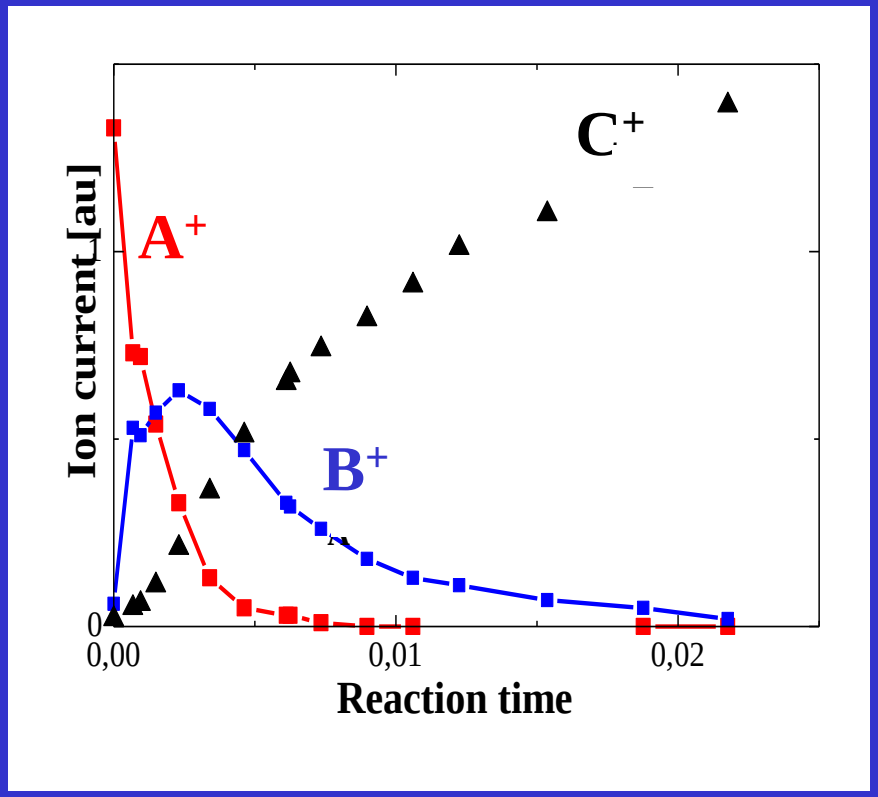

Reaction rate coefficient

$$\frac{dA^+}{dt} = -k_{UNI} A^+ = -A^+ / \tau_{UNI}$$

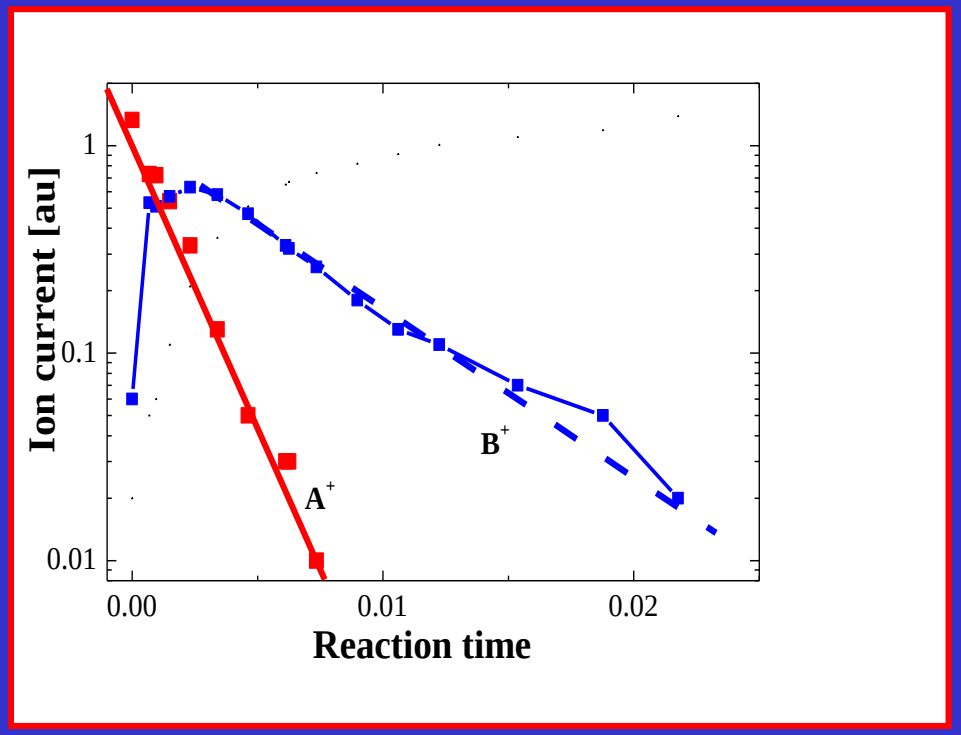

Unimolecular reactions

$$A^+ \rightarrow product$$

$$[A^+]_t = [A^+]_{t=0} \cdot e^{-k_{UNI} t} = [A^+]_{t=0} \cdot e^{-t/\tau_{UNI}}$$

Reaction rate coefficient

$$\frac{dA^+}{dt} = -k_{UNI} A^+ = -A^+ / \tau_{UNI}$$

$$A^+ \rightarrow B^+ \rightarrow C^+$$

$$A^+ \rightarrow B^+ \rightarrow C^+$$

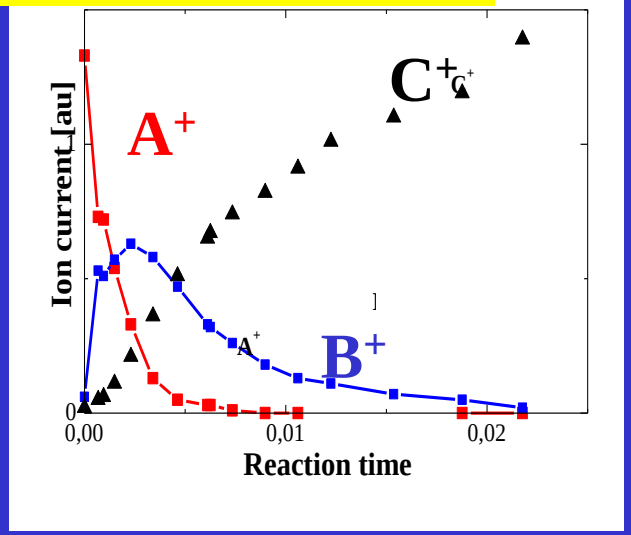

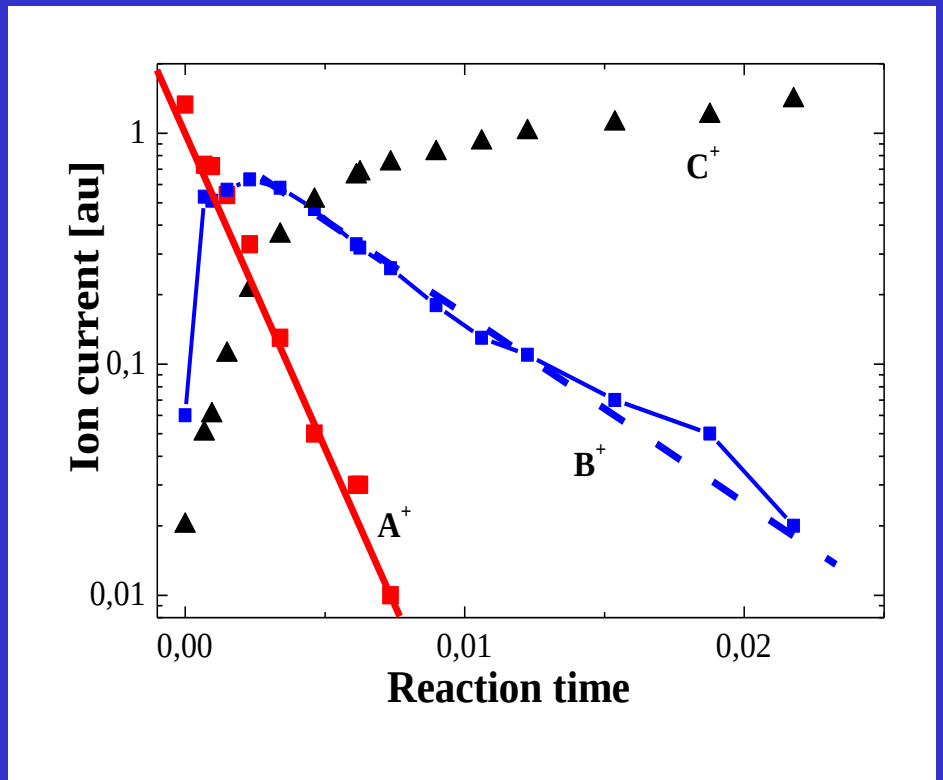

Example

Photodissociation

$$H_3^+ + h\nu \rightarrow (H_3^{+*}) \rightarrow H^+ + H_2$$

$$[A^+]_t = [A^+]_{t=0} \cdot e^{-k_{UNI}t} = [A^+]_{t=0} \cdot e^{-t/\tau_{UNI}}$$

$$D_3^+ + h\nu \rightarrow (D_3^*) \rightarrow D^+ + D_2$$

Radiative lifetime

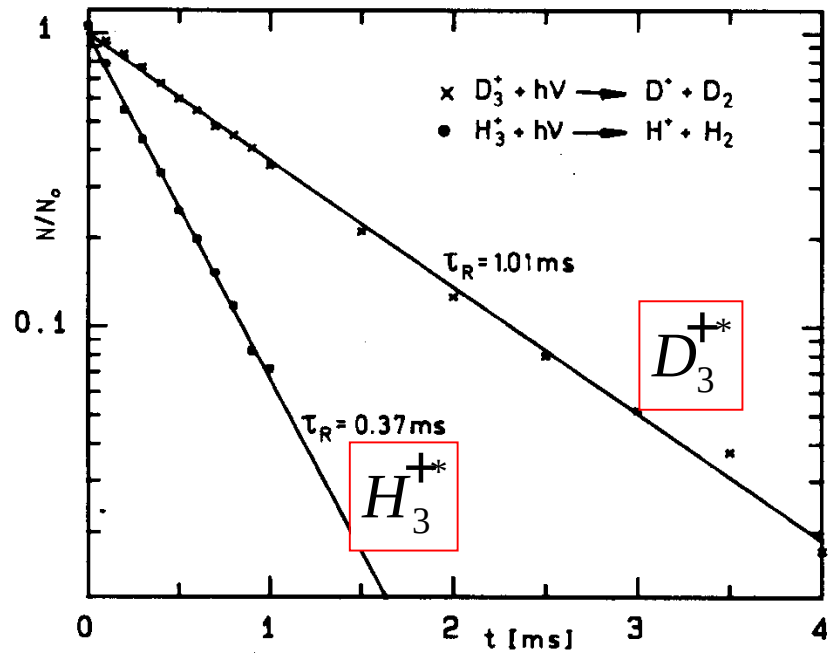

Figure 87. Direct determination of radiative lifetimes of highly exited H_3^+ and D_3^+ ions. Externally created ions were injected into the ring electrode trap, and their spontaneous radiative decay was probed by delayed CO_2 laser-induced fragmentation. Loss by processes other than radiative decay is excluded on the depicted time scale and at the low pressure ($< 10^{-9}$ mbar).

excitation

Radiative decay of $H_3^+(v)$

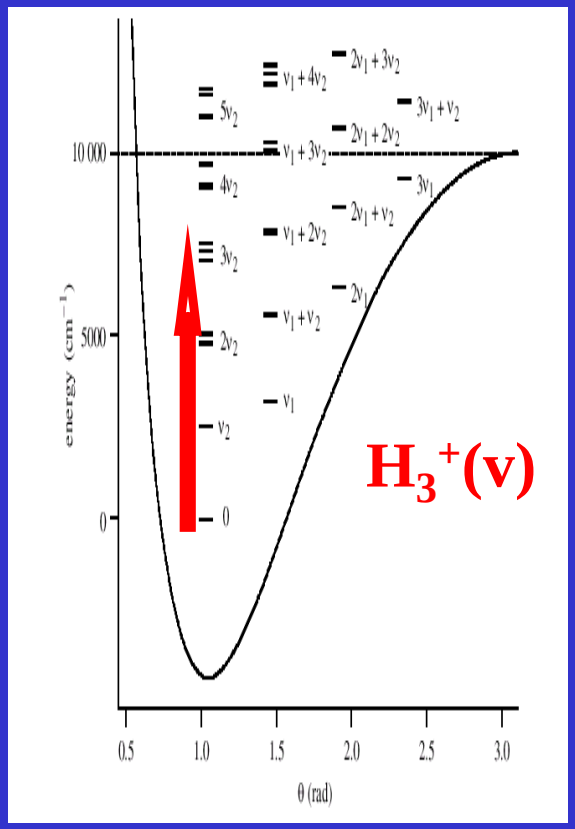

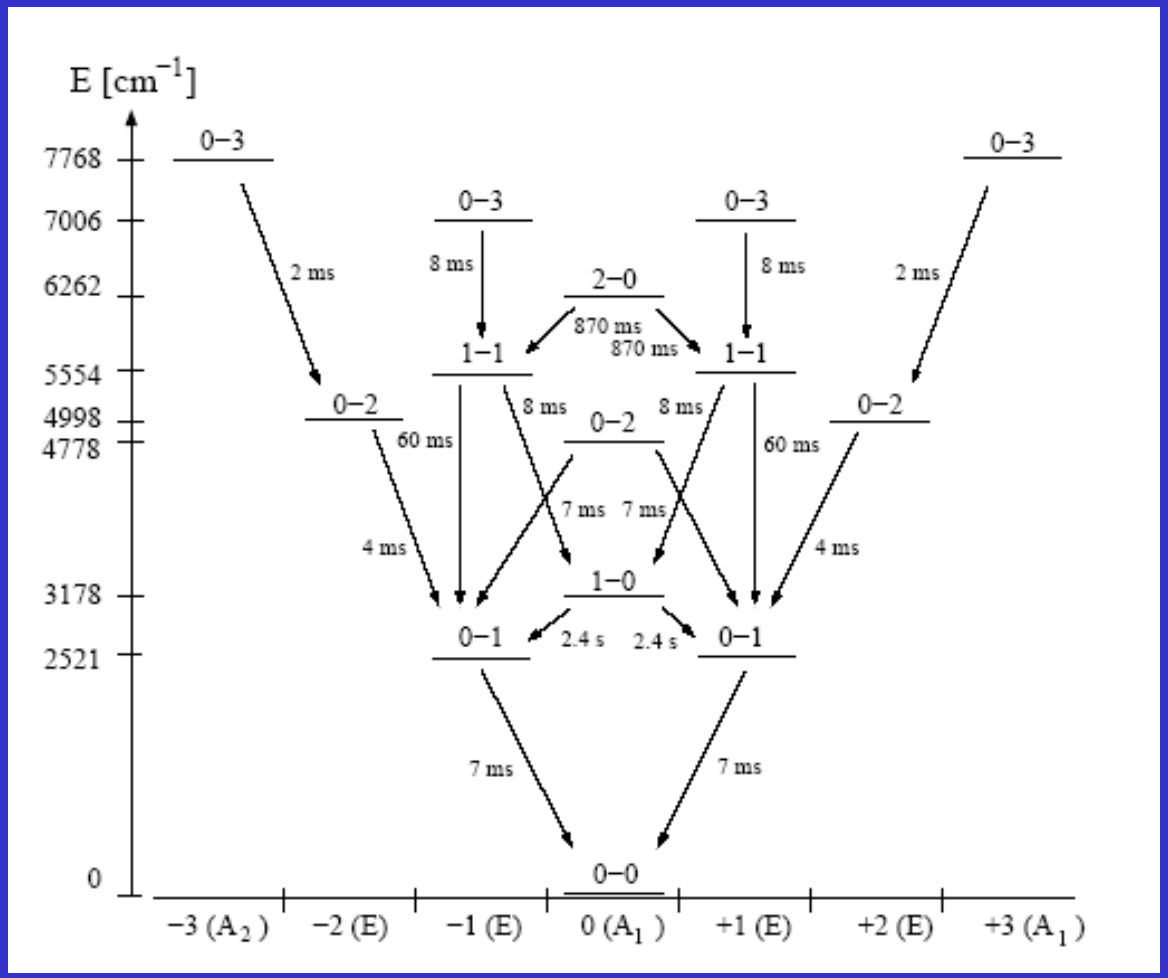

Radiative lifetime

Reakce II.řádu

$2\,A \rightarrow P$

$A + B \rightarrow P$

Binary reactions Reaction rate coefficient

$$A^+ + B \rightarrow C^+ + D$$

$$[k_{BIN}] = cm^3 s^{-1}$$

$$\frac{d[A^+]}{dt} = -k_{BIN}[A^+][B]$$

Often it is written in simpler form using A^+ instead of $[A^+]$

$$\frac{dA^+}{dt} = -k_{BIN} A^+ B$$

Binary reactions Reaction rate coefficient

$$A^+ + B \rightarrow C^+ + D$$

$$\frac{d[A^+]}{dt} = -k_{BIN}[A^+][B]$$

For $[A^+] << [B]$

$$[A^+]_t = [A^+]_{t=0} \cdot e^{-k[B]t}$$

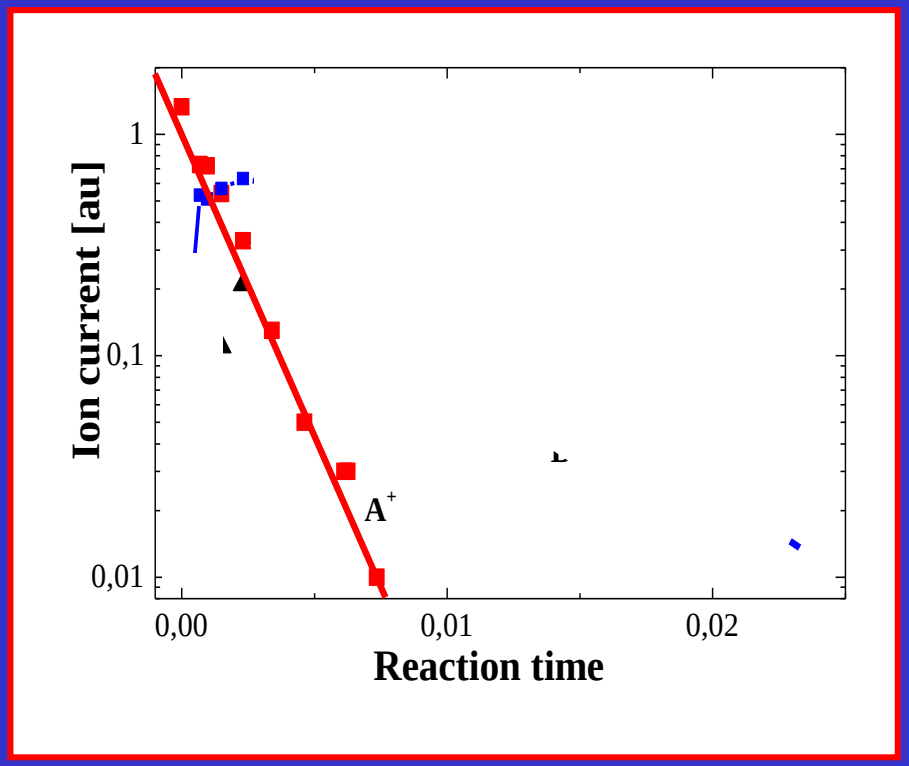

Binary reactions Reaction rate coefficient

$$A^+ + B \rightarrow C^+ + D$$

$$\frac{dA^+}{dt} = -k_{BIN} A^+ B$$

$$[A^+]_t = [A^+]_{t=0} \cdot e^{-k[B]t}$$

Sequence of reactions

$$A^+ + B \rightarrow A_1^+ + C$$
$$A_1^+ + B \rightarrow A_2^+ + D$$

$$A^+ \rightarrow A_1^+ \rightarrow A_2^+$$

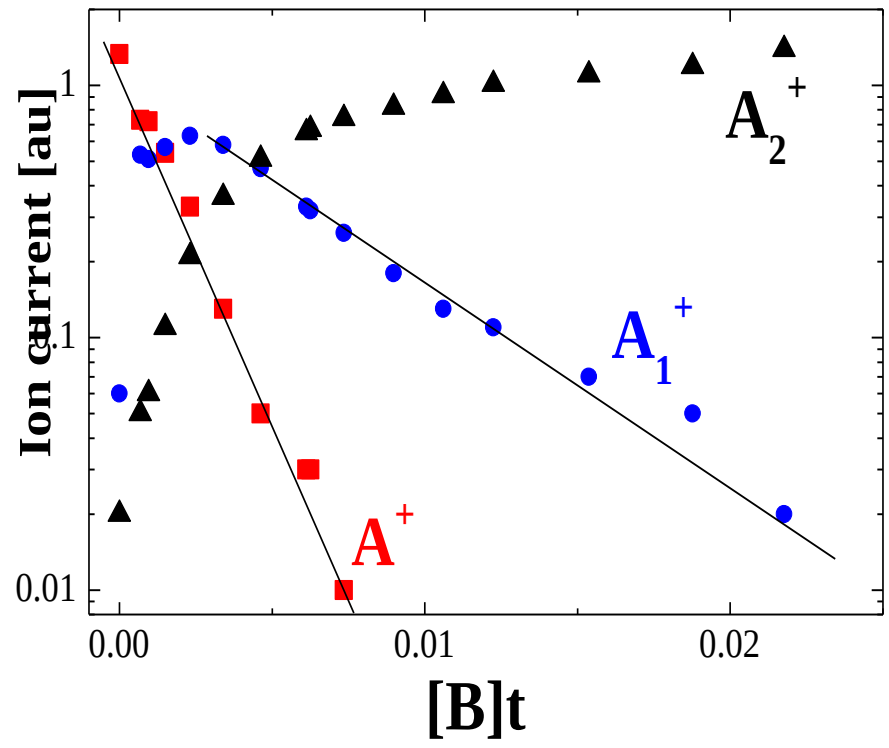

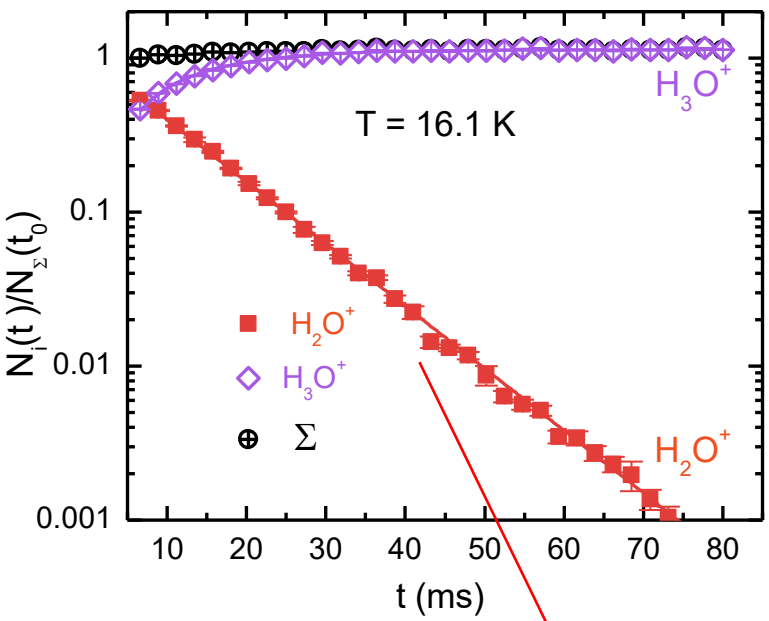

$$\mathbf{H_2O^+ + H_2 \rightarrow H_3O^+ + H}$$

$$A^+ \quad + \quad B \rightarrow C^+ \quad + \quad D$$

$$\frac{dA^+}{dt} = -k_{BIN} A^+ B$$

$$[A^+]_t = [A^+]_{t=0} \cdot e^{-k[B]t}$$

Sequence of reactions

$$OH^+ + H_2 \rightarrow H_2O^+ + H$$

$$H_2O^+ + H_2 \rightarrow H_3O^+ + H$$

Experiment in 22-pole trap

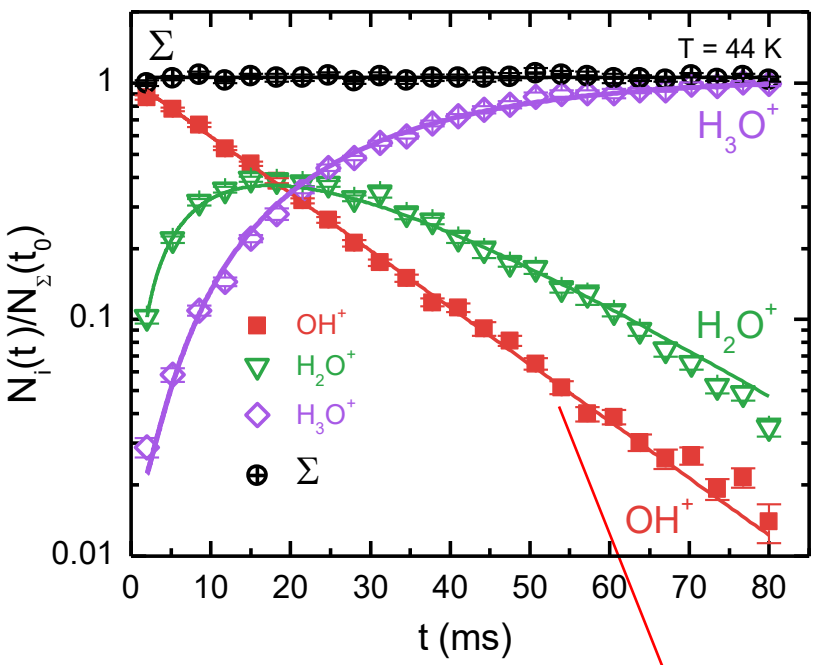

$$A^+ + B \rightarrow C^+ + D$$

$$\frac{dA^+}{dt} = -k_{BIN} A^+ B$$

$$[A^+]_t = [A^+]_{t=0} \cdot e^{-k[B]t}$$

$$O^+ + H_2 \rightarrow OH^+ + H$$

$$OH^+ + H_2 \rightarrow H_2O^+ + H$$

$$H_2O^+ + H_2 \rightarrow H_3O^+ + H$$

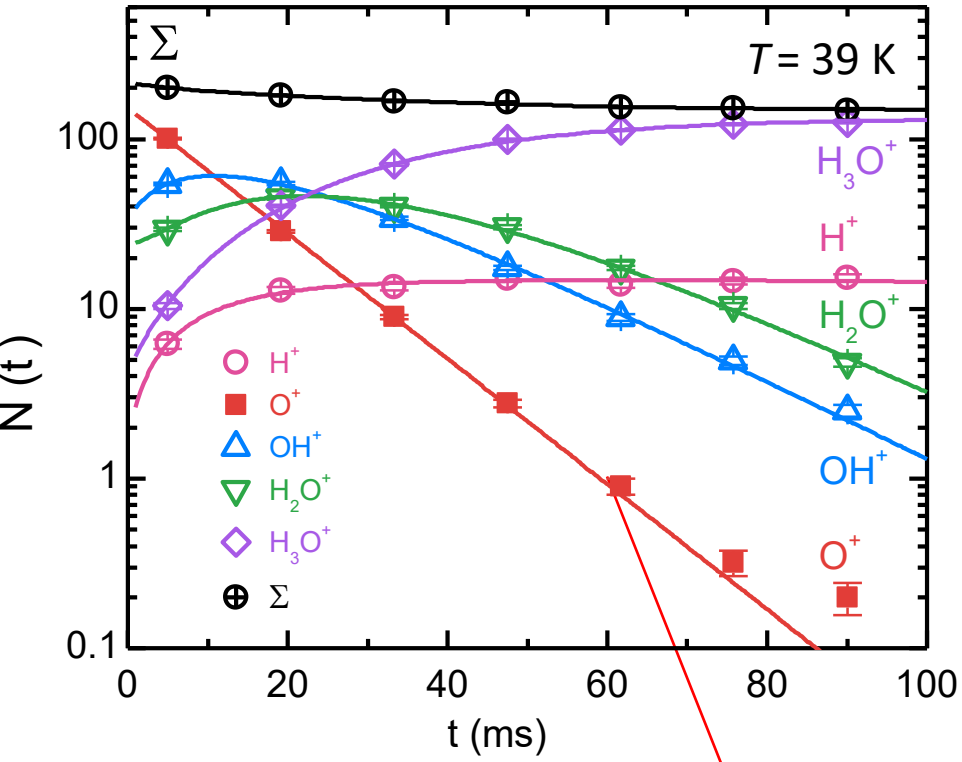

$$A^+ + B \rightarrow C^+ + D$$

$$\frac{dA^+}{dt} = -k_{BIN} A^+ B$$

$$[A^+]_t = [A^+]_{t=0} \cdot e^{-k[B]t}$$

Oxygen and its components in the interstellar medium

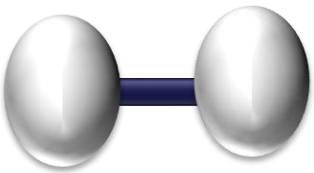

O_2, P. F. Goldsmith 2002

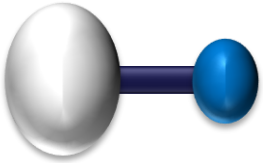

OH^+, F. Wyrowski 2010

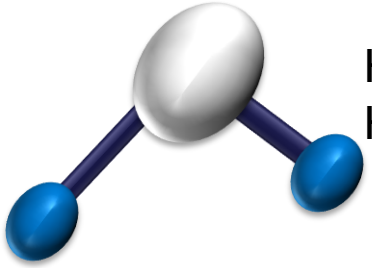

H_2O, A. C. Cheung 1969
H_2O^+, V. Ossenkopf 2010

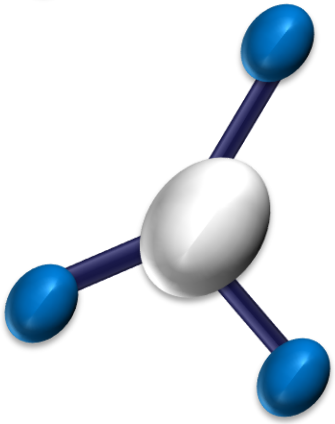

H_3O^+, J. M. Hollis 1986

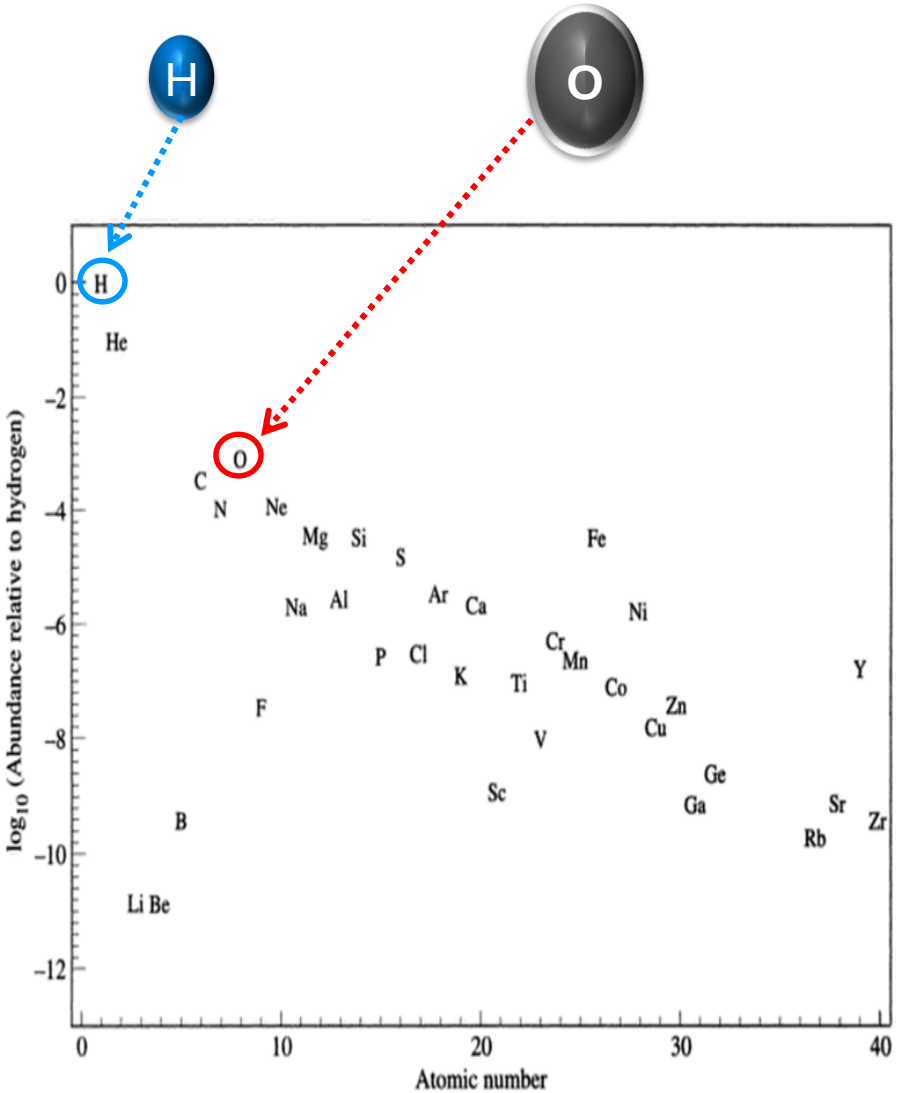

The Astrophysical Journal, 754:105 (22pp), 2012 August 1 doi:10.1088/0004-637X/754/2/105

2012

THE CHEMISTRY OF INTERSTELLAR OH^+, H_2O^+, AND H_3O^+: INFERRING THE COSMIC-RAY IONIZATION RATES FROM OBSERVATIONS OF MOLECULAR IONS

David Hollenbach[1], M. J. Kaufman[2], D. Neufeld[3], M. Wolfire[4], and J. R. Goicoechea[5]

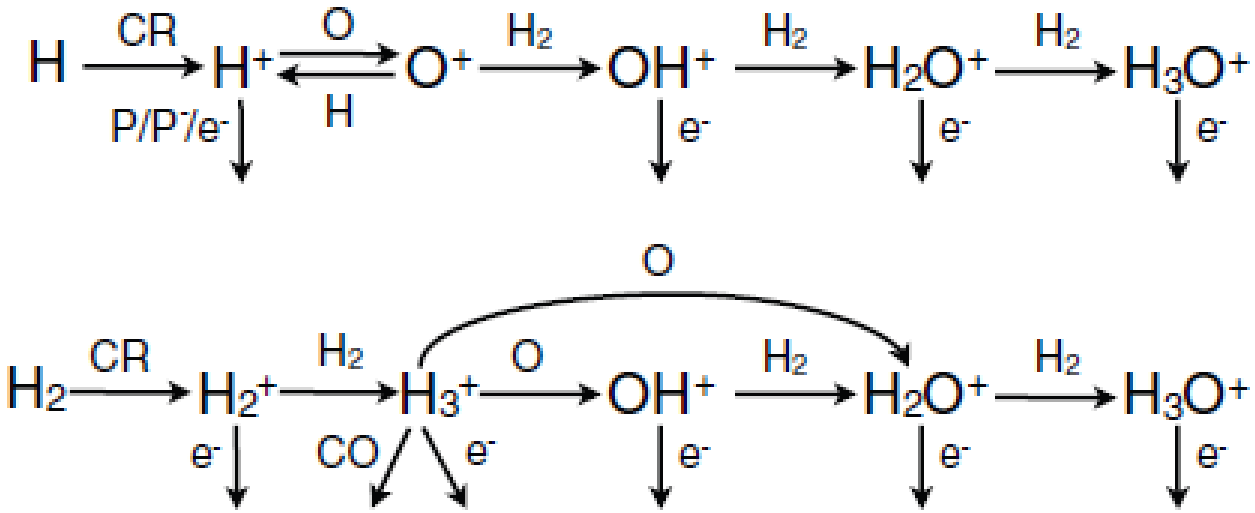

Interstellar Hydrides

Maryvonne Gerin,[1,2] David A. Neufeld,[3,4] and Javier R. Goicoechea[5]

Annu. Rev. Astron. Astrophys. 2016. 54:181–225

First published online as a Review in Advance on July 22, 2016

The *Annual Review of Astronomy and Astrophysics* is online at astro.annualreviews.org

2016

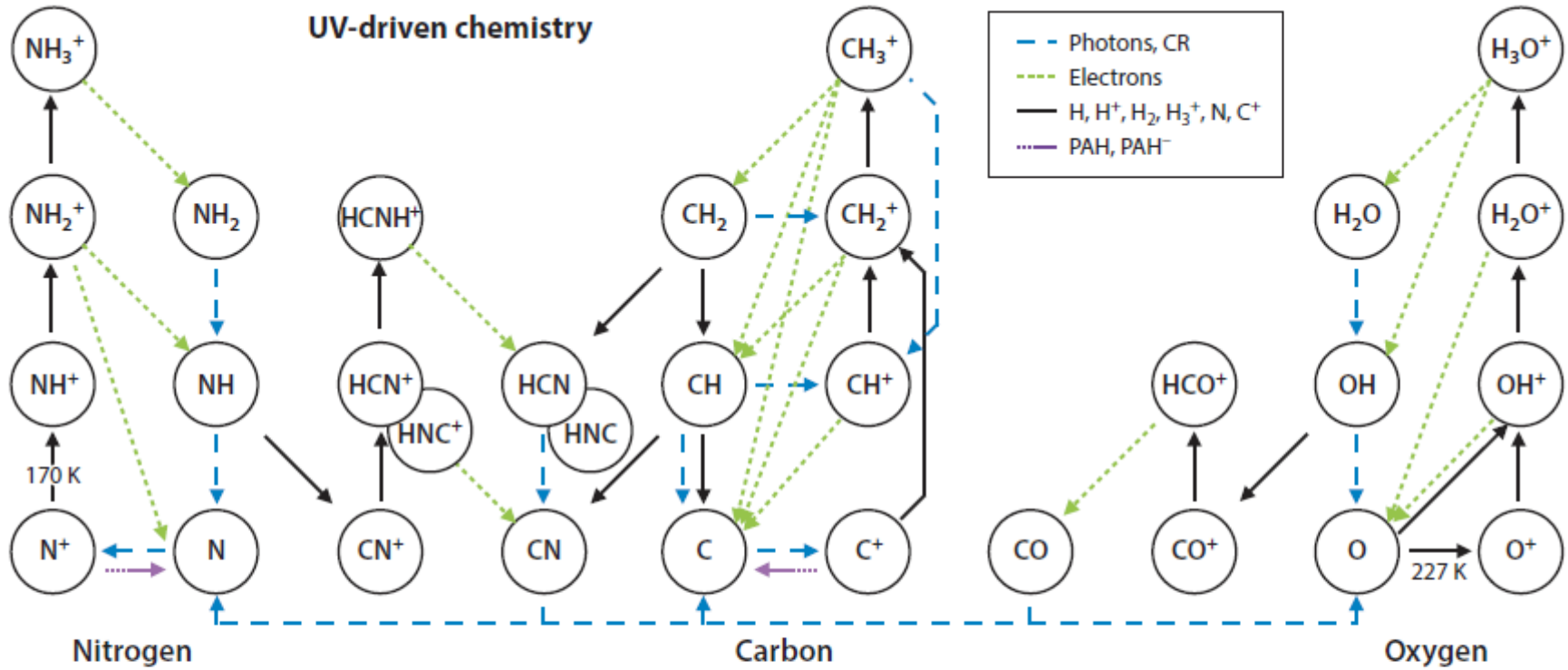

Figure 3

Illustration of the chemical network initiating the carbon, oxygen, and nitrogen chemistry in diffuse cloud conditions ($n_H = 50$ cm^3, $A_V = 0.4$ mag, $\chi = 1$). The black arrows show the reactions with H, H^+, H_2, H_3^+, C^+, and N, with values of the endothermicity for the reaction between N^+ and H_2 and for the charge exchange reaction between O and H^+. Note that CH_2^+ is formed in the slow radiative association reaction between C^+ and H_2. The dashed blue arrows indicate the reactions induced by FUV photons or cosmic rays (CR). Dissociative recombination reactions with electrons are shown with green dotted arrows. Purple arrows show the neutralization reactions on dust grains and polycyclic aromatic hydrocarbons (PAHs). Adapted from Godard et al. (2014) with permission.

$O^+ + H_2 \rightarrow OH^+ + H$

2015

THE JOURNAL OF PHYSICAL CHEMISTRY A
Article
pubs.acs.org/JPCA

Accurate Time-Dependent Wave Packet Calculations for the $O^+ + H_2 \rightarrow OH^+ + H$ Ion–Molecule Reaction

N. Bulut,[†] J.F. Castillo,[‡] P. G. Jambrina,[‡] J. Klos,[§] O. Roncero,[∥] F. J. Aoiz,[‡] and L. Bañares[*,‡]

J. Phys. Chem. A 2015, 119, 11951−11962

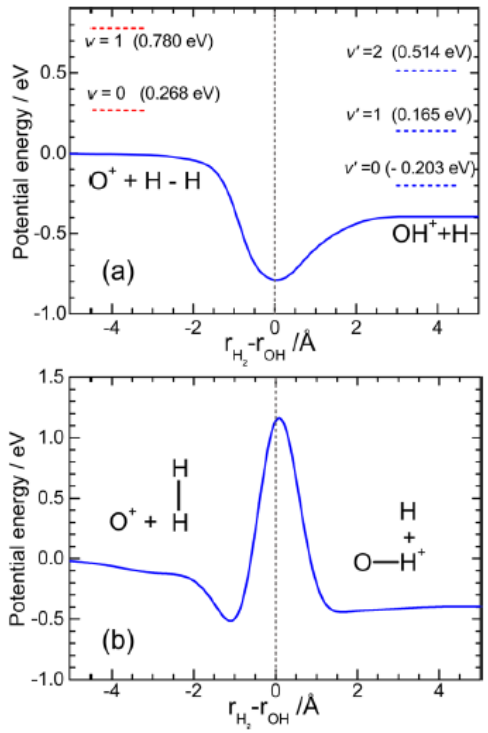

Figure 1. Minimum energy path for the $O^+ + H_2 \rightarrow OH^+ + H$ reaction calculated on the MMG PES[10] as a function of $r_{H_2} - r_{OH}$. (a) Collinear configuration, $\widehat{OHH}$ angle $\alpha = 180°$. The dashed horizontal lines indicate the energy of the initial H_2 $v = 0$ and $v = 1$, and final OH^+ $v' = 0$, $v' = 1$, and $v' = 2$ vibrational states. (b) Perpendicular configuration $\widehat{OHH}$ angle $\alpha = 90°$.

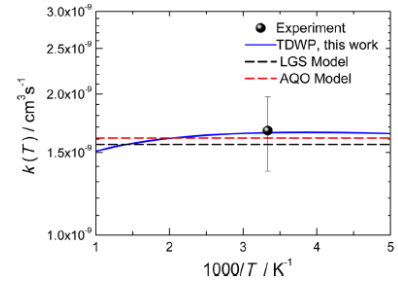

Figure 9. Thermal rate constants for the $O^+ + H_2$ reaction. Blue solid line: TDWP. Solid circle: experimental result from ref 7. Black dashed line: Langevin model. Red dashed line: AQO model.

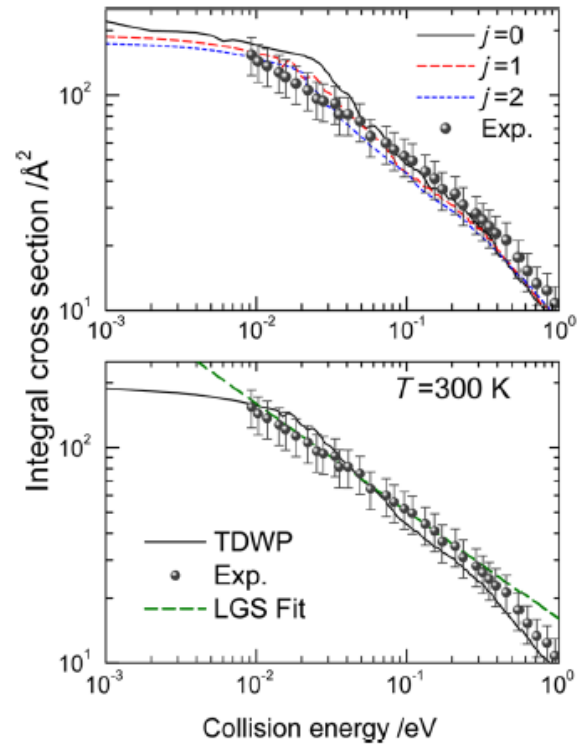

Figure 8. Top: total reaction cross section as a function of collision energy for the $O^+ + H_2(v=0,j)$ reactions. Solid black line: $j = 0$. Red dashed line: $j = 1$. Blue short-dashed line: $j = 2$. Solid circles: experimental results from ref 7. Bottom: Total reaction cross section as a function of collision energy for the $O^+ + H_2(v=0,\langle j \rangle)$ reaction averaged over the thermal rotational population at 300 K. Black solid line: TDWP. Solid circles: experimental results from ref 7. Green dashed line: Langevin model, $\sigma_r(E_c) = AE_c^{-1/2}$; $A = 16$ Å^2 eV$^{1/2}$.

$$O^+ + H_2 \rightarrow OH^+ + H$$

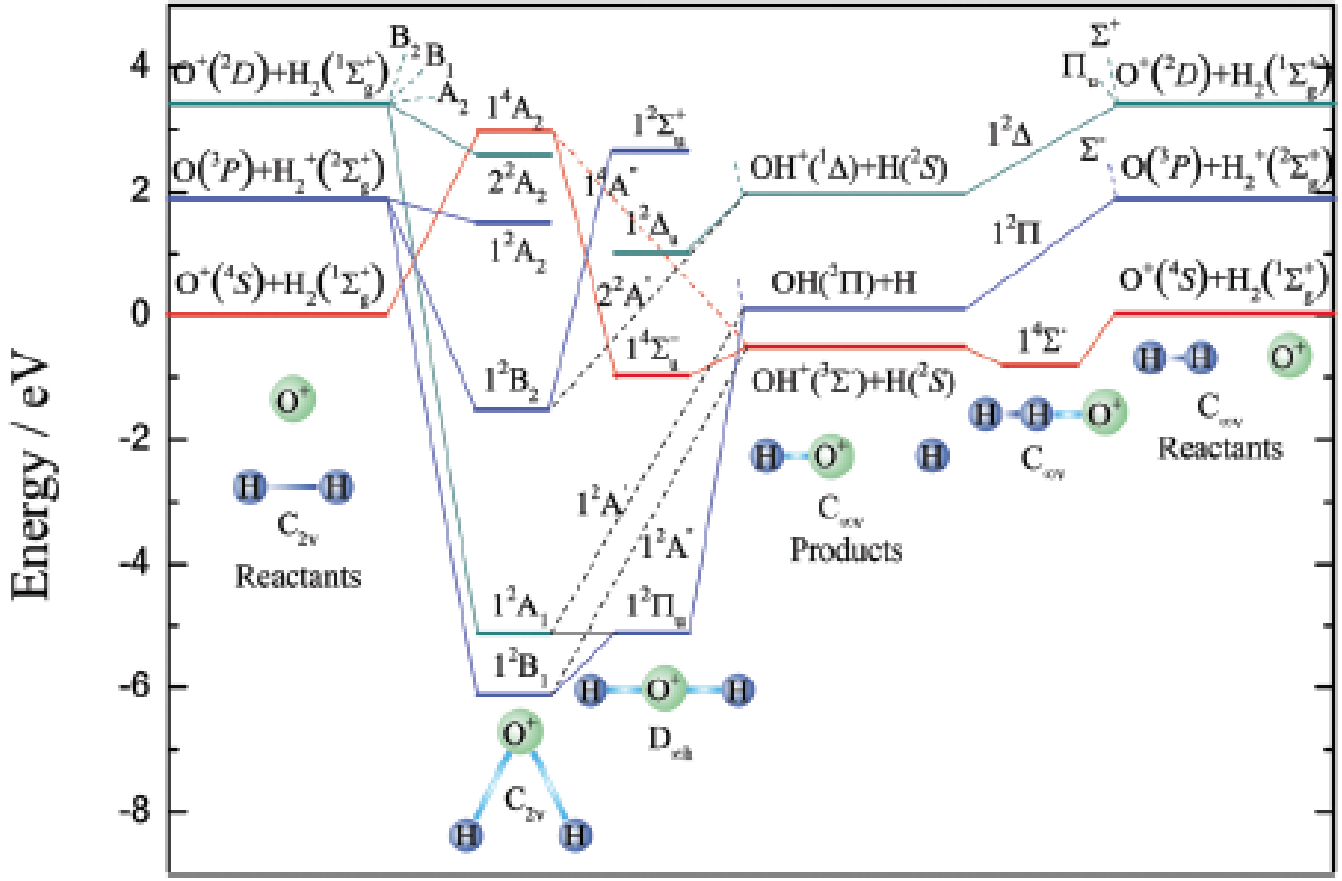

Fig. 1 Electronic correlation diagram for reactant, intermediate, and product arrangements of the H_2O^+ system under C_{2v}, $C_{\infty v}$, and $D_{\infty h}$ symmetries. The PESs of the title reaction are plotted by the red lines. This diagram is an adaptation of that reported in ref. 24.

$$O^+ + D_2 \rightarrow OD^+ + D$$

Dynamics studies of $O^+ + D_2$ reaction using the time-dependent wave packet method

Ziliang Zhu[a,b], Li Li[b], Qiju Li[b] and Bing Teng[a]

[a]College of Physics, Qing dao University, Qing dao, People's Republic of China; [b]Shandong Peninsula Engineering Research Center of Comprehensive Brine Utilization, Weifang University of Science and Technology, Shouguang, People's Republic of China

ABSTRACT

Based on the potential energy surface (PES) reported by Li *et al.* (Phys. Chem. Chem. Phys. **20**, 1039 (2018)), the initial state dynamics calculation of $O^+ + D_2$ ($v = 0, j = 0$) reaction was conducted using the time-dependent wave packet method with a second order split operator. Dynamics properties such as reaction probability, integral cross section, differential cross section, and distribution of products were calculated and compared with available experimental and theoretical results. The present integral cross section values were in good agreement with experimental results. In addition, the differential cross section indicates that the mechanism of the complex-formation reaction plays a dominant role during the reaction.

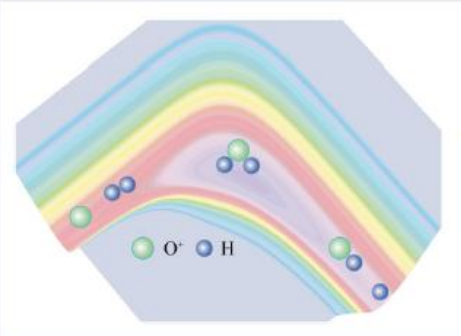

ARTICLE HISTORY
Received 15 November 2018
Accepted 7 May 2019

KEYWORDS
Reaction probability; $O^+ + D_2$ reaction; integra cross section; time-dependent wave packet

1. Introduction

The reactions of $O^+ + H_2$, D_2 and HD isotopes have been extensively studied in recent years because of their enhanced modelling capability for ion-molecule reactions that occur in interstellar chemistry, planetary ionospheres, and combustion processes [1,2]. Dynamics properties such as rate coefficients, cross sections, and product angle-recoil velocity distributions of these reactions have been determined using a series of experimental techniques [3–10]. Li and coworkers employed a triple-quadruple double-octopole apparatus with dissociative charge transfer reactions ($Ne^+ + O_2 \rightarrow Ne + O^+(^4S,^2D) + O$, $He^+ + O_2 \rightarrow He + O^+(^4S,^2D,^2P) + O$) and octopole ion trap techniques, in order to measure the cross section of $O^+ + H_2/D_2$ reaction in the energy range of 0.01–10 eV [10].

The potential energy surface (PES) of the reaction $O^+ + H_2$ has been studied theoretically a lot in recent decades. In 2004, Martínez and coworkers [11] utilised CCSD(T) method with cc-pVQZ basis set to determine the analytical PES of $O^+ + H_2$ system ground state by fitting about 600 *ab initio* points. Then, numerous dynamics calculations [12–22] of $O^+ + H_2$ reaction and its isotopic variants were reported, which were based on PES [11]. Recently, Li and coworkers [20] reported a new PES of $O^+ + H_2$ by fitting about 63,000 *ab initio* points using the permutation invariant

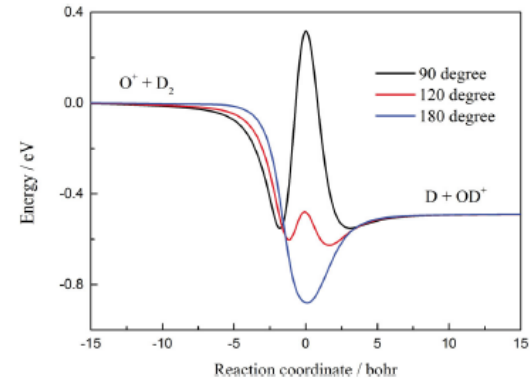

Figure 1. Minimum energy path of $O^+ + D_2$ PES for 90, 120, and 180 degrees.

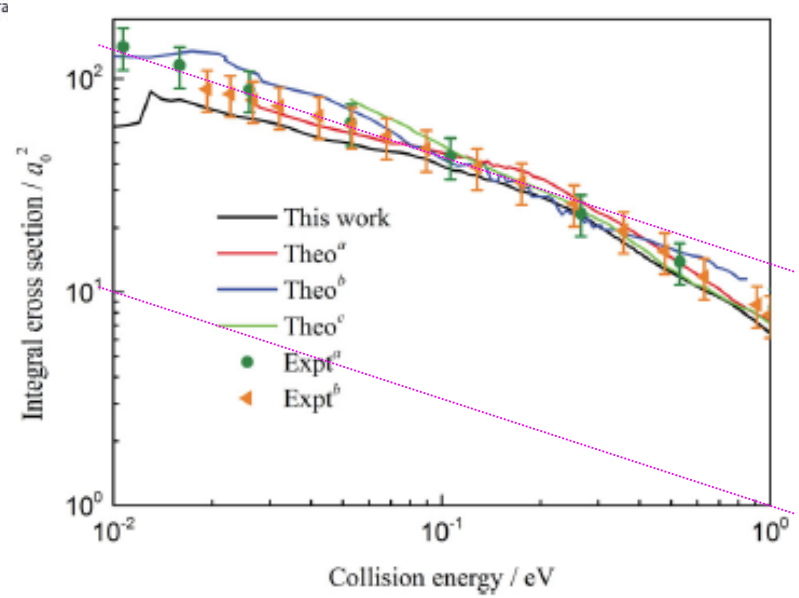

Figure 3. Total integral cross section of $O^+ + D_2(v = 0, j = 0) \rightarrow OD^+ + D$ reaction as well as experimental and theoretical results, reported in Refs. [10] (Expt^a), [7] (Expt^b), [14] (Theo^a), [16] (Theo^b), and [22] (Theo^c).

2018

$$O^+ + H_2 \rightarrow OH^+ + H$$

PCCP

PAPER

View Article Online
View Journal | View Issue

Check for updates

Cite this: *Phys. Chem. Chem. Phys.*, 2018, 20, 1039

A new potential energy surface of the OH_2^+ system and state-to-state quantum dynamics studies of the $O^+ + H_2$ reaction†

Wentao Li,*[ab] Jiuchuang Yuan,[b] Meiling Yuan,[c] Yong Zhang,[d] Minghai Yao[a] and Zhigang Sun*[b]

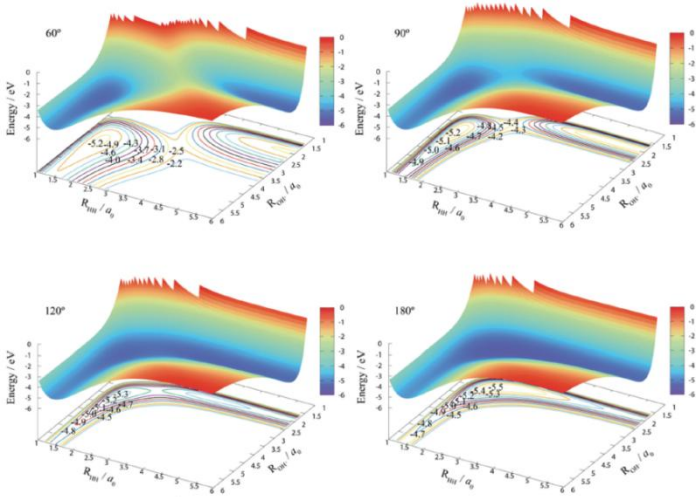

Fig. 2 Potential energy surfaces for O^+–H–H angles of 60°, 90°, 120°, and 180°.

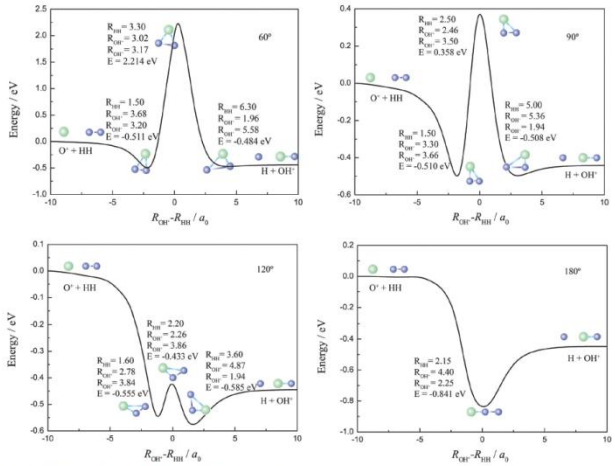

Fig. 3 Minimum energy paths for the new PES at four O^+–H–H angles.

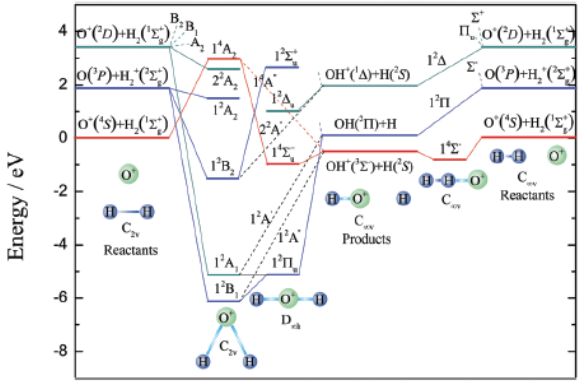

Fig. 1 Electronic correlation diagram for reactant, intermediate, and product arrangements of the H_2O^+ system under C_{2v}, $C_{\infty v}$, and $D_{\infty h}$ symmetries. The PESs of the title reaction are plotted by the red lines. This diagram is an adaptation of that reported in ref. 24.

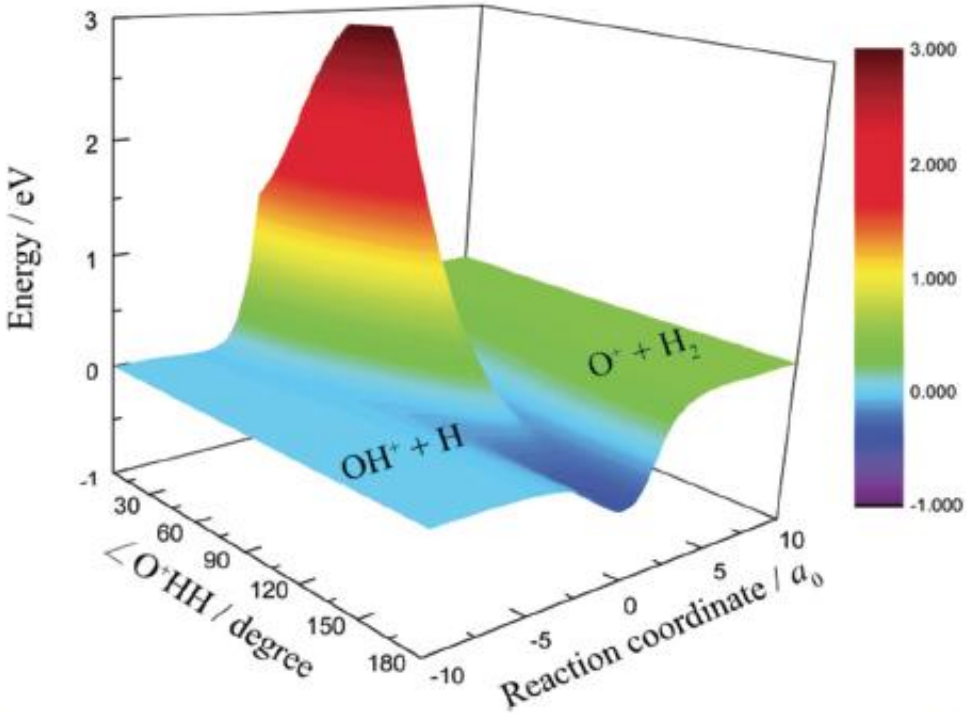

Fig. 4 Minimum energy paths of the new PES as a function of the bond–bond angle.

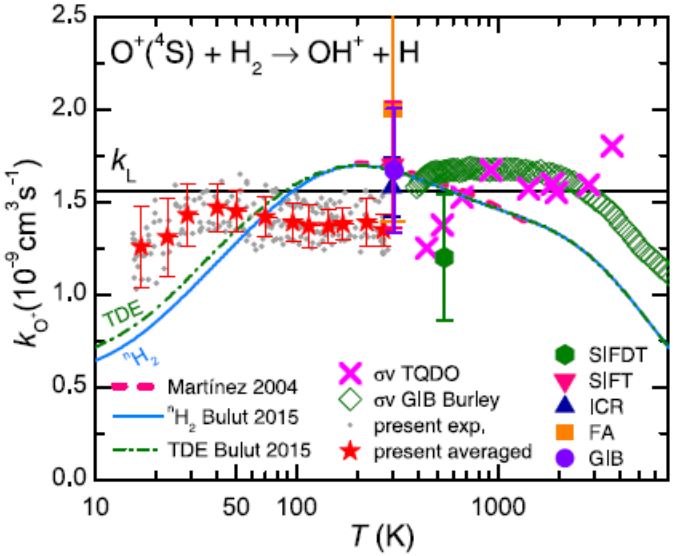

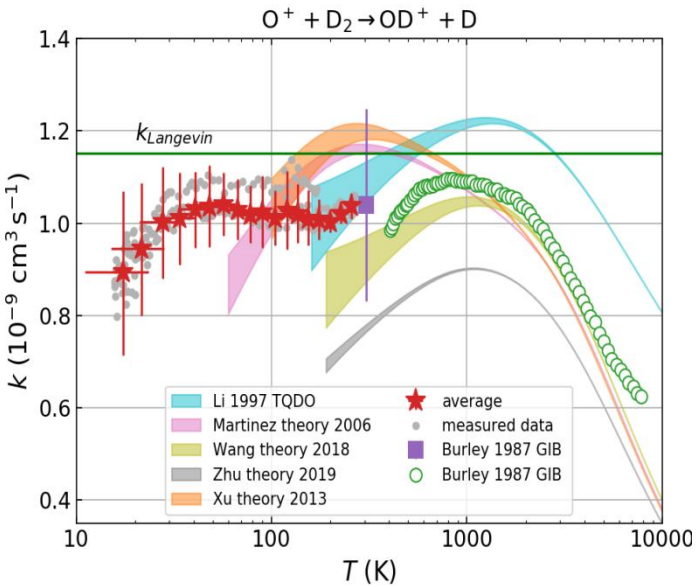

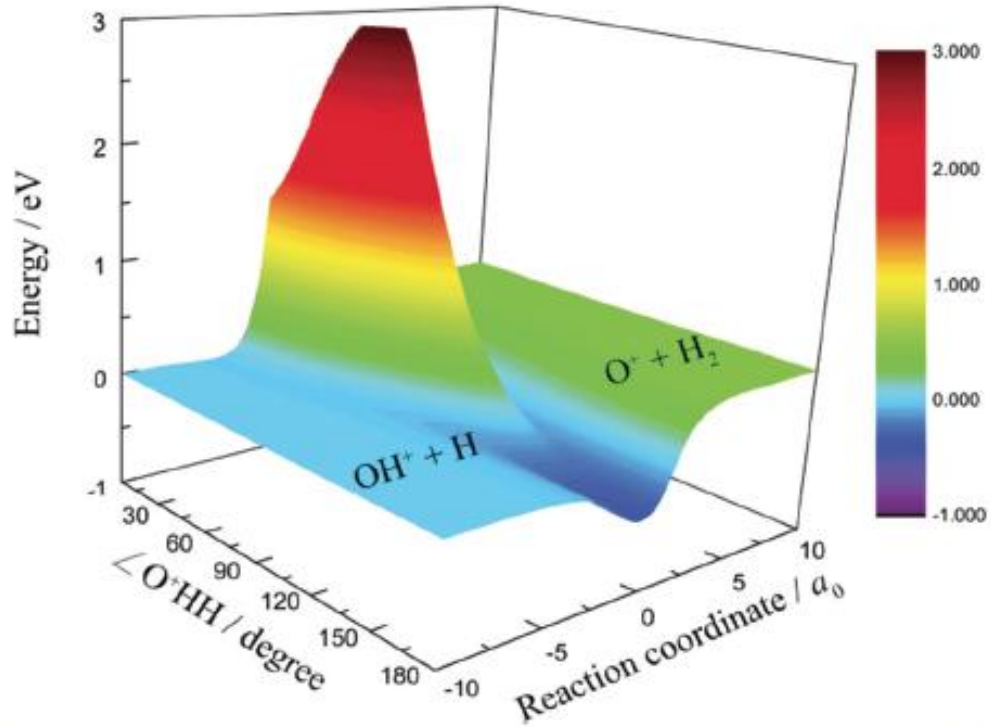

Fig. 4 Minimum energy paths of the new PES as a function of the bond–bond angle.

Oxygen evolution in interstellar medium

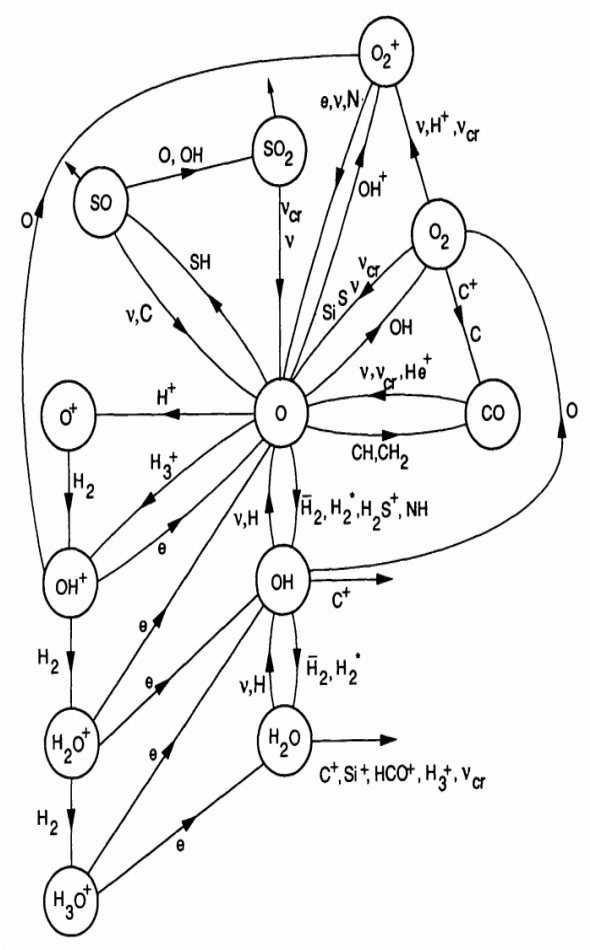

$$O^+ \xrightarrow{H_2} OH^+ \xrightarrow{H_2} H_2O^+ \xrightarrow{H_2} H_3O^+$$

$$O^+ + H_2 \rightarrow OH^+ + H \quad \Delta H_0 = -0.54 \text{ eV}$$

$$H_3O^+ + e \rightarrow H_2O + H$$

$O^+ + H_2$ reaction in 22 pole ion trap

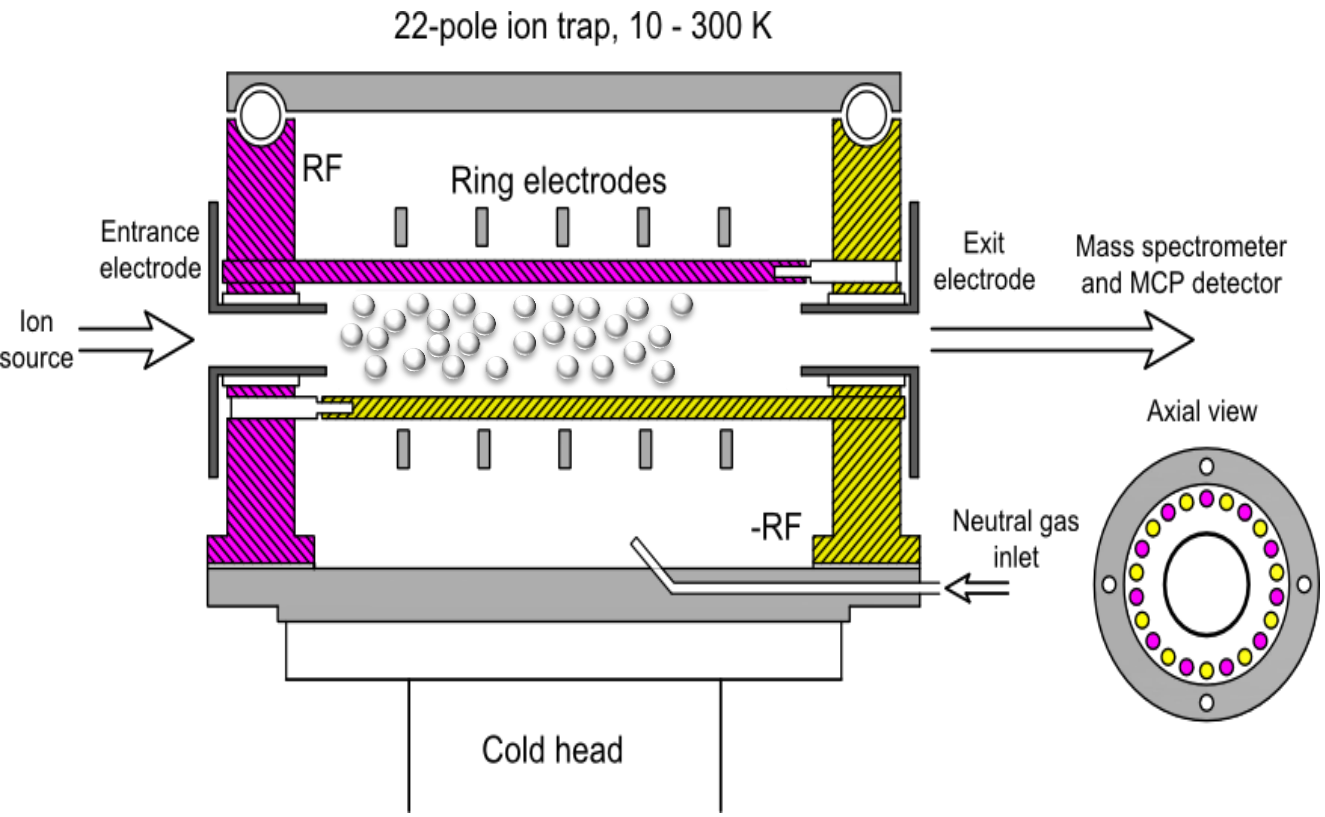

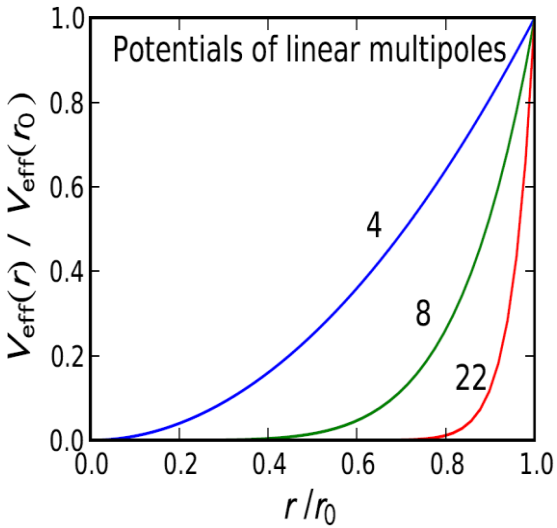

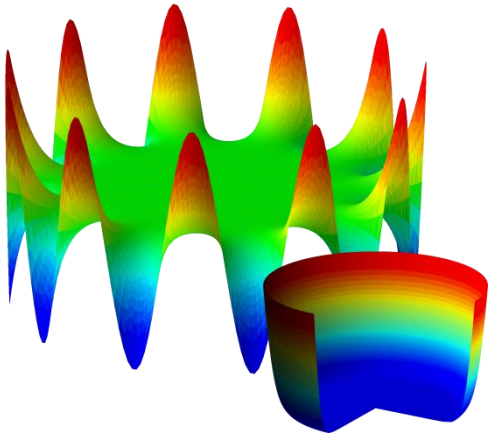

$O^+ + H_2$ reaction in 22 pole ion trap

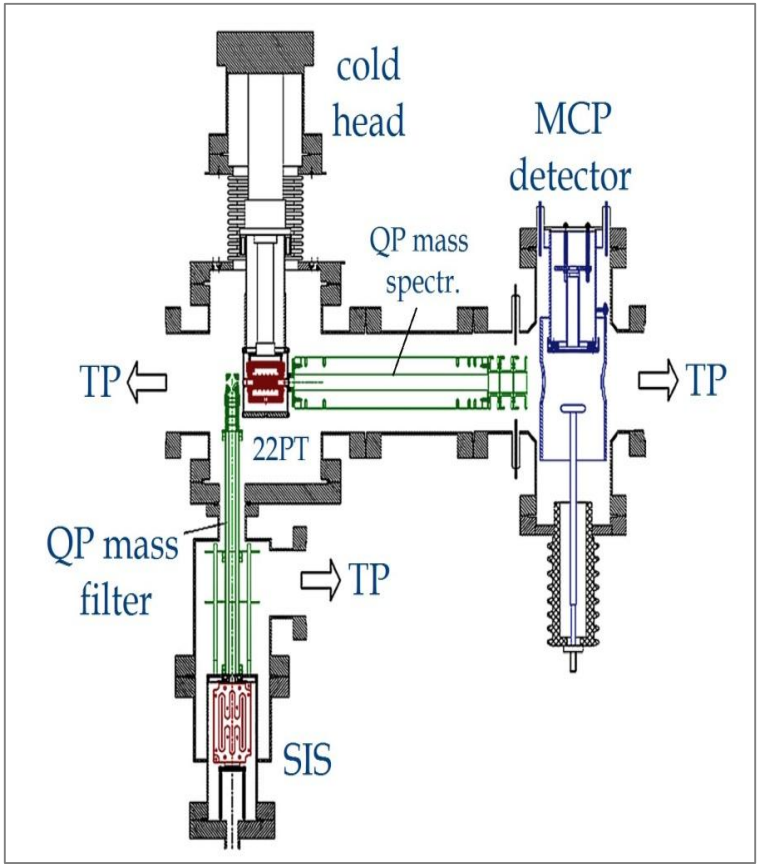

- Různé konfigurace pro různé experimenty
- Chladící hlavy na 22PT a zdroji H chladí až do 11 K a 7 K
- Ionty se produkují v iontovém zdroji
- QP hmotnostní filtr vpouští do pasti jen ionty, které vybereme
- QP hmotnostní spektrometr a detektor jednotlivých iontů

The Astrophysical Journal, 856:100 (6pp), 2018 April 1 https://doi.org/10.3847/1538-4357/aab106

2018

OH^+ Formation in the Low-temperature $O^+(^4S) + H_2$ Reaction

Artem Kovalenko, Thuy Dung Tran, Serhiy Rednyk, Štěpán Roučka, Petr Dohnal, Radek Plašil, Dieter Gerlich, and Juraj Glosík
Department of Surface and Plasma Science, Faculty of Mathematics and Physics, Charles University, Prague, Czech Republic; radek.plasil@mff.cuni.cz
Received 2017 December 18; revised 2018 February 7; accepted 2018 February 18; published 2018 March 28

$$O^+(^4S) + H_2 \xrightarrow{k_{O^+}} OH^+ + H; \quad \Delta H = -0.54\ \text{eV}.$$

The Astrophysical Journal, 854:25 (5pp), 2018 February 10 https://doi.org/10.3847/1538-4357/aaa0d8

2018

Formation of H_2O^+ and H_3O^+ Cations in Reactions of OH^+ and H_2O^+ with H_2: Experimental Studies of the Reaction Rate Coefficients from $T = 15$ to 300 K

Thuy Dung Tran, Serhiy Rednyk, Artem Kovalenko, Štěpán Roučka, Petr Dohnal, Radek Plašil, Dieter Gerlich, and Juraj Glosík
Department of Surface and Plasma Science, Faculty of Mathematics and Physics, Charles University, V Holešovičkách 2, Prague, 180 00, Czech Republic; stepan.roucka@mff.cuni.cz
Received 2017 October 24; revised 2017 December 8; accepted 2017 December 8; published 2018 February 7

$$OH^+ + H_2 \xrightarrow{k_{OH^+}} H_2O^+ + H, \quad \Delta H = -1.02\ \text{eV},$$

$$H_2O^+ + H_2 \xrightarrow{k_{H_2O^+}} H_3O^+ + H, \quad \Delta H = -1.7\ \text{eV},$$

$$H \xrightarrow{CR} H^+ \xrightarrow{O} O^+ \xrightarrow{H_2} OH^+ \xrightarrow{H_2} H_2O^+ \xrightarrow{H_2} H_3O^+.$$

$$H_2 \xrightarrow{CR} H_2^+ \xrightarrow{H_2} H_3^+ \xrightarrow{O} OH^+ \xrightarrow{H_2} H_2O^+ \xrightarrow{H_2} H_3O^+.$$

$O^+ + H_2$ time evolution of components

N_2O in source

Without mass filter

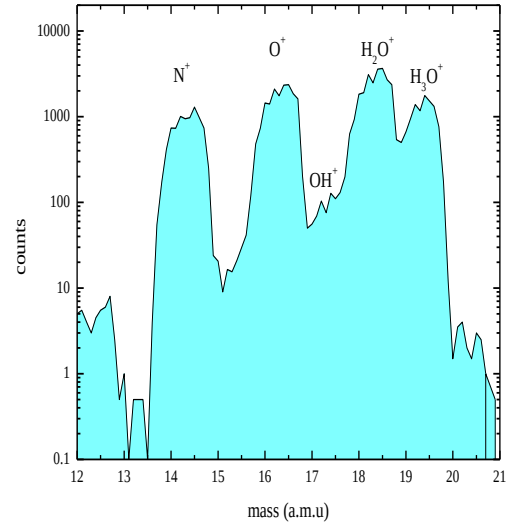

$$O^+ + H_2 \rightarrow OH^+ + H$$

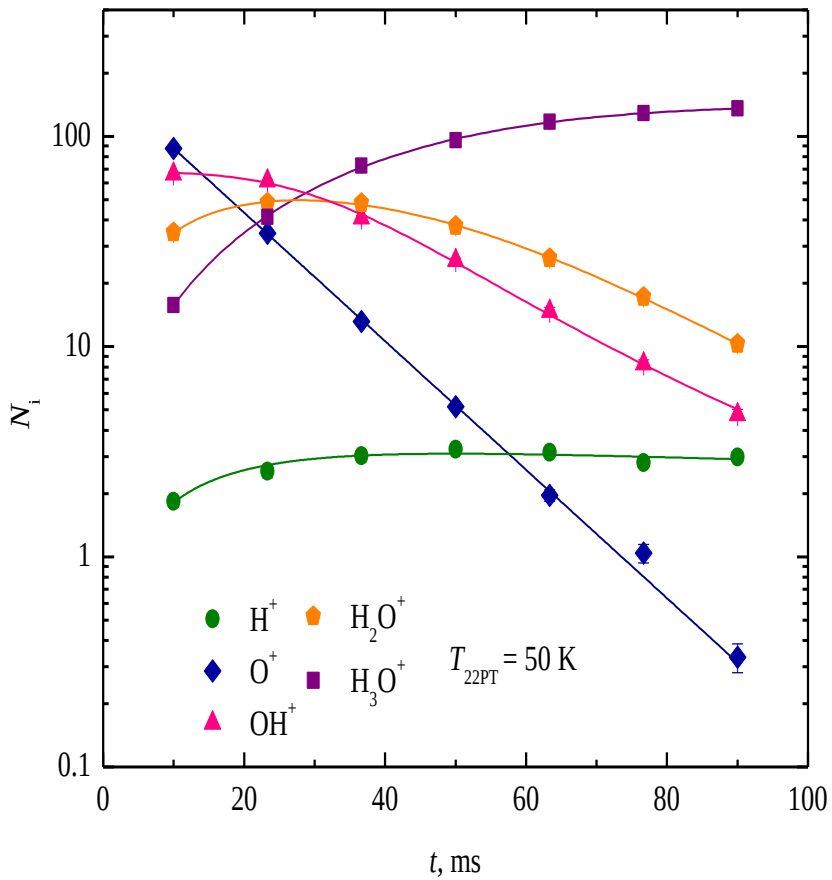

With mass filter

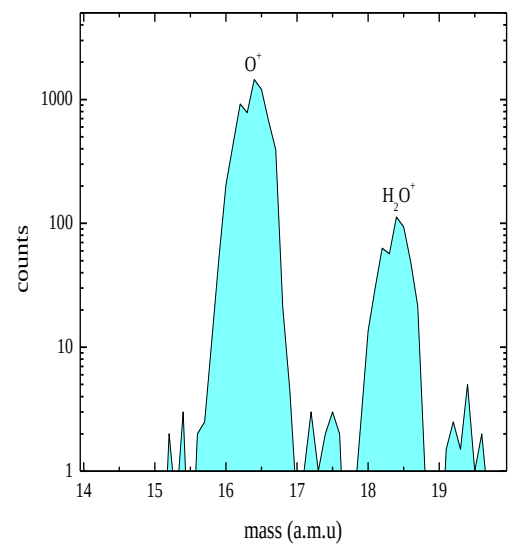

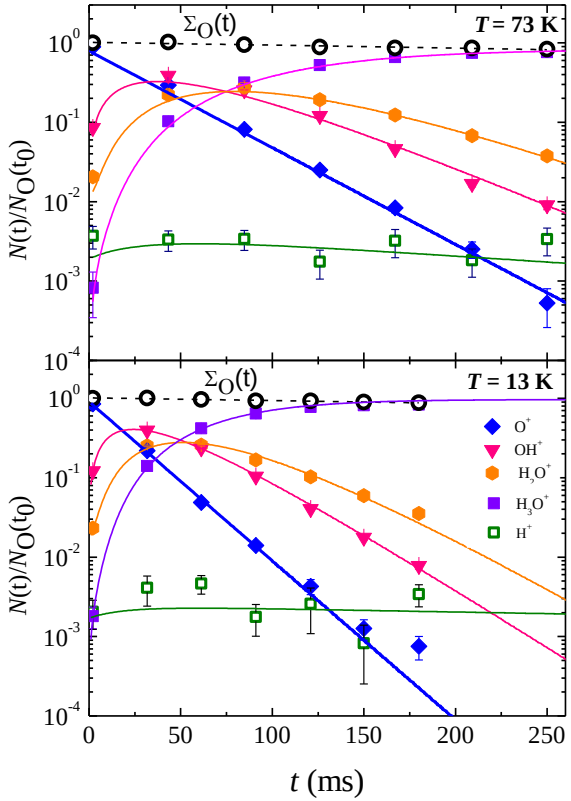
$\Sigma_O(t)$
T = 73 K
T = 13 K
$N(t)/N_O(t_0)$
O^+
OH^+
H_2O^+
H_3O^+
H^+
t (ms)

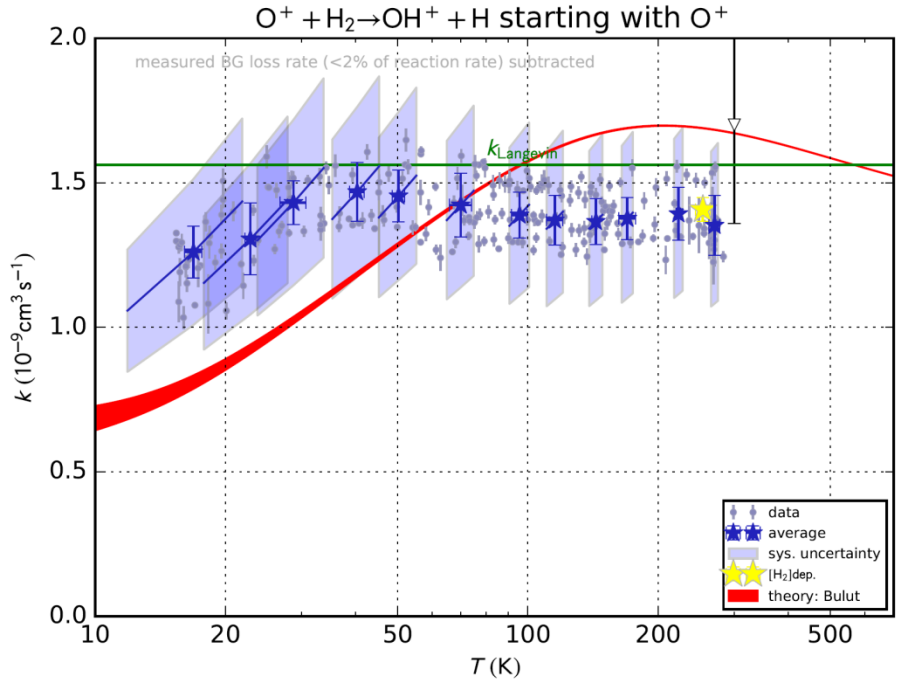
$O^+ + H_2 \rightarrow OH^+ + H$ starting with O^+
measured BG loss rate (<2% of reaction rate) subtracted
$k_{Langevin}$
$k\ (10^{-9} cm^3 s^{-1})$
T (K)
data
average
sys. uncertainty
$[H_2]$dep.
theory: Bulut

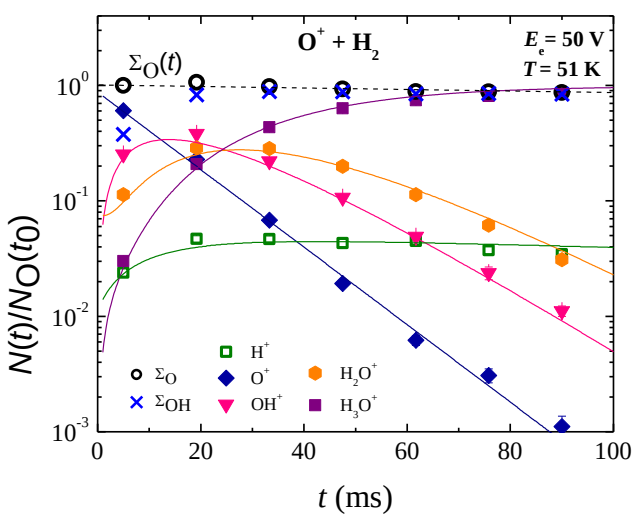
$O^+ + H_2$
E_e = 50 V
T = 51 K
$\Sigma_O(t)$
$N(t)/N_O(t_0)$
Σ_O
Σ_{OH}
H^+
O^+
OH^+
H_2O^+
H_3O^+
t (ms)

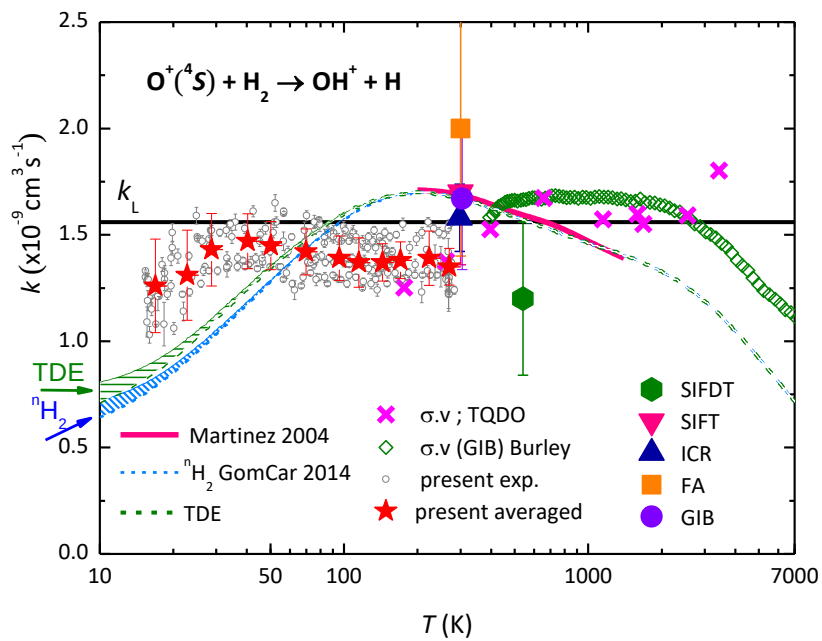
$O^+(^4S) + H_2 \rightarrow OH^+ + H$
k_L
TDE
$^nH_2$
$k\ (x10^{-9} cm^3 s^{-1})$
Martinez 2004
$^nH_2$ GomCar 2014
TDE
σ.v ; TQDO
σ.v (GIB) Burley
present exp.
present averaged
SIFDT
SIFT
ICR
FA
GIB
T (K)

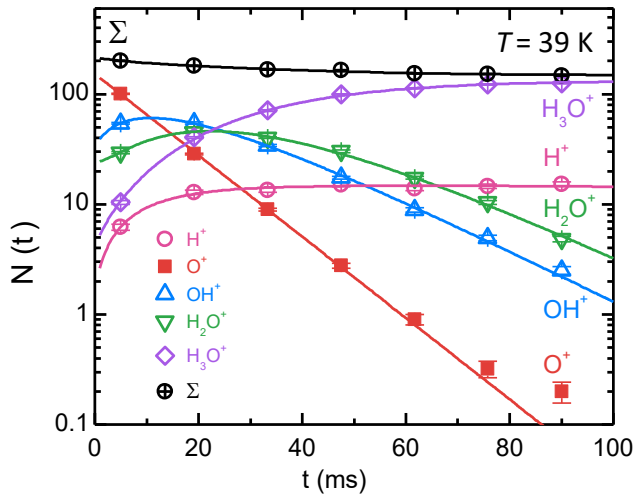
Σ
T = 39 K
H3O+
H+
H2O+
OH+
O+
N (t)
t (ms)
H+
O+
OH+
H2O+
H3O+
Σ

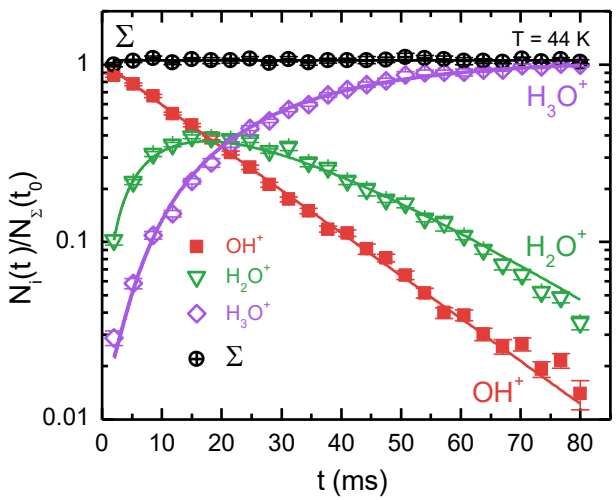
Σ
T = 44 K
H3O+
H2O+
OH+
Ni(t)/NΣ(t0)
t (ms)
OH+
H2O+
H3O+
Σ

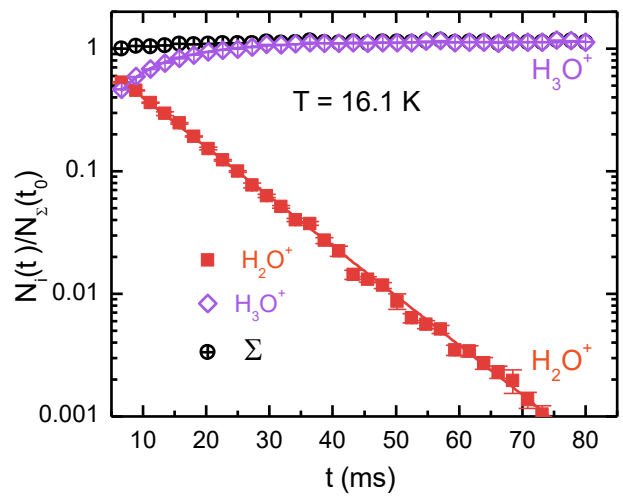
H3O+
T = 16.1 K
Ni(t)/NΣ(t0)
H2O+
H3O+
Σ
H2O+
t (ms)

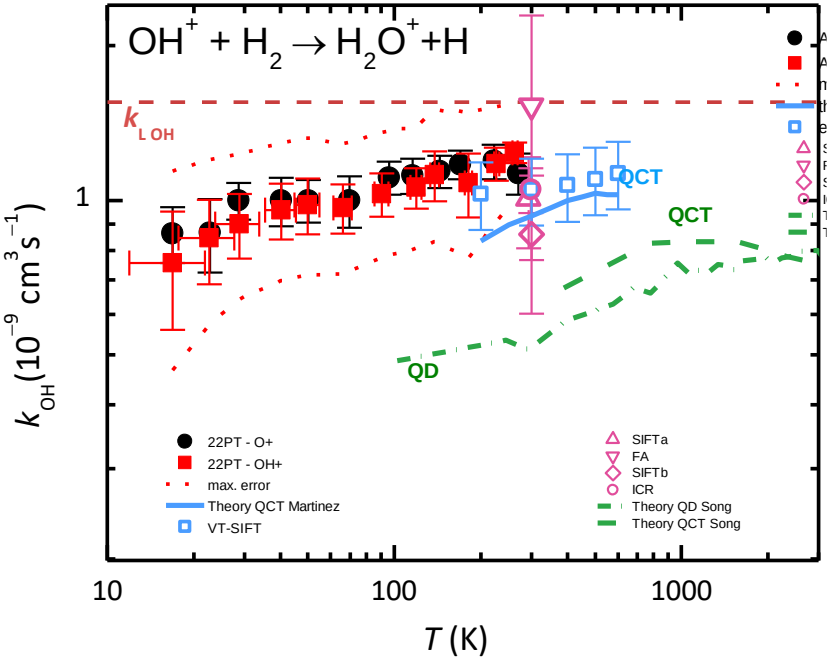
OH+ + H2 → H2O+ +H
k L OH
QCT
QCT
QD
22PT - O+
22PT - OH+
max. error
Theory QCT Martinez
VT-SIFT
SIFTa
FA
SIFTb
ICR
Theory QD Song
Theory QCT Song
k OH (10−9 cm3 s−1)
T (K)

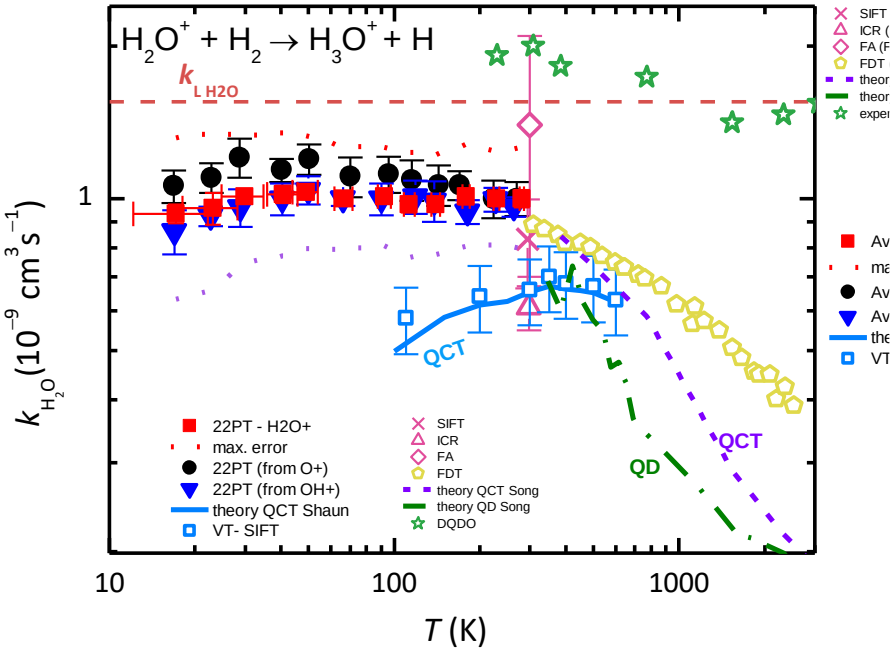
H2O+ + H2 → H3O+ + H
k L H2O
QCT
QCT
QD
22PT - H2O+
max. error
22PT (from O+)
22PT (from OH+)
theory QCT Shaun
VT- SIFT
SIFT
ICR
FA
FDT
theory QCT Song
theory QD Song
DQDO
k H2O (10−9 cm3 s−1)
T (K)

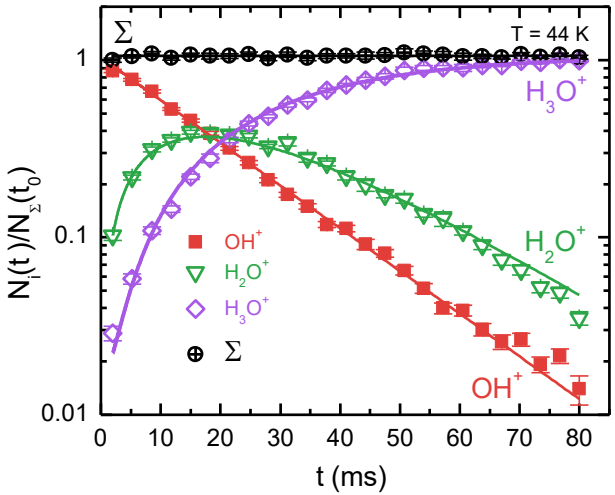
Σ
T = 44 K
H3O+
H2O+
OH+
OH+
H2O+
H3O+
Σ
Ni(t)/NΣ(t0)
t (ms)

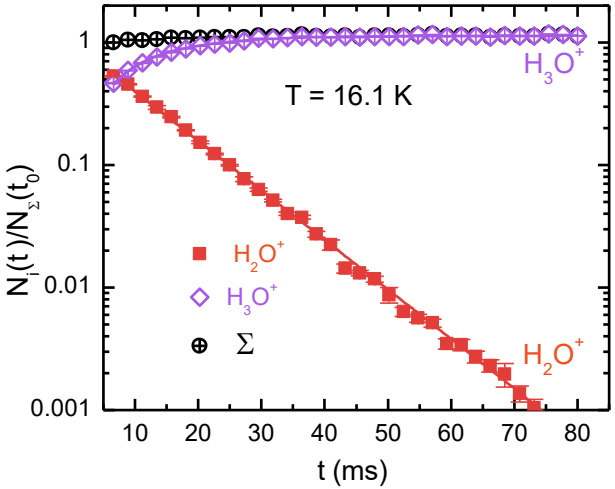
T = 16.1 K
H3O+
H2O+
H2O+
H3O+
Σ
Ni(t)/NΣ(t0)
t (ms)

2018

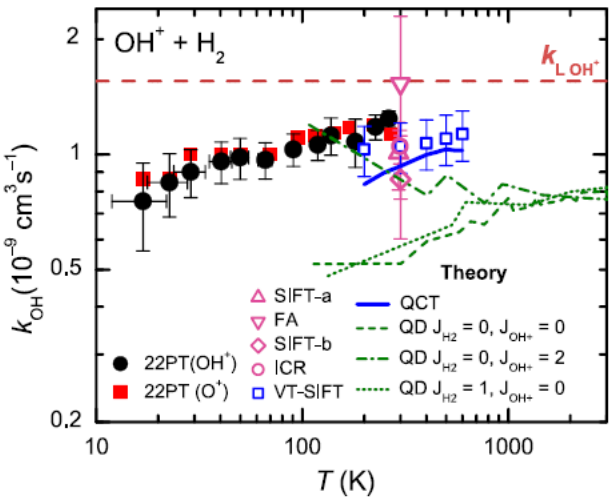

Figure 4. Temperature dependence of the rate coefficient k_{OH^+} of the reaction of OH^+ with normal hydrogen. The averaged data obtained in experiments with OH^+ and O^+ ions injected into the trap are indicated by full circles and squares, respectively. The systematic error due to pressure measurement is 20%. The dashed horizontal line ($k_{L\ OH^+}$) indicates the Langevin collisional rate coefficient. The previous results at 300 K are FA (Fehsenfeld et al. 1967), ICR (Kim et al. 1975), SIFT-a (Jones et al. 1981), and SIFT-b (Shul et al. 1988). The temperature dependencies of k_{OH^+} calculated (QCT) and measured (VT-SIFT) by Martinez et al. (2015) are indicated by the full line and open squares, respectively. The dashed, dotted, and dash-dotted lines represent the phenomenological rate coefficients ($v\sigma$) derived from the theoretical QD cross-sections (Song et al. 2016a) corresponding to different rotational states of reactants as indicated in the legend.

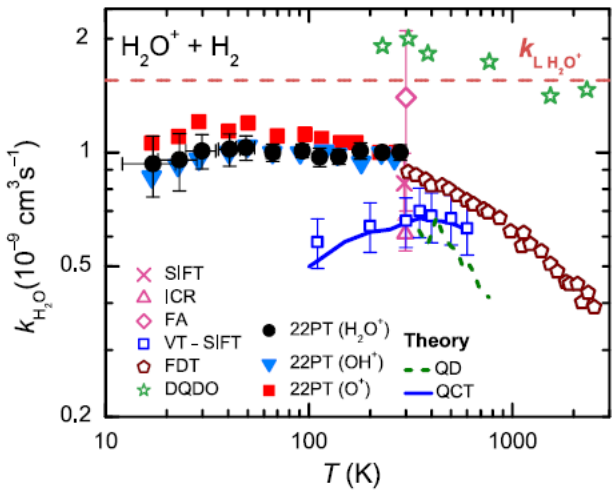

Figure 5. Temperature dependence of the reaction rate coefficient $k_{H_2O^+}$ of the reaction of H_2O^+ with normal hydrogen. The averaged data obtained in experiments with H_2O^+, OH^+, and O^+ ions injected into the trap are indicated by full circles, triangles, and squares, respectively. The systematic error due to pressure determination is 20%. The dashed horizontal line ($k_{L\ H_2O^+}$) indicates the Langevin collisional rate coefficient. The previous results at 300 K are FA (Fehsenfeld et al. 1967), ICR (Kim et al. 1975), FDT (Dotan et al. 1980), and SIFT (Jones et al. 1981). The values measured (VT-SIFT) and calculated (QCT) by Ard et al. (2014) are indicated by the open squares and by the full line (QCT), respectively. The dashed line and stars represent the phenomenological rate coefficients ($v\sigma$) derived from the theoretical QD, and experimental DQDO cross-sections (Song et al. 2016b). The uncertainty of the DQDO results is 50%.

Fig. 4

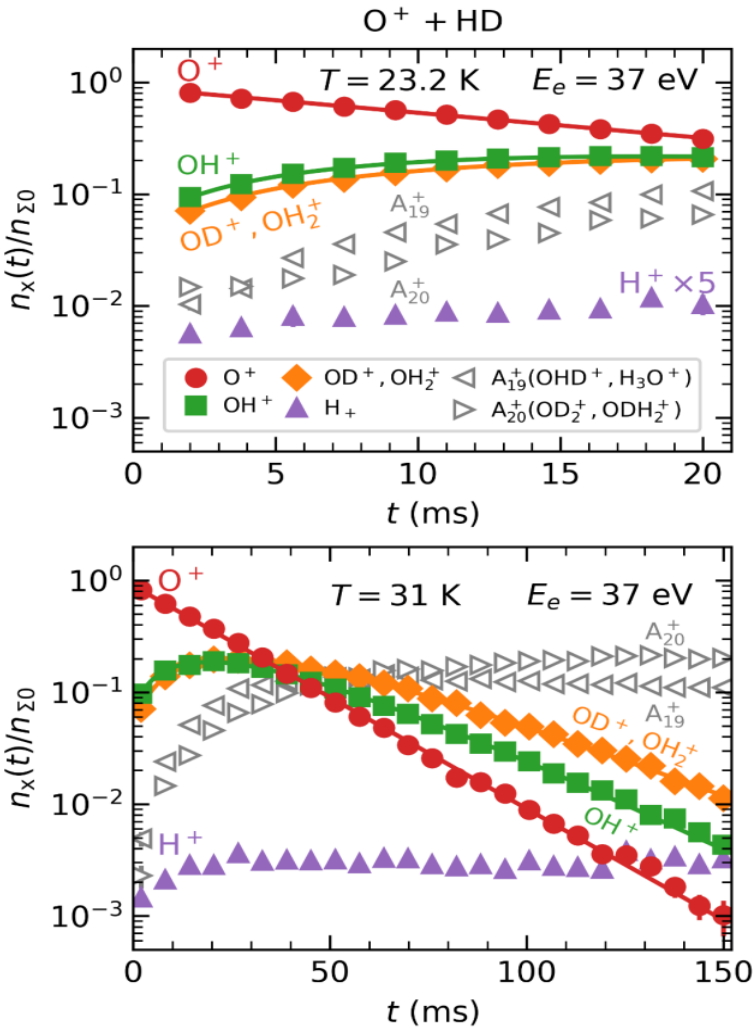
O⁺ + HD
T = 23.2 K
E_e = 37 eV
O⁺
OH⁺
OD⁺, OH₂⁺
A₁₉⁺
A₂₀⁺
H⁺ ×5
O⁺
OH⁺
OD⁺, OH₂⁺
H₊
A₁₉⁺(OHD⁺, H₃O⁺)
A₂₀⁺(OD₂⁺, ODH₂⁺)
n_x(t)/n_ΣO
t (ms)
T = 31 K
E_e = 37 eV
O⁺
A₂₀⁺
A₁₉⁺
OD⁺, OH₂⁺
OH⁺
H⁺
n_x(t)/n_ΣO
t (ms)

Fig. 5

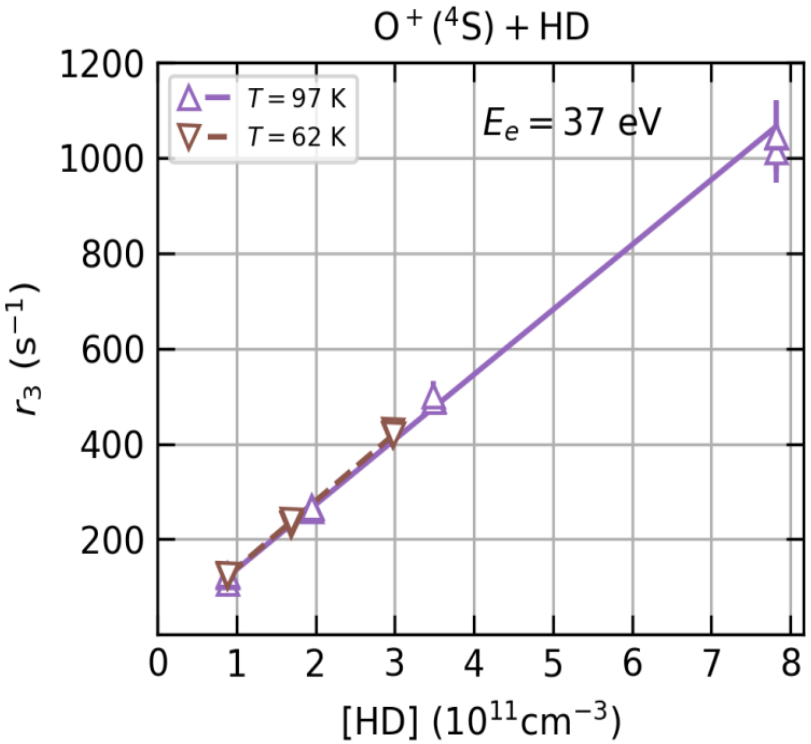
O+ (4S) + HD
T = 97 K
T = 62 K
Ee = 37 eV
r3 (s−1)
[HD] (1011cm−3)
1200
1000
800
600
400
200
0
1
2
3
4
5
6
7
8

Fig. 6

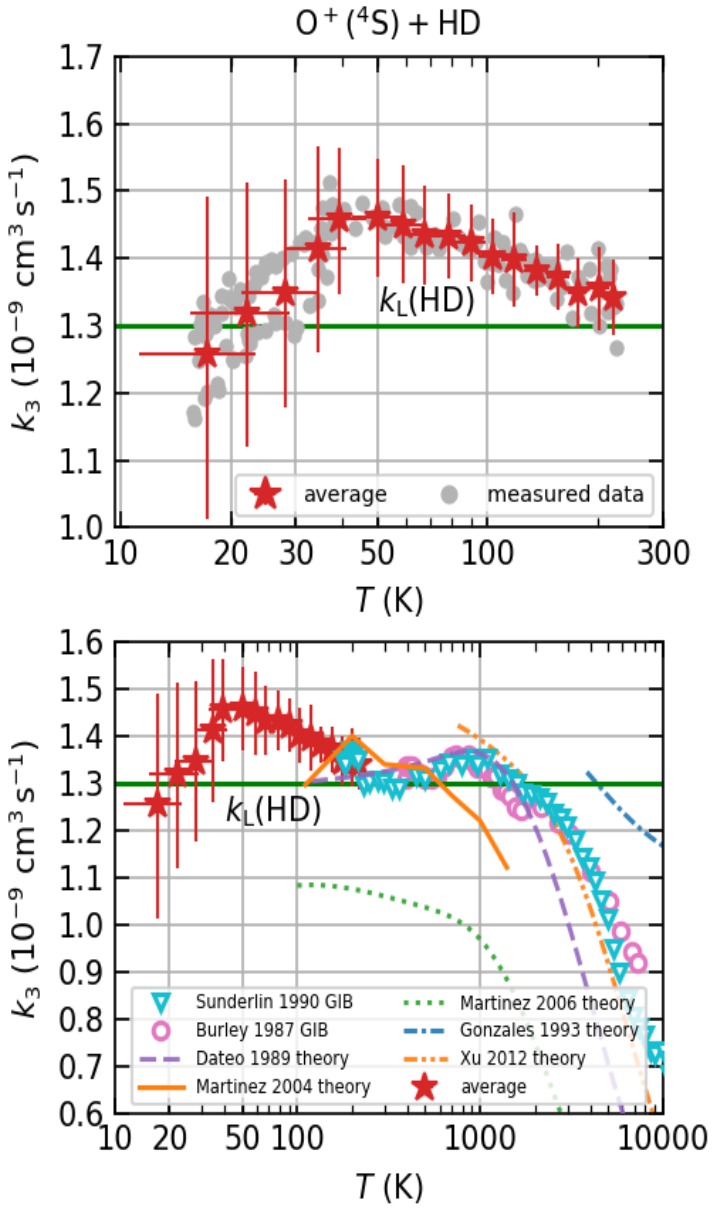
O+ (4S) + HD
k3 (10−9 cm3 s−1)
T (K)
kL(HD)
average
measured data
Sunderlin 1990 GIB
Burley 1987 GIB
Dateo 1989 theory
Martinez 2004 theory
Martinez 2006 theory
Gonzales 1993 theory
Xu 2012 theory
average

09. 10. 2019, correction for 3% H2

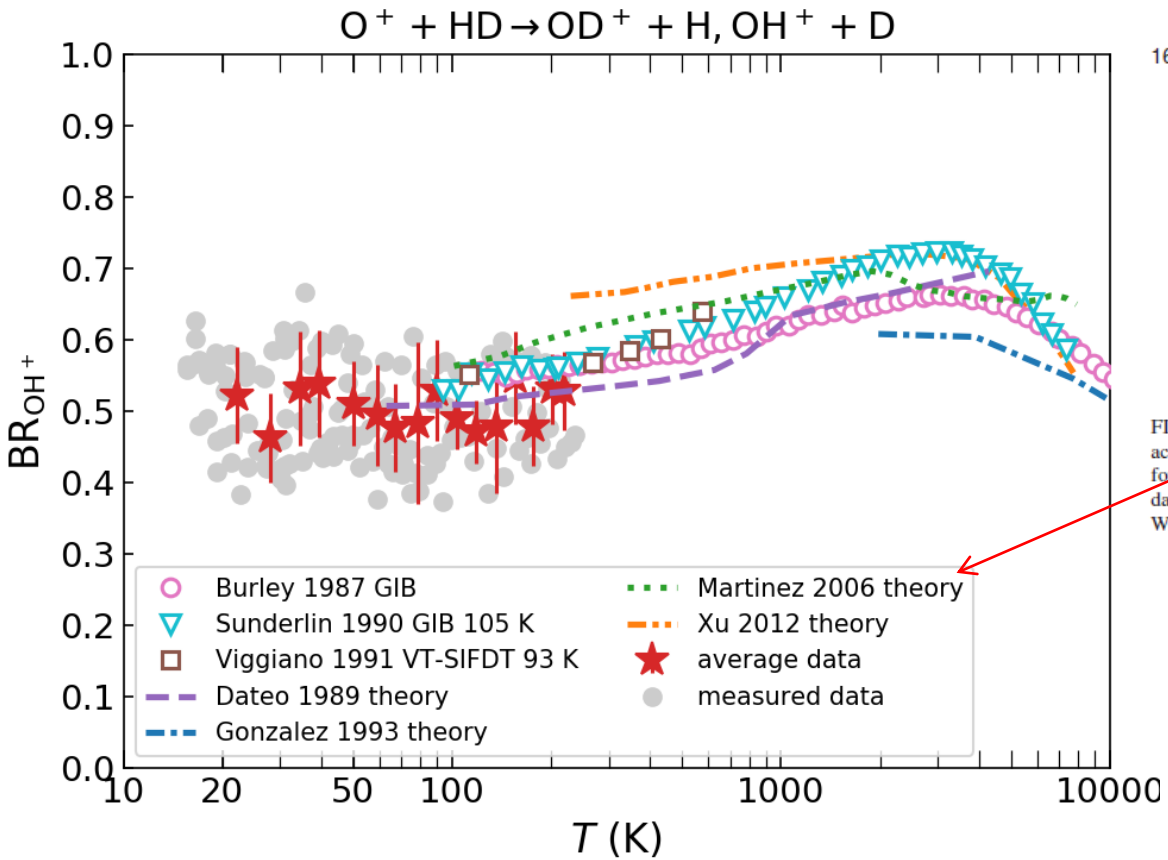

164305-5 The $O^+ + H_2(v=0, j=0) \rightarrow OH^+ + H$ ion-molecule reaction

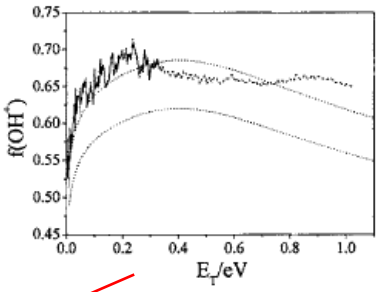

FIG. 5. HD-RWP intramolecular isotopic effect of $O^+ + HD(v=0, j=0)$ reaction expressed in terms of the $f(OH^+)$ fraction. The experimental results for reaction $O^+ + HD(300\ K)$ are also represented as the highest and lower data, considering a 5% experimental error (Ref. 10): (—) $WP_1(HD)$, (--) $WP_2(HD)$, and (···) Expt.

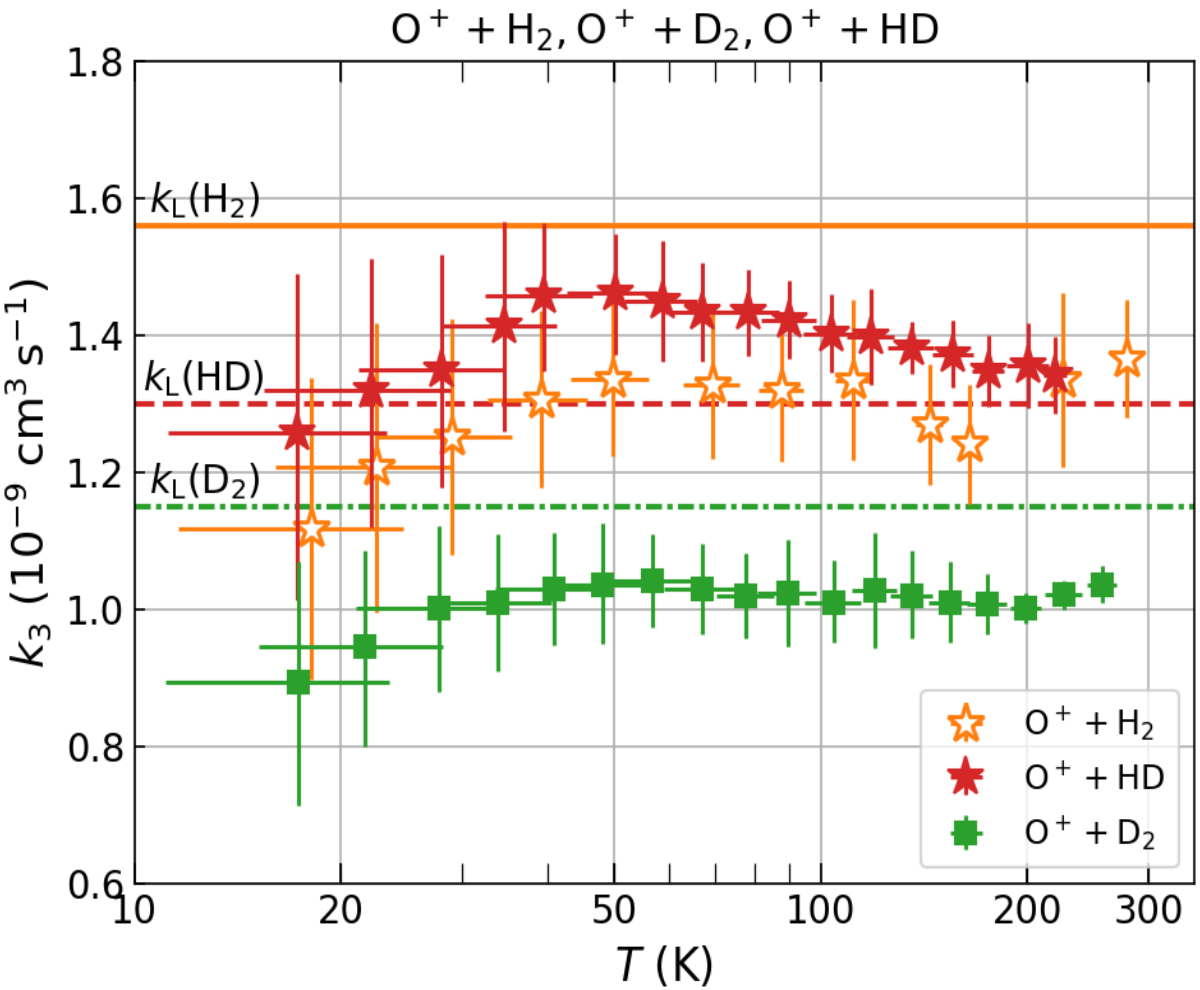
$O^+ + H_2, O^+ + D_2, O^+ + HD$
$k_L(H_2)$
$k_L(HD)$
$k_L(D_2)$
k_3 (10^{-9} cm^3 s^{-1})
T (K)
1.8
1.6
1.4
1.2
1.0
0.8
0.6
10
20
50
100
200
300
$O^+ + H_2$
$O^+ + HD$
$O^+ + D_2$

Binary reactions

$$A^+ + B \rightarrow C^+ + D$$

$$\frac{dA^+}{dt} = -k_{BIN} A^+ B$$

$$[k_{BIN}] = cm^3 s^{-1}$$

$$A^+ + B \rightarrow A_1^+ + C$$

$$\rightarrow A_2^+ + C$$

Reaction cannels

Branching ratio

Single collision

$$H_2^+ + Ar \quad \Rightarrow \quad ArH^+ + H$$

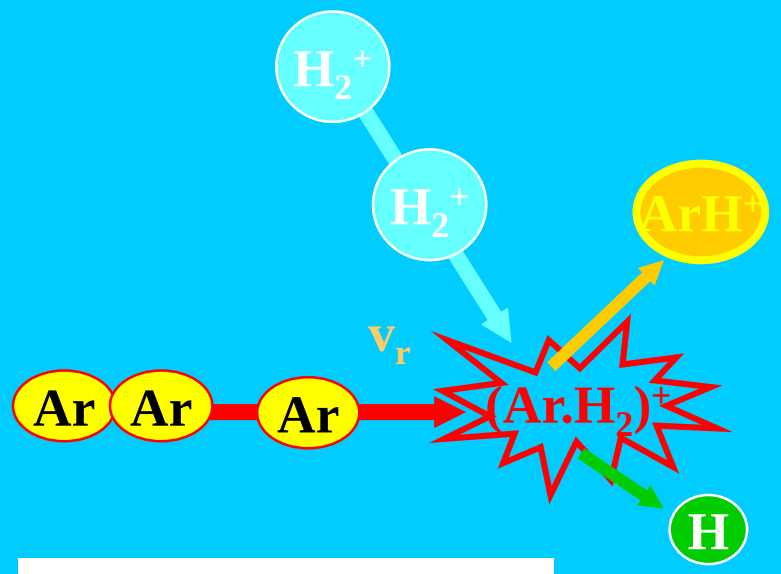

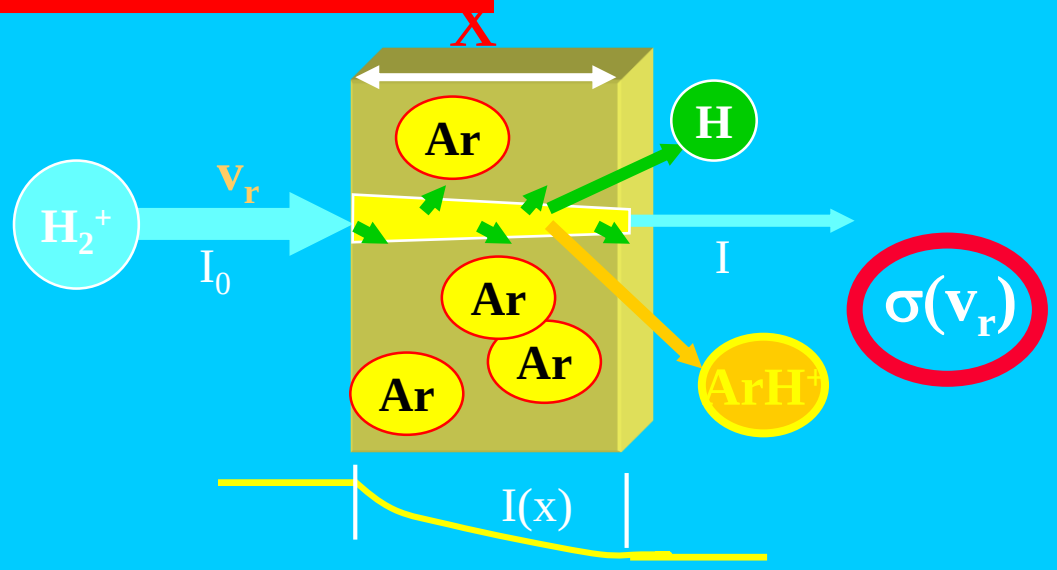

reaction cross section

$$\mathbf{I = I_0 \exp(-\sigma n_{Ar} x)}$$

Proportionality factor

$$\frac{dI}{dx} \sim -IN \qquad \frac{dI}{dx} = -\sigma IN$$

$$\frac{dI}{Idx} = \frac{d\ln(I)}{dx} = -\sigma N$$

$$I(x) = I_0 \exp(-\sigma N x)$$

Single collision

$$H_2^+ + Ar \Rightarrow ArH^+ + H$$

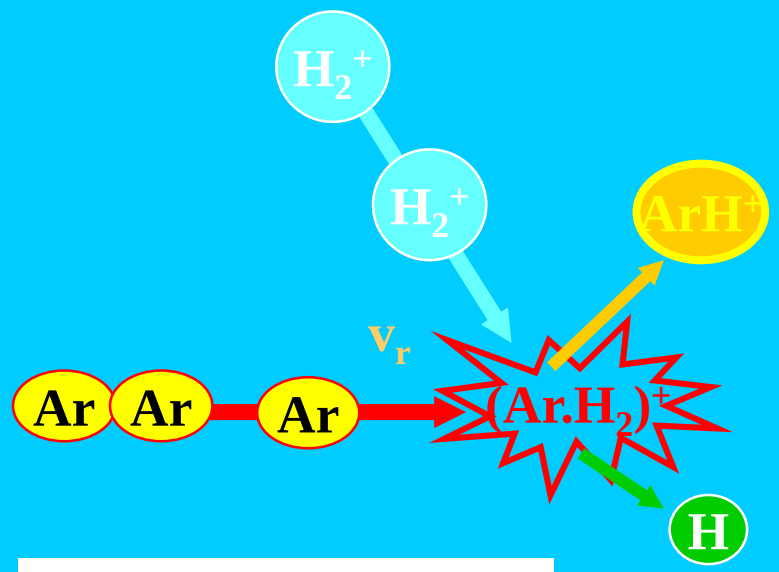

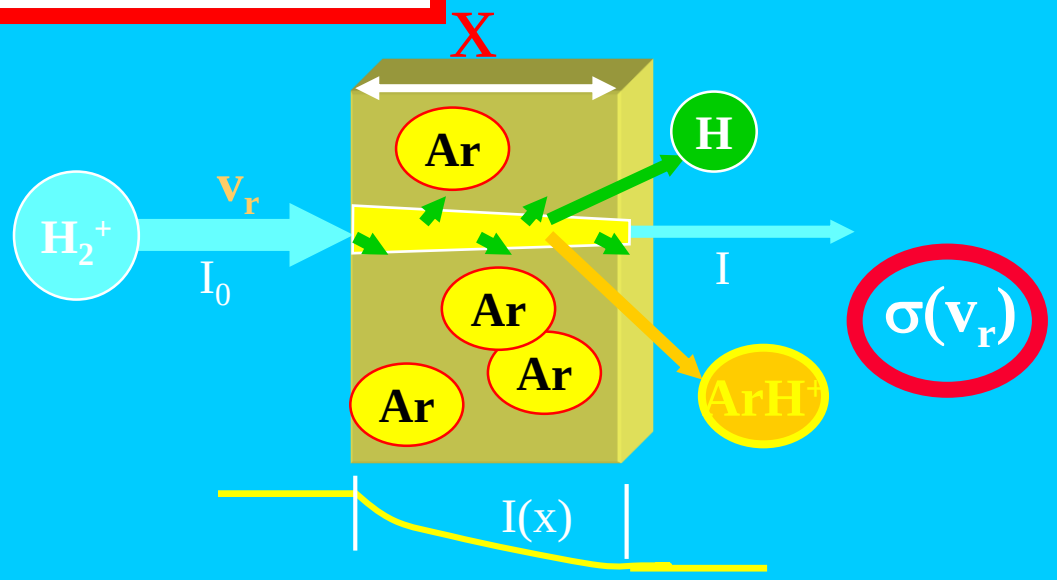

reaction cross section

$$I = I_0 \exp(-\sigma n_{Ar} x)$$

$$\nu_{coll} = nV_{rel} = n\nu S = n\nu\pi\delta^2 = n\nu\sigma$$

$$\nu_{coll} = n\nu\sigma$$

$$\frac{dI}{dt} = -\frac{I}{\tau_{coll}} = -I\nu_{coll}$$

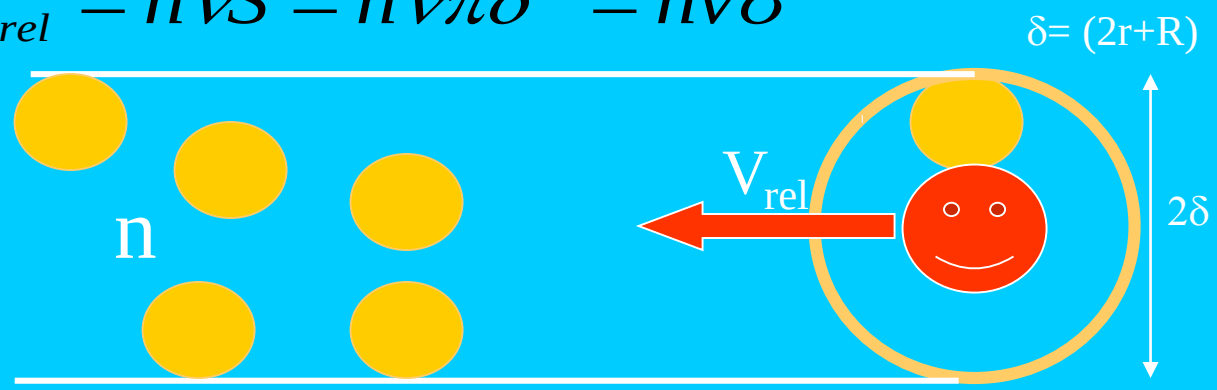

$$I(t) = I_0 \exp(-\nu_{coll} t) = I_0 \exp(-\sigma n \nu_{rel} t)$$

Simple picture of ion – molecule interaction

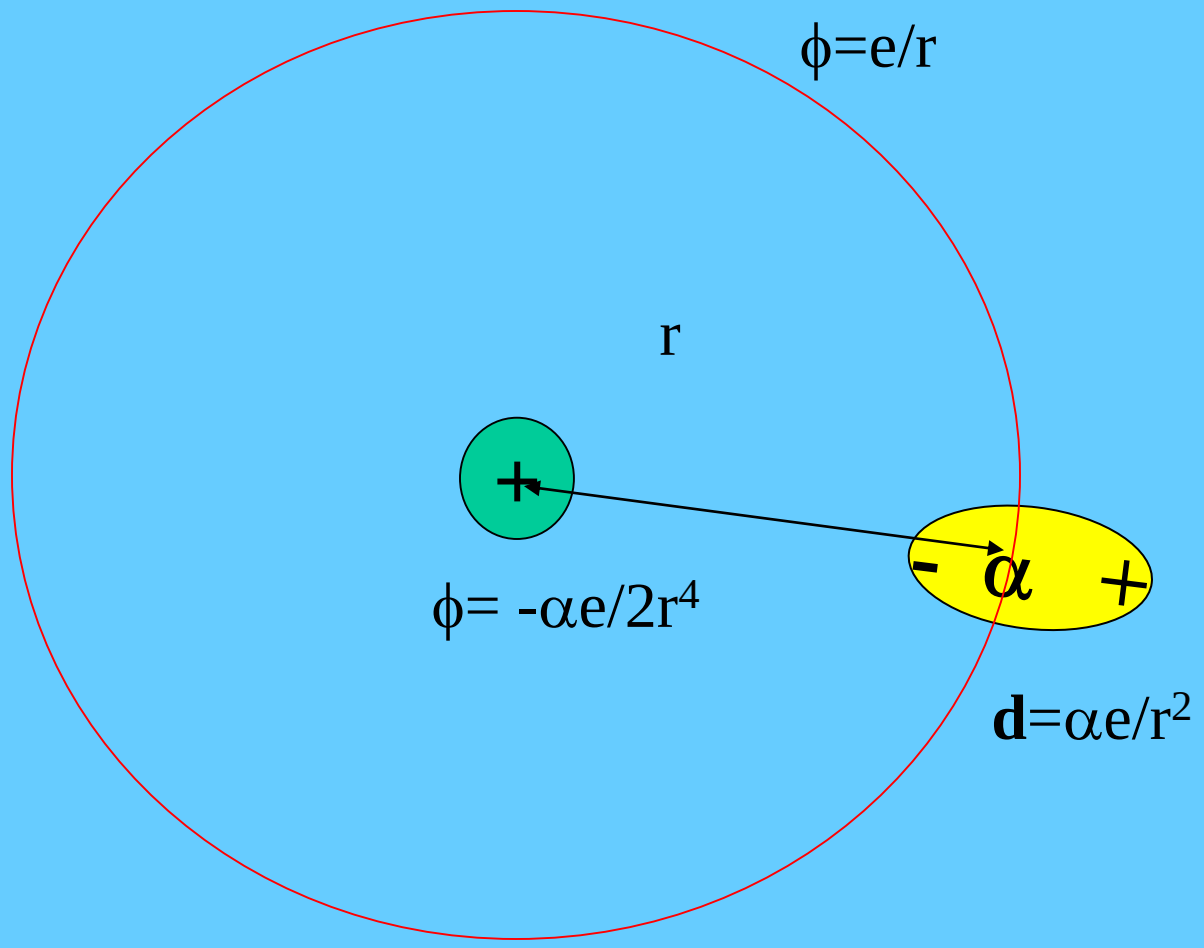

$E(ion) = 2d/r^3 = 2\alpha e/r^5$

α - polarisability

$F(ion) = 2\alpha e^2/r^5$

$U(pot) = -\alpha e^2/2r^4$

Two particles interaction

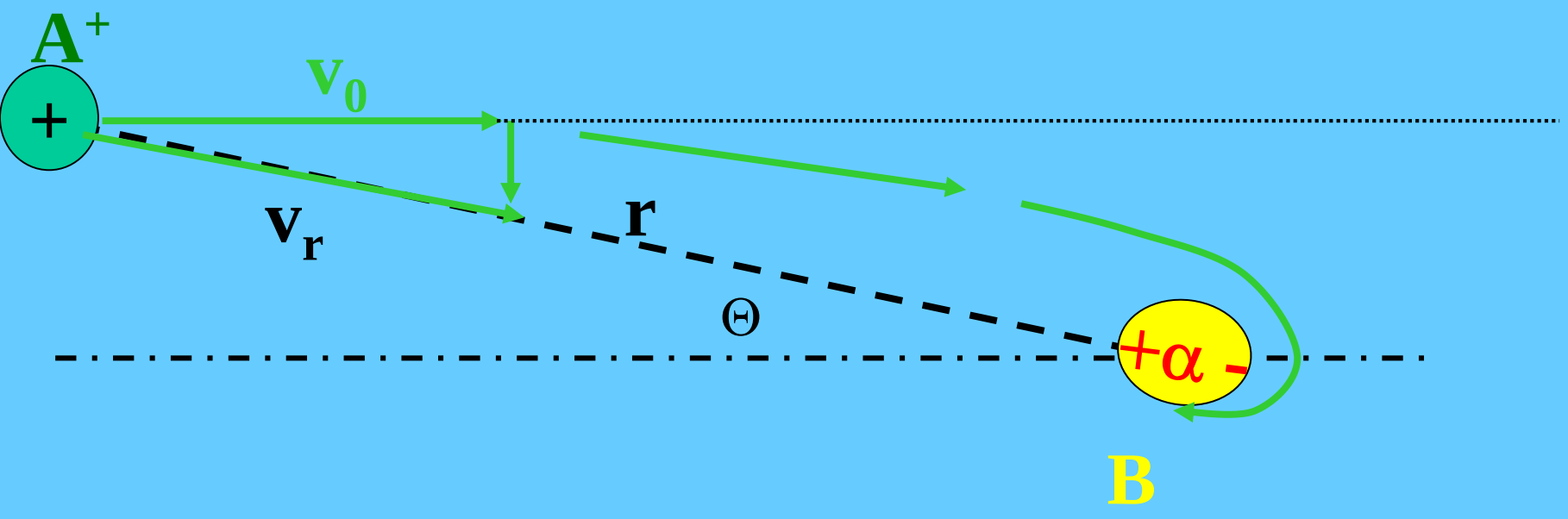

Simple picture

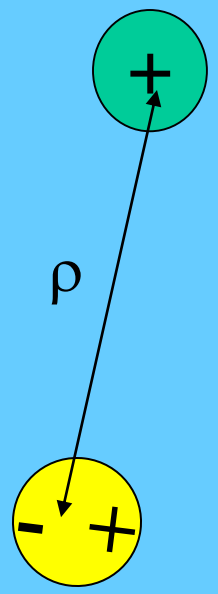

$F(\rho) \sim 2\alpha e^2/\rho^5$

$U(pot) = -\alpha e^2/2r^4$

$U(kin)=\mu v_0^2/2$

For U(pot) > U(kin) we have capture ➔

Capture is for $r<\rho$ where $U(\rho, pot) = U(\rho, kin)$

➔ $\mu v_0^2/2 = \alpha e^2/2\rho^4$

➔ $\sigma \sim \pi\rho^2 = \{\pi^2\alpha e^2/2\,(\mu v_0^2/2)\}^{1/2}$

➔ $\sigma \sim \pi e/v_0\,\{\alpha/\mu\}^{1/2}$

Using SI units: $$\sigma_0 = \pi\rho_0^2 = \frac{2\pi e}{v_0(4\pi\varepsilon_0)}\sqrt{\frac{\alpha}{\mu}}$$

Ion induced dipole interaction

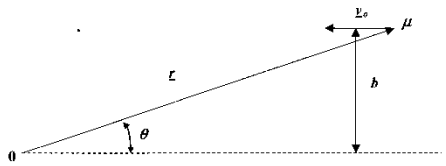

Figure 1
The coordinates for an ion–molecule collision in the scattering center system. The vector **r** with polar coordinate r and θ indicates the position of a particle of reduced mass μ relative to the stationary scattering center at the origin. The vector $\mathbf{v}_o$ indicates the initial relative velocity and b the impact parameter.

$$E = (1/2)\mu v_0^2$$

$$E = (1/2)\mu(\dot{r}^2 + r^2\dot{\theta}^2) + V(r)$$

$$L = \mu v_0 b = \mu r^2 \dot{\theta}$$

$$E = (1/2)\mu\dot{r}^2 + (1/2)\mu r^2\dot{\theta}^2 + V(r)$$

$$U(r) = (1/2)\mu r^2\dot{\theta}^2 + V(r)$$

$$U(r) = \frac{Eb^2}{r^2} + V(r)$$

$$E = (1/2)\mu\dot{r}^2 + U(r)$$

metastabile orbit

$$(1/2)\mu\dot{r}^2 = 0 \quad \Rightarrow E = U(r_0)$$

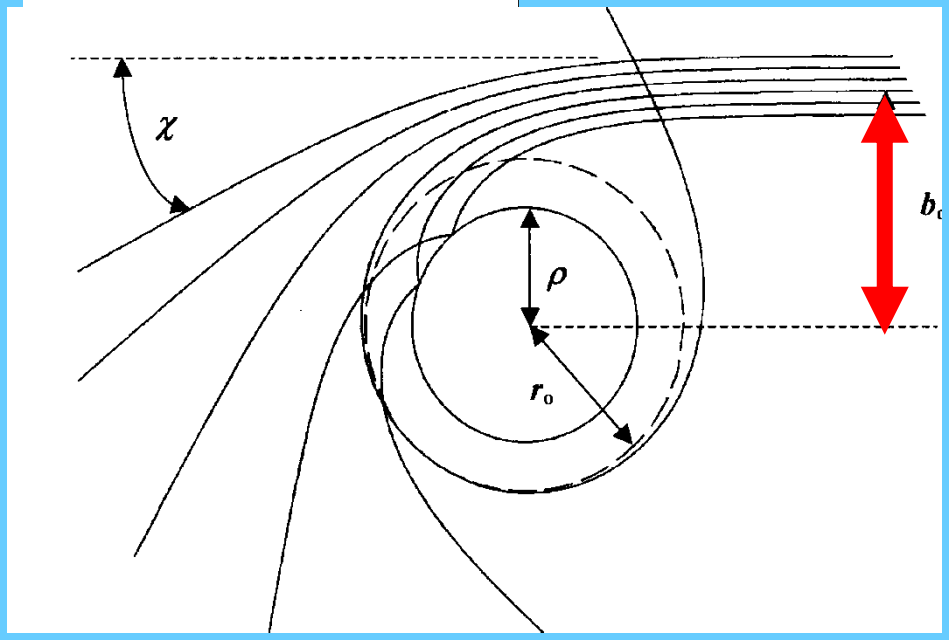

Figure 2
Trajectories for ion–induced dipole collisions in the scattering center system calculated from Eqn. (7) with b/b_o equal to 1.1500, 1.1000, 1.0500, 1.0001, 1.0000, 0.9500, and 0.9000 corresponding to deflection angles χ equal to −28.6°, −40.2°, −61.2°, −299.9°, −infinity (dashed circle), −139.4°, and −80.1°, respectively. A hard sphere of radius ρ represents the structure of the ion–molecule pair.

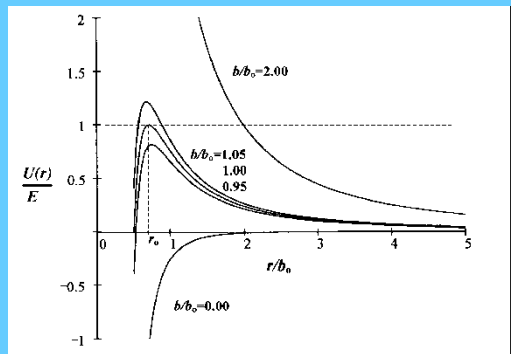

Figure 3
Plots of the effective potential *vs.* r from Eqn. (9). For a fixed energy the plots represent the indicated impact parameters b. Turning points occur where the horizontal dashed line intersects a $U(r)$ plot. A metastable circular orbit of radius r_o (Eqn. (12)) occurs when b equals b_o (Eqn. (13)).

For ion induced dipole force

$$r_0 = \left(\frac{\alpha e^2}{(4\pi\varepsilon_0)^2 \mu v_0^2}\right)^{1/4}$$

$$b_0 = \sqrt{2} r_0$$

$$\sigma_0 = \pi b_0^2 = \frac{2\pi e}{v_0 (4\pi\varepsilon_0)} \sqrt{\frac{\alpha}{\mu}}$$

Collisional rate coefficient

$$\sigma_0 = \pi\rho_0^2 = \frac{2\pi e}{v_0(4\pi\varepsilon_0)}\sqrt{\frac{\alpha}{\mu}} \sim \frac{1}{v_0}\sqrt{\frac{\alpha}{\mu}}$$

Exothermic reaction

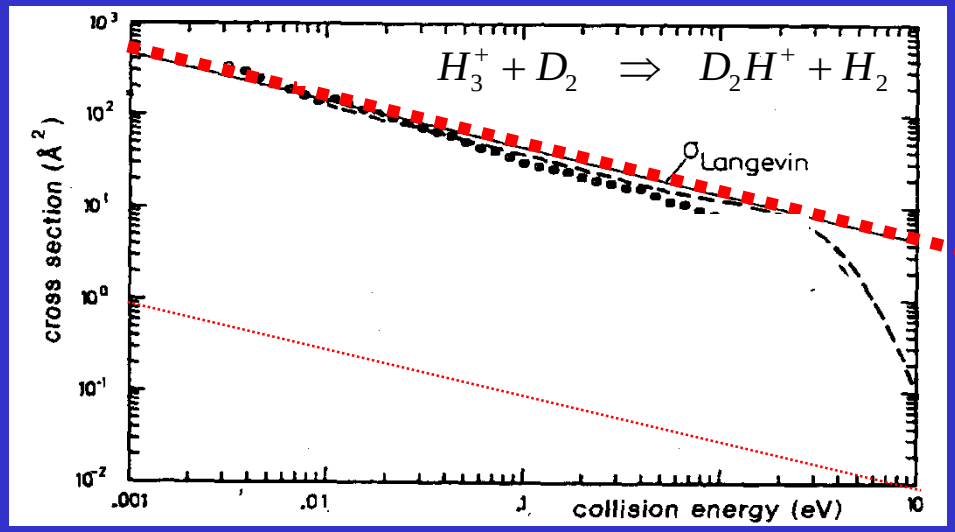

$$\sigma_{collisional} \sim \frac{1}{v_0}$$

k(T)=<vσ> → $k = \int_{Max(T)} v\sigma(v)dv = k(T)$

k(T) reaction rate coefficient

k_{coll}(T) collision rate coefficient

k_{coll}(T) ~ collision frequency

Collision rate coefficient

$$\sigma_0 = \pi\rho_0^2 = \frac{2\pi e}{v_0(4\pi\varepsilon_0)}\sqrt{\frac{\alpha}{\mu}} \sim \frac{1}{v_0}\sqrt{\frac{\alpha}{\mu}}$$

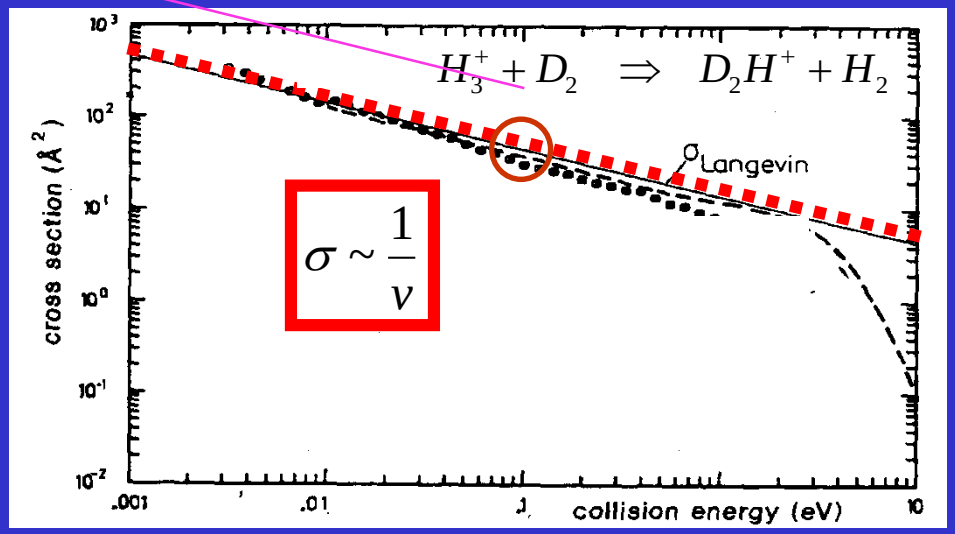

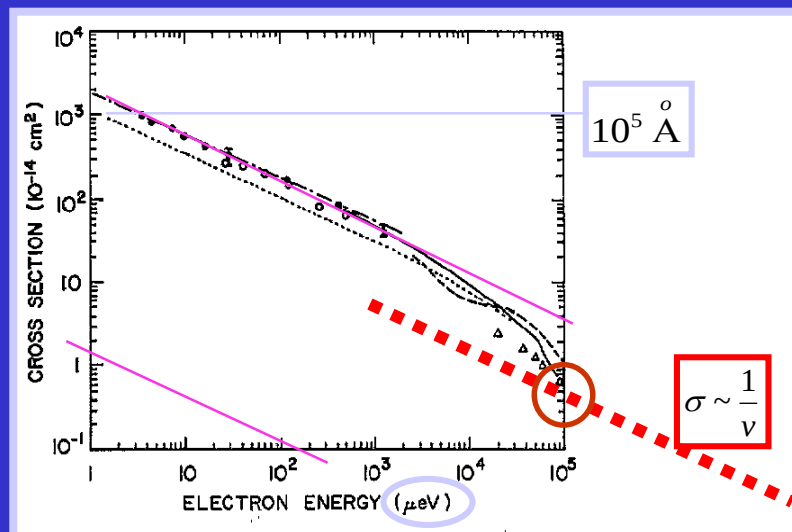

Figure 3. Cross sections for electron attachment to CCl_4. ●, $\bar{\sigma}_e$-K(np); —·—, $\sigma_e(v)$-K(np) (Frey *et al* 1994b); ○, $\bar{\sigma}_e$-K(np) (Ling *et al* 1992); ——, free electrons (Hotop 1994); - - -, free electrons (Orient *et al* 1989); △, free electrons (Christodoulides and Christophorou (1971); -----, theory (Kłots 1976).

k(T)=<vσ> → $k = \int_{Max(T)} v\sigma(v)dv = k(T)$

k(T) reaction rate coefficient

k_{coll}(T) collision rate coefficient

k_{coll}(T)~collision frequency

Collision rate coefficient -Langevin rate coefficient

$$\sigma_0 = \pi\rho_0^2 = \frac{2\pi e}{v_0(4\pi\varepsilon_0)}\sqrt{\frac{\alpha}{\mu}}$$

$$\sigma_{coll} = \sigma_L = const\,\frac{1}{v}\sqrt{\frac{\alpha}{\mu}} \sim \sigma_0\frac{v_0}{v}\,cm^2$$

$$k_{coll}(T) = <\sigma v> \sim <\sigma_0\frac{v_0}{v}v> \sim const$$

$$k_{coll} = k_{coll} = const\sqrt{\frac{\alpha}{\mu}} \sim 3.34x10^{-9}\sqrt{\frac{\alpha}{\mu}}\,cm^3 s^{-1};$$

α in Debye

μ in atomic units

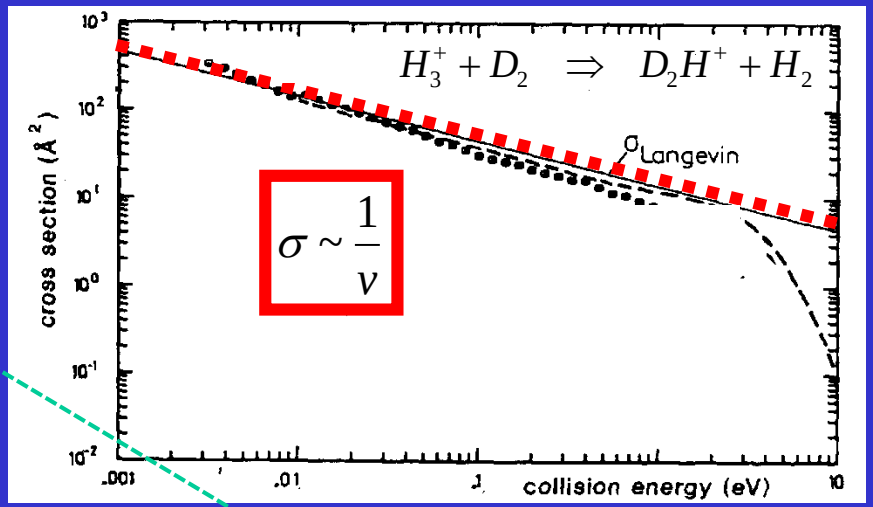

	α
H	~0.666793
He	~0.204956
Li	~24.3
C	~1.76
Ar	~1.64
CO	~1.95
H_2	~0.8
C_2H_4	~4.5

$k_L \sim 10^{-9} cm^3 s^{-1}$

Ind. dipole d=$\alpha e/r^2$ → $[\alpha]=[dr^2/e]=[err^2/e]=[r^3]$

$\alpha \sim dr^2/e$ → if $r \sim A$ and $d \sim eA$ → $\alpha \sim A^3$

Cross section of IMR

$$H_3^+ + D_2 \rightarrow D_2H^+ + H_2$$

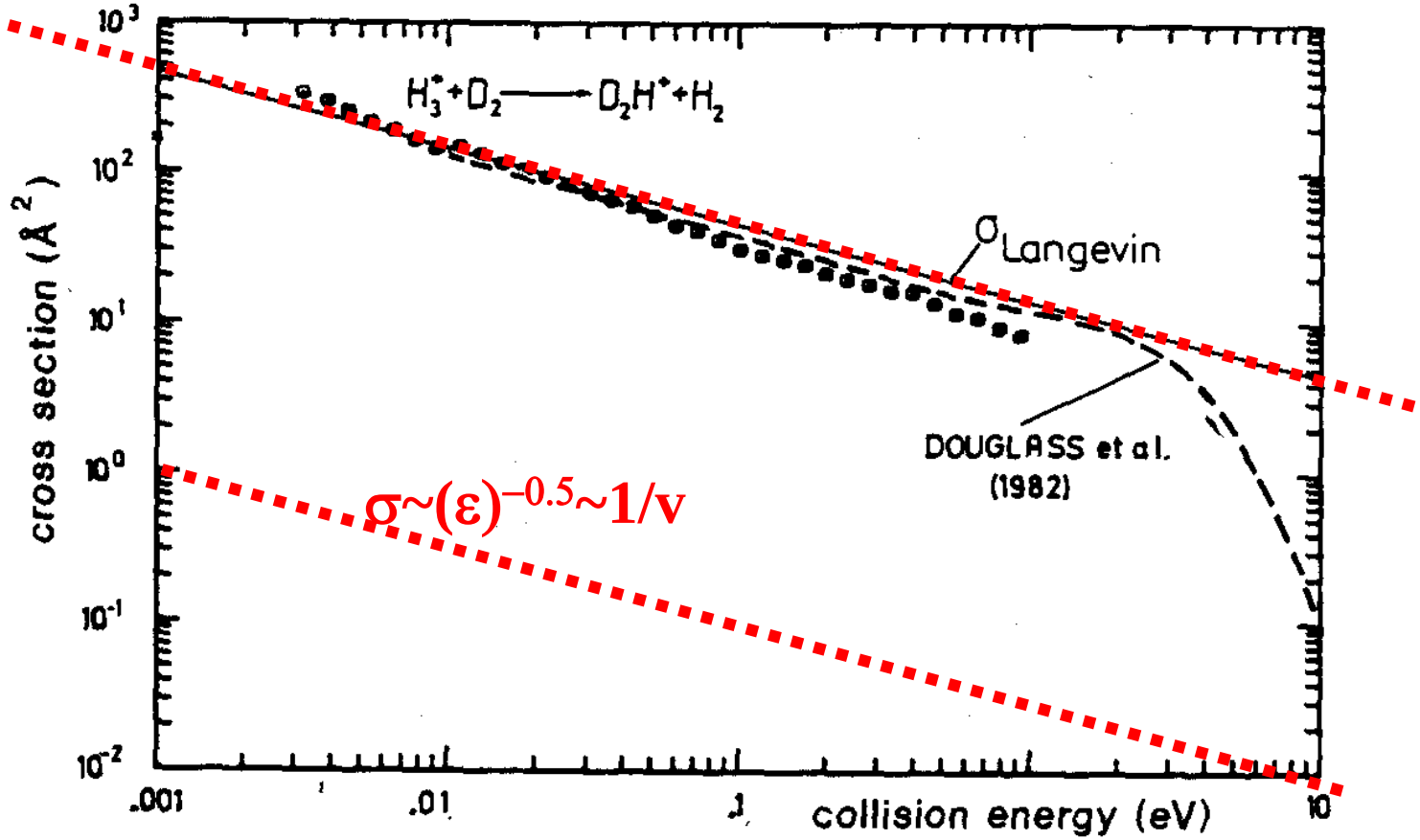

Figure 55. Comparison of the cross section for the proton transfer reaction $H_3^+ + D_2 \rightarrow D_2H^+ + H_2$ obtained with a conventional (dashed line) (Dougless et al., 1982) and our new slow merged beam apparatus (●).

$$\sigma_{coll} = \sigma_L = const \frac{1}{v}\sqrt{\frac{\alpha}{\mu}} \sim \sigma_0 \frac{v_0}{v} cm^2$$

Cross section IMR

$$D_3^+ + H_2 \rightarrow H_2D^+ + D_2$$

Endothermic reaction

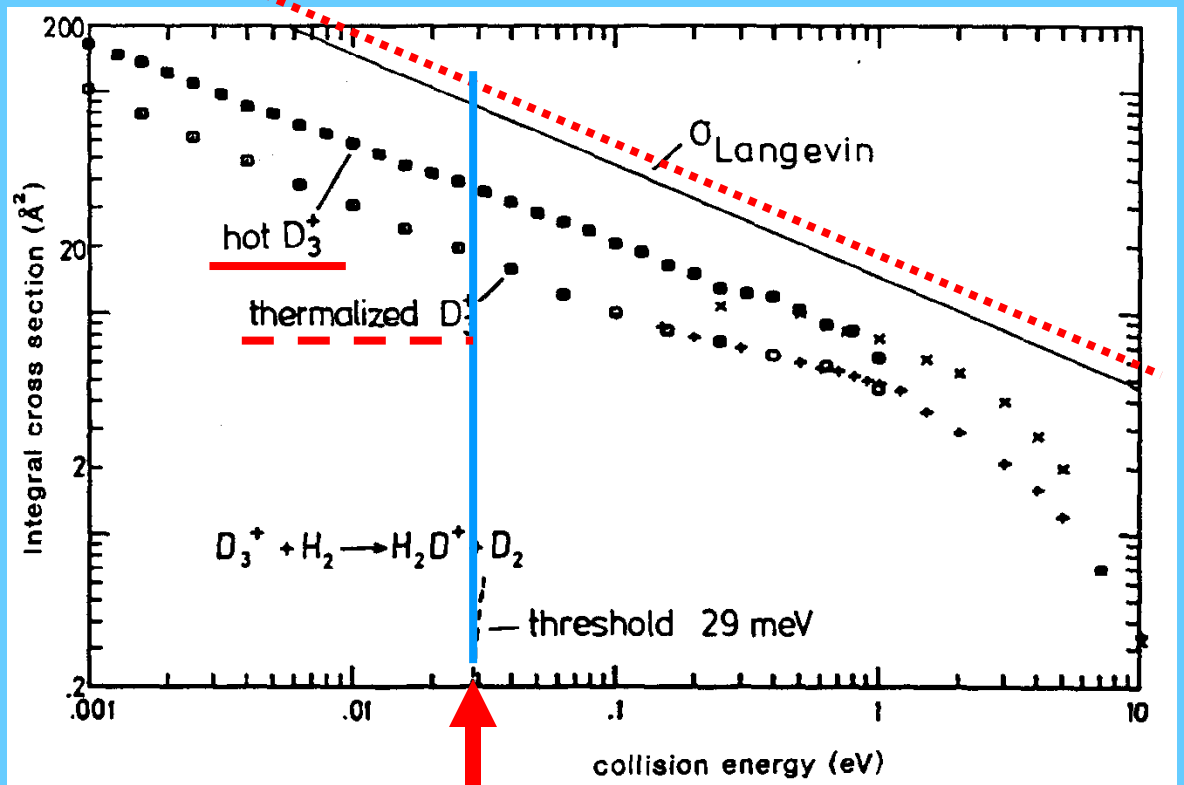

Figure 56. Integral cross sections for the 29 meV endothermic reaction $D_3^+ + H_2 \rightarrow H_2D^+ + D_2$ with hot D_3^+ (~2 eV internal energy) and ~350 K thermalized D_3^+. The merged beam results (●, ⊙) are, in the overlapping energy range, in good agreement with earlier guided ion-beam experiments (Piepke, 1980), recorded under similar storage ion source conditions (+, ×). The cross sections are significantly lower than the Langevin value.

Cross section IMR

$$He^+ + O_2 \rightarrow O^+ + O + He$$

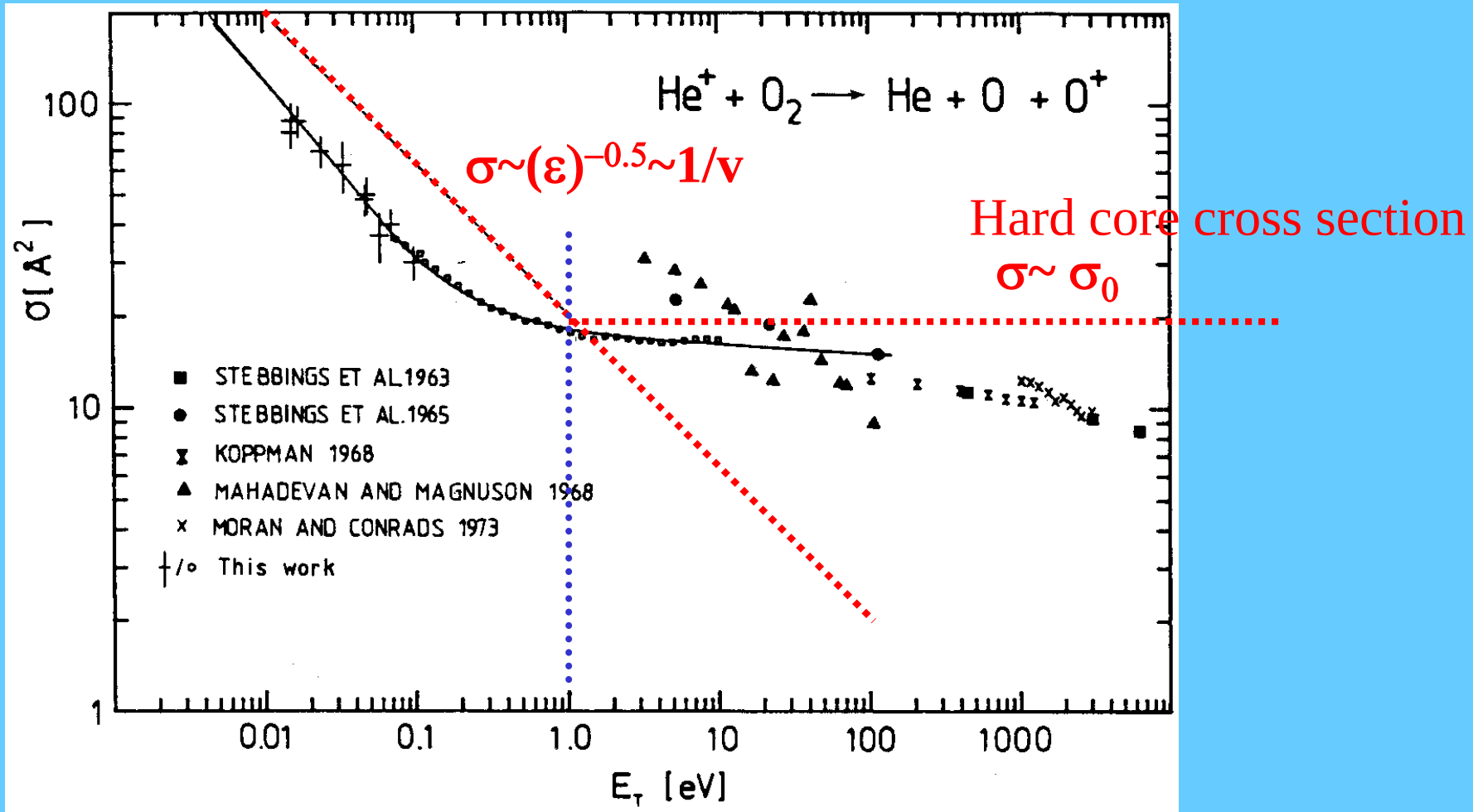

Figure 61. Integral cross sections for the dissociative charge transfer $He^+ + O_2 \rightarrow O^+ + O + He$. The guided-ion-beam results (○) have been extended to lower energies using the trapped ion beam method (+). The data at higher energies are from several other beam experiments, the references of which are compiled in Bischof and Linder (1986). The solid line is an effective cross section calculated using an analytical expression given in the text.

Decay of plasma – change of plasma composition

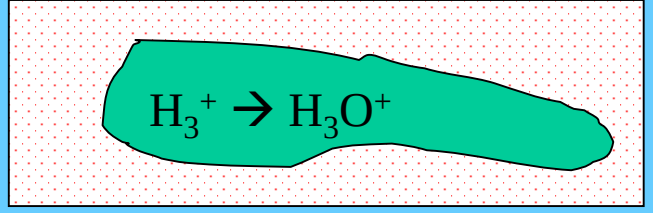

$H_3^+ + H_2O \rightarrow H_3O^+ + H_2$

Ion density in low temperature plasma, e.g. DC discharge $[H_3^+] \sim 10^{10} cm^{-3}$

"Pure He" … grade 5 …. 99.999% ….0.001 % of impurities

Water impurities $\sim 10^{-5}$ Torr $\rightarrow 3x10^{11} cm^{-3}$

$$\frac{dH_3^+}{dt} = -k[H_3^+].[H_2O] = -[H_3^+]/\tau_{H2O}$$

$$[H_3^+] = [H_3^+]_0.\exp(-k[H_2O]t) = [H_3^+]_0.\exp(-t/\tau_{H2O})$$

$$\tau = \frac{1}{k[H_2O]} \sim \frac{1}{(2.10^{-9})x(3.10^{11})} \sim 0.0017s \sim 1.7ms$$

Collision rate coefficient -Langevin rate coefficient

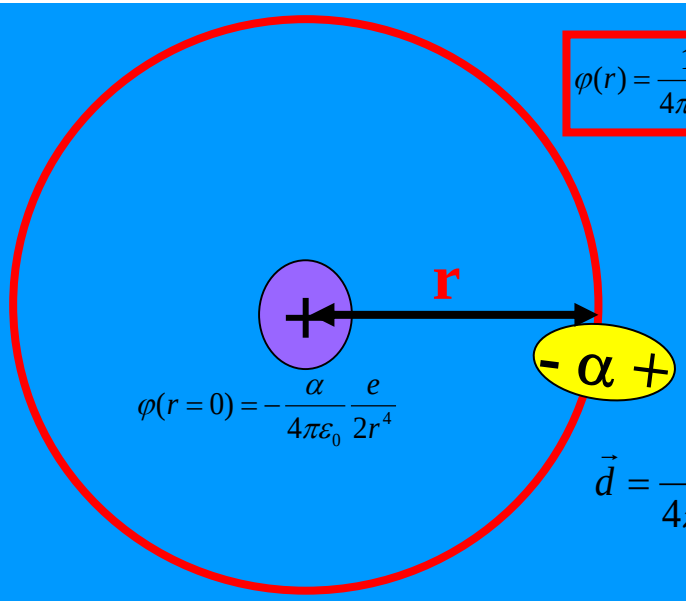

$$\varphi(r) = \frac{1}{4\pi\varepsilon_0}\frac{e}{r}$$

$$\varphi(r=0) = -\frac{\alpha}{4\pi\varepsilon_0}\frac{e}{2r^4}$$

$$\vec{d} = \frac{\alpha}{4\pi\varepsilon_0}\frac{e}{r^2}\frac{\vec{r}}{r}$$

α - polarizability

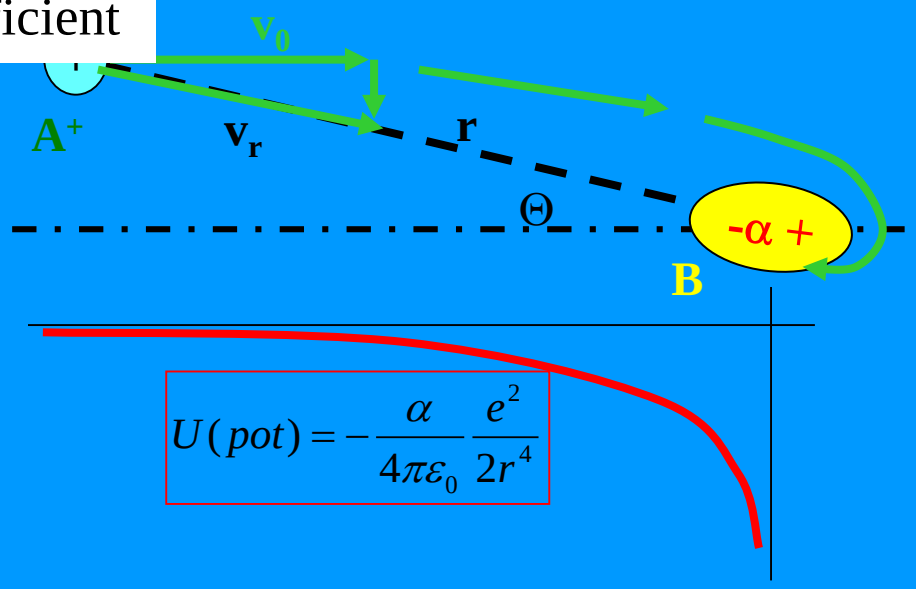

$$U(pot) = -\frac{\alpha}{4\pi\varepsilon_0}\frac{e^2}{2r^4}$$

pro U(pot) < U(kin) je záchyt ➔
Záchyt pro r<ρ kde U(ρ, pot) = U(ρ, kin)

$$\frac{\mu v_0^2}{2} = \frac{\alpha}{4\pi\varepsilon_0}\frac{e^2}{2r^4}$$

Collision cross section of IMR

Langevin cross section of IMR

$$\sigma = \pi\rho_0^2 = \frac{2\pi e}{v_0}\sqrt{\frac{\alpha}{4\pi\varepsilon_0\mu}}$$

$k_{coll}(T)$ collision rate coefficient

Langevin rate coefficient

$$\sigma = \pi\rho_0^2 \sim \frac{1}{v_0}\sqrt{\frac{\alpha}{\mu}} \sim \frac{1}{\sqrt{E}}$$

Collision cross section of IMR

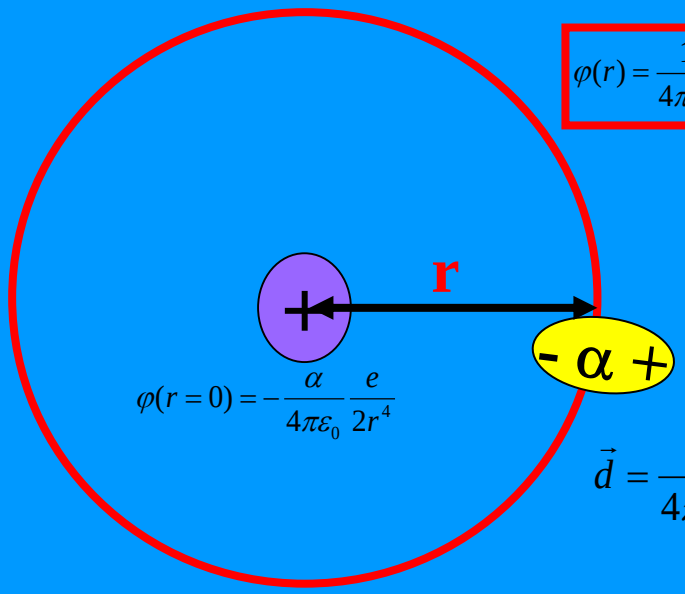

$$\varphi(r) = \frac{1}{4\pi\varepsilon_0}\frac{e}{r}$$

$$\varphi(r=0) = -\frac{\alpha}{4\pi\varepsilon_0}\frac{e}{2r^4}$$

$$\vec{d} = \frac{\alpha}{4\pi\varepsilon_0}\frac{e}{r^2}\frac{\vec{r}}{r}$$

α - polarizovatelnost

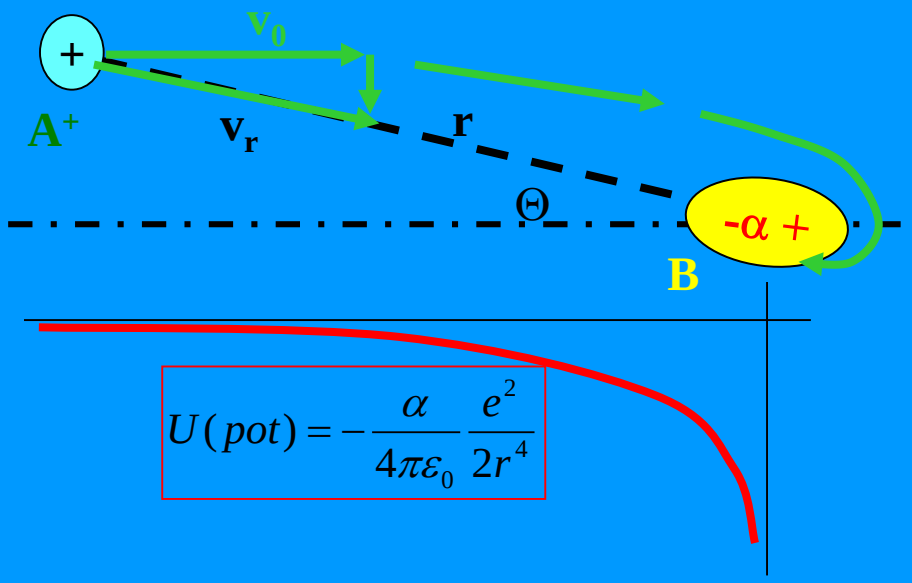

$$U(pot) = -\frac{\alpha}{4\pi\varepsilon_0}\frac{e^2}{2r^4}$$

pro U(pot) < U(kin) je záchyt ➔
Záchyt pro r<ρ kde U(ρ, pot) = U(ρ, kin)

$$\frac{\mu v_0^2}{2} = \frac{\alpha}{4\pi\varepsilon_0}\frac{e^2}{2r^4}$$

$$\sigma = \pi\rho_0^2 = \frac{2\pi e}{v_0(4\pi\varepsilon_0)}\sqrt{\frac{\alpha}{\mu}}$$

$$\sigma = \pi\rho_0^2 \sim \frac{1}{v_0}\sqrt{\frac{\alpha}{\mu}} \sim \frac{1}{\sqrt{E}}$$

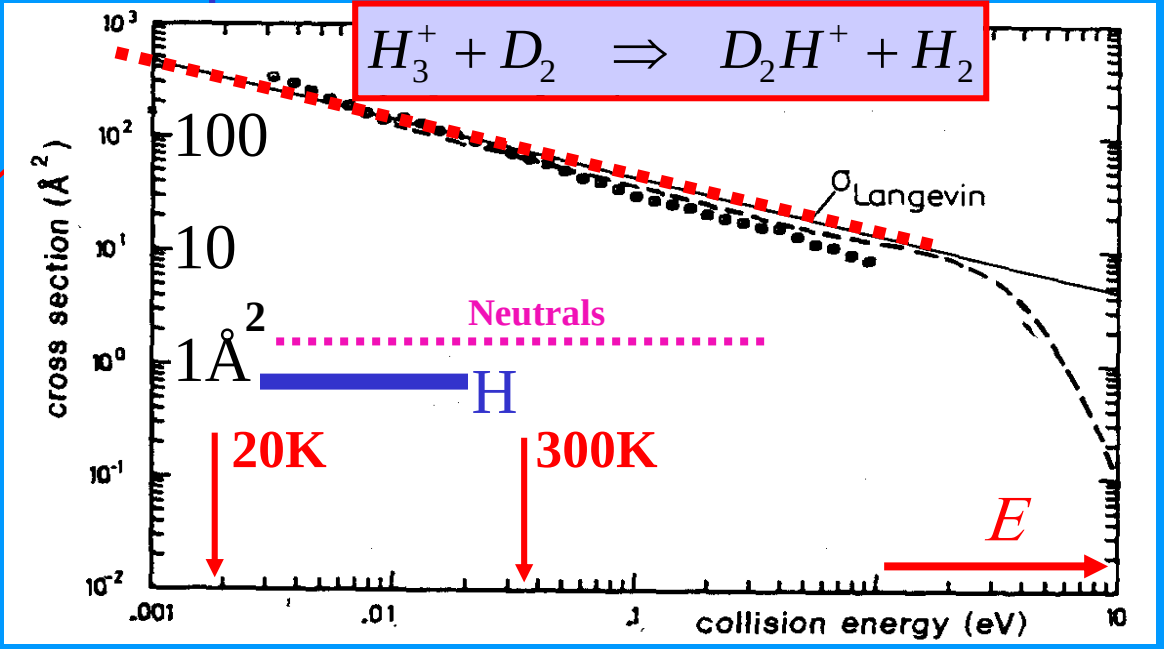

Reaction Rate of IMR relevant for ionosphere

k_{IMR}

$k_{coll} \sim 10^{-9} cm^3 s^{-1}$

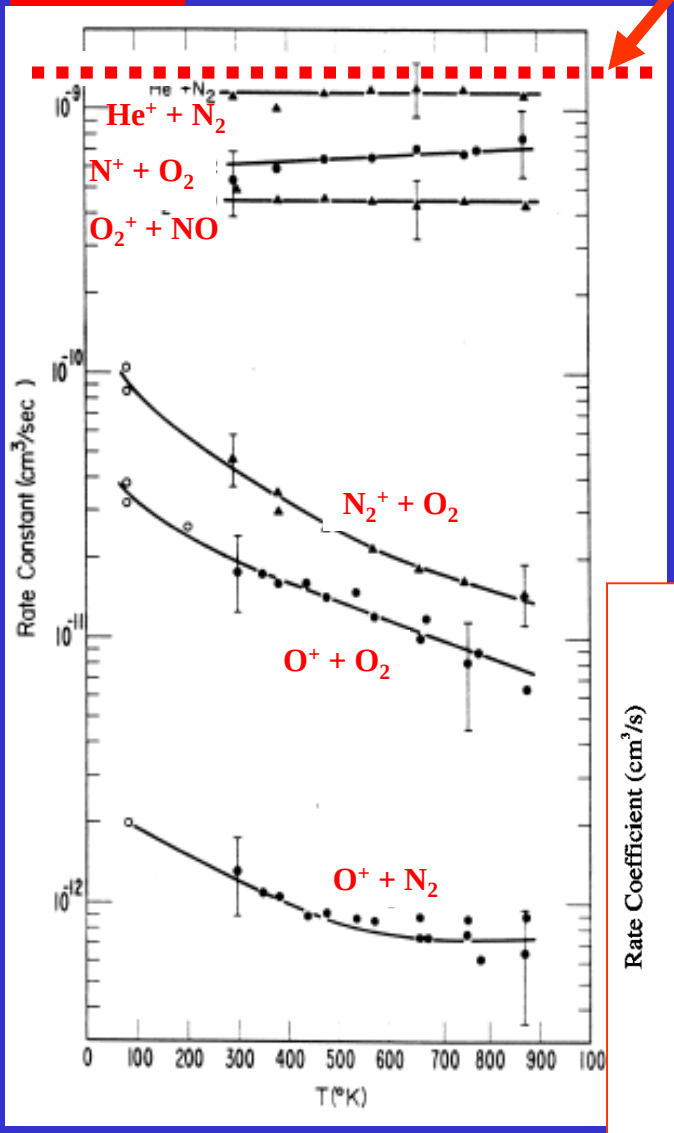

1975-90

1990-00

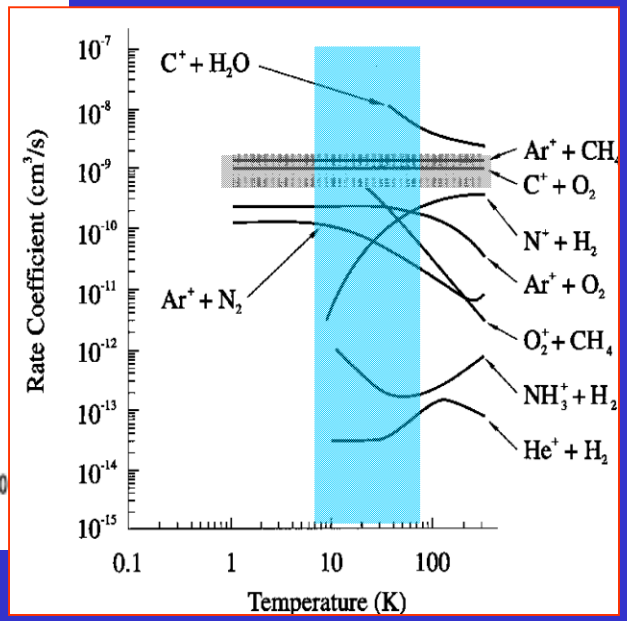

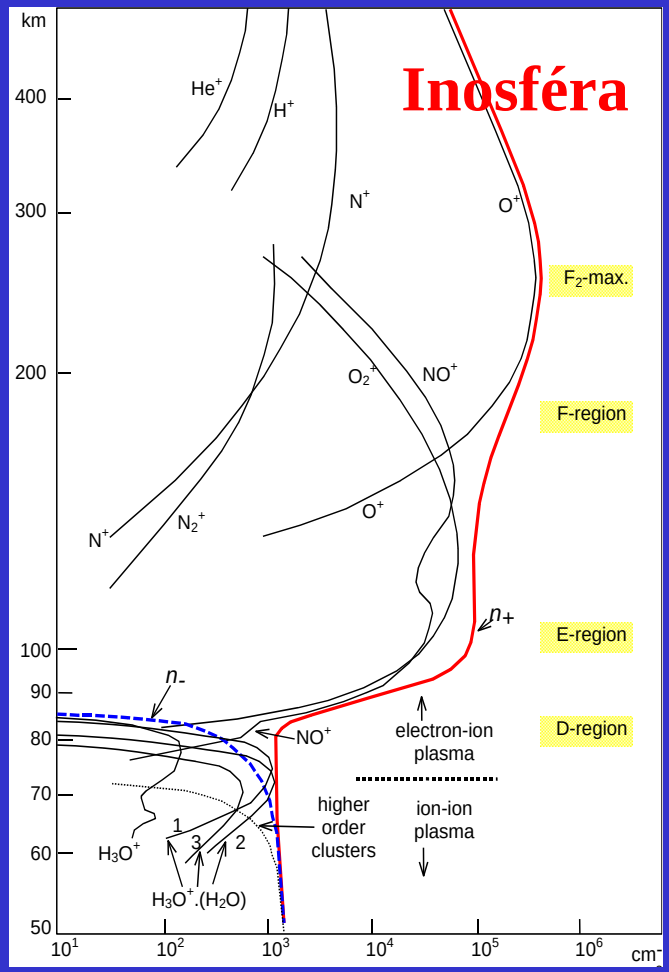

IMR thermal

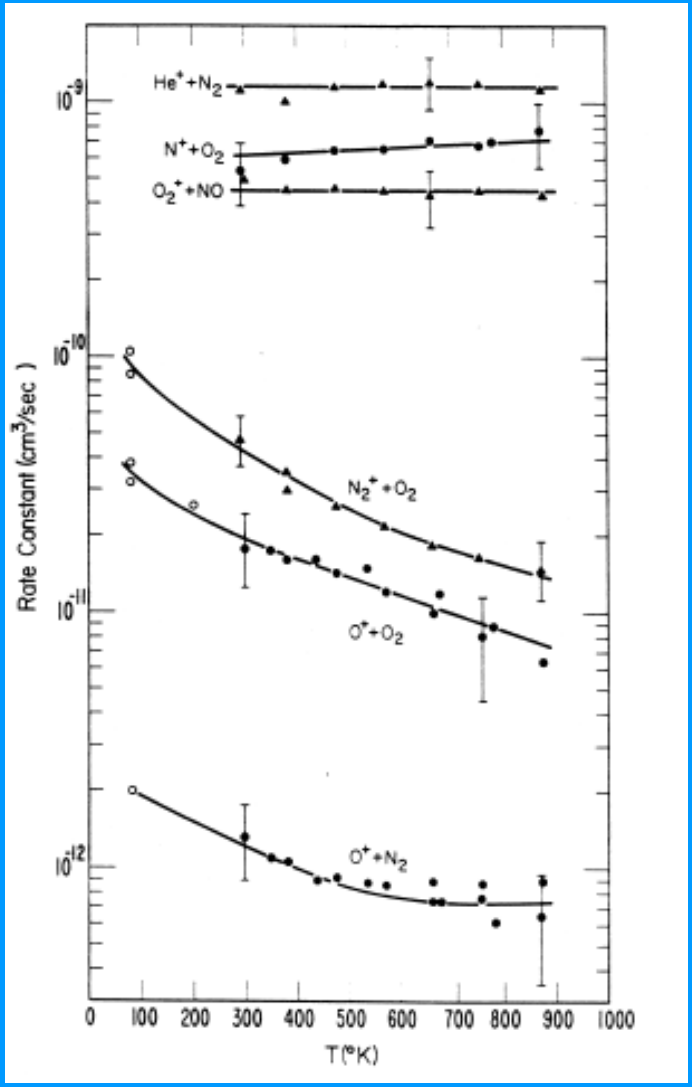

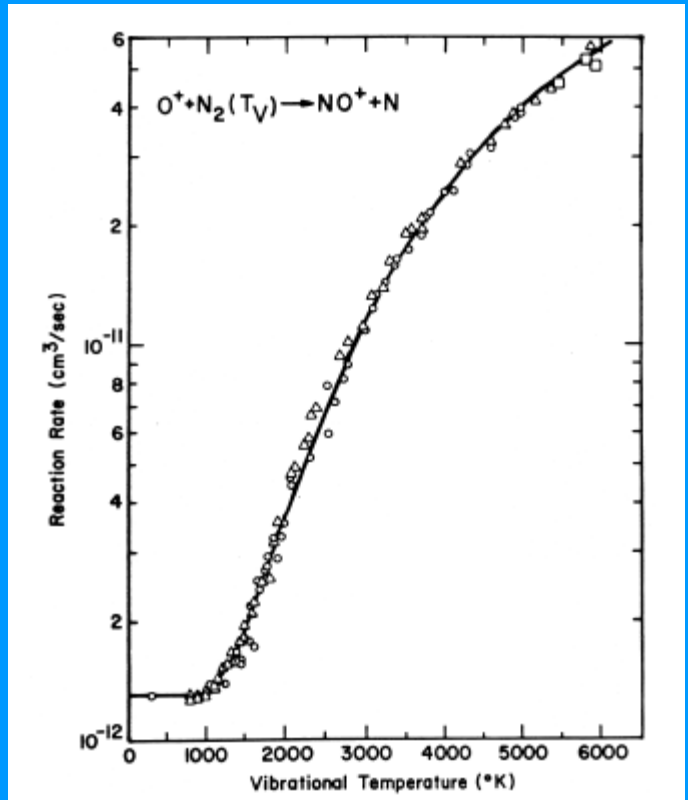

Fig. 12. Measurements of the variation of the rate coefficient for the reaction of $O^+ + N_2 \rightarrow NO^+ + N$ with the vibrational temperature of N_2 [16].

Ionic composition of the atmosphere

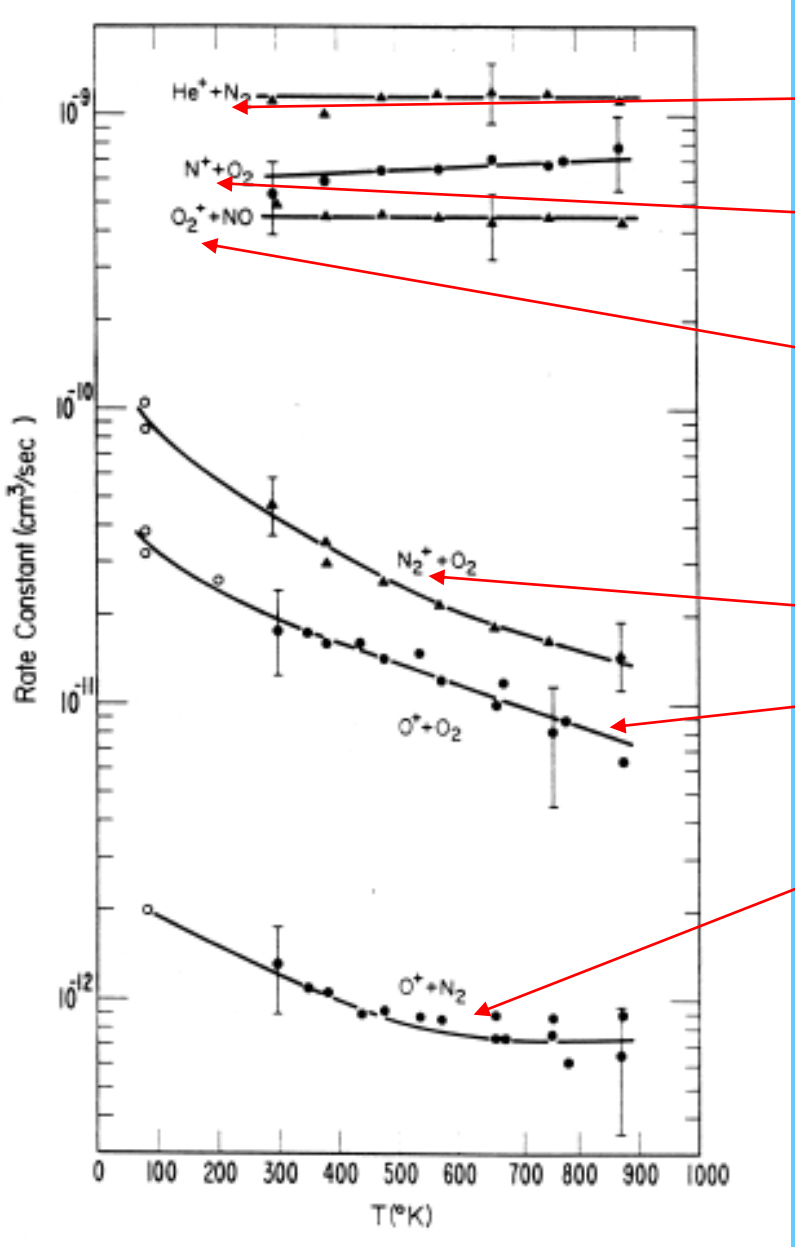

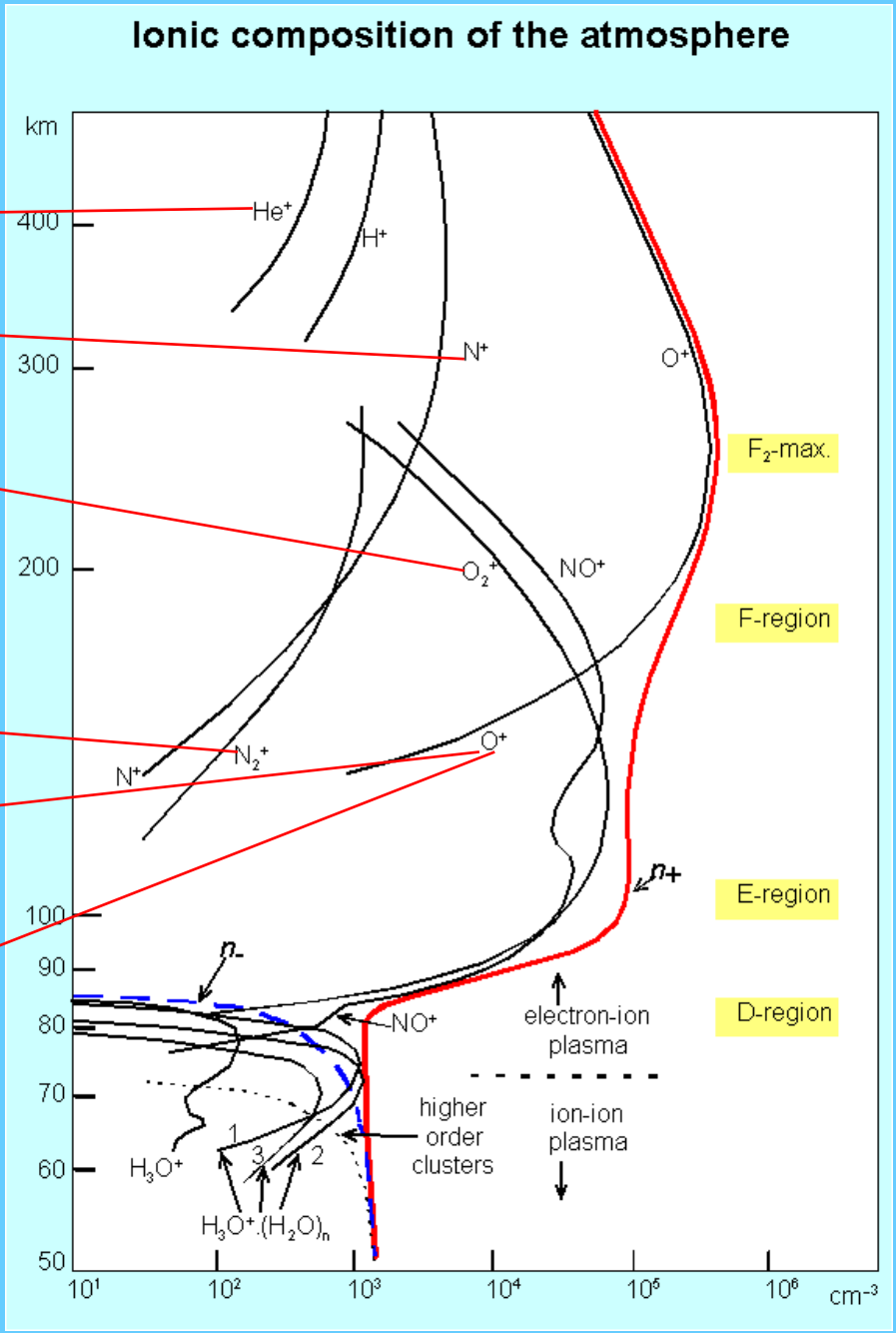

The ion chemistry of the lower atmosphere

Binary reactions

Ternary reactions

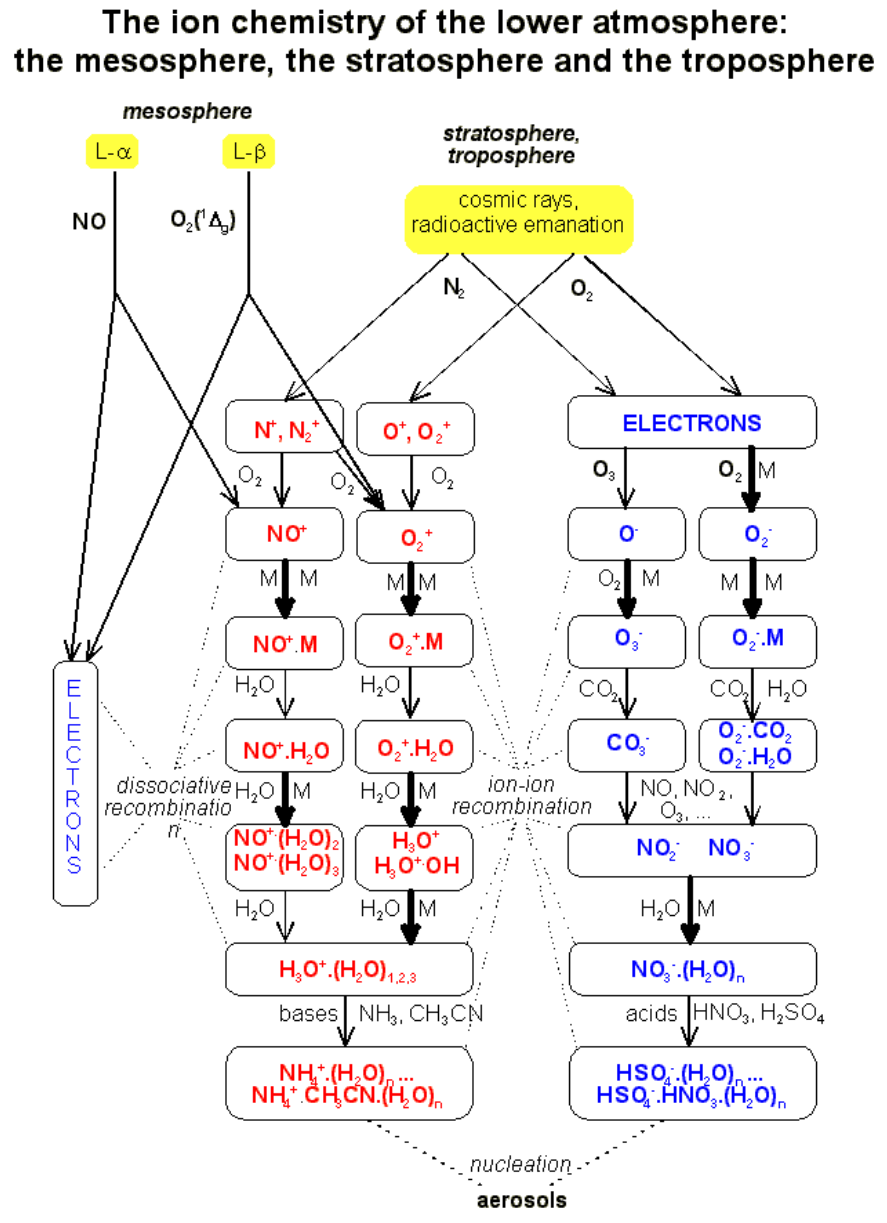

Branching ratio of IMR

$$AB^+ + C \underset{\tau_{-1}}{\overset{k_1}{\leftrightarrow}} (A.BC^+)^{\#} \xrightarrow{\tau_2} AB + C^+$$

$$\xrightarrow{\tau_3} AC + B^+$$

$$\xrightarrow{\tau_4} AC^+ + B$$

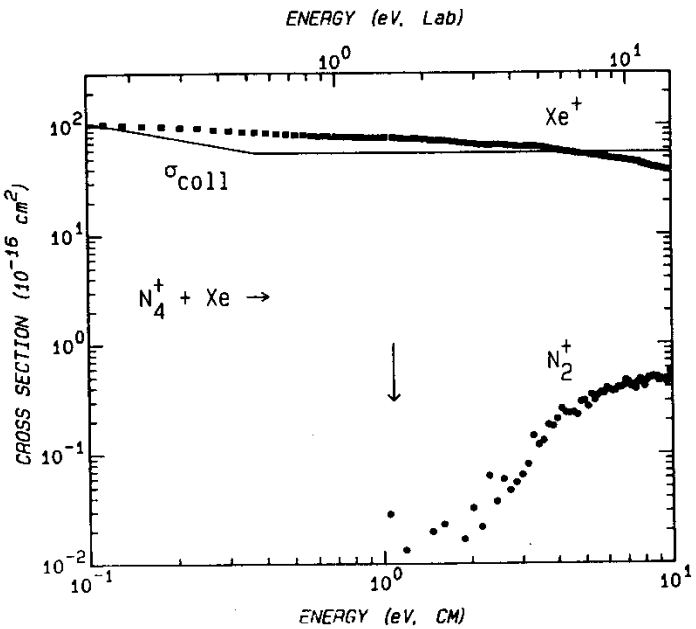

Fig. 4. Cross-sections for reaction of N_4^+ with Xe as a function of relative kinetic energy (lower x-axis) and laboratory energy (upper x-axis). Cross-sections are normalized to 100% isotopic abundance as described in the text. Circles are CID (reaction 4); squares, CT (reaction 5); and triangles, ligand exchange (reaction 6). The vertical arrow shows the N_2^+–N_2 bond strength of 1.09 eV. The solid line represents the LGS collision cross-section, Eq. 7, at low energy and the hard sphere collision cross-section of 54 Å^2 at higher energy.

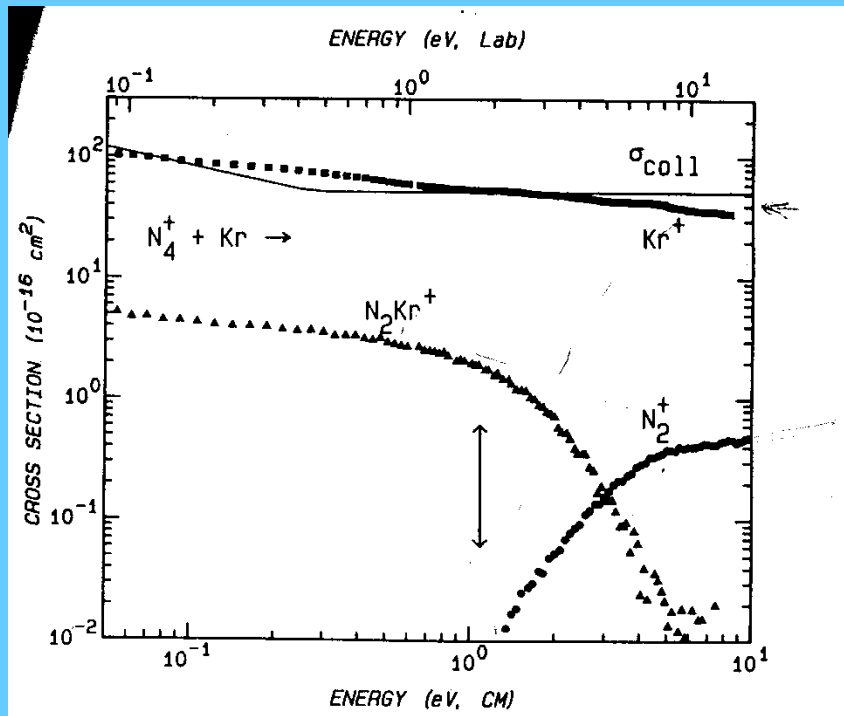

Fig. 3. Cross-sections for reaction of N_4^+ with Kr as a function of relative kinetic energy (lower x-axis) and laboratory energy (upper x-axis). The cross-sections are normalized to 100% isotopic abundance as described in the text. Circles are CID (reaction 4); squares, CT (reaction 5); and triangles, ligand exchange (reaction 6). The vertical arrow shows the N_2^+–N_2 bond strength of 1.09 eV. The solid line represents the LGS collision cross-section, Eq. 7, at low energy and the hard sphere collision cross-section of 51 Å^2 at higher energy.

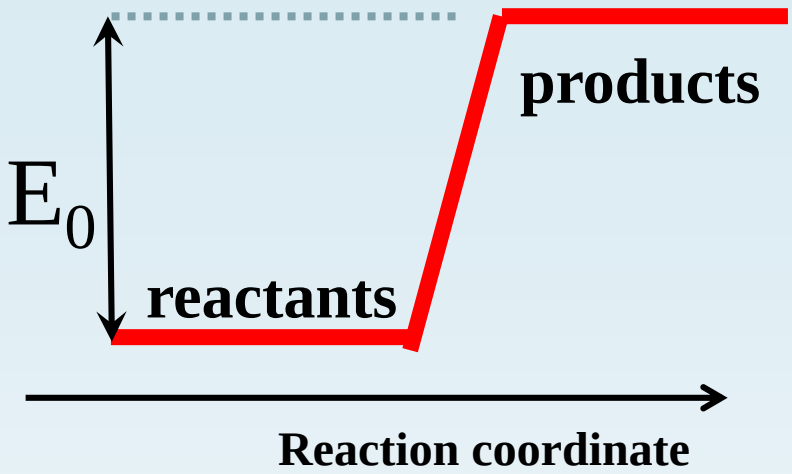

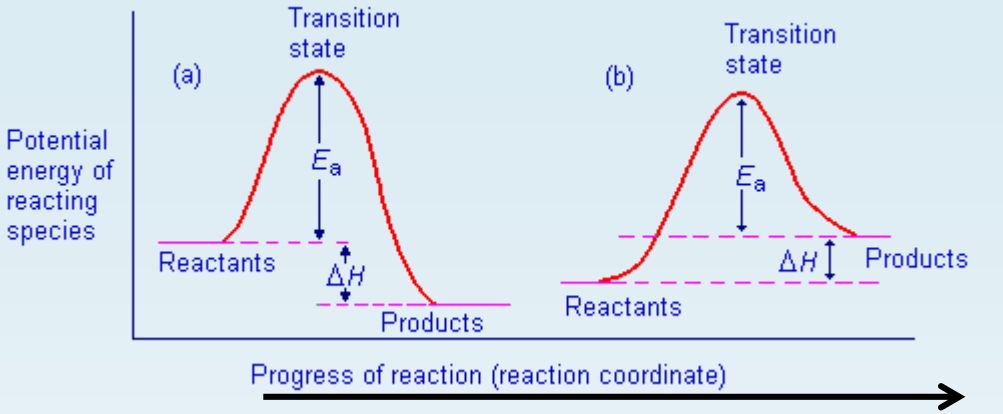

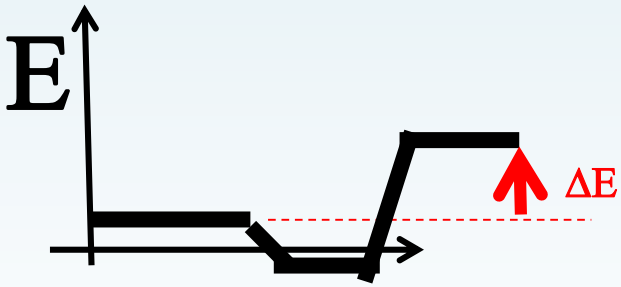

Reaction coordinate

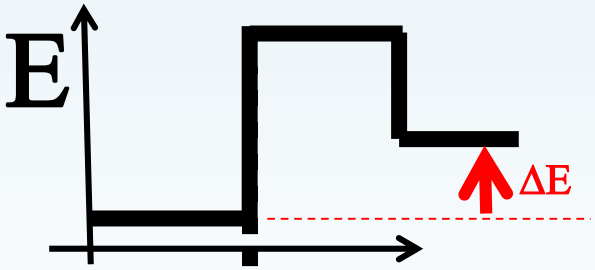

Reaction coordinate

Reaction coordinate

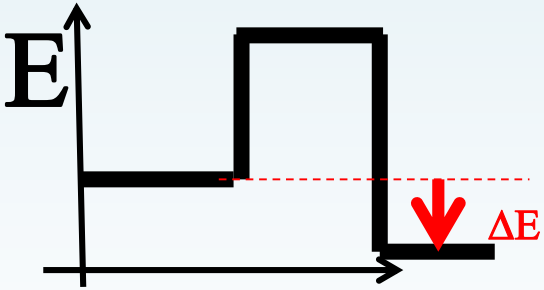

Reaction coordinate

Endothermic

Exothermic

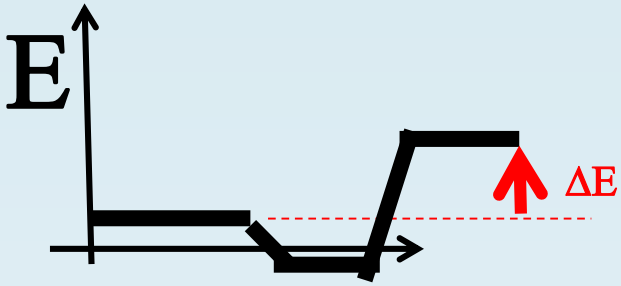

Reaction coordinate

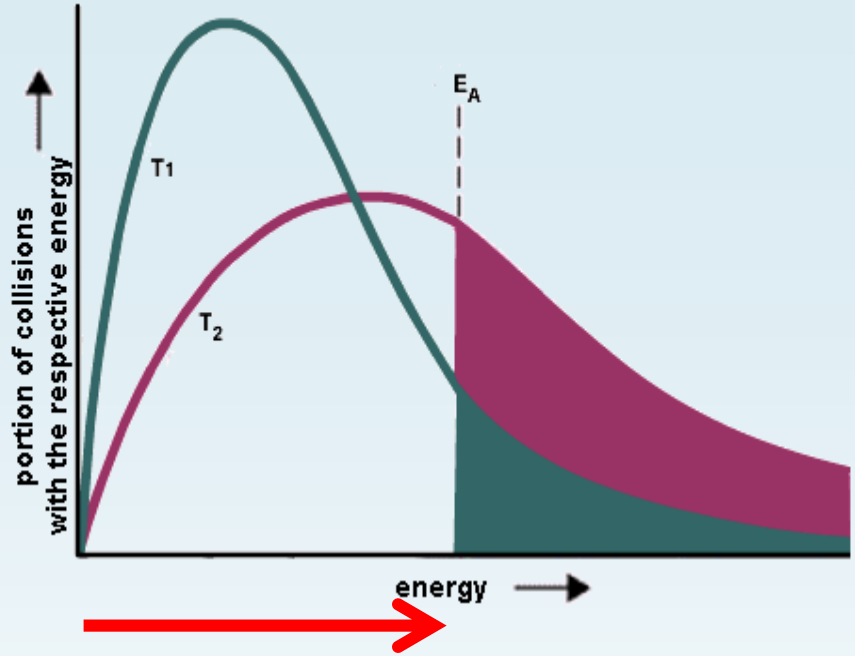

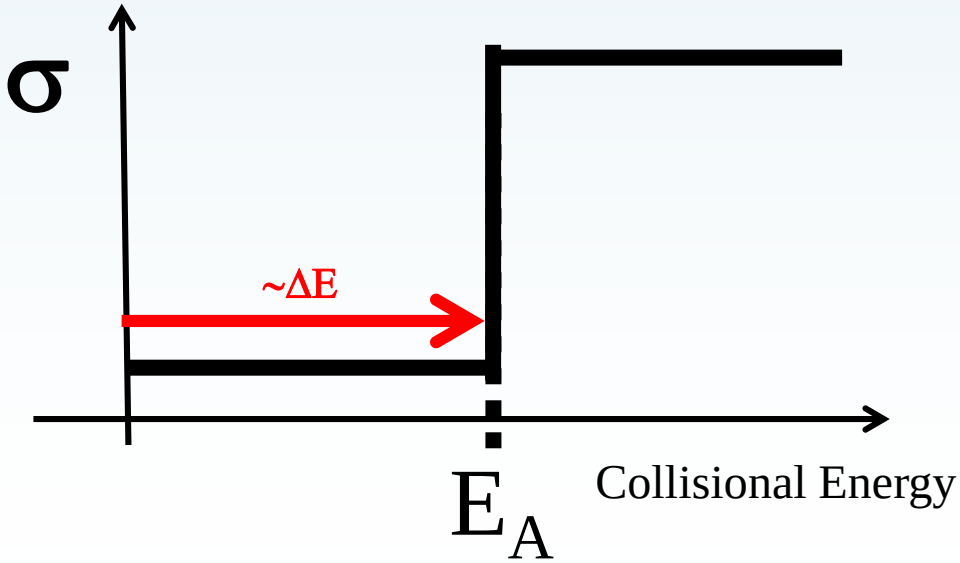

ΔE ……. E_A

Reaction coordinate

Collisional Energy

Kinetics of elementary process

k(T)=<vσ> → $$k = \int_{Max(T)} f(v).v.\sigma(v)dv = k(T)$$

$$\nu \sim N v \sigma$$

$$\tau \sim 1/Nk$$

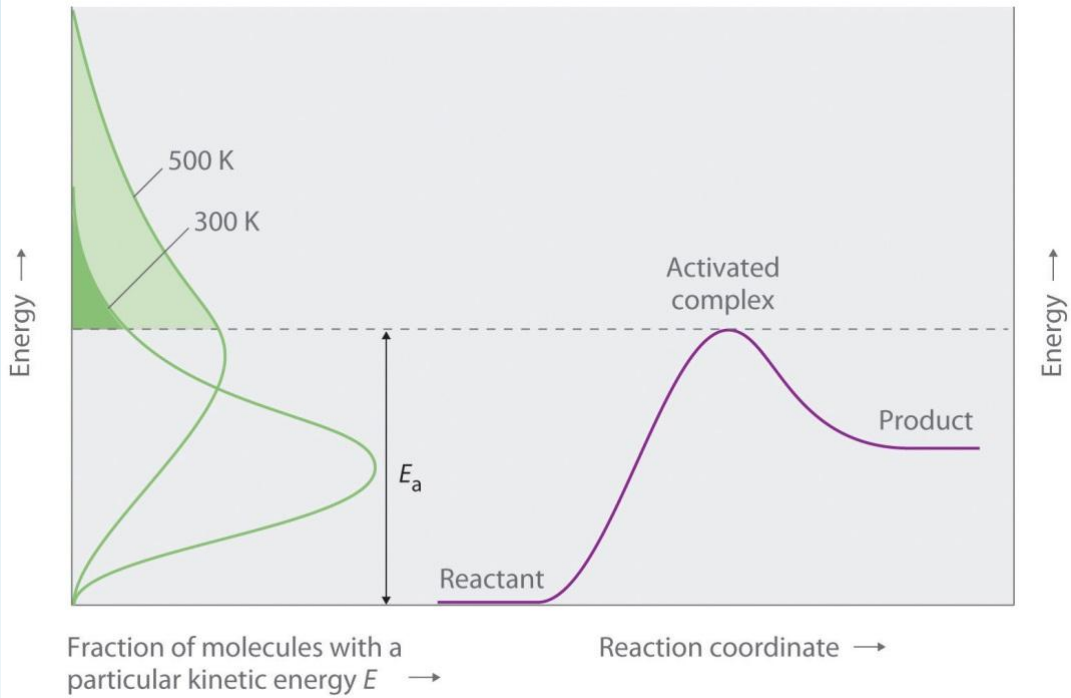

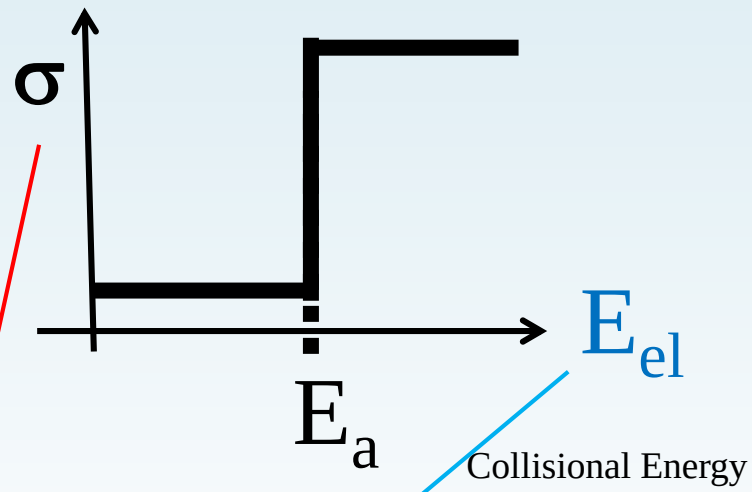

The thermally averaged rate constant $\alpha_{th}(T)$ (in a.u.) is obtained from the energy-dependent cross-section $\sigma(E)$ as

$$\alpha_{th}(T) = \frac{8\pi}{(2\pi kT)^{3/2}} \int_0^\infty \sigma(E_{el}) e^{-\frac{E_{el}}{kT}} E_{el} dE_{el} , \quad (4)$$

where T is the temperature. Temperature dependencies $\alpha_{th}(T)$ for different rovibrational transitions $v \rightarrow v'$ obtained using equation (4) are shown in Fig. 3 as solid lines.

Overview

Electronic Transitions:
ΔE = 1-15 eV
Visible-UV

Vibrational Transitions:
ΔE = 0.1-1 eV
Infrared

Rotational Transitions:
ΔE = 0.01-0.1 eV
(sub)-Millimeter

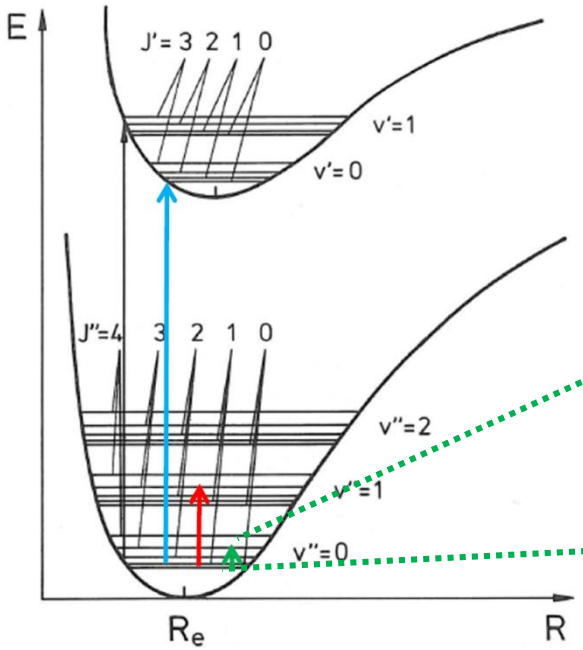

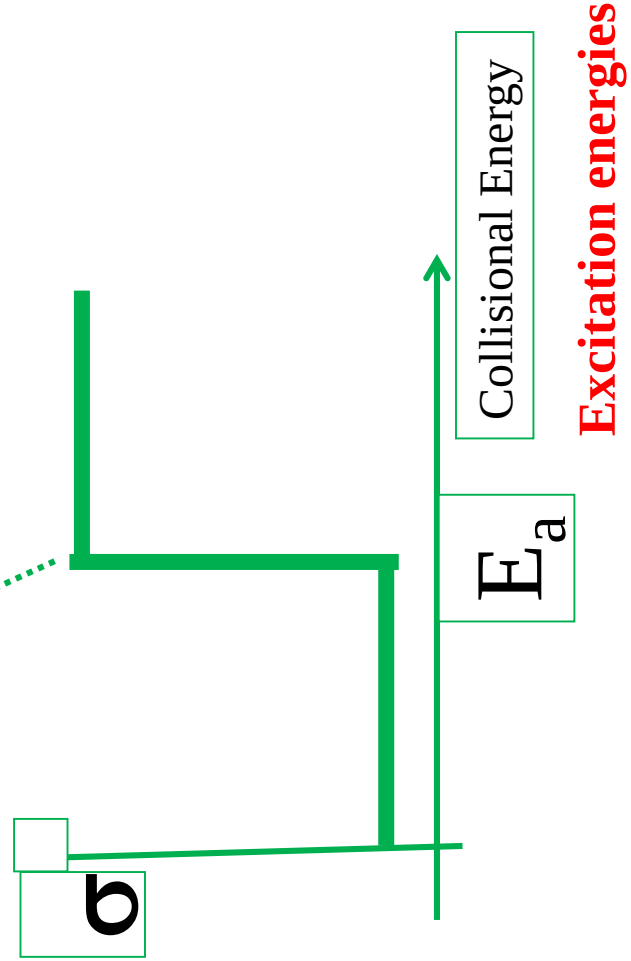

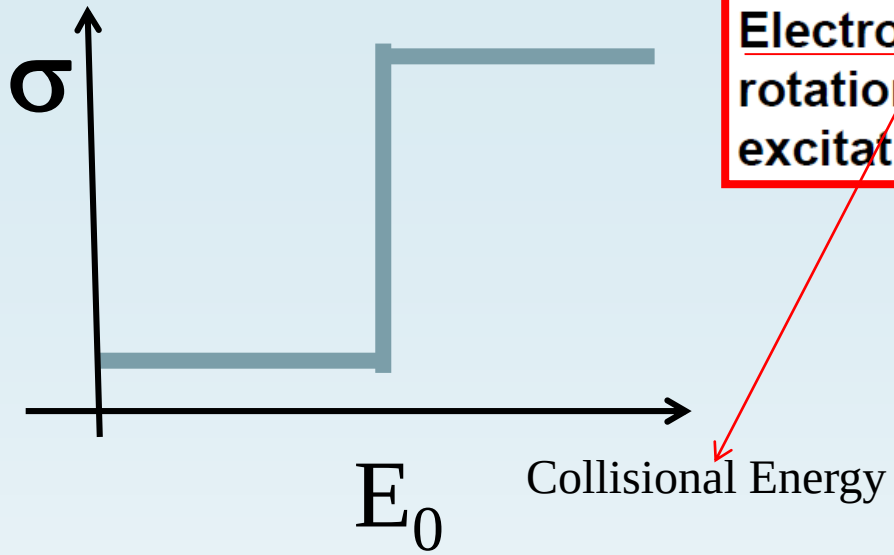

Electron impact rotational excitation of CH^+

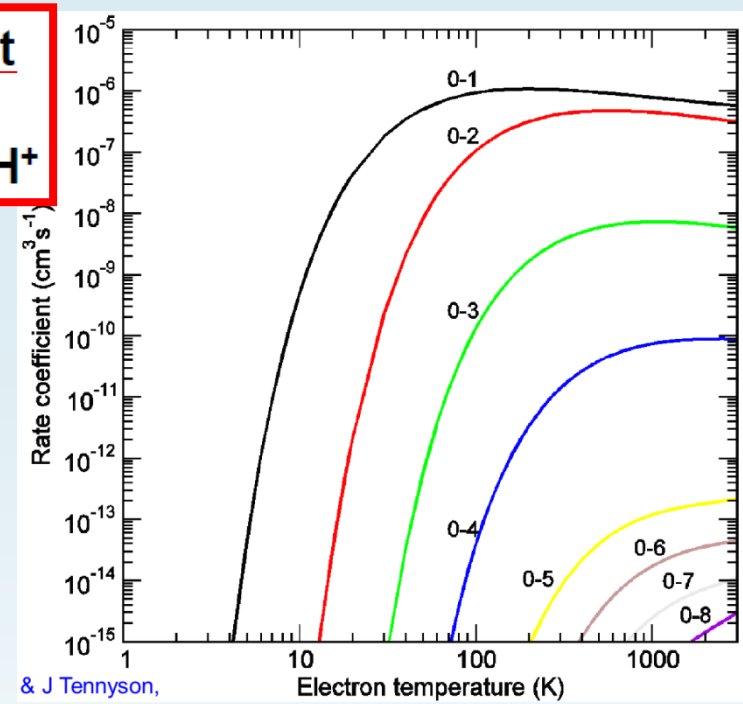

ΔE ……. E_A **….activation energy E_a**

The thermally averaged rate constant $\alpha_{th}(T)$ (in a.u.) is obtained from the energy-dependent cross-section $\sigma(E)$ as

$$\alpha_{th}(T) = \frac{8\pi}{(2\pi kT)^{3/2}} \int_0^\infty \sigma(E_{el}) e^{-\frac{E_{el}}{kT}} E_{el} dE_{el}\,, \qquad (4)$$

where T is the temperature. Temperature dependencies $\alpha_{th}(T)$ for different rovibrational transitions $v \rightarrow v'$ obtained using equation (4) are shown in Fig. 3 as solid lines.

For further discussion, it is convenient to represent the cross-section $\sigma(E_{el})$ in the form

$$\sigma(E_{el}) = \frac{\pi}{k^2} P(E_{el})\,, \qquad (5)$$

where k is the wave vector of the incident electron, $P(E_{el})$ is the probability for vibrational (de-)excitation at collision energy E_{el}.

$$k = A\, e^{-\frac{E_a}{RT}}$$

activation energy

pre-exponential factor

average kinetic energy

$$\ln k = \ln A - \frac{E_a}{RT}$$

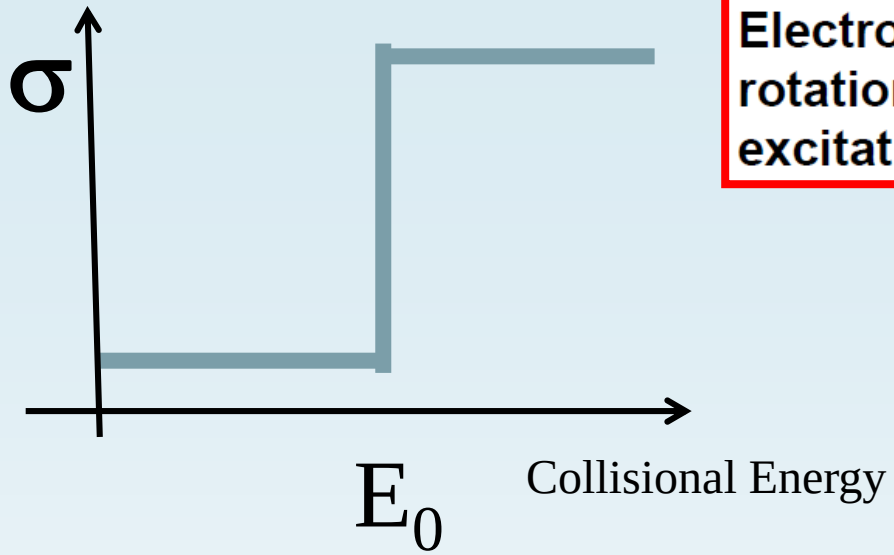

Electron impact rotational excitation of CH^+

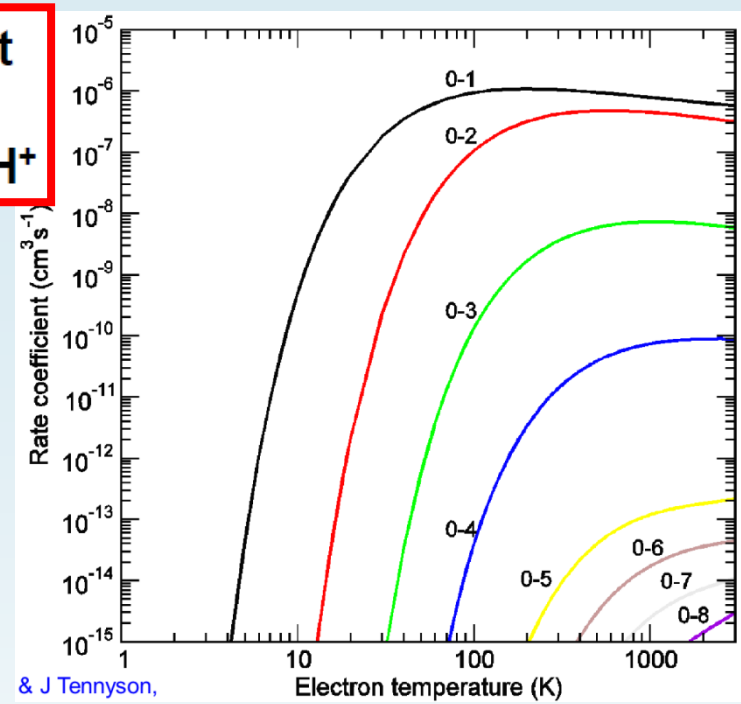

Arrhenius plot

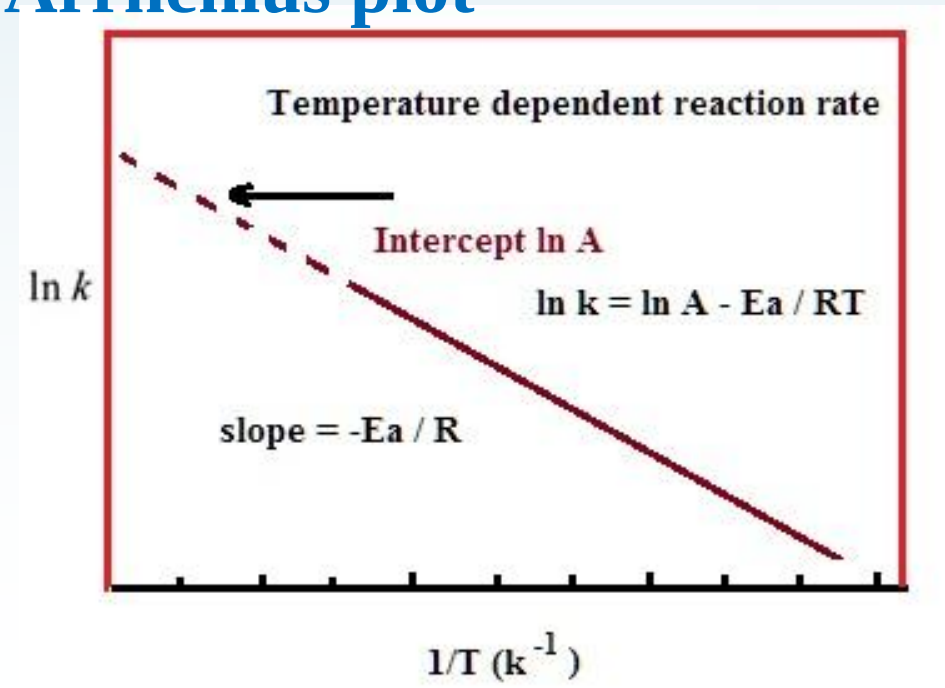

$$k = A e^{-\frac{E_a}{RT}}$$

activation energy

pre-exponential factor

average kinetic energy

$$\ln k = \ln A - \frac{E_a}{RT}$$

Energies of H_2 and D_2

1eV corresponds to ~ 11604K

H_2	B_e=60.80
D_2	B_e=30.429
HD	B_e=45.655

	j	E/meV	E/in K	300K	250K	80K	35K	low
H_2	0	0	0	0.128	0.150	0.248	0.25	1/4
	1	14.7	170.6	0.657	0.694	0.75	0.75	3/4
	2	44	510.6	0.117	0.098	0.002	0	
	3	87	1009.5	0.092	0.055	0	0	
	4	145	1682.6	0.004	0.0016	0	0	
	5	215	2494.9	0.001	0.0002	0	0	
D_2	0	0	0	0.179	0.213	0.552	0.664	2/3
	1	7.3	84.71	0.202	0.227	0.329	0.333	1/3
	2	22	255.29	0.383	0.384	0.114	0.002	
	3	44	510.6	0.115	0.098	0.004	0	
	4	72	835.5	0.098	0.066	0.0001	0	
	5	108	1253.2	0.015	0.008	0	0	
HD	0	0	0					1
	1	11.04	128.1					
	2	33.05	383.4					

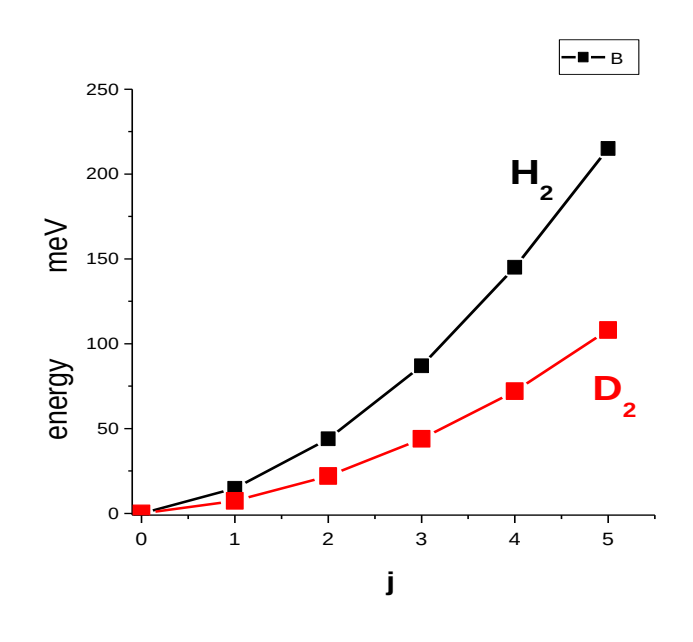

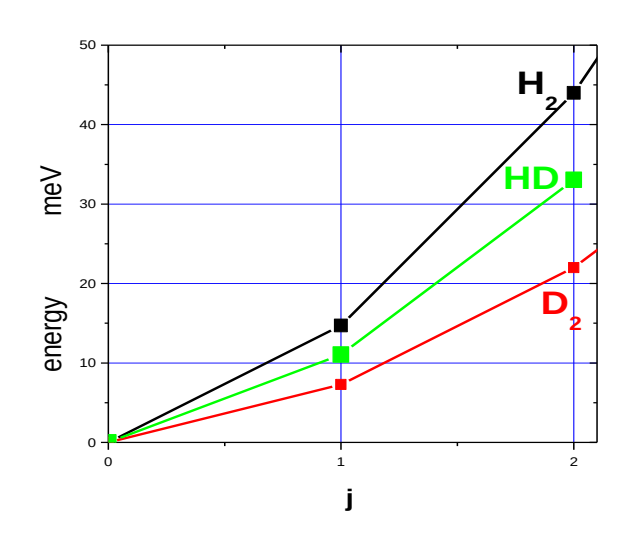

H_2 and D_2 are taken from O. Wick dissertation
HD is calculated using B_e from Herzberg and comparison with H_2 from table

$$OD^- + H_2 \rightarrow OH^- + HD, \quad \Delta H = 24.0 \text{ meV}. \qquad (2)$$

1eV corresponds to ~ 11604K

$$k = A e^{-\frac{E_a}{RT}}$$

activation energy

pre-exponential factor

average kinetic energy

$$\ln k = \ln A - \frac{E_a}{RT}$$

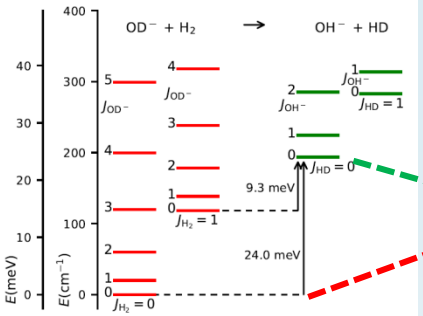

Fig. 1. Rotational energy levels of the reactants (left-hand side) and products (right-hand side) for reaction (1). The rotational constants for OD^-, OH^-, HD, and H_2 are taken from the literature (Huber & Herzberg 1979; Rehfuss et al. 1986; Matsushima et al. 2006). The two arrows indicate that 24.0 meV of translational energy are needed to reach the threshold at 0, while 9.3 meV are sufficient for reaction with ortho-H_2 ($J_{H_2} = 1$).

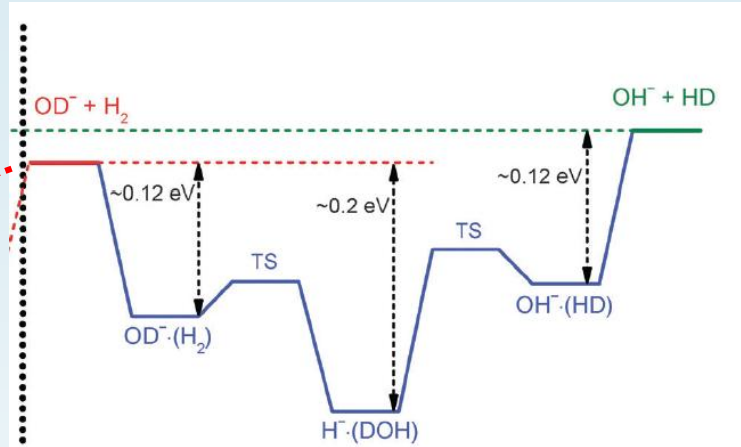

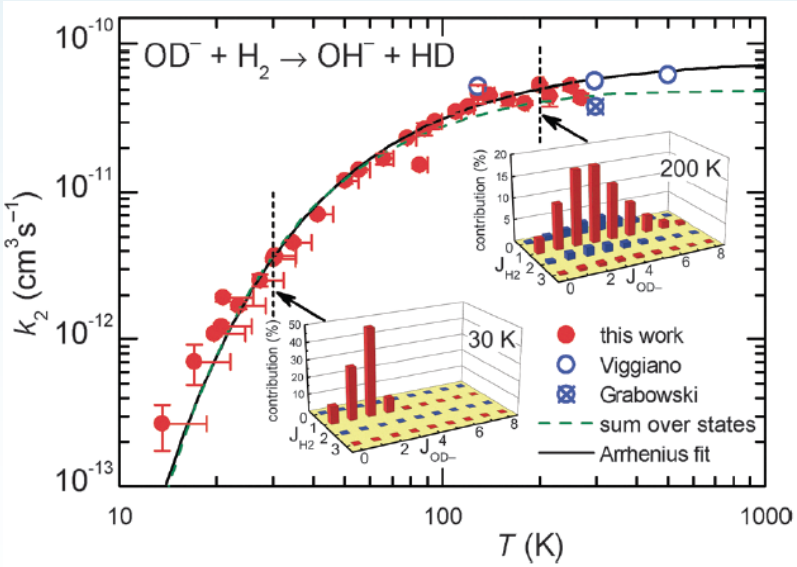

Temperature dependence of the rate coefficient k_2

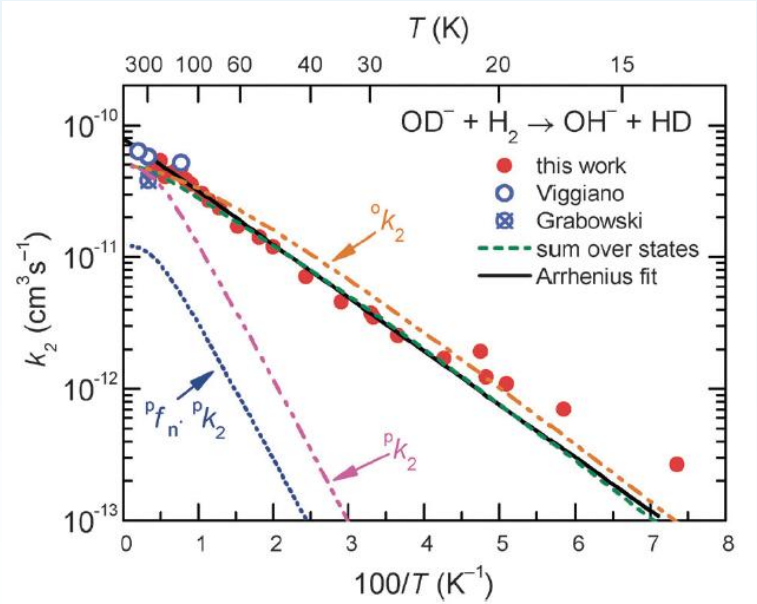

Arrhenius plot of rate coefficient k_2 for reaction (2)

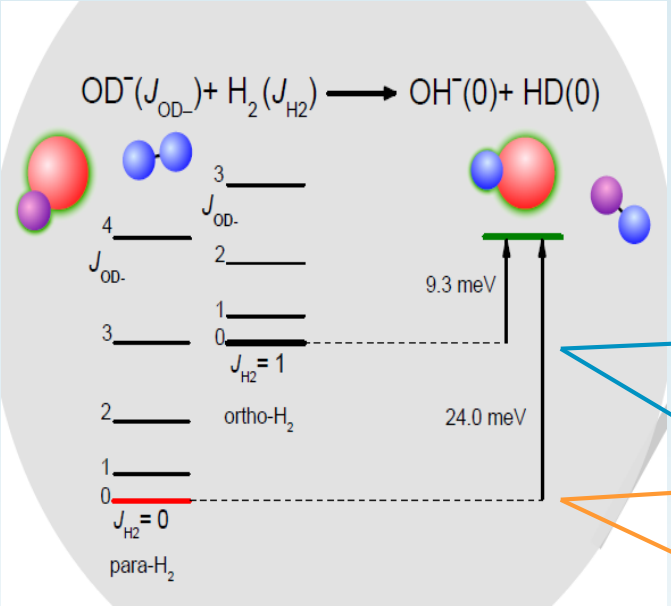

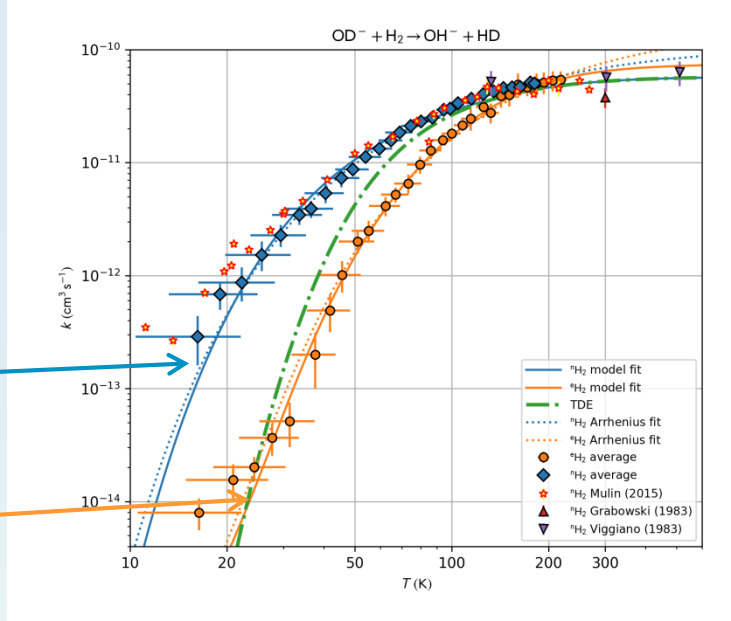

$$^{o/p}k_2 = \frac{1}{^{o/p}f} k_{20} \Sigma_{JOD-} \quad \Sigma_{JH2}^{o/p}\left(P_{JH2}P_{JOD-}e^{\frac{-Max\{(\Delta H - E_{JH2} - E_{JOD-});0\}}{k_B T}}\right)$$

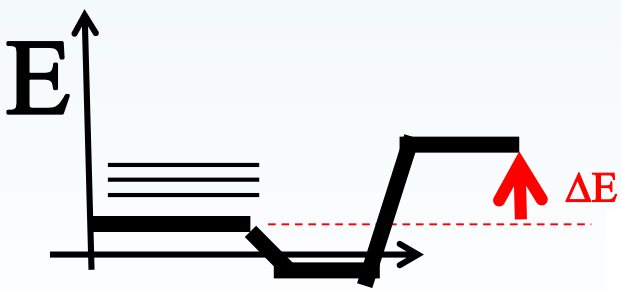

Reaction coordinate

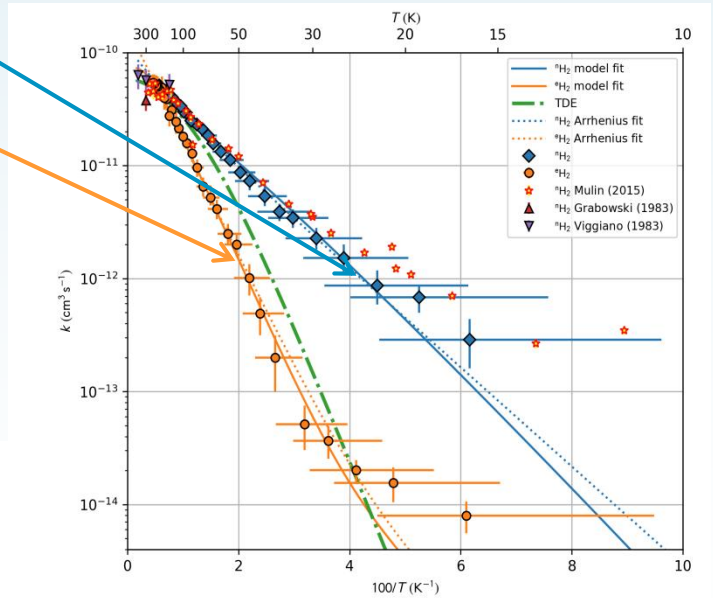

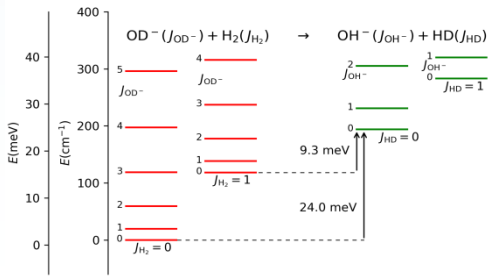

ELSEVIER

International Journal of Mass Spectrometry and Ion Processes 134 (1994) 67–71

International Journal of Mass Spectrometry and Ion Processes

Short communication

Observations of Arrhenius behaviour over 56 decades: dissociation of N_4^+ ions

J. Glosík[a,b], V. Skalský[a,b], W. Lindinger[a]

$$N_4^+ + He \xrightarrow{k_2} N_2^+ + N_2 + He$$

$$k_2 = A \exp\left(-\frac{3E_a}{2E_b}\right) = A \exp\left(-\frac{E_a}{kT_b}\right)$$

The equilibrium constant K_c for the formation and destruction of N_4^+, described by Eqs. (4) and (8)

$$K_c = \frac{k_{forward}}{k_{reverse}} = \frac{k_3}{k_2} \qquad (11)$$

is expressed in the van't Hoff formula,

$$RT \ln K_p = -\Delta G_p = -\Delta H_p + T\Delta S_p \qquad (12)$$

where ΔG_p, ΔH_p and ΔS_p (subscript p means constant pressure) is the free energy, enthalpy and entropy change, respectively, $K_p = K_c(R'T)^{\Delta n}$ and Δn is the mole change in the reaction. In reaction (10), $\Delta n = -1$. For more details see Ref. 22.

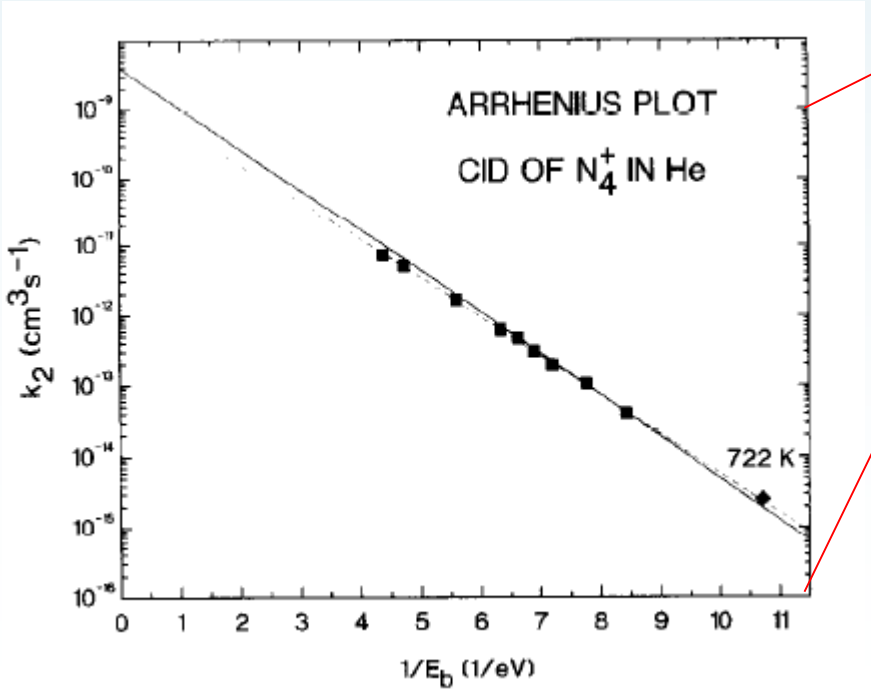

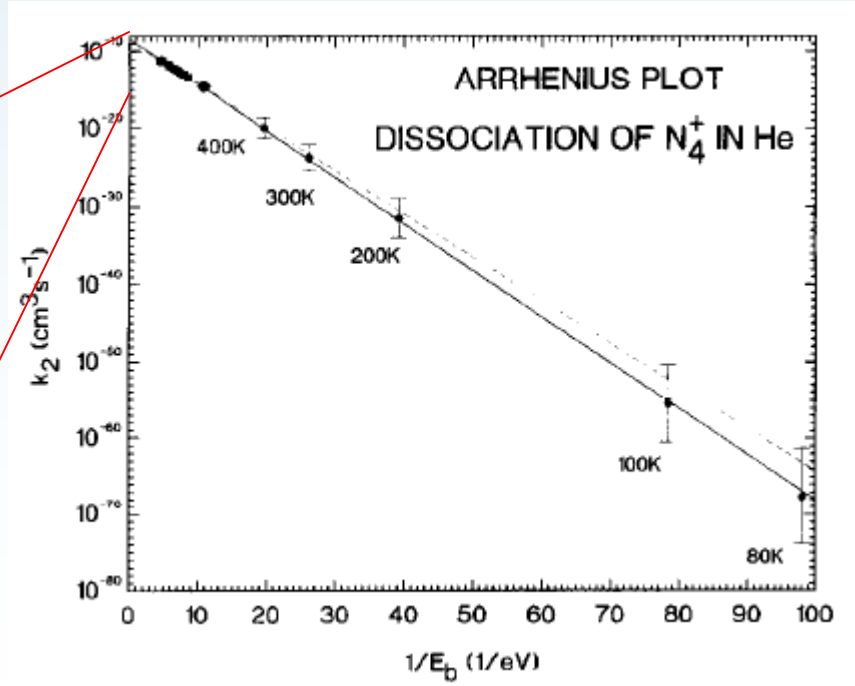

Princip akce a reakce

Henri Louis Le Chatelier
(1850-1936)

Karl Ferdinand Braun
(1850-1918)

Při ovlivňování rovnováhy se uplatňuje princip akce a reakce aplikovaný na chemické děje, známý pod názvem ***Le Chatelierův-Braunův princip***:

Porušení rovnováhy vnějším zásahem (akcí) vyvolá děj (reakci), který směřuje ke zrušení účinku vnějšího zásahu (akce).

Chemická rovnováha je takový stav soustavy, v němž se z makroskopického hlediska nemění její složení, i když v ní neustále probíhají chemické děje.

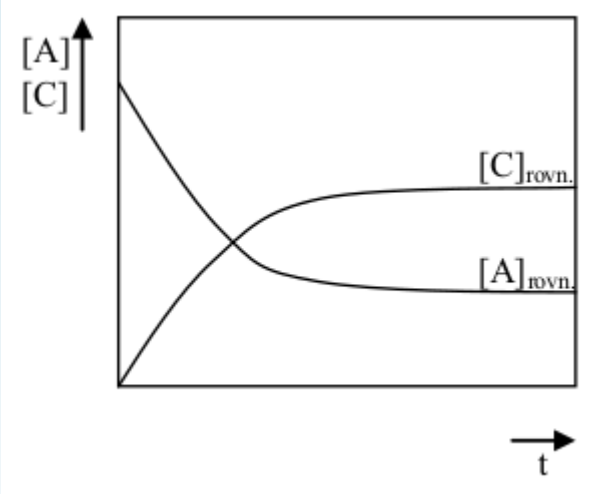

Obr. 22-1: Příklad časových změn skutečné okamžité látkové koncentrace látek pro vratnou reakci

Uvažujeme vratnou endotermickou reakci:

$$A + B \rightleftharpoons C + D$$ endotermická reakce $(\Delta H > 0)$

$$\alpha A + \beta B \rightleftharpoons \gamma C + \delta D \qquad (22\text{-}1)$$

A, B, C, D ... symboly chemických látek

A, B – výchozí látky neboli reaktanty

C, D – produkty

$\alpha, \beta, \gamma, \delta$ ..... stechiometrické koeficienty

b. **látkových koncentrací**

$$K_c = \frac{[C]^{\gamma}[D]^{\delta}}{[A]^{\alpha}[B]^{\beta}} \qquad (22\text{-}3)$$

K_c . rovnovážná konstanta vyjádřená pomocí látkových koncentrací

$[A]$ skutečná (nikoli analytická) rovnovážná látková koncentrace látky; písmeno v závorce označuje chemickou látku, horní index odpovídající stechiometrický koeficient – viz (22-1)

$$\Delta G_r^{\circ} = -RT \ln K_a \qquad (22\text{-}6)$$

ΔG_r° ..... reakční Gibbsova energie za standardních podmínek

R ..... molární plynová konstanta

T ..... termodynamická teplota

K_a ..... rovnovážná konstanta vyjádřená pomocí aktivit

IMR
Energy dependence

$$N_4^+ + He \rightarrow N_2^+ + N_2 + He$$

Endothermic IMR

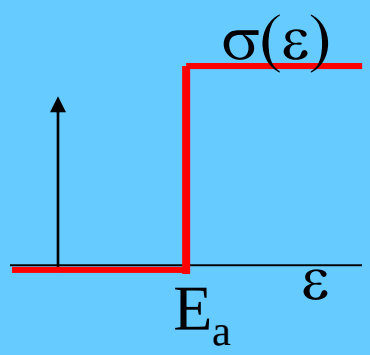

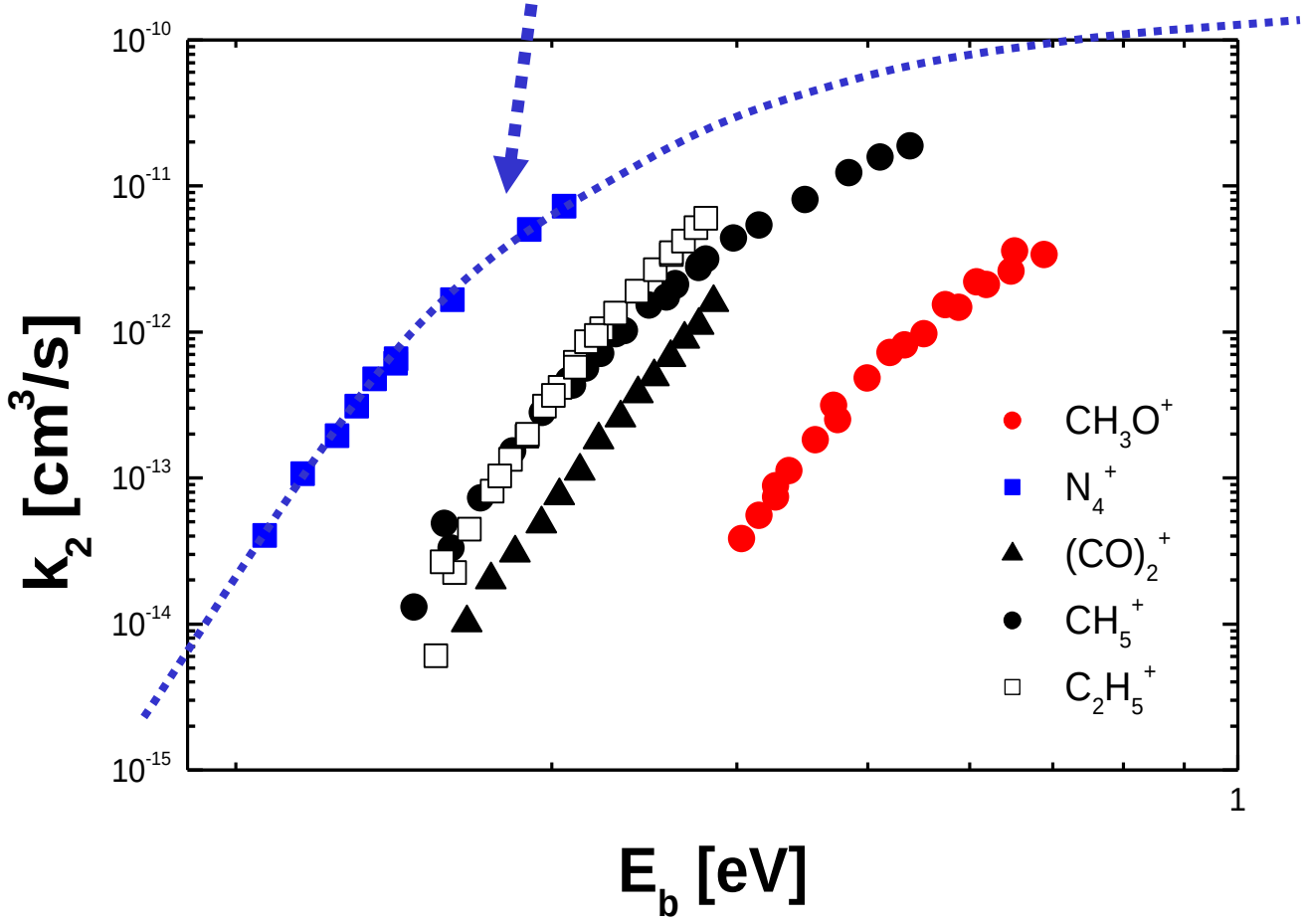

CID – binary process

$$CO^{+} \cdot N_2 \quad + \quad N_2 \xrightarrow{k_{CID}} product$$

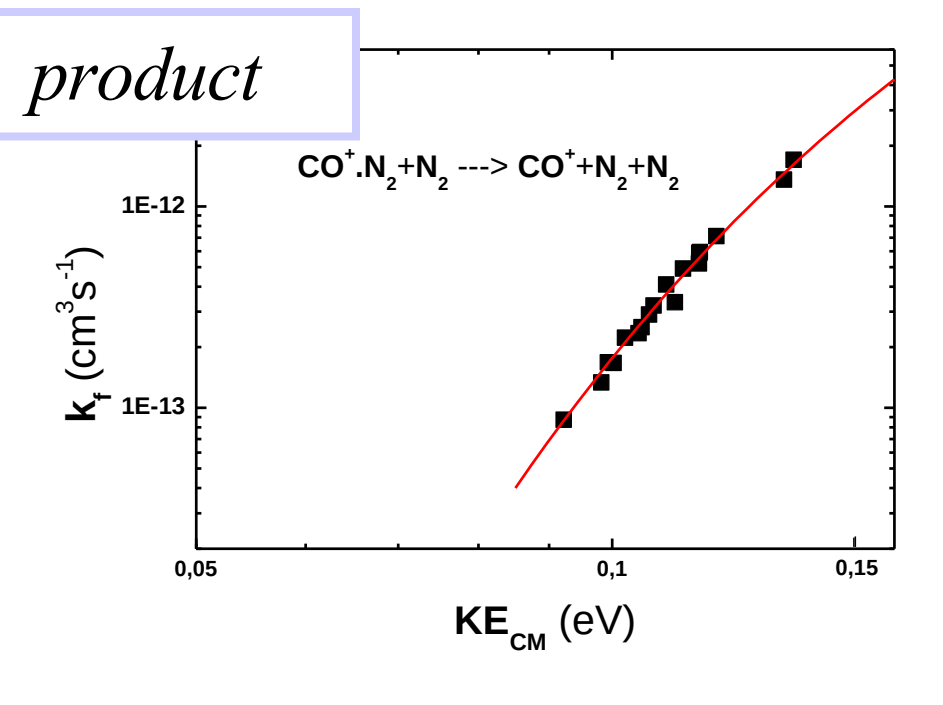

Association reactions - three body reactions

$$CO^{+} \quad + \quad N_2 \quad + \quad N_2 \xrightarrow{k_{ASOC}} CO^{+} \cdot N_2 \quad + \quad N_2$$

$$CO^{+} \cdot N_2 \quad + \quad N_2 \underset{k_r}{\overset{k_f}{\rightleftharpoons}} CO^{+} \quad + \quad N_2 \quad + \quad N_2$$

IMR k = k(1/E) diagram

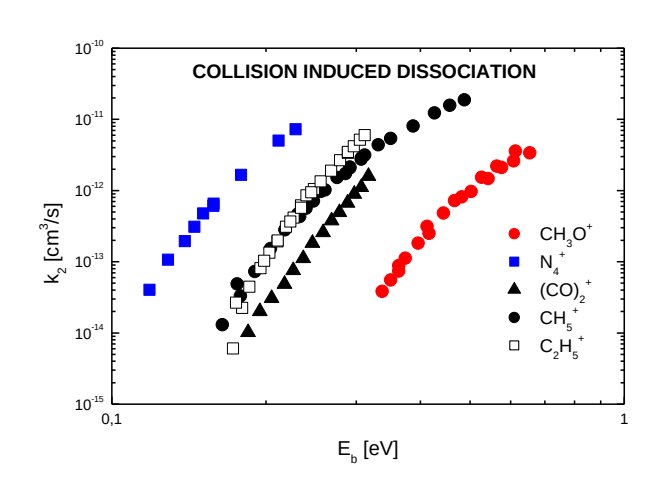

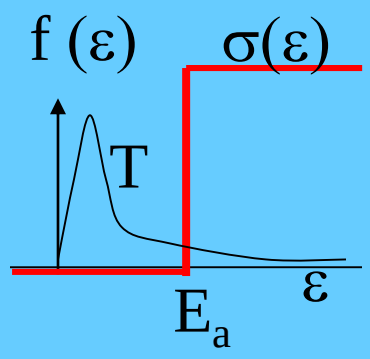

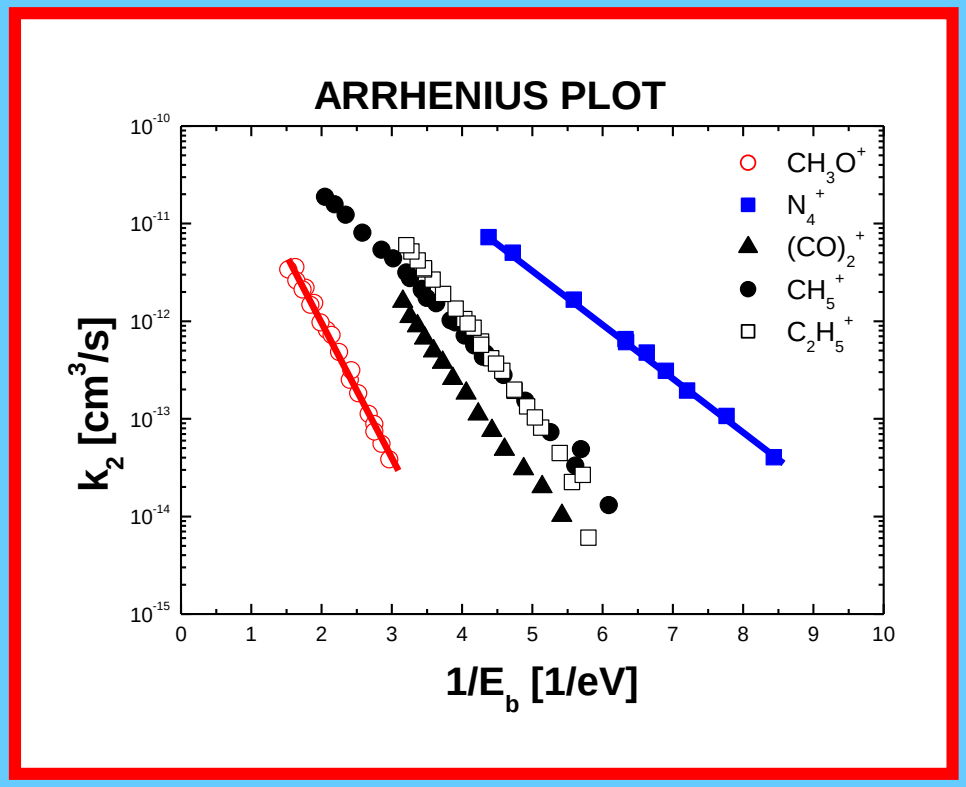

The Arrhenius Equation

Experimental observation : k=Aexp(-B/T)
1889 Arrhenius sugested expression:

$k=Aexp(-E_a/RT)$ Arrhenius equation

A - pre exponential factor or Frequency factor
E_a – activation energy

Better definition is $\ln k = (-E_a/RT) + \ln A$
Dependence of lnk versus 1/T will have a slope equal $-E_a/R$

Boltzmann's Distribution Law

Boltzmann distribution law

$$N_i/N = [\exp(-\varepsilon_\iota /kT)]/[\Sigma \exp(-\varepsilon_\iota /kT)]$$

$$N_2/N_1 = \exp(-(\varepsilon_2-\varepsilon_1)/kT)$$

$$N_i/N = g_i [\exp(-\varepsilon_\iota /kT)]/g$$

g – molecular partition function

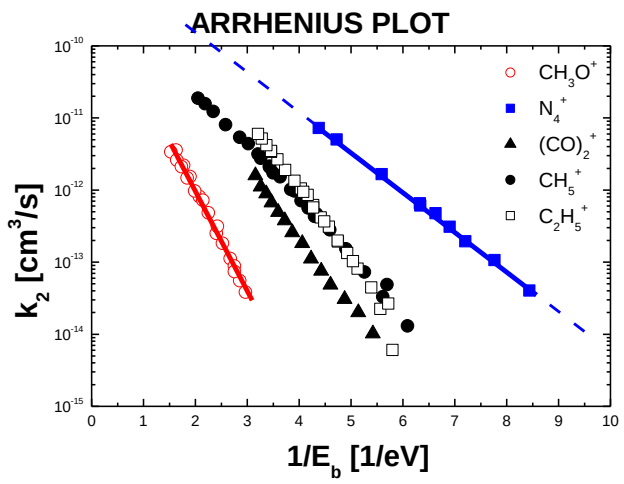

Endothermic reactions

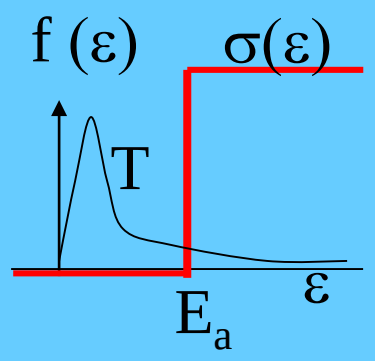

Fraction of collisions, f(ε), with energy ε

f(ε) = dN(ε)/N= exp(- ε /kT)d ε/kT

Fraction of molecules with energy > ε is :

$$F = \int_{\varepsilon}^{\infty} f(\varepsilon')\mathrm{d}\varepsilon' = \int_{E}^{\infty} \frac{1}{kT}\exp(-\varepsilon'/\mathrm{kT})\mathrm{d}\varepsilon' = \exp(-\varepsilon/\mathrm{kT}) = \exp(-E/\mathrm{RT})$$

A + B → products

$dN_A/dt = -kN_AN_B$

$dN_A/dt = Z_{AB}\exp(-E/RT) = N_AN_B\sigma\langle u_r\rangle \exp(-E/RT)$

$k = \sigma\langle u_r\rangle \exp(-E/RT)$

From experiment

$k = A\exp(-E_a/RT)$

Potential energy surface 3D

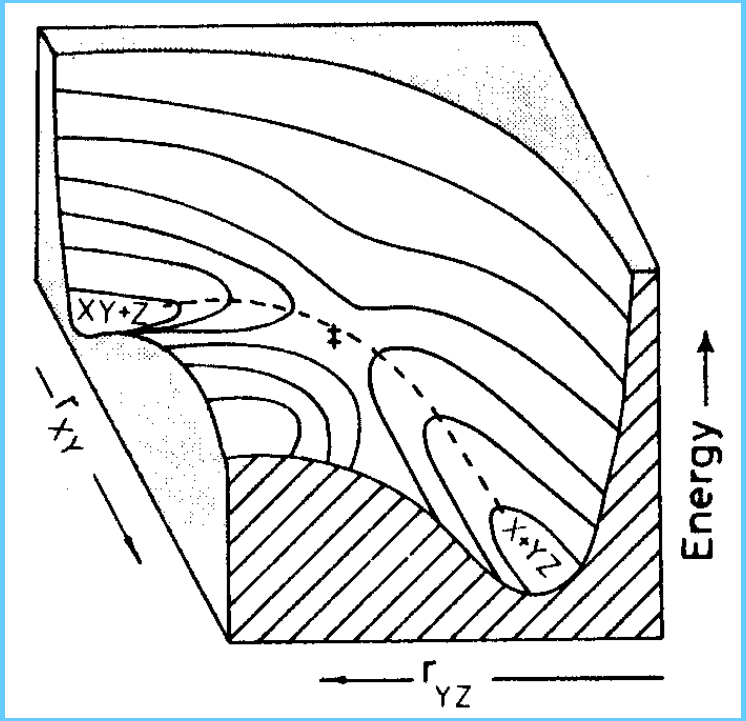

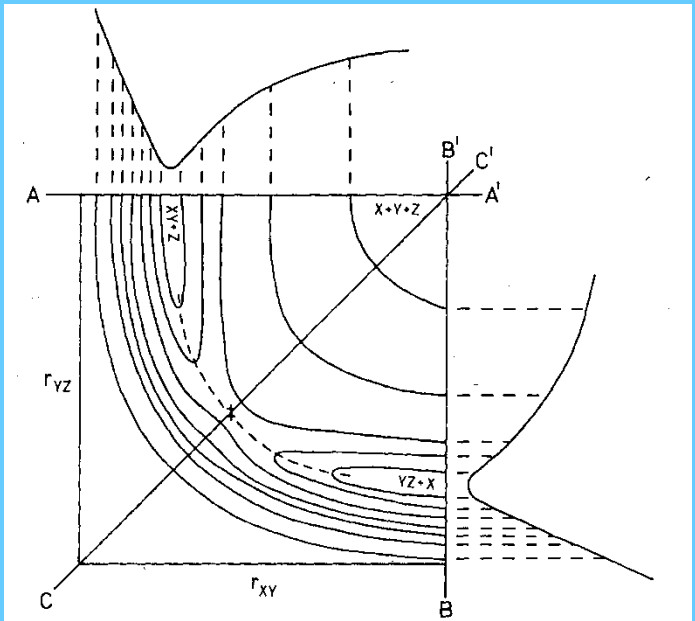

Figure 45 Contour representation of a potential energy surface for the replacement reaction XY + Z → X + YZ.

$$XY + Z \rightarrow ZY + X$$

Reaction coordinate

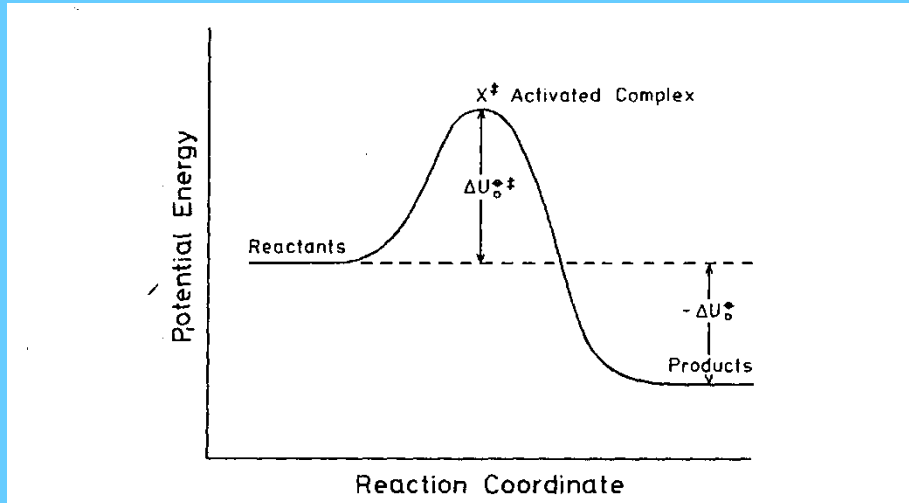

Figure 46 Variation in potential energy along the reaction coordinate for any elementary reaction at zero Ke

Temperature dependence of IMR - CID

COLLISION INDUCED DISSOCIATION

$$AB^+ + M \xrightarrow{k} A^+ + B + M$$

CID - can be considered as binary process

$$N_4^+ + He \rightarrow N_2^+ + N_2 + He$$

Bond energy ~1eV

$[N_4^+] = [N_4^+]_0 \exp(-E_A/kT)$

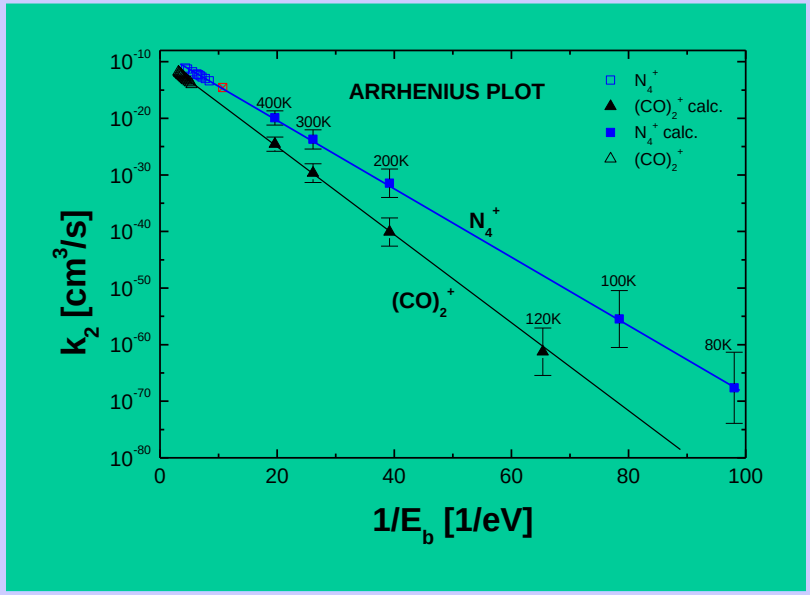

Can be considered also as unimolecular decay !!!

$$N_4^+ \rightarrow N_2^+ + N_2$$

J. Glosik, V. Skalsky and W. Lindinger,
Observation of Arrhenius behaviour over 56 decades: Dissociation of N_4^+ Ions, Int. J. Mass .Spectr. Ion Proc., **134**, 67, 1994
J. Glosik, V. Skalsky, C. Praxmarer, D. Smith, W. Freysinger and W. Lindinger,
Dissociation of Kr_2^+, N_2Ar^+, $(CO)_2^+$, CH_5^+ and $C_2H_5^+$ Ions Drifting in He, J. Chem. Phys., **101**, 3792, 1994

IMR thermal

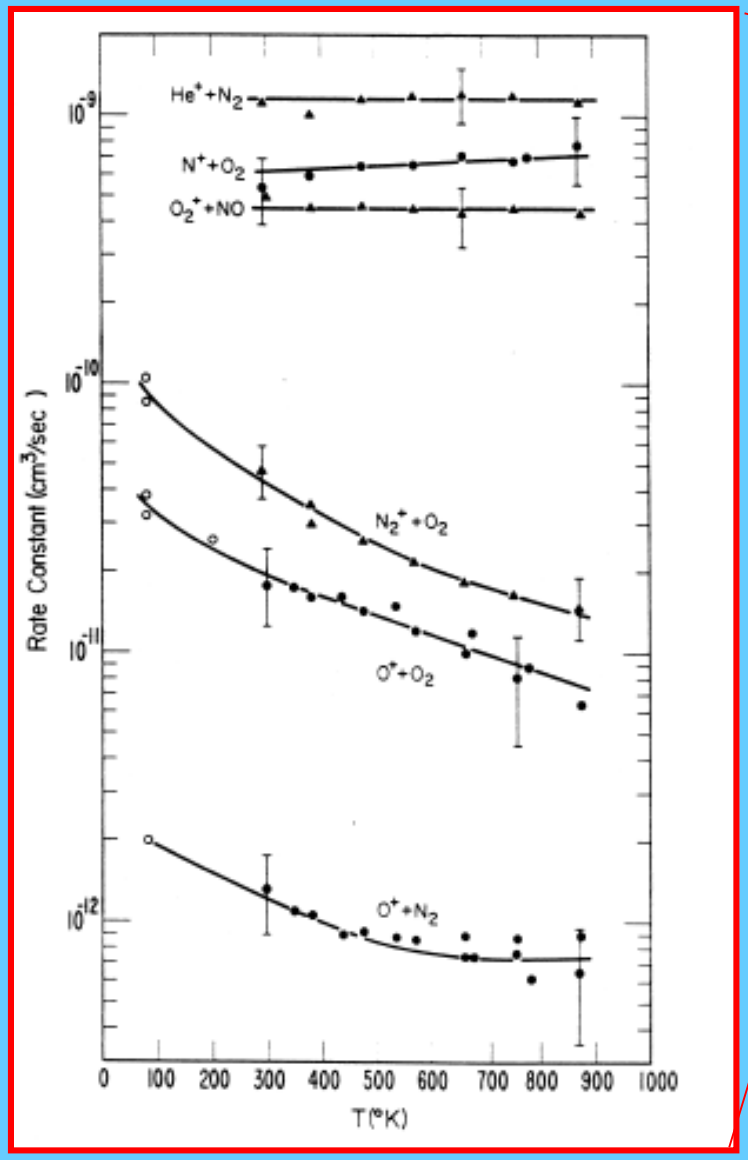

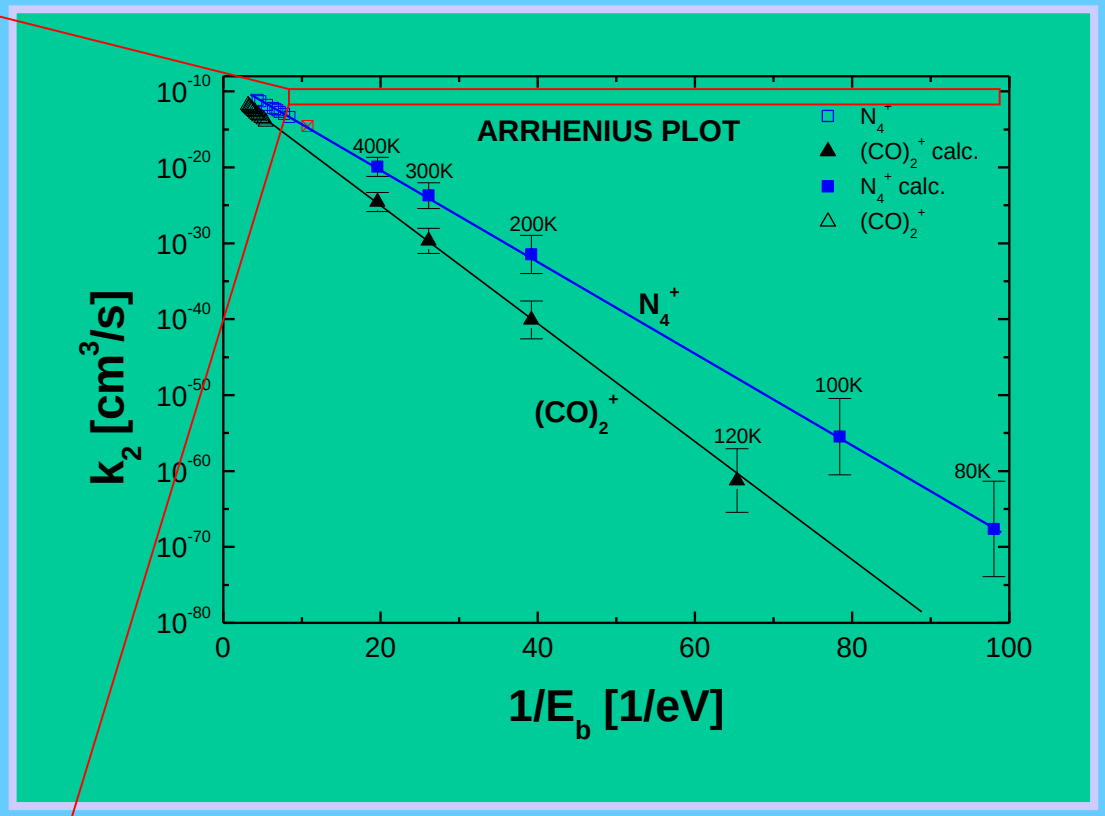

$$[N_4^+] = [N_4^+]_0 \exp(-E_A/kT)$$

IMR Energy dependence eV region

Endothermic IMR

$$N_4^+ + He \rightarrow N_2^+ + N_2 + He$$

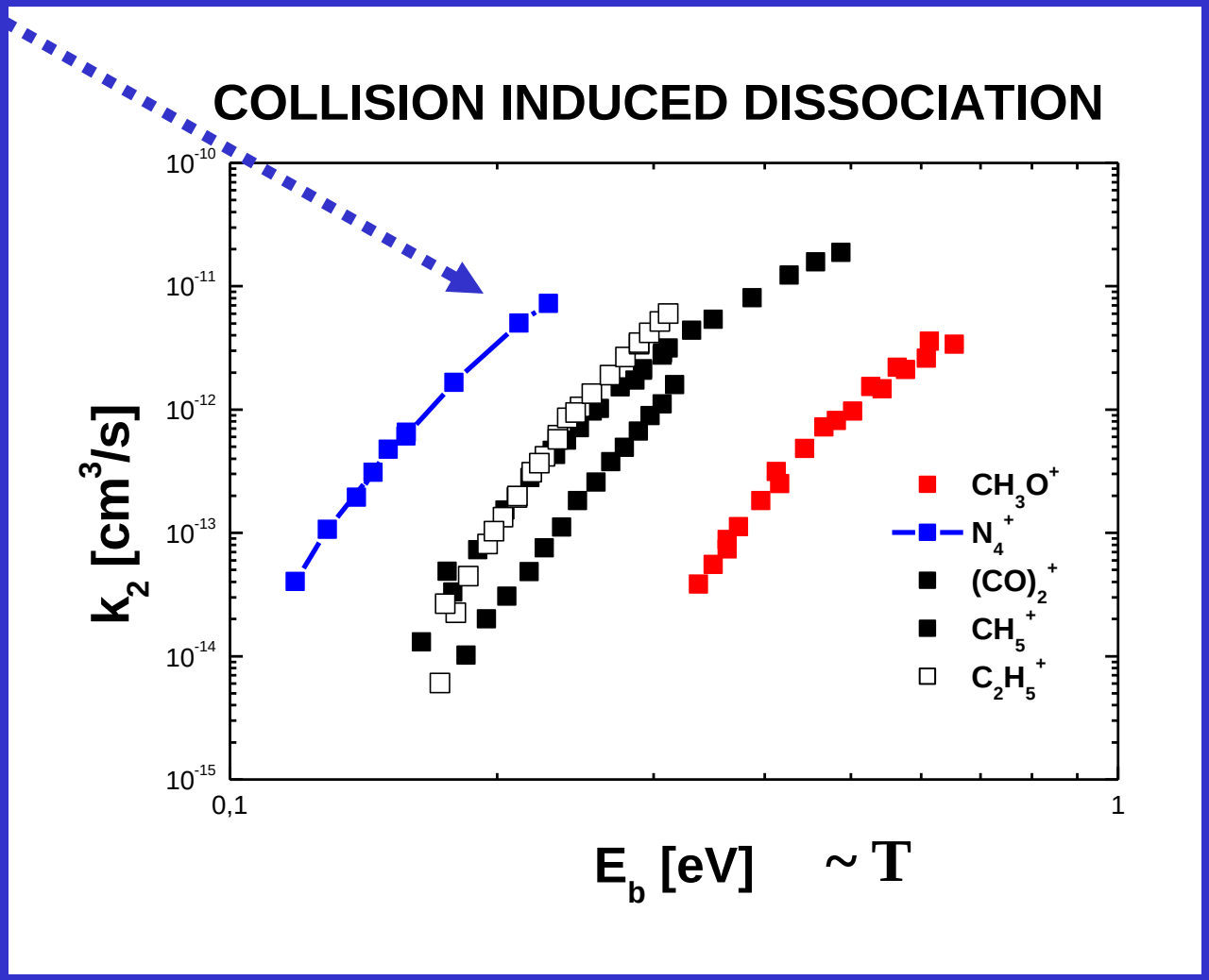

At this point without discussion

Reaction rate coefficients

Typical values of at 300K (approximate values)

	reactants		products	rate coefficient
Electron atomic ion rec.	$A^+ + e^-$	➔	$A + h\nu$	$\sim 10^{-11} cm^3 s^{-1}$
Electron - ion recomb.	$O_2^+ + e^-$	➔	$O + O$	$2x10^{-7} cm^3 s^{-1}$
Electron – cluster ion recomb.	$H_5^+ + e^-$	➔	products	$3.5x10^{-6} cm^3 s^{-1}$
Ion – ion recombination	$Ar^+ + Cl^-$	➔	$Ar + Cl$	$2x10^{-8} cm^3 s^{-1}$
Ion – molecule reactions	$H_2^+ + H_2$,	➔	$H_3^+ + H$	$2x10^{-9} cm^3 s^{-1}$
	$H_3^+ + H_2 + He$	➔	$H_5^+ + He$	$k_{eff\ BIN} = k_3 x[He]$
				$k_3 < 2x10^{-29} cm^6 s^{-1}$
Attachment	$CCl_4 + e^-$		$Cl^- + CCl_3$	$\sim 10^{-7} cm^3 s^{-1}$
Penning ionization	$He^* + Ar$		$Ar^+ + e^- + He$	$7x10^{-11} c$.

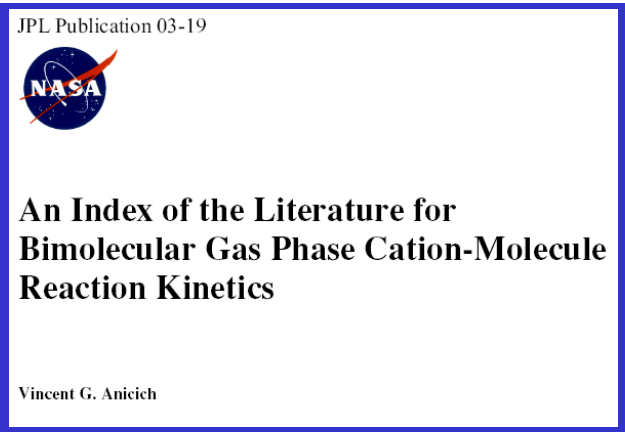
JPL Publication 03-19

An Index of the Literature for Bimolecular Gas Phase Cation-Molecule Reaction Kinetics

Vincent G. Anicich

Rate coefficients

Introduction xi
Bimolecular Reactions xiii
Comments on Termolecular Reactions xiv
Notes on the Table xv
Methods Used in Citation xvi
Journals Cited xvii
Publications by Journal xix
The Authors of the articles in this bibliography xx
References for Introduction xxii
The Table of Ion-Molecule Reactions with Reference Numbers 1

H_n^+ 1
HeH_n^+ 29
LiH_n^+ 49
$As_mH_n^+$ 592
$Se_mH_n^+$ 594
$Br_mH_n^+$ 594

National Aeronautics and Space Administration

Jet Propulsion Laboratory
California Institute of Technology
Pasadena, California

November 2003

A^+		B		products			%	k[cm^3s^{-1}]	T		
C^+	+	C_2H_6	→	Products					300	MS	6406
C^+	+	CH_2CCH_2	→	$C_4H_2^+$	+	H_2	0.40	1.40×10^{-9} ±20	300	SIFT	8207
				$C_3H_3^+$	+	CH	0.25				
				$C_2H_2^+$	+	C_2H_2	0.20				
				$C_3H_4^+$	+	C	0.15				
C^+	+	CH_3CCH	→	$C_4H_2^+$	+	H_2	0.30	1.90×10^{-9} ±25	300	SIFT	8207
				$C_3H_4^+$	+	C	0.30				
				$C_3H_3^+$	+	CH	0.20				
				$C_2H_2^+$	+	C_2H_2	0.10				
				$C_2H_3^+$	+	CCH	0.10				
C^+	+	CH_3CHCH_2	→	$C_2H_3^+$	+	$CHCH_2$	0.30	2.00×10^{-9} ±25	300	SIFT	8207
				$C_3H_3^+$	+	CH	0.20				
				$C_3H_3^+$	+	CH_3	0.15				
				$C_2H_2^+$	+	C_2H_4	0.15				
				$C_3H_6^+$	+	C	0.10				
				$C_4H_3^+$	+	H_2 + H	0.10				

Importance of Ion-Molecule Reactions

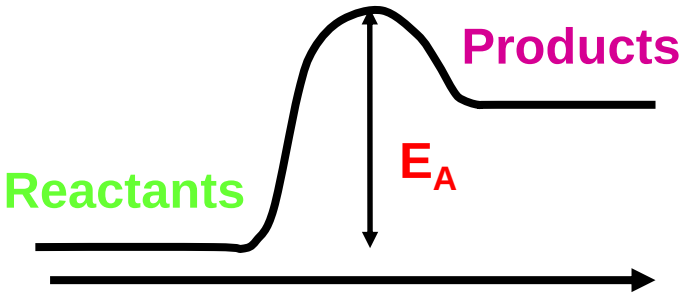

Arrhenius:

$$k(T) = \langle \sigma v \rangle = \mathbf{A} \exp(-E_A/kT)$$

Neutral-Neutral Reactions

$$\mathbf{A} \approx 10^{-11}\ \mathrm{cm^3/s}$$
$$E_A \approx 2000\ \mathrm{K}$$
$$T_{MC} = 10\ \mathrm{K}$$

Ion-Molecule Reactions

$$10^{-7}\ \mathrm{cm^3/s} > \mathbf{A} > 10^{-9}\ \mathrm{cm^3/s}$$
$$E_A \approx 0\ \mathrm{K}$$

Cosmic Ray Ionization → **Ion-Molecule Reactions** → Recombination

E. Herbst, The Physics and Chemistry of Interstellar MCs (1993)

Details of Potential Energy Surface

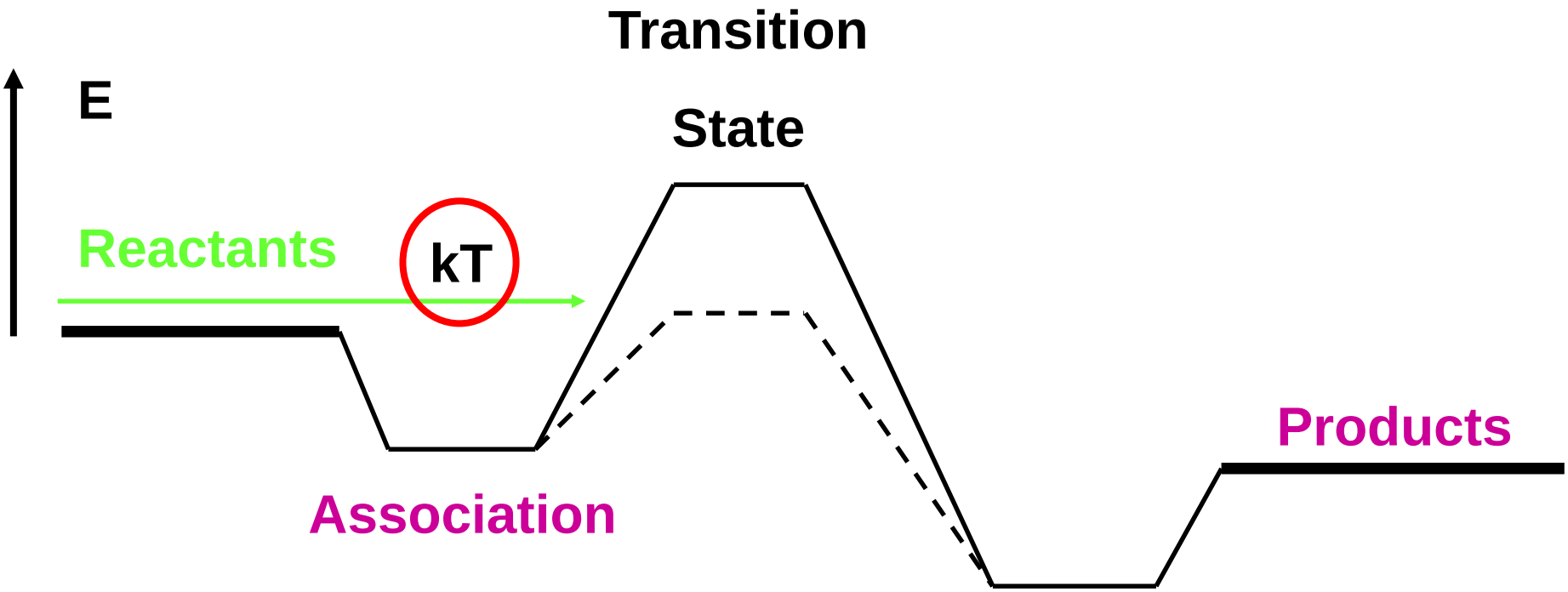

Rotational Energy, Zero Point Energy and Fine Structure Energy

Example I: Negative Temperature Dependence

$$NH_3^+ + H_2 \rightarrow NH_4^+ + H$$

Gas Phase Formation of Ammonia

$$NH_n^+ + H_2 \rightarrow NH_{n+1}^+ + H$$

$n = 0,1,2,3$

Implications of a barrier along reaction path

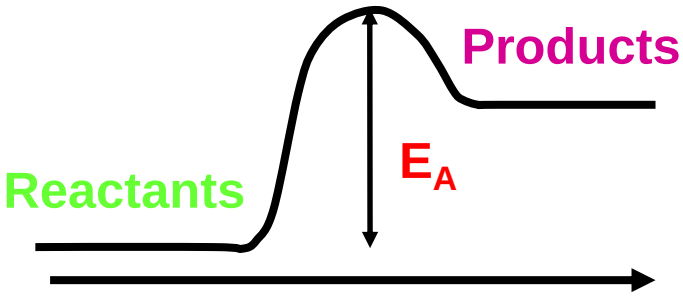

Arrhenius:

$$k(T) = \langle \sigma v \rangle = A \exp(-E_A/kT)$$

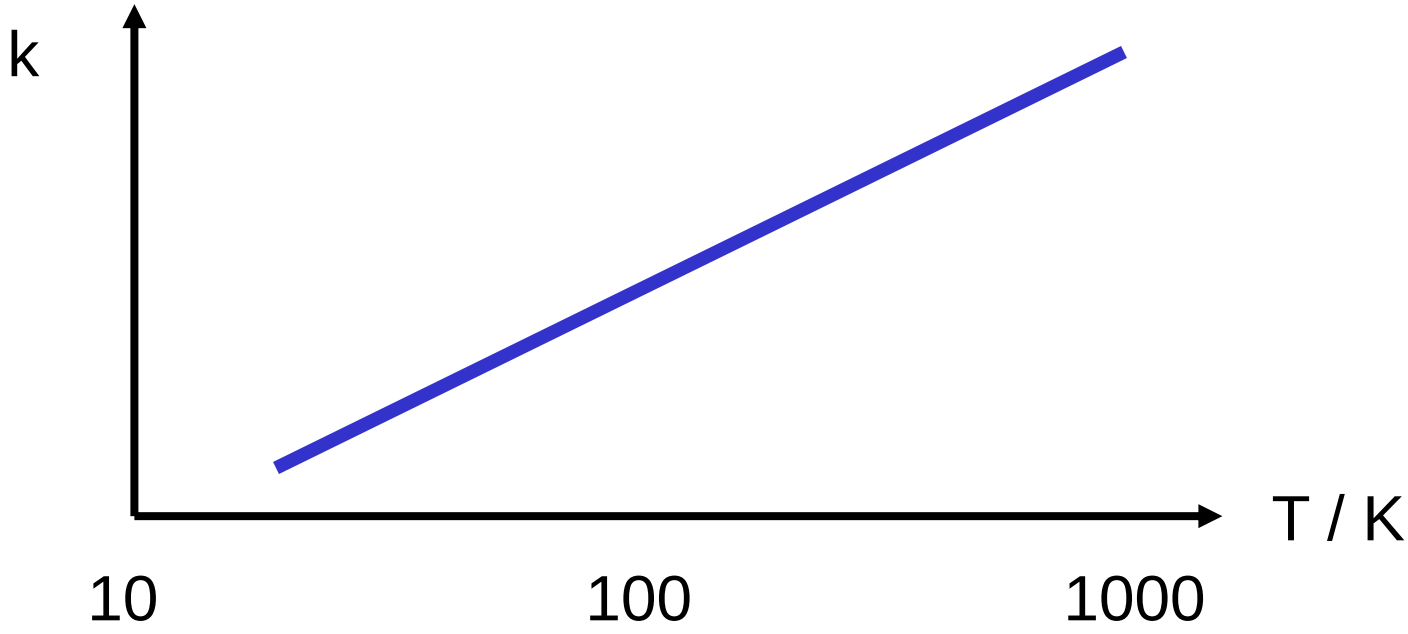

Negative Temperature Dependence

$$NH_3^+ + H_2 \rightarrow NH_4^+ + H$$

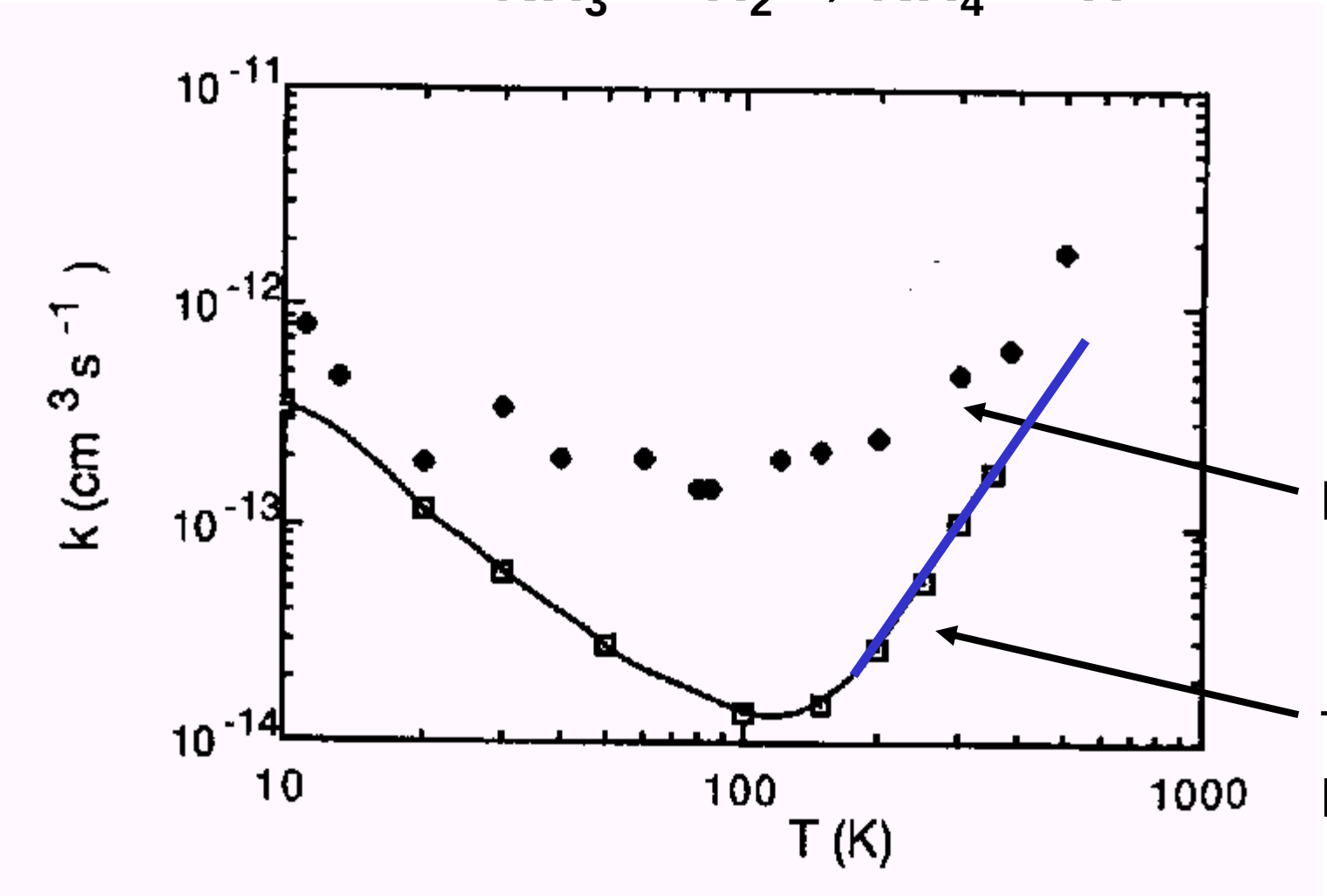

Herbst et al. J.Chem.Phys. 1991

Lowest energy path for
$NH_3^+ + H_2 \rightarrow NH_4^+ + H$

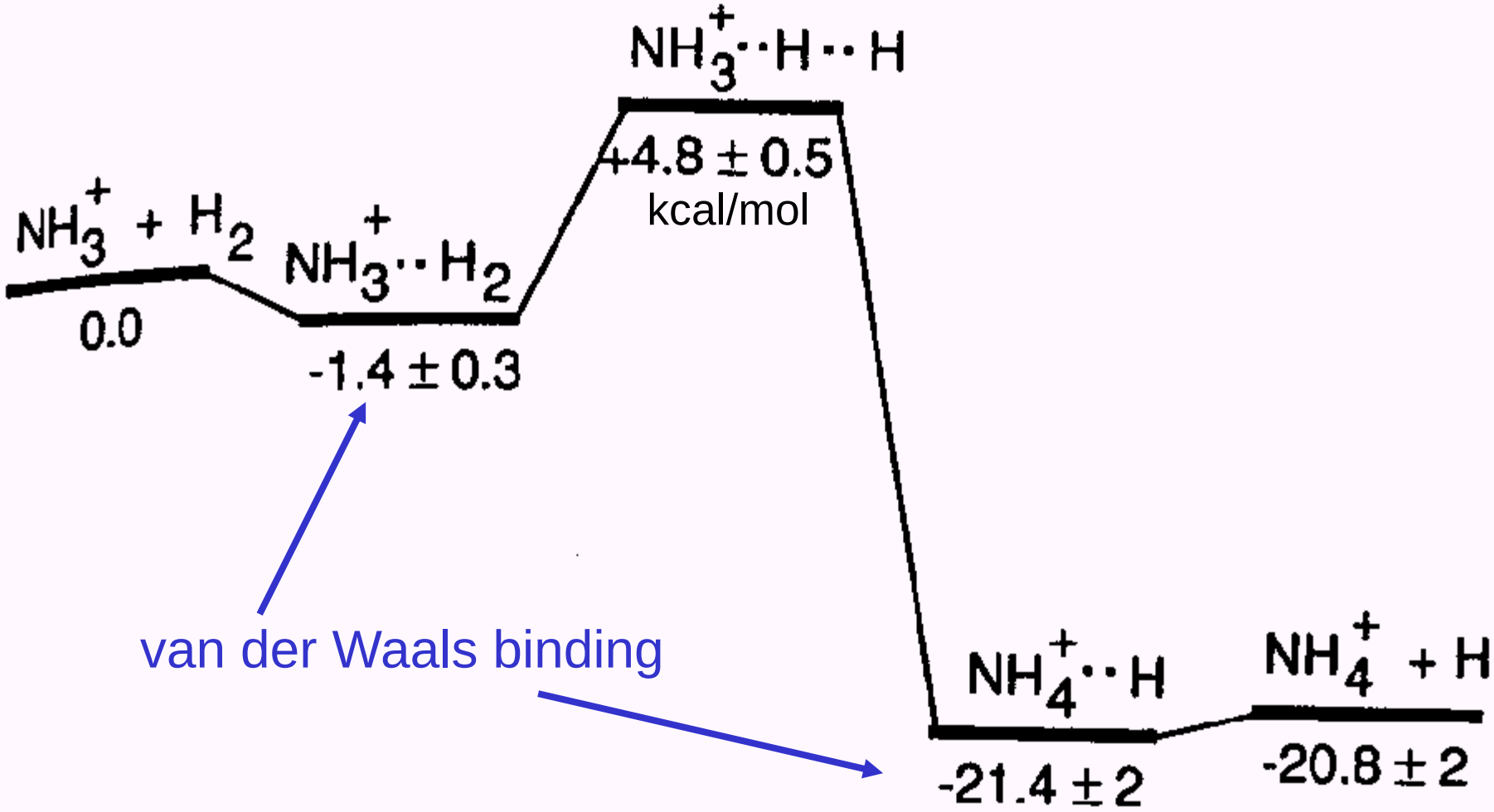

Herbst et al. J.Chem.Phys. 1991

Negative Temperature Dependence

$$NH_3^+ + H_2 \rightarrow NH_4^+ + H$$

- $k << k_L$ — 1 in 10000 collisions leads to reaction
- Turnover at 100 K
- barrier height 4.8 kcal/mol (2400 K)
- Tunneling is a dominant mechanism at low temperatures

Ion molecule reactions

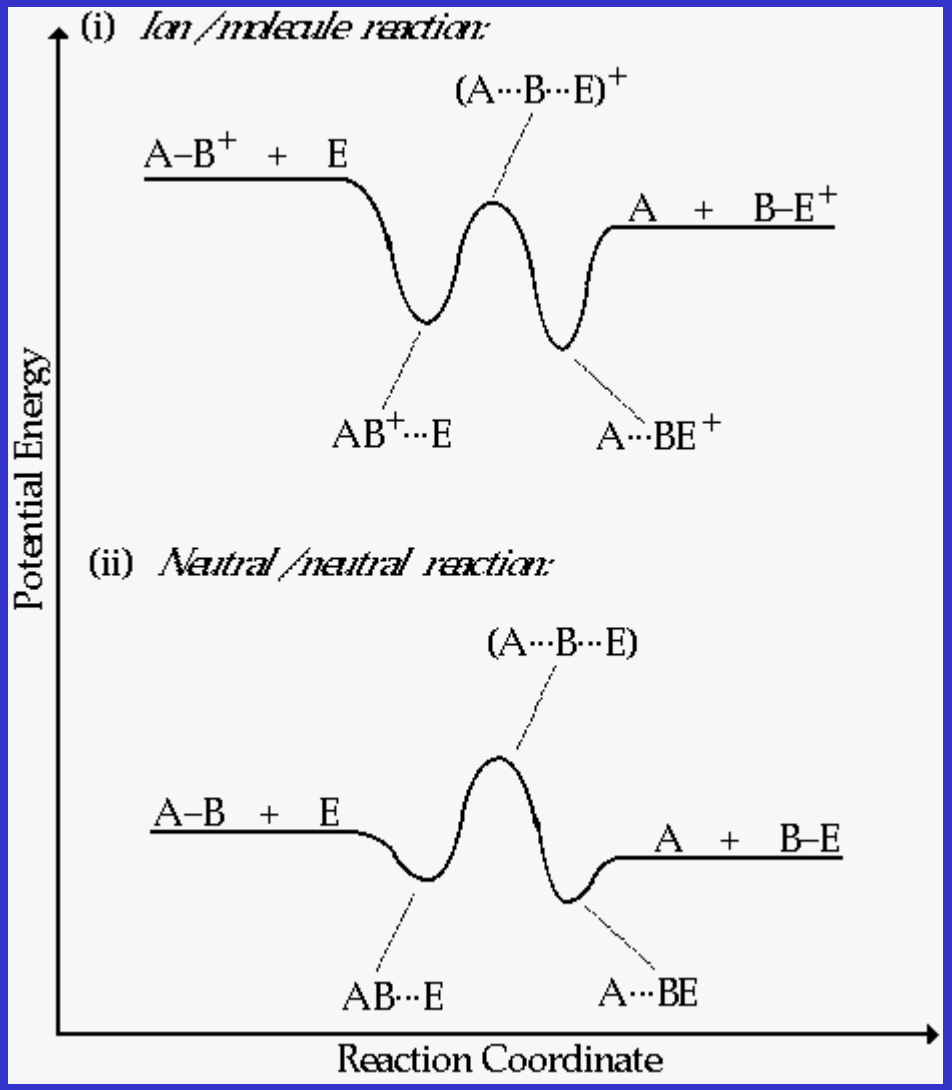

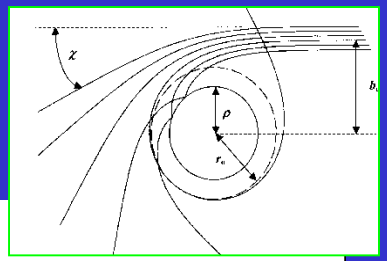

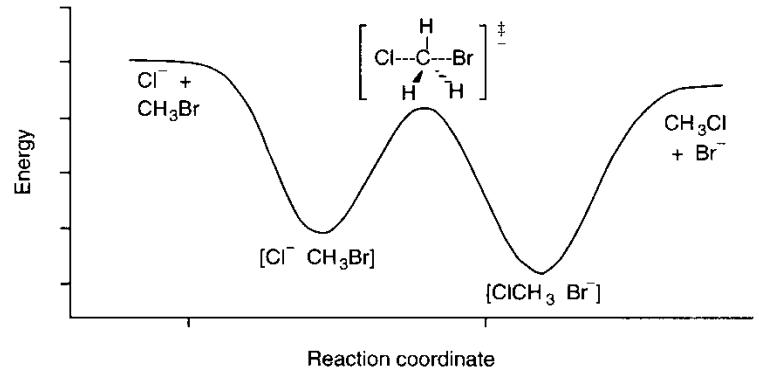

Figure 1
Double-well potential energy surface for the reaction of Cl^- with CH_3Br (after Olmstead and Brauman (*3*)).

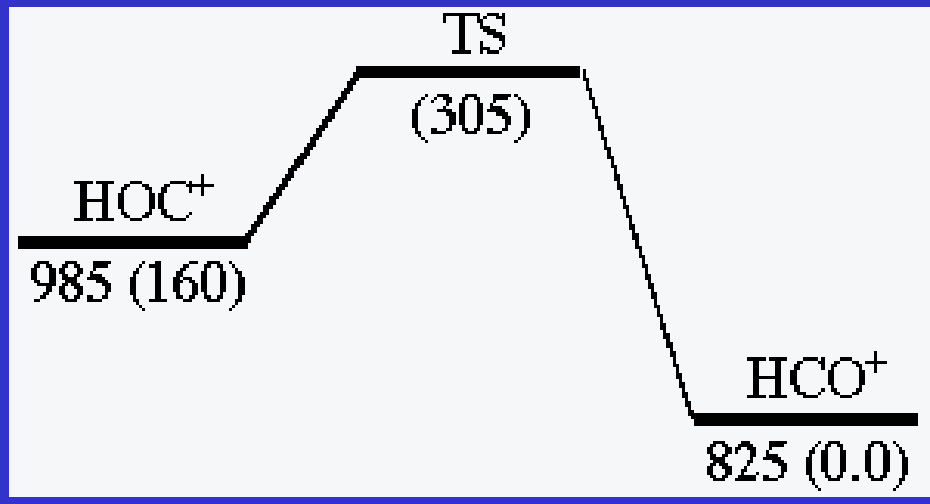

Závislost reakční rychlosti na teplotě

Reaction mechanism

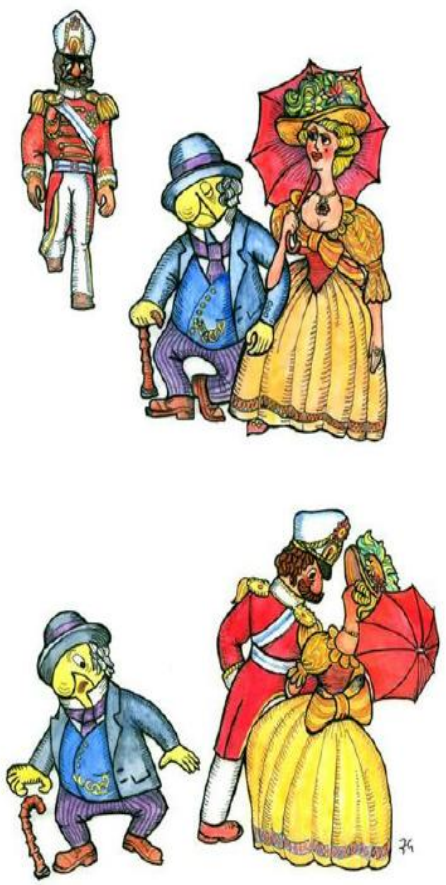

Reaction Mechanisms in Pictures: Spectator Stripping

Reaction Mechanisms in Pictures: Long-Lived Complex Formation

Reaction coordinate

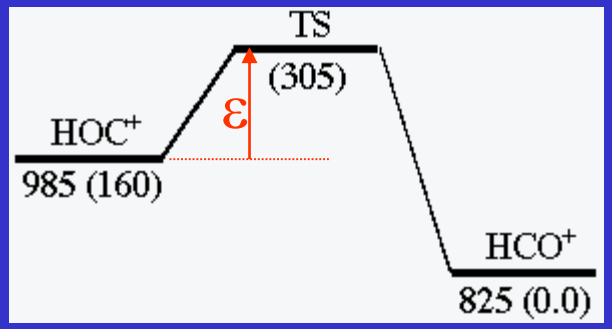

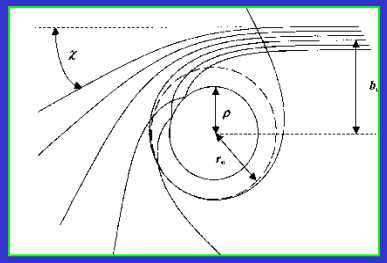

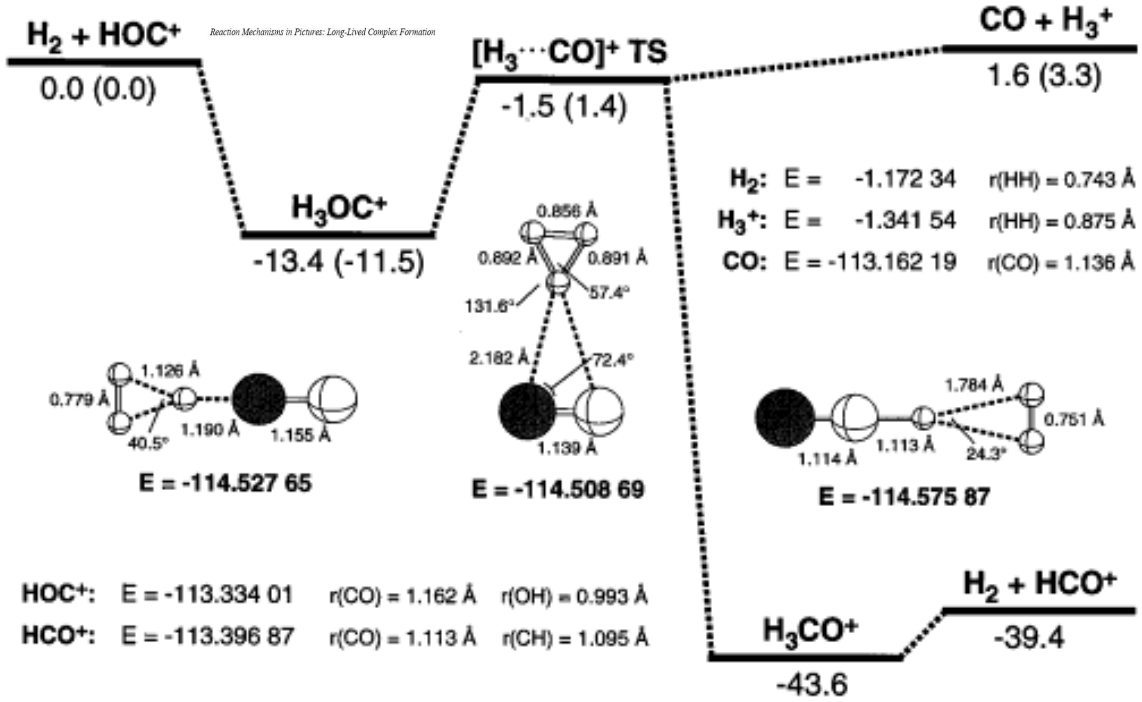

FIG. 1.—The minimum energy potential pathway from $HOC^+ + H_2$ reactants to two sets of products: $HCO^+ + H_2$ and $CO + H_3^+$. The computed relative energies (kcal mol^{-1}) listed for the stationary points (reactants, complexes, transition state, and products) are given without and with zero-point energy corrections. Corrected values are in parentheses. The structures of the two complexes and transition state are shown with bond lengths in angstroms (Å) and bond angles in degrees. Calculated absolute energies are in hartrees (1 H = 3.16×10^5 K).

Potential energy 3D

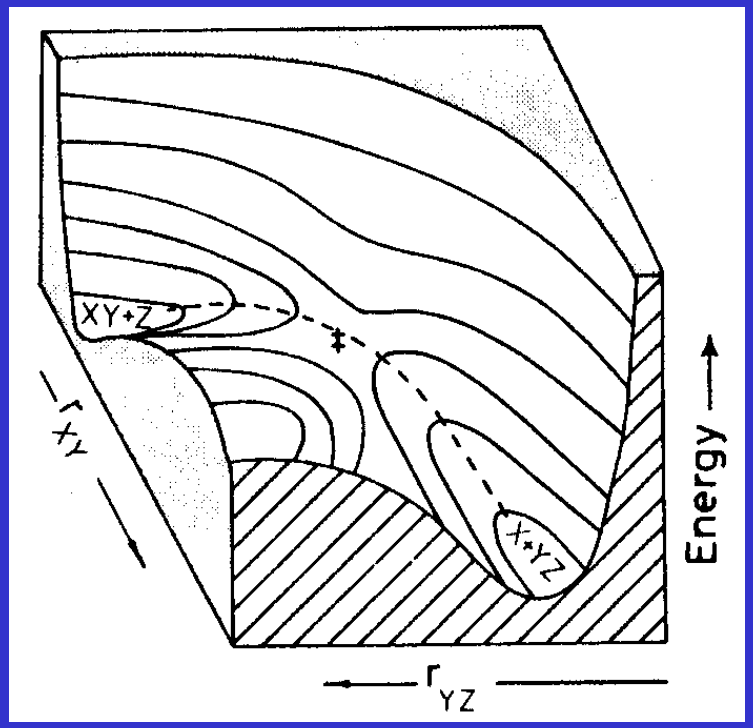

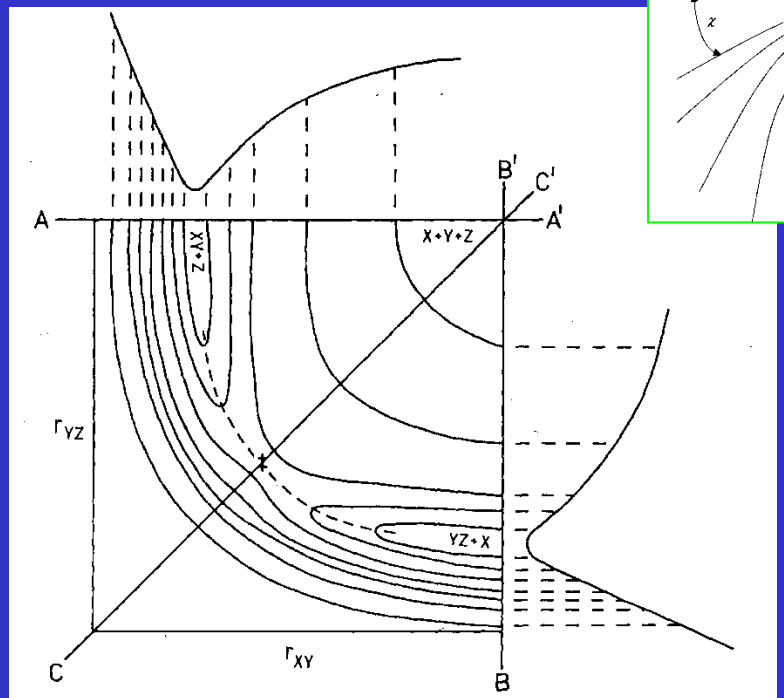

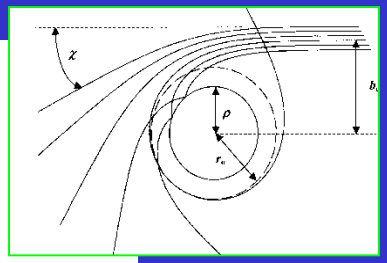

Figure 45 Contour representation of a potential energy surface for the replacement reaction XY + Z → X + YZ.

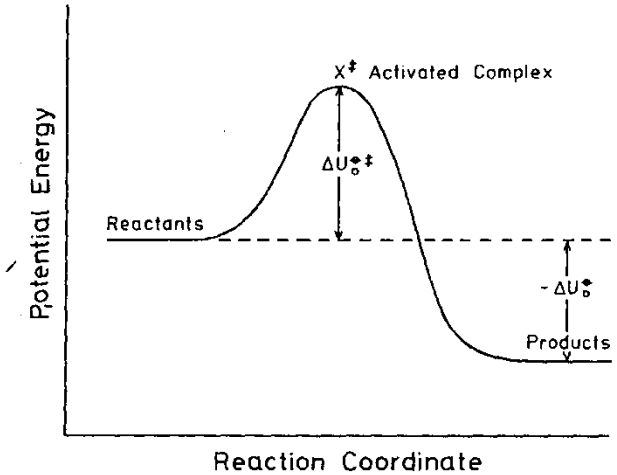

Figure 46 Variation in potential energy along the reaction coordinate for any elementary reaction at zero Ke

Reaction proceeding via intermediate states

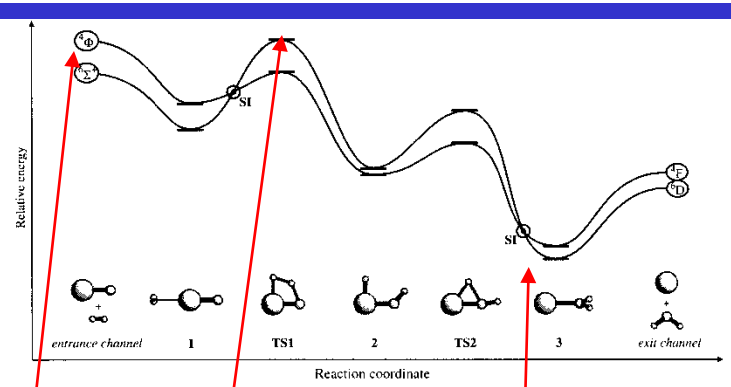

Figure 3
Reaction pathways on the sextet and quartet potential energy surfaces for the gas-phase reaction $H_2 - FeO^+ \rightarrow Fe^+ + H_2O$ (reproduced by permission of Wiley-VCH from (*31*)).

Table 5
Computed energies (kJ mol^{-1}) of stationary points for the activation of H_2 by FeO^+ (D_0 relative to separated FeO^+ ($^6\Sigma^+$) + H_2).

	BP86[a]	B3LYP[a]	B3LYP[b]	CCSD(T)[b]	CASPT2[c]
$FeO^+(^4\Phi) + H_2$	53	33	31	52	80
^{6}1	−68	−64	−53	−50	−22
^{4}1	−68	−28	−23	1	15
^{6}TS1	29	35	40	53	77
^{4}TS1	0	3	4	31	24
^{6}2	−139	159	142	−130	−61
^{4}2	170	−171	−160	−124	−121
^{6}TS2	−28	−54	−48	27	
^{4}TS2	−128	−141	−124	−91	
^{6}3	−226	−307	−276	291	−280
^{4}3	260	−330	−312	−280	
$Fe^+(^6D) + H_2O$	−16	−161	−139	−133	−151
$Fe^+(^4D) + H_2O$	−34	−171	−157	−156	

[a] Wachters basis for Fe, Dunning TZ2P basis for H and O (*64*). [b] Modified Ahlrichs TZVP basis for Fe, 6-311 + + G(2df,2p) for H and O (*65*). [c] ANO [8s7p6d4f2 g] basis for Fe, [3s2p1d] and [5s4p3d2f] for H and O, respectively (*63*).

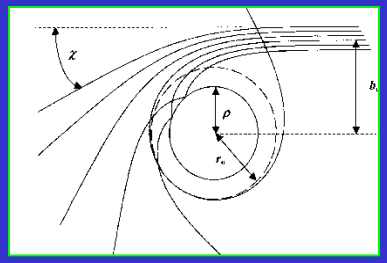

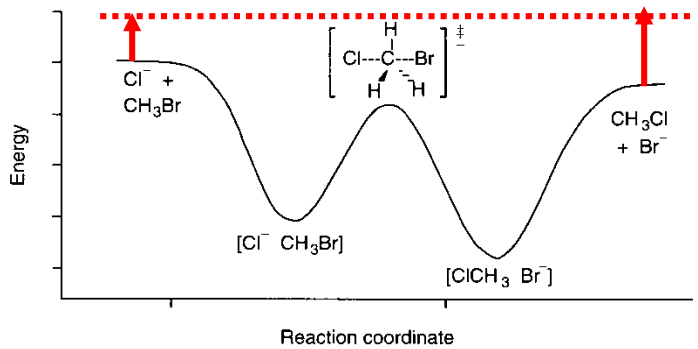

Figure 1
Double-well potential energy surface for the reaction of Cl^- with CH_3Br (after Olmstead and Brauman (*3*)).

Rate Law

- **rate = $k[A]^x[B]^y$**
- **rate order = x + y**
- **knowledge of order can help control reaction**
- **rate must be experimentally determined**

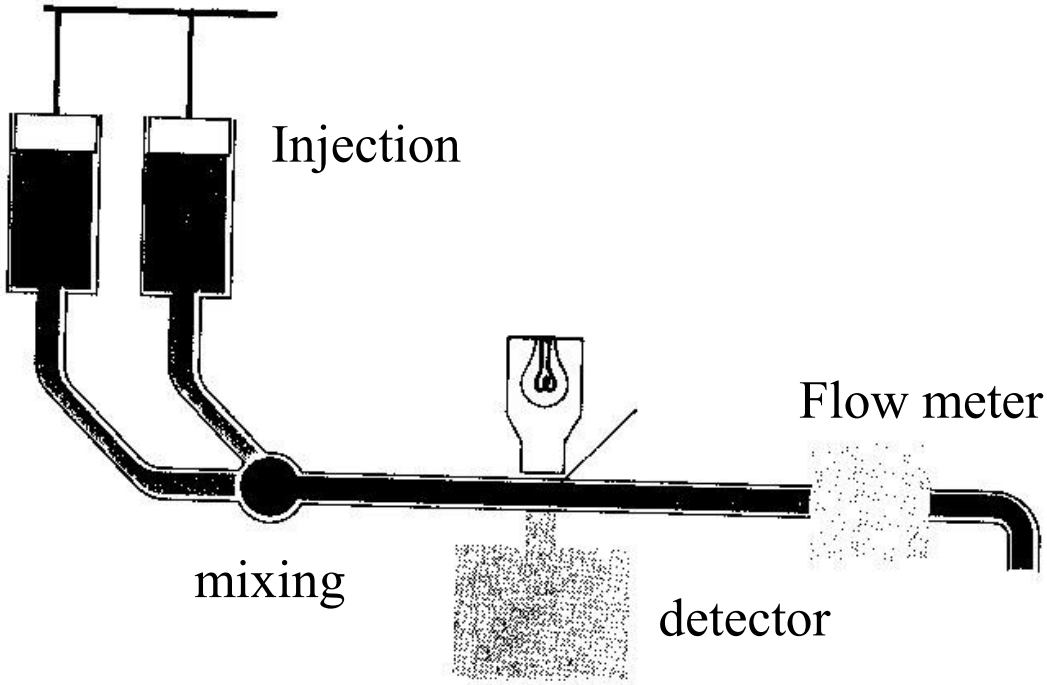

FA– Flowing Afterglow principle

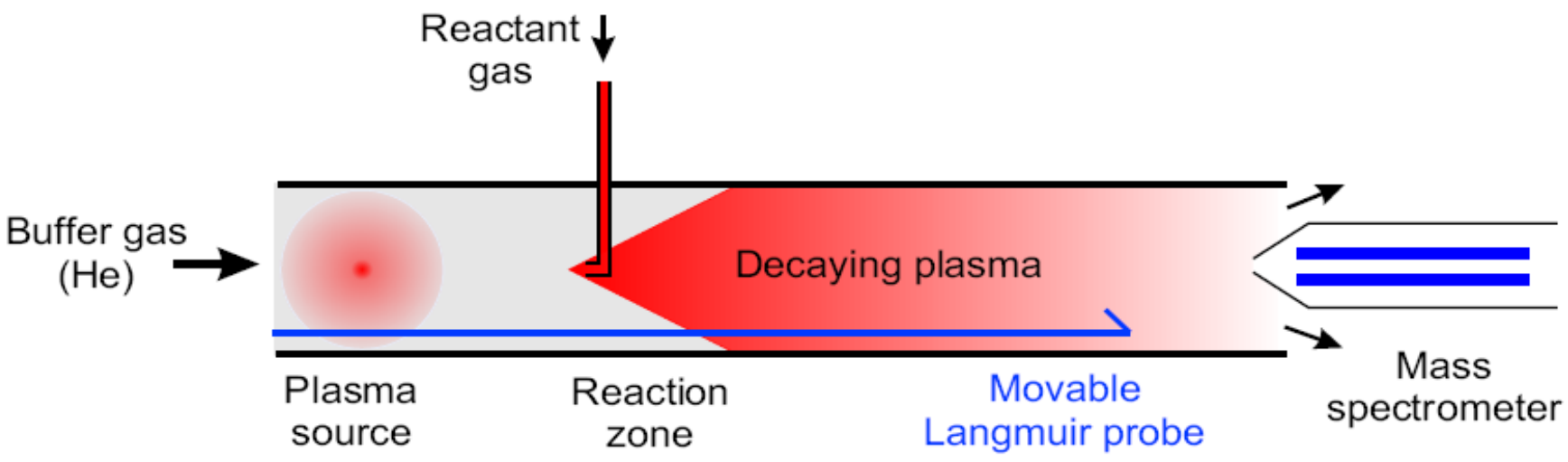

Figure 1.1: The basic principle of FA and FALP techniques.

Techniques for study of IMR – FALP 1965

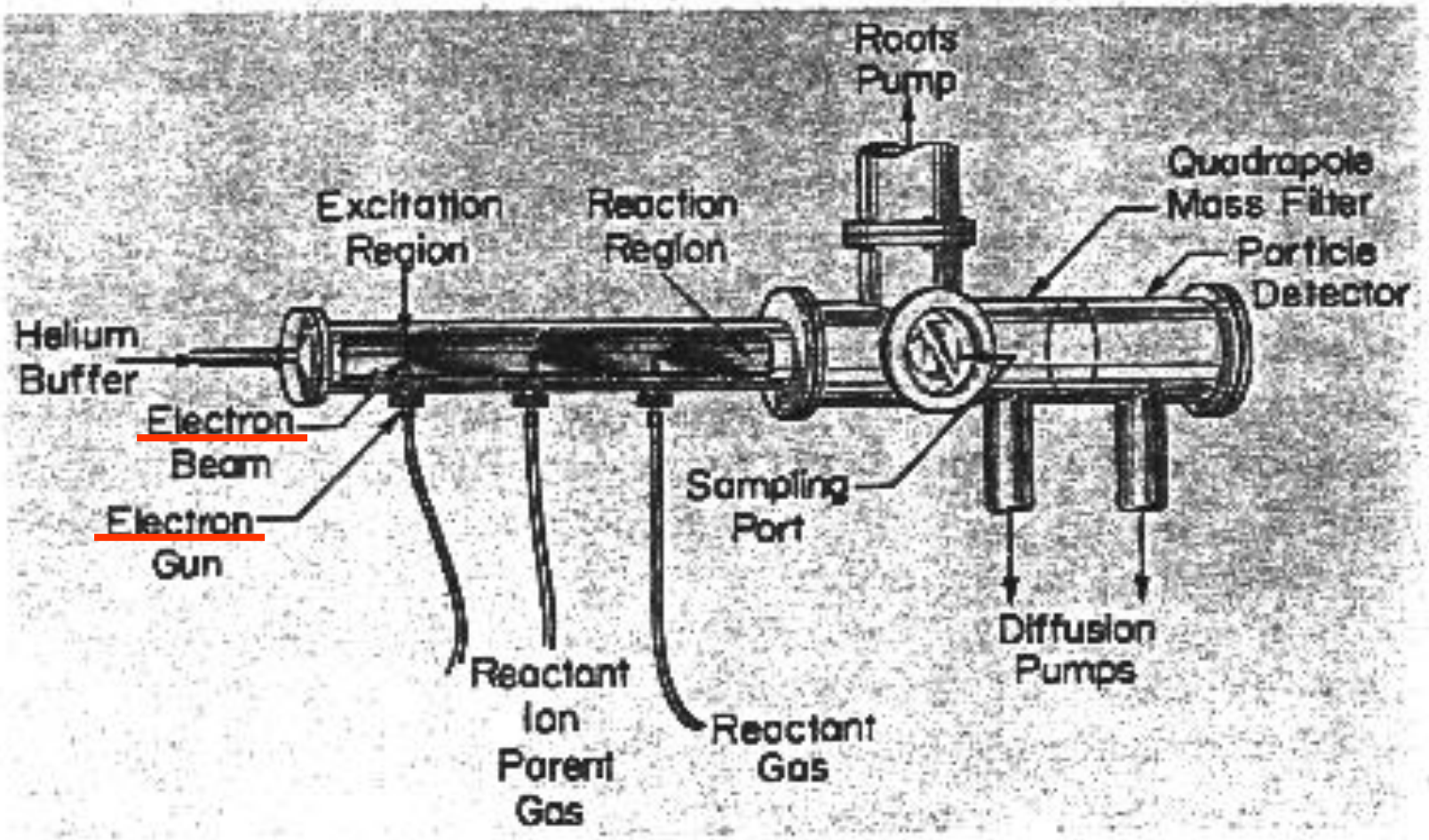

FIG. 1. Pictorial representation of the flowing afterglow tube.

Experimental studies of IMR ➔FA

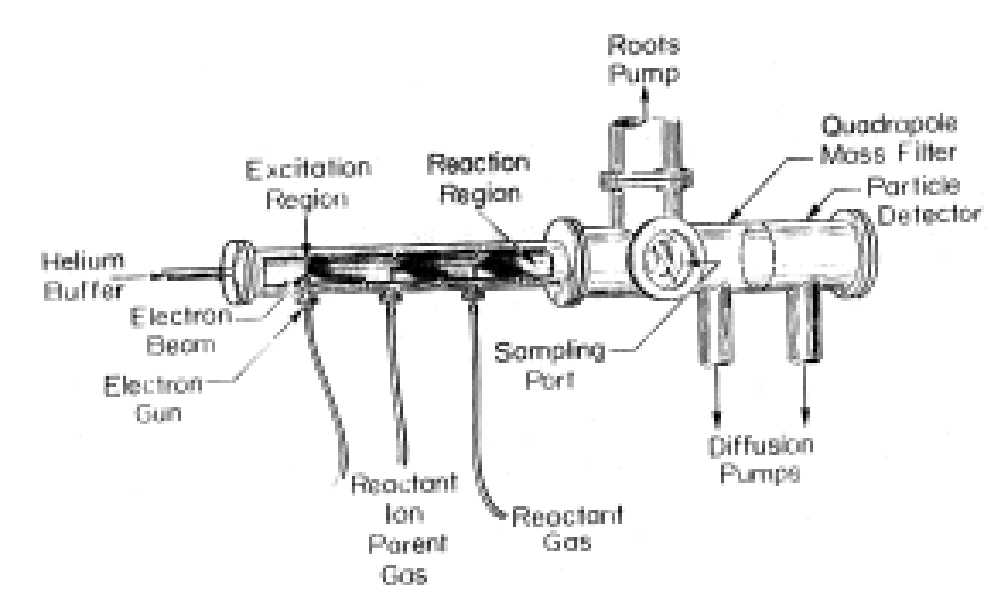

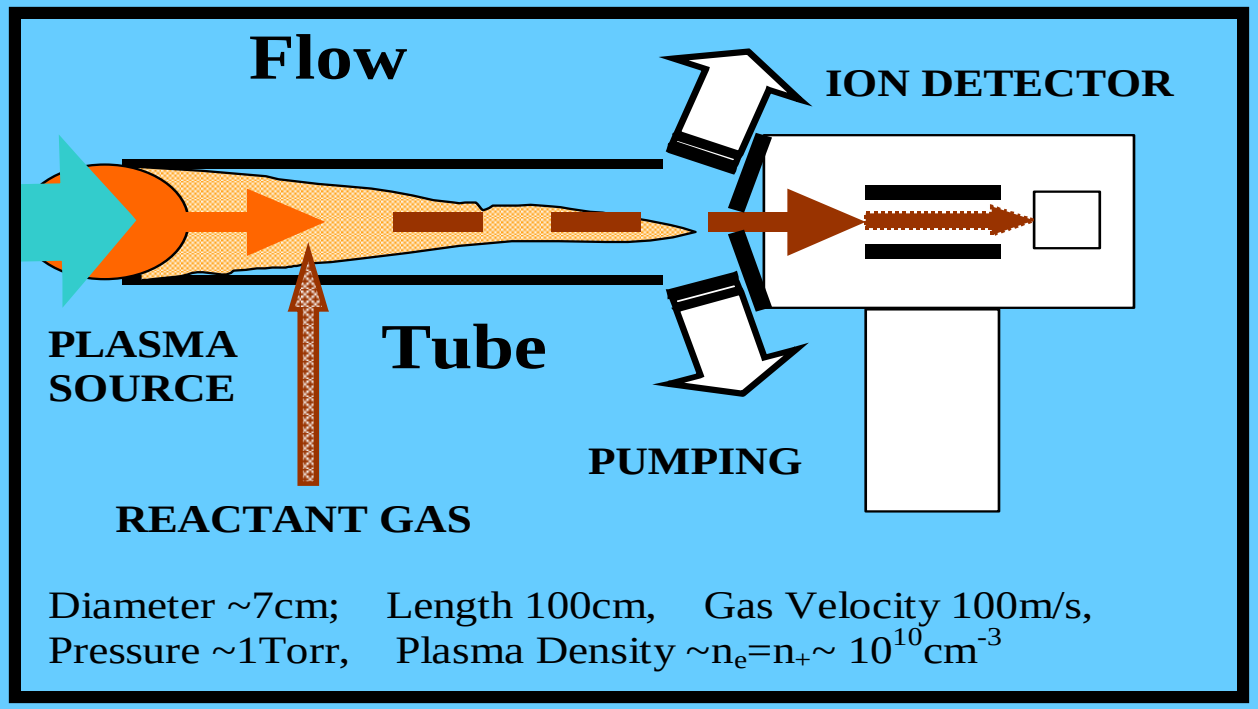

Techniques for study of IMR

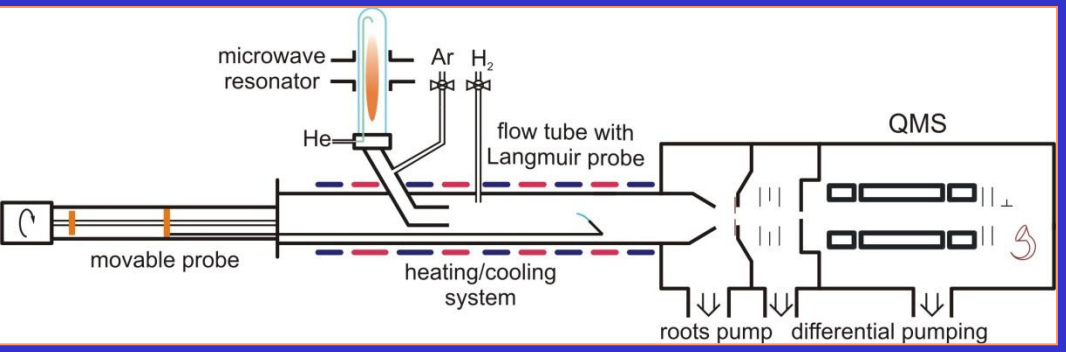

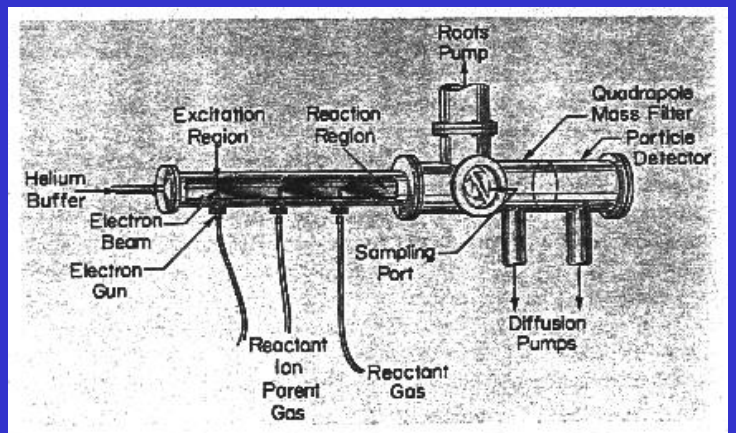

FIG. 1. Pictorial representation of the flowing afterglow tube.

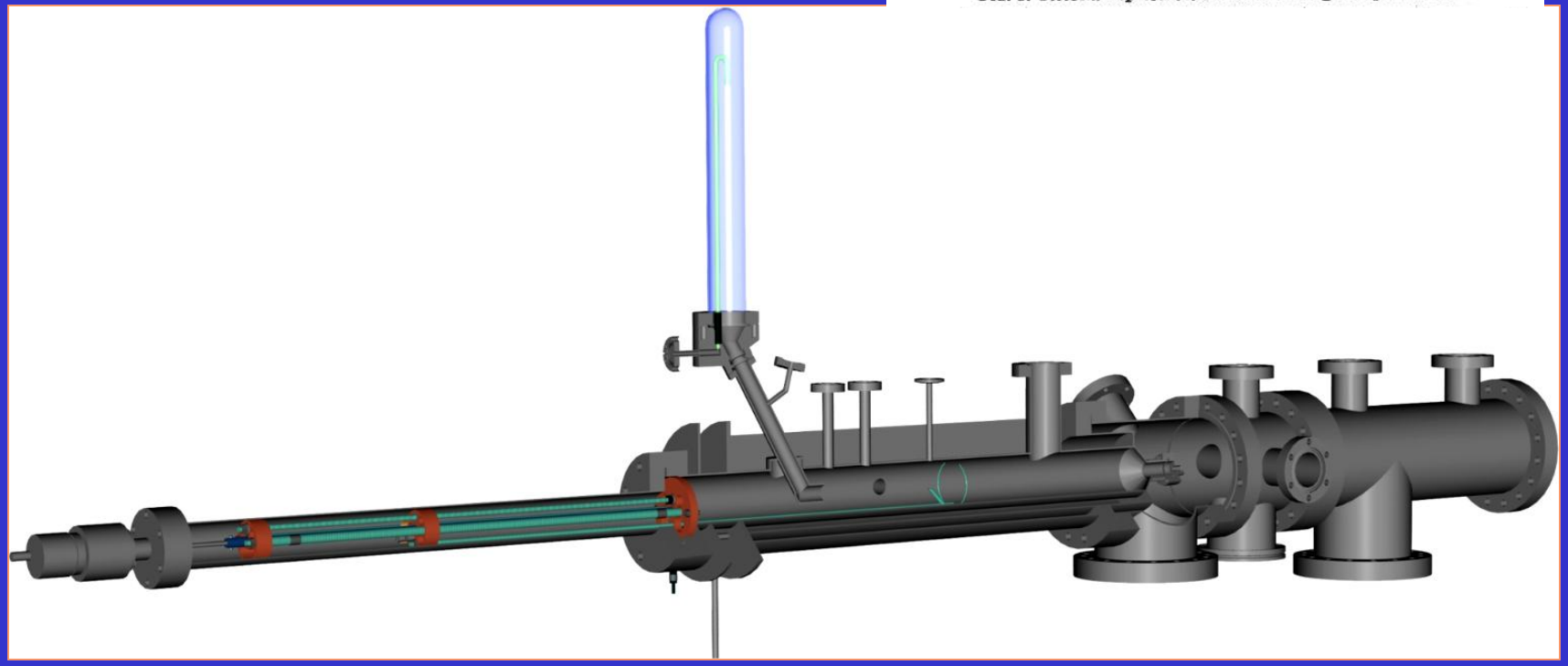

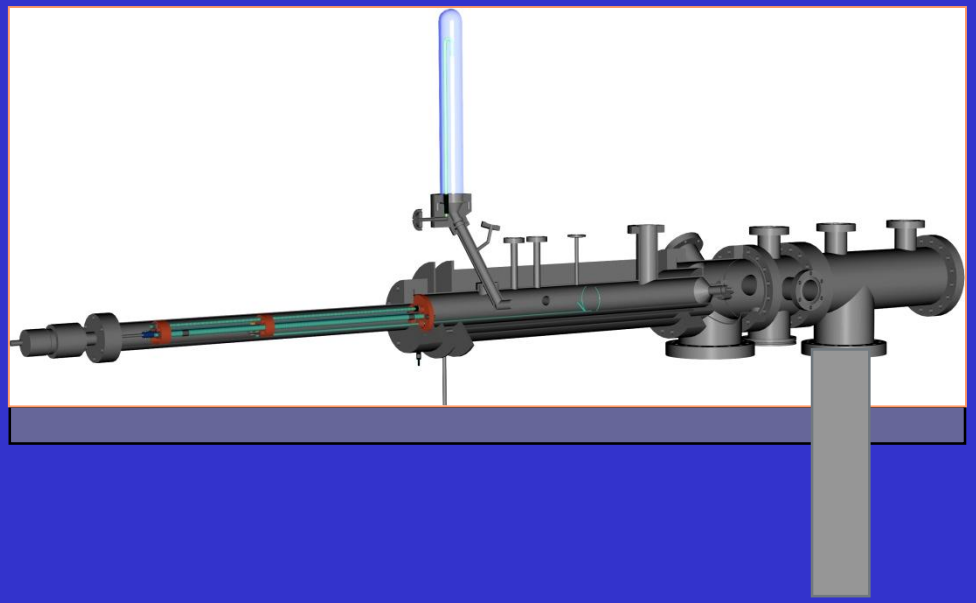

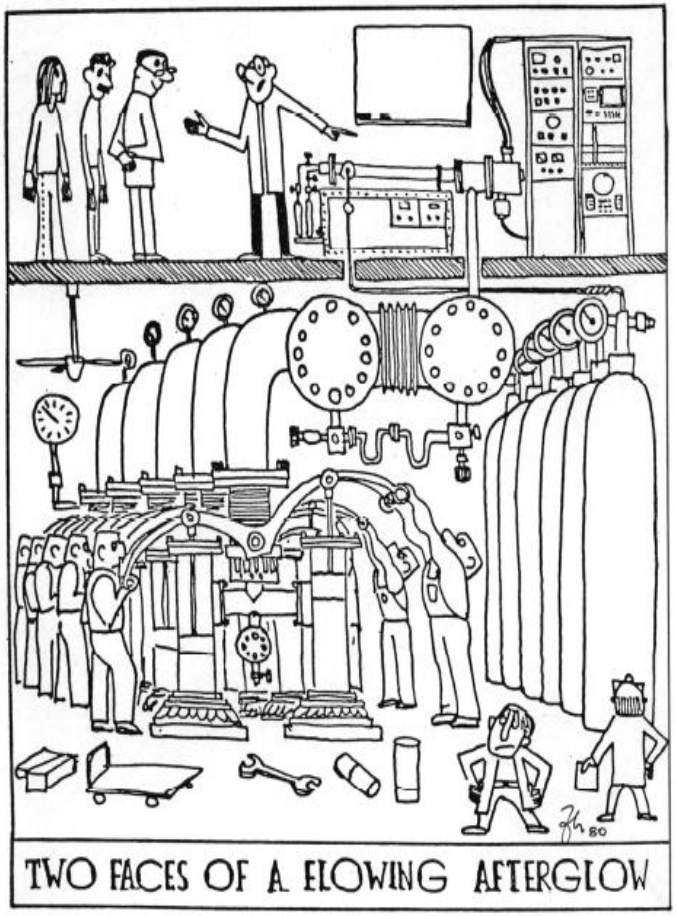

Two faces of a flowing afterglow.

(Opening picture to a seminar in Boulder, 1980)

Techniques for study of IMR

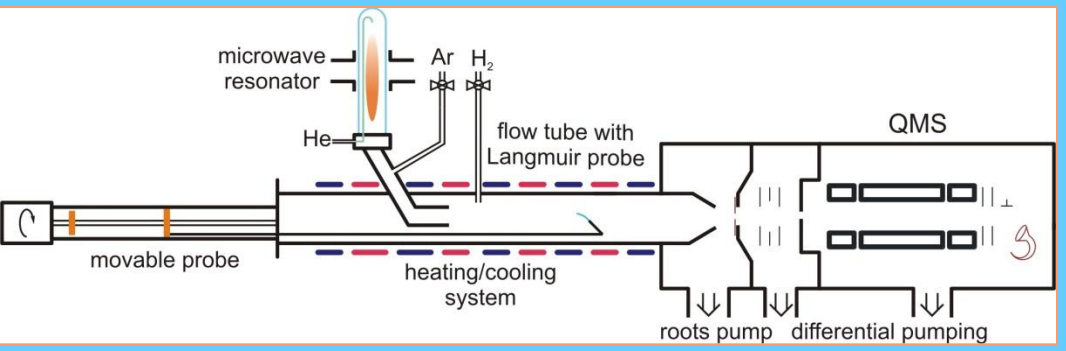

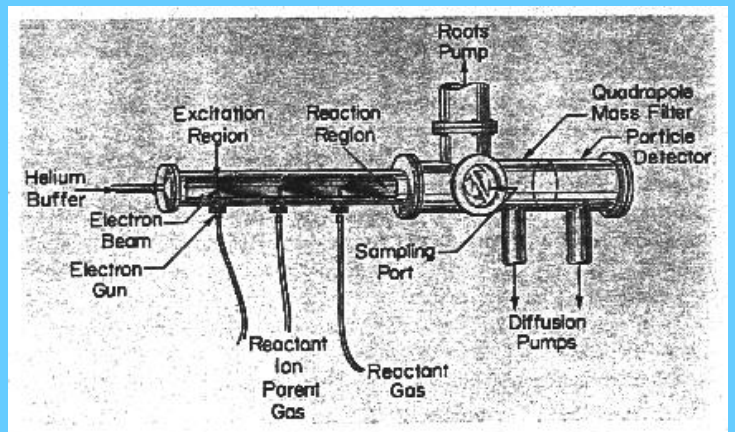

FIG. 1. Pictorial representation of the flowing afterglow tube.

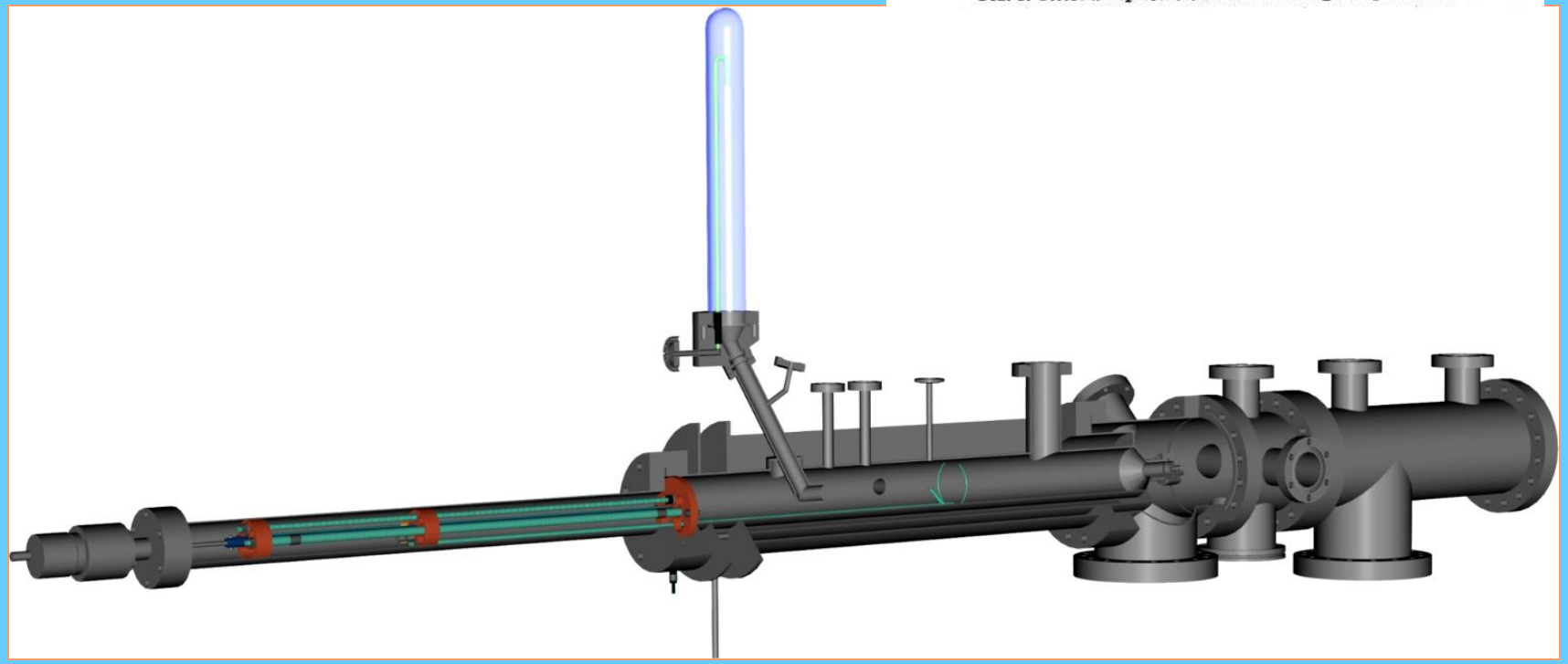

FA – Flowing Afterglow

100-700 K

$$H_3^+ + CO \Rightarrow HCO^+ + H$$

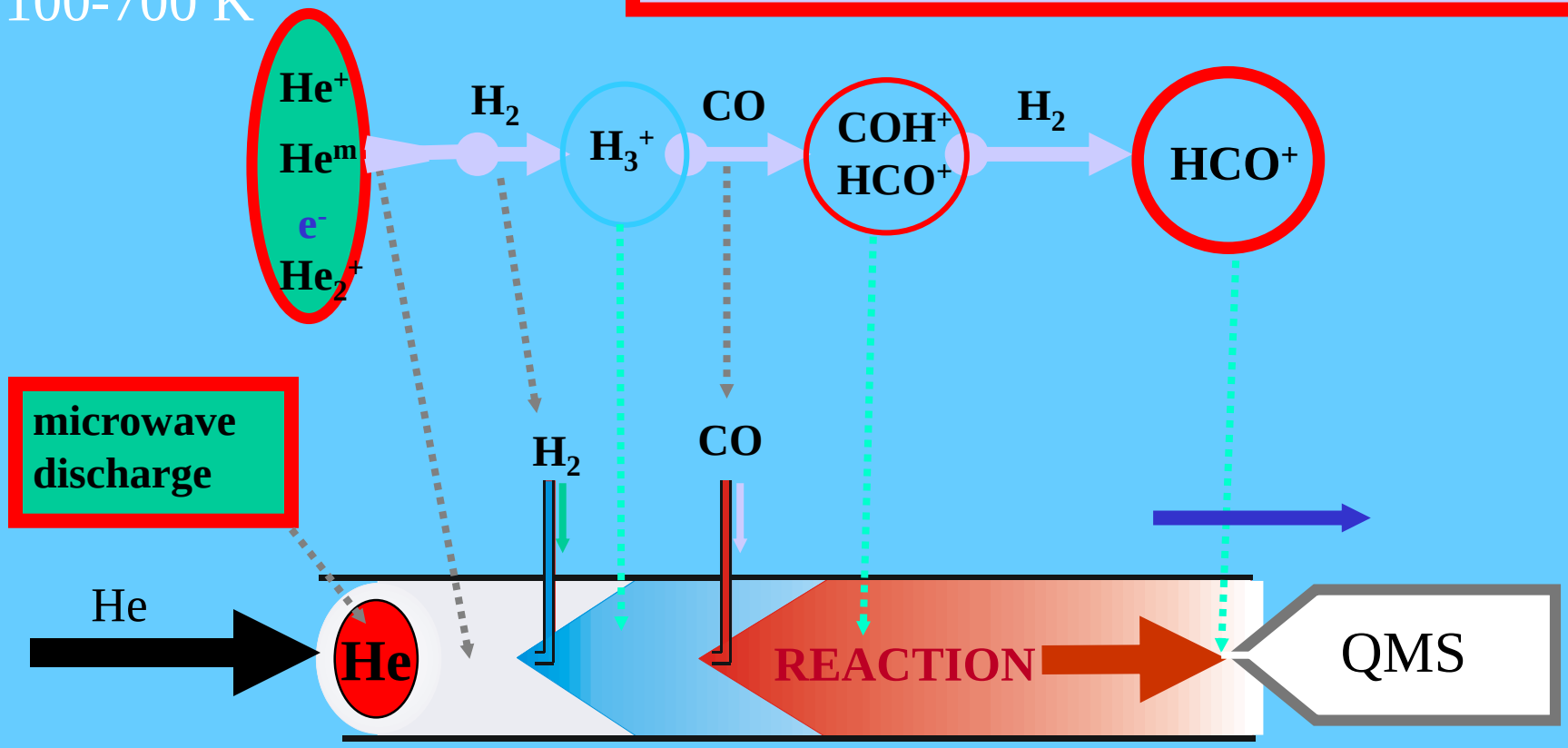

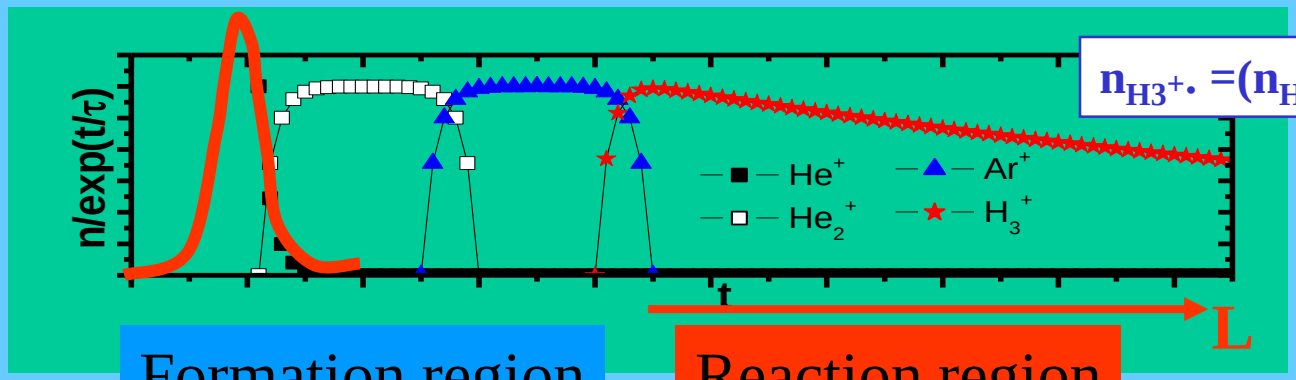

$$n_{H3^+}. = (n_{H3^+}).\ _0\ \exp(-kn_{Ar}t)$$

$$t = L/v$$

Formation region

Reaction region

FA – Flowing Afterglow

100-700 K

$$H_3^+ + CO \Rightarrow HCO^+ + H$$

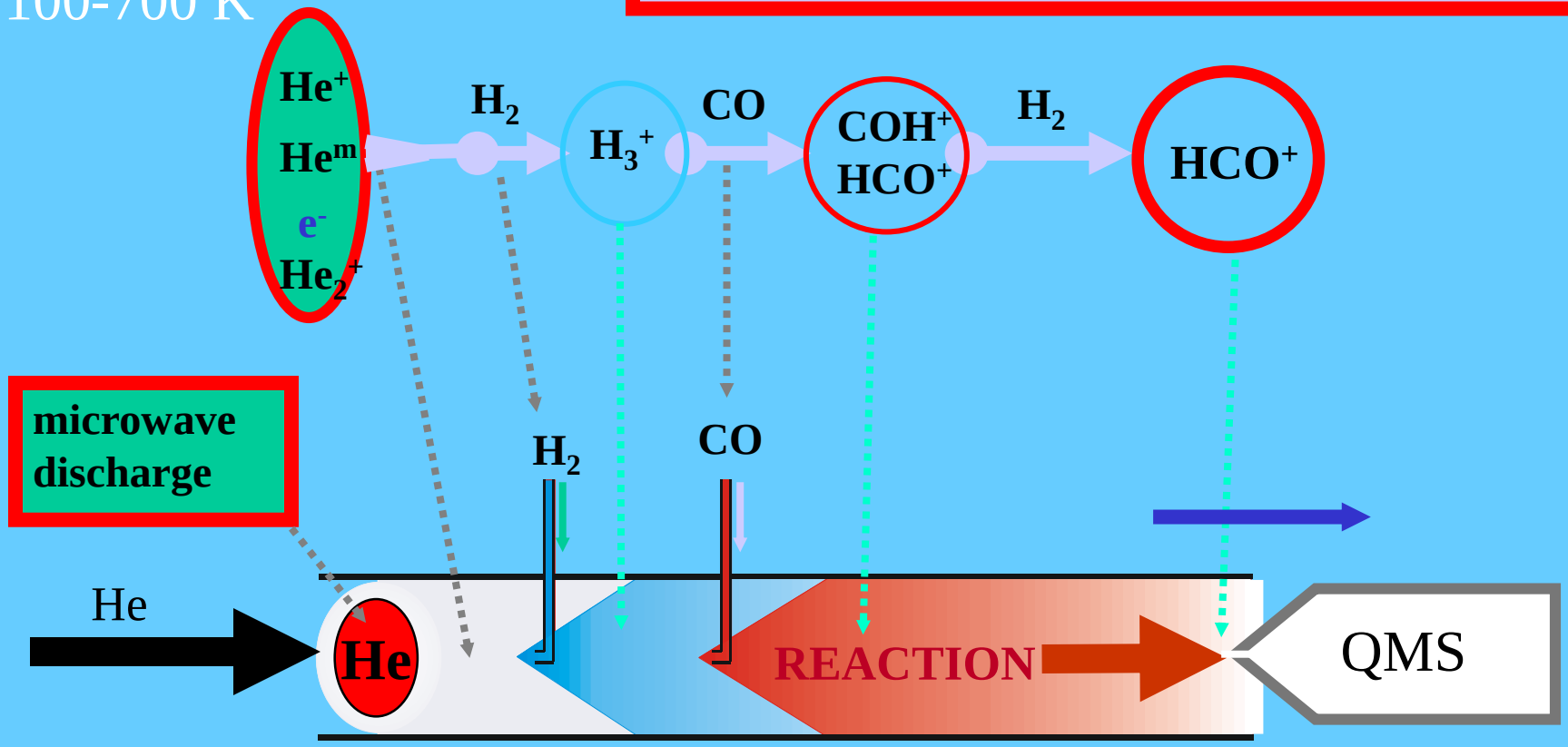

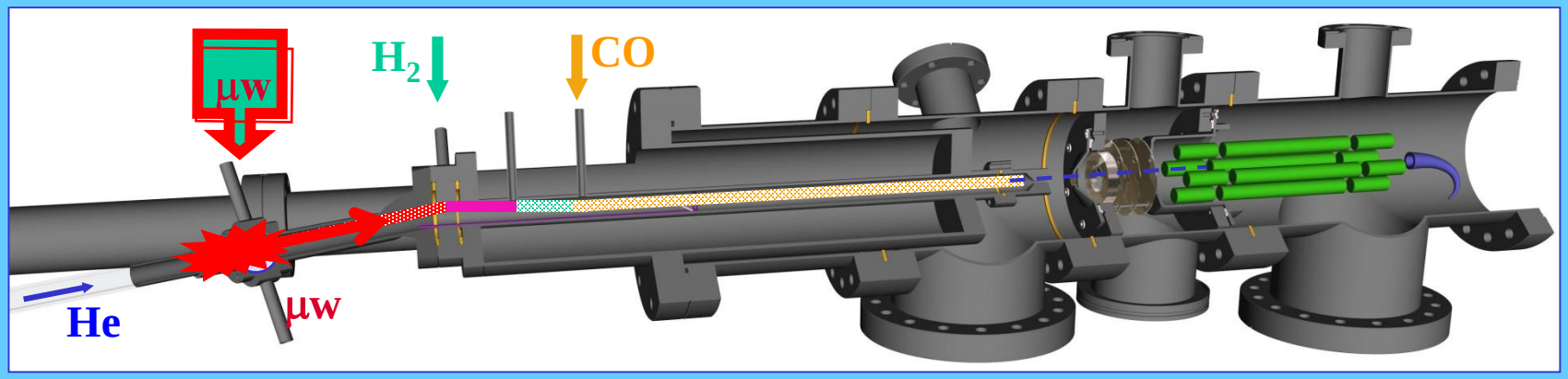

FA– Flowing Afterglow 2005

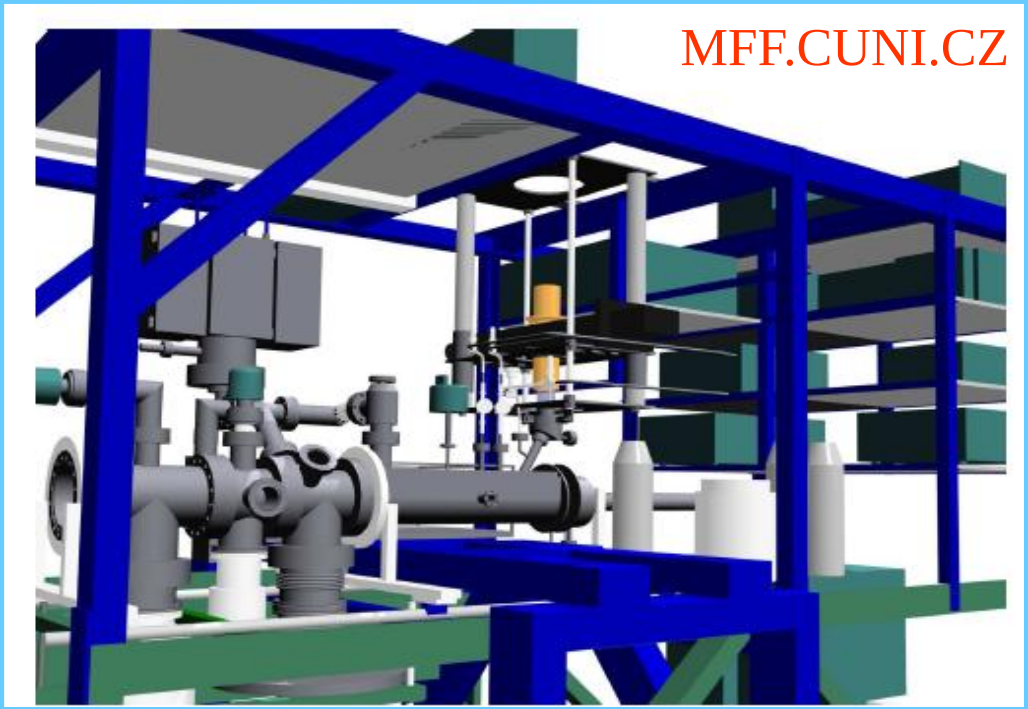

FA– Flowing Afterglow 2005

MFF.CUNI.CZ

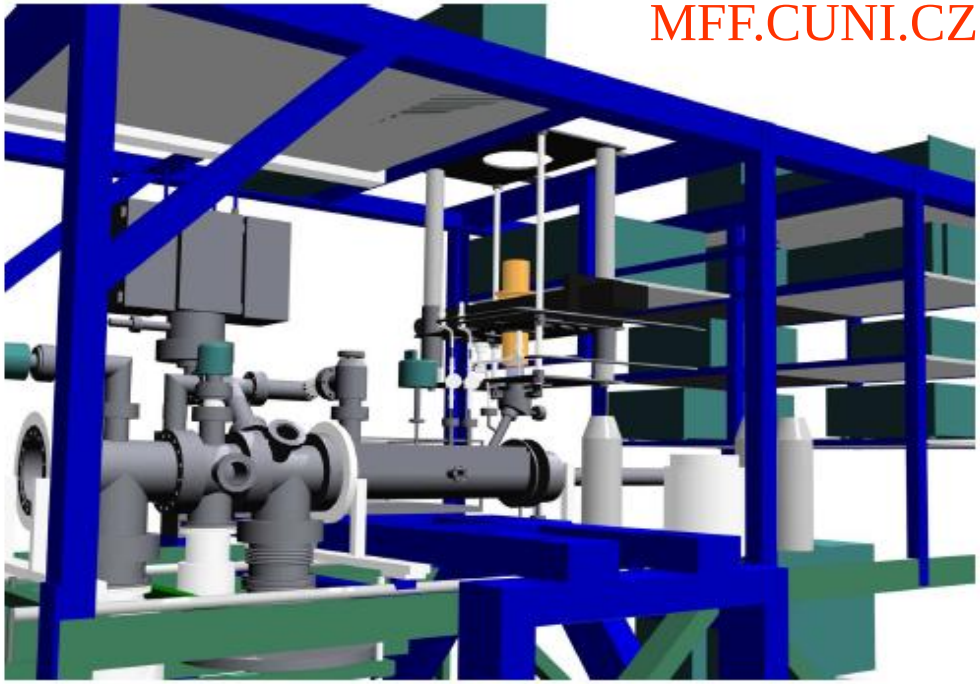

FA– Flowing Afterglow 1965 -2006

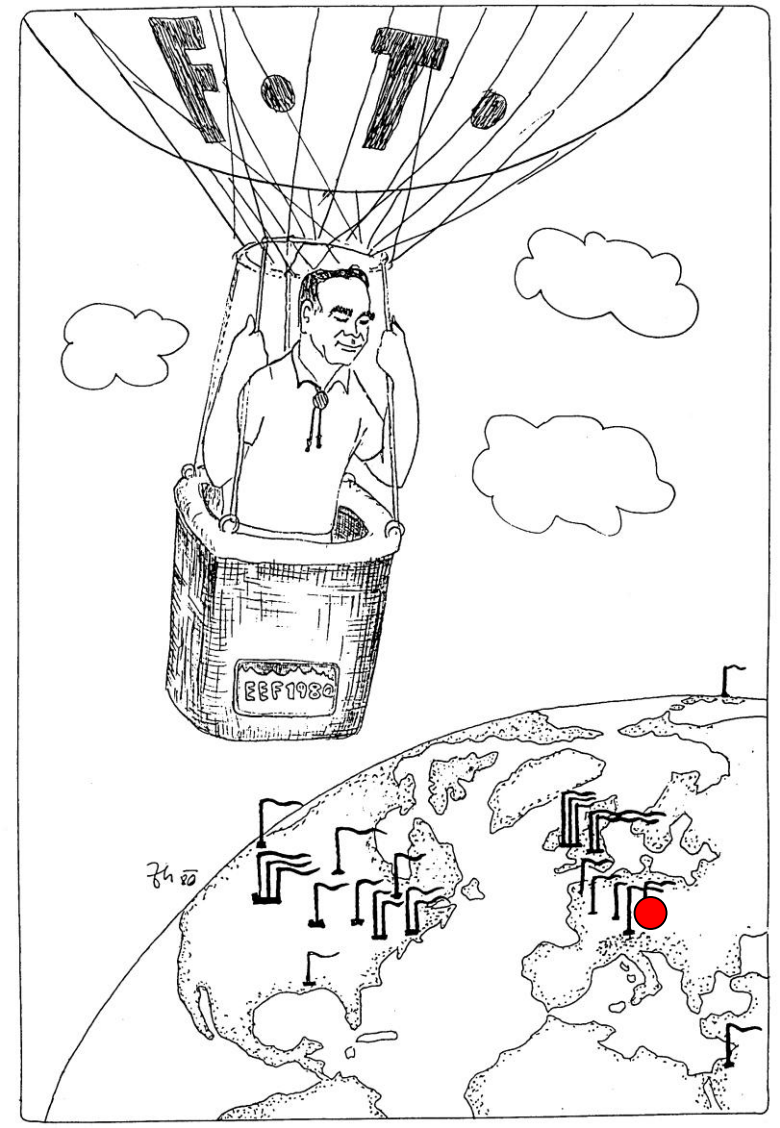

CU – Chemistry 1980:
Eldon Ferguson watching the flow-tube centers

MFF.CUNI.CZ

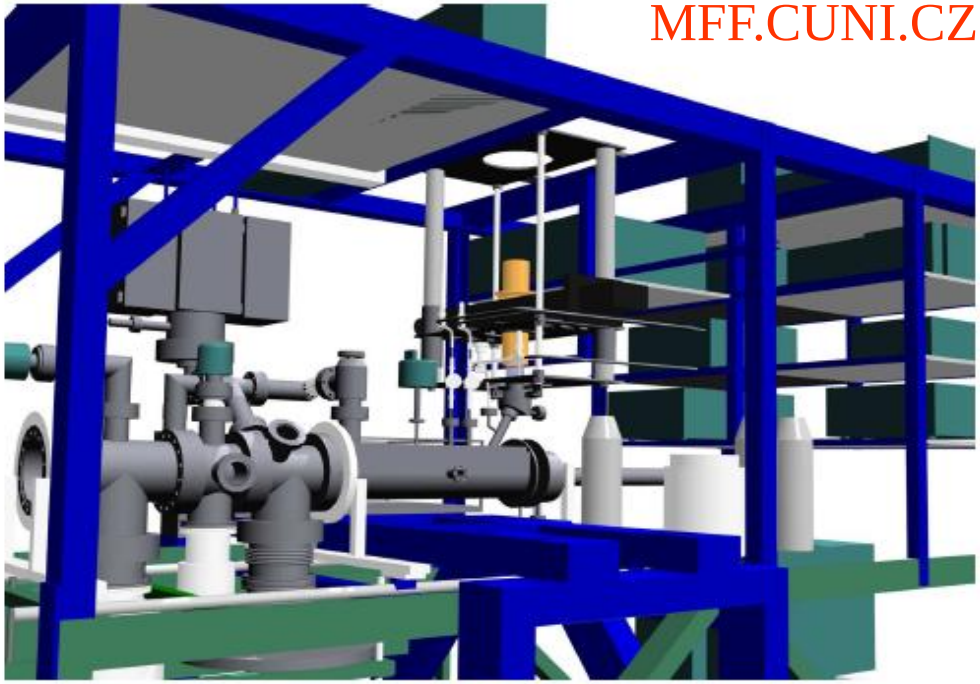

FALP – MFF.CUNI.CZ

Plasma, IMR, Recombination Diagnostics

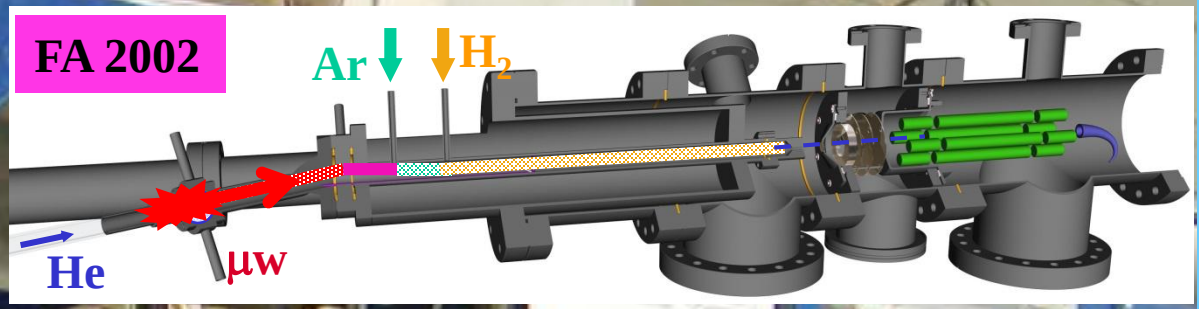

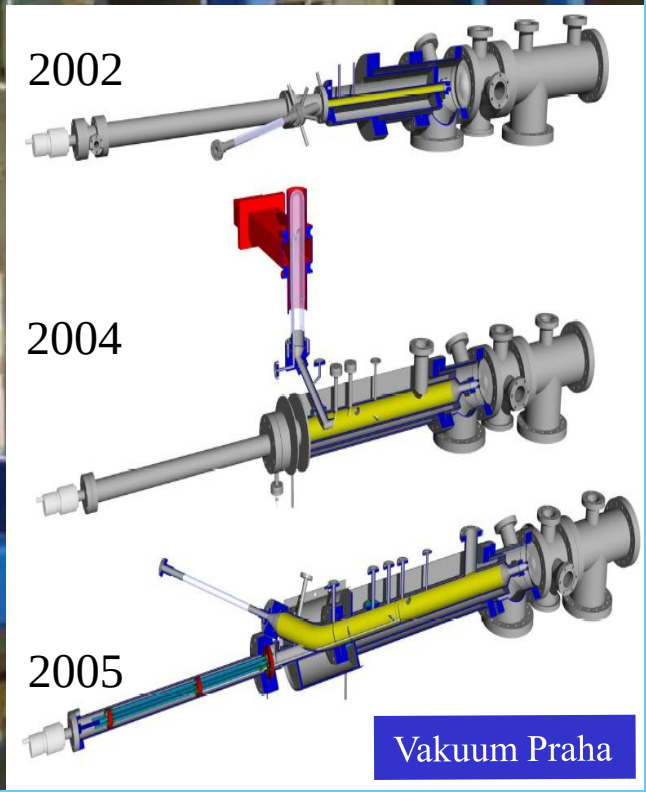

Vakuum Praha

O.Novotný

Principle of Flowing Afterglow Langmuir Probe - FALP

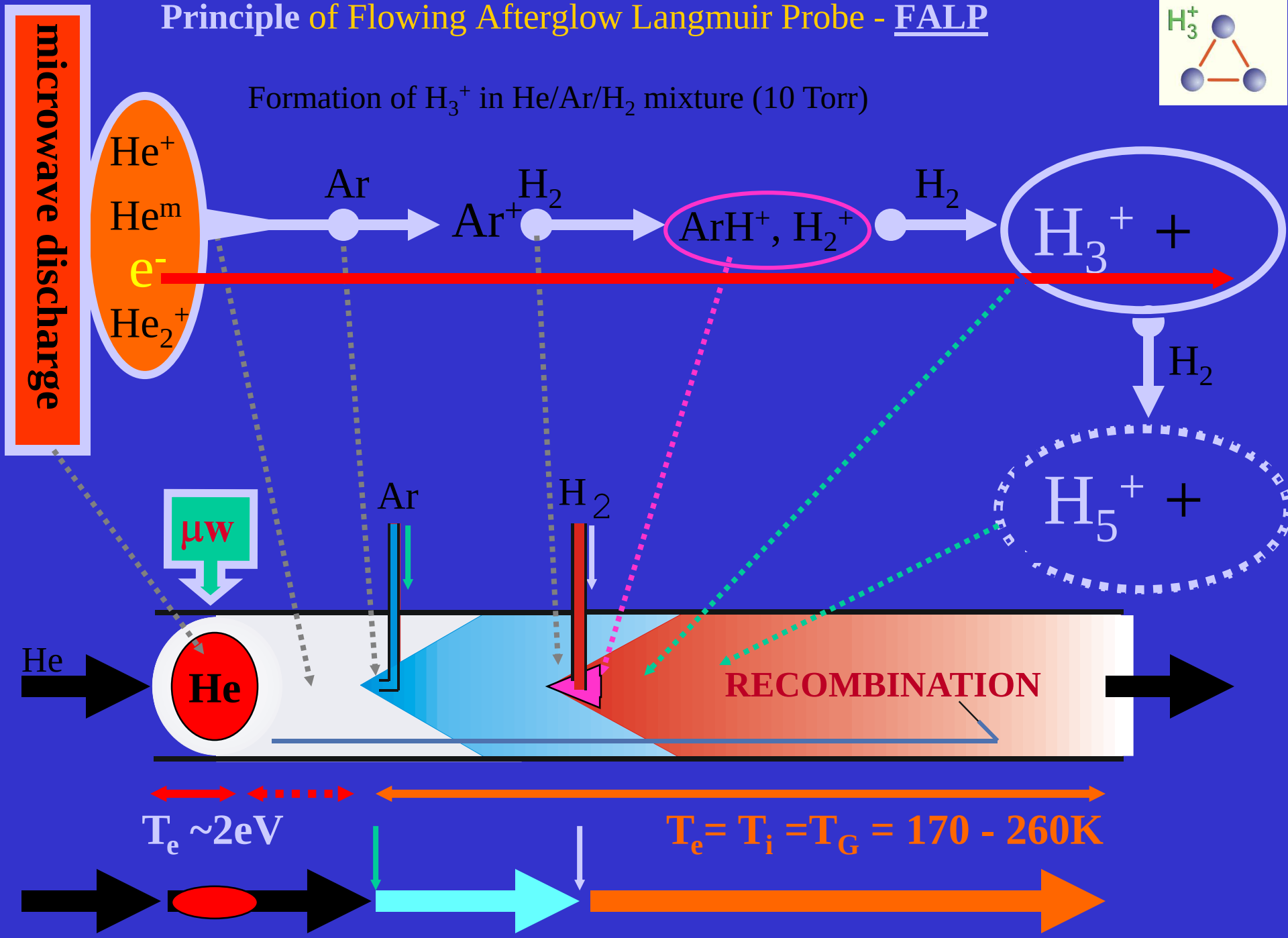

Apparatus -FALP

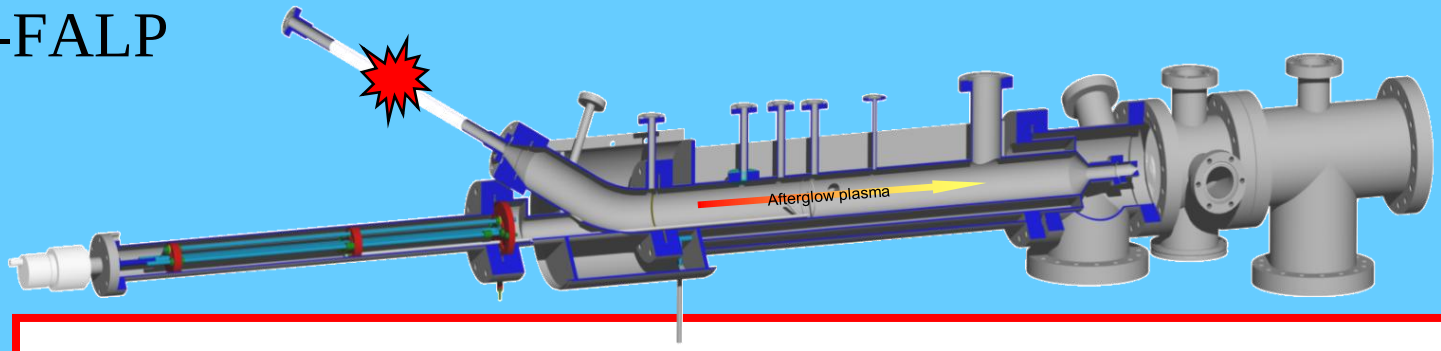

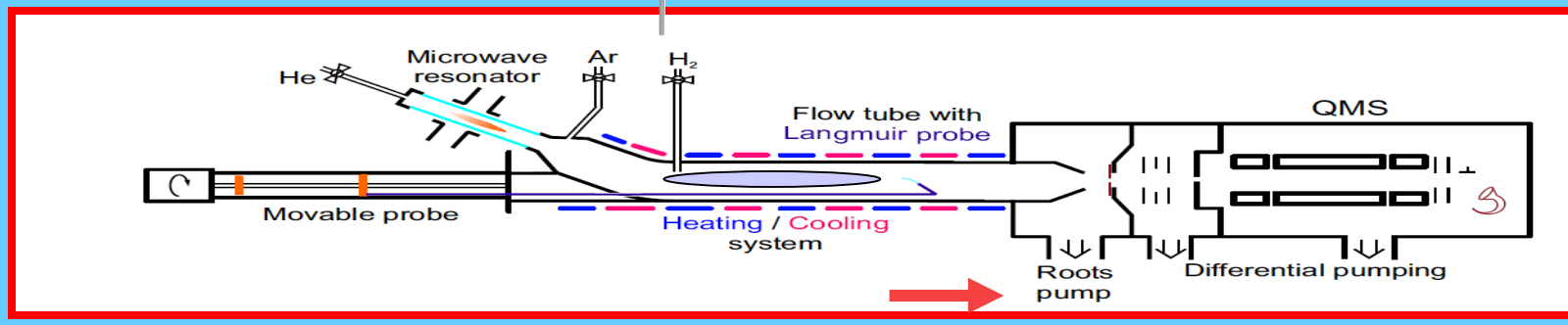

Kinetics

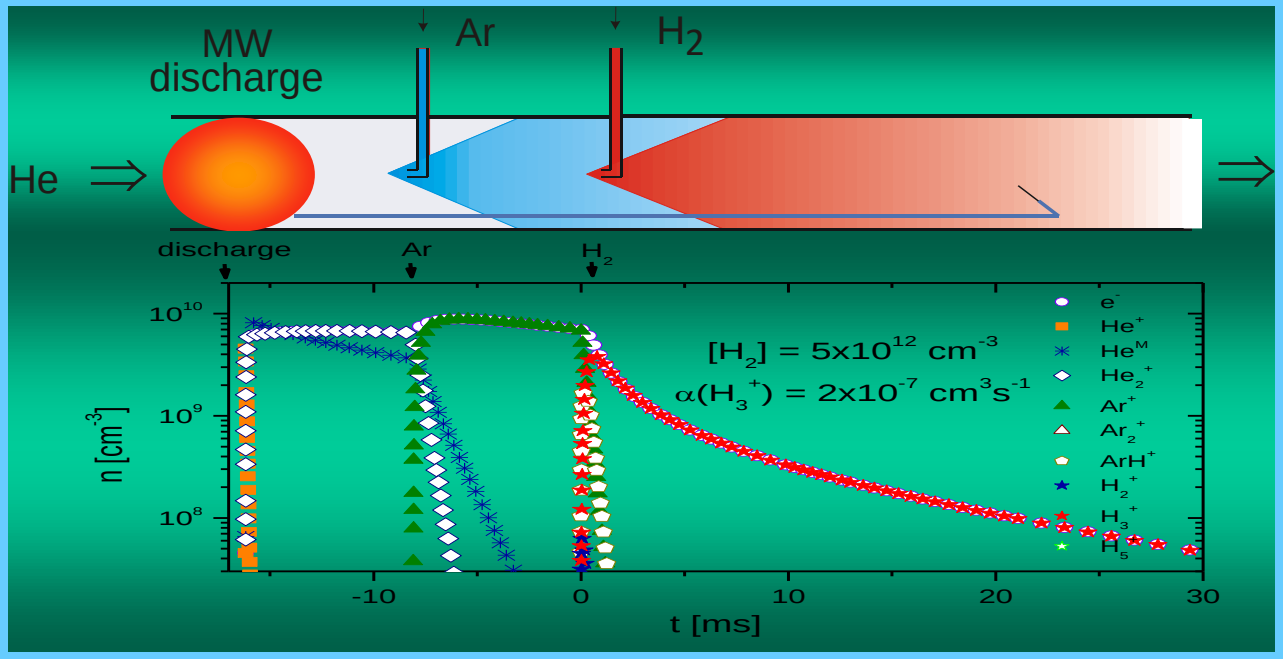

$\alpha \sim 5x10^{-9}$ cm^{3}s^{-1}

Plasma decay can be monitored up to 35 cm ➔ 65 ms, Temperature – 130 - 300 K Pressure up to 12 Torr

Evolution along the flow tube

$$[A^+]_L = [A^+]_{L=0} \cdot e^{-DL/\lambda^2 v}$$

$$[A^+]_L = [A^+]_{L=0} \cdot e^{-const_1 . D_0 p_0 L/Q} = [A^+]_{L=0} \cdot e^{-const_2 . L/Q}$$

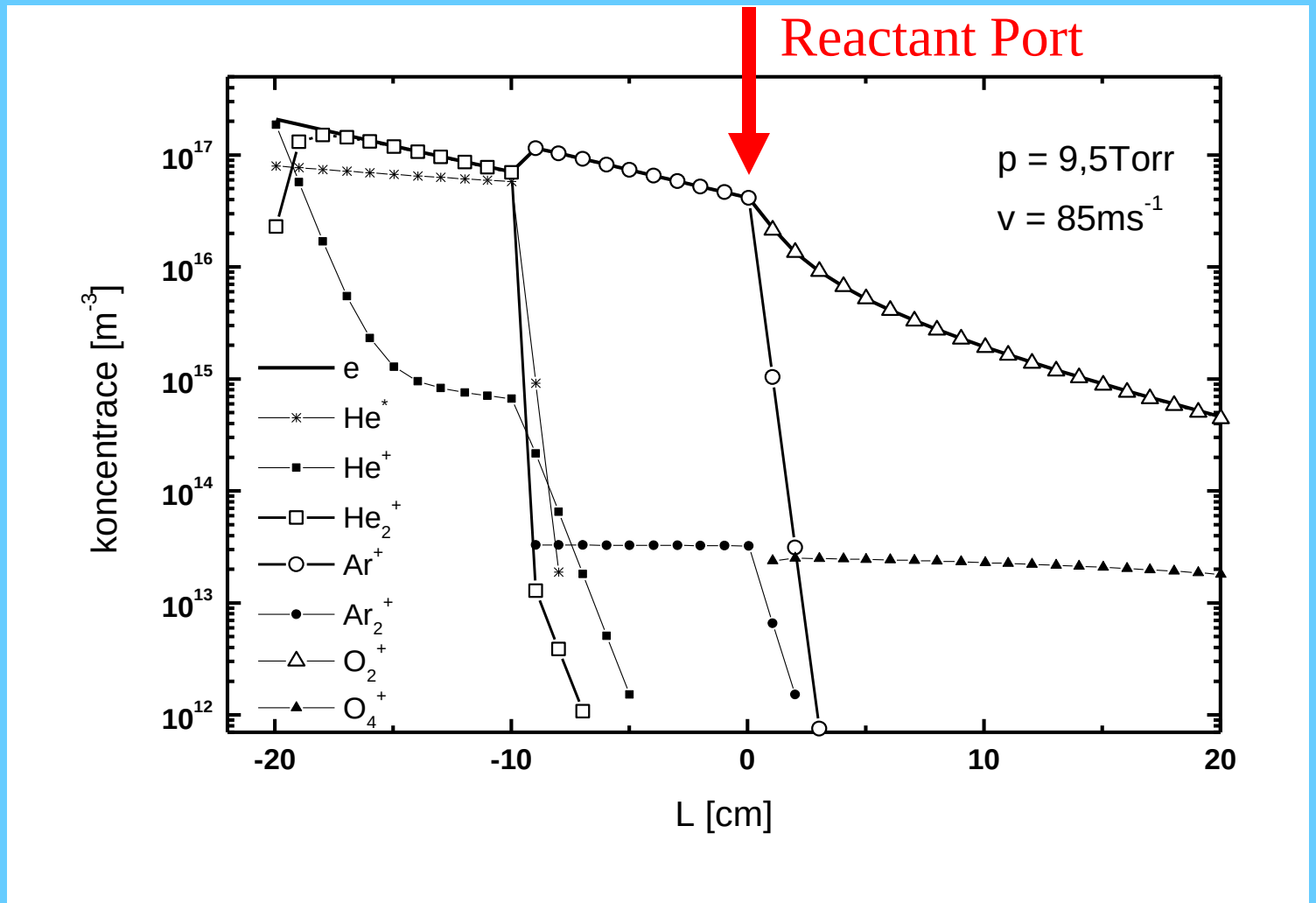

Ion-molecule reactions

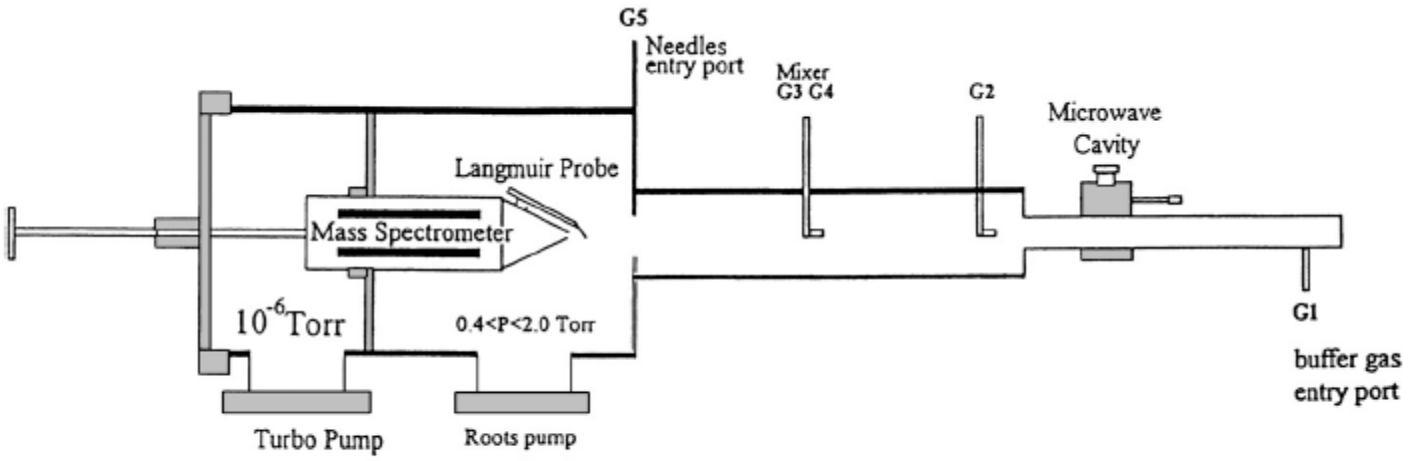

Fig. 12. Schematic view of the Rennes FALP-MS [164]

Flowing Afterglow 1968

Professor David Smith

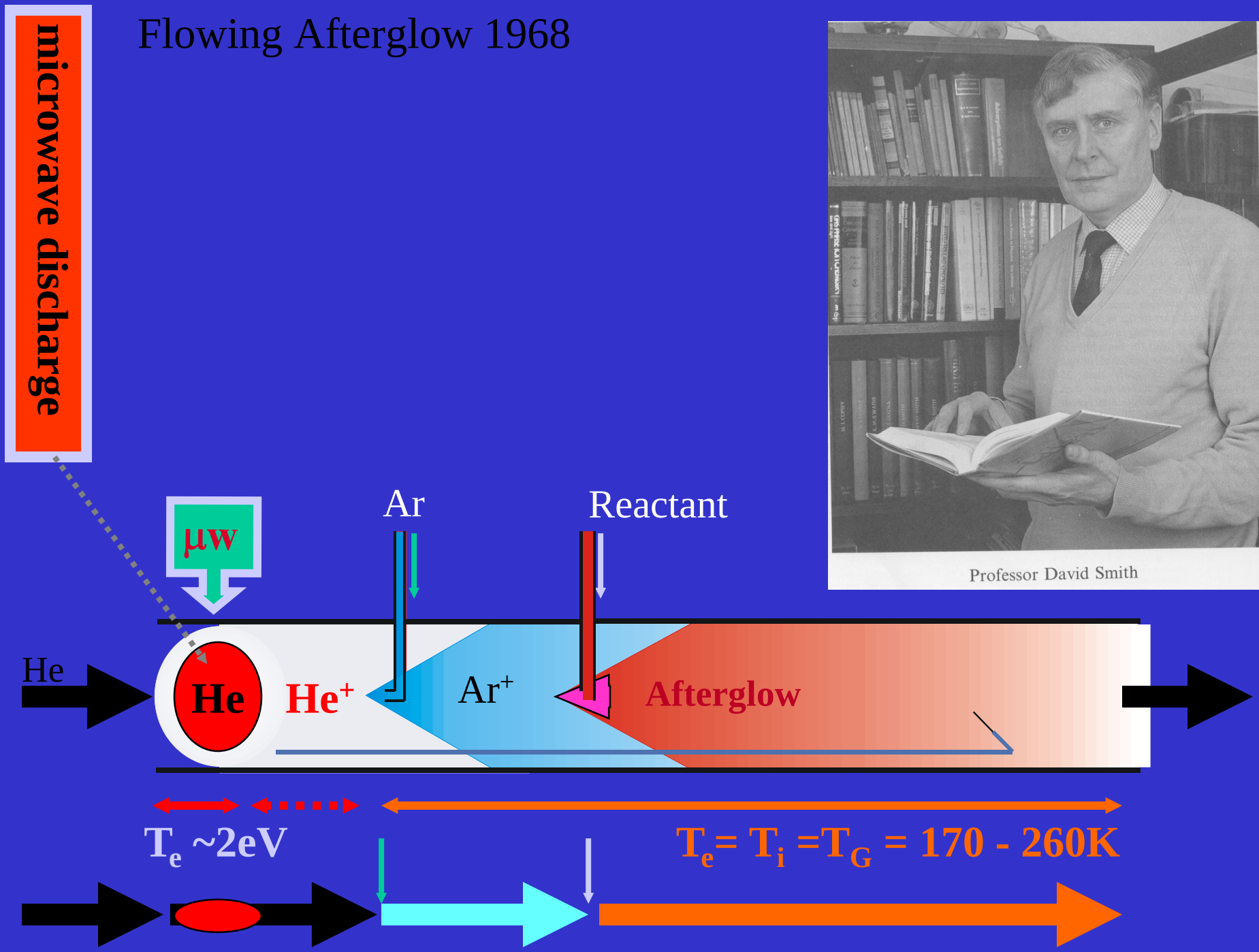

Selected Ion Flow Tube - SIFT

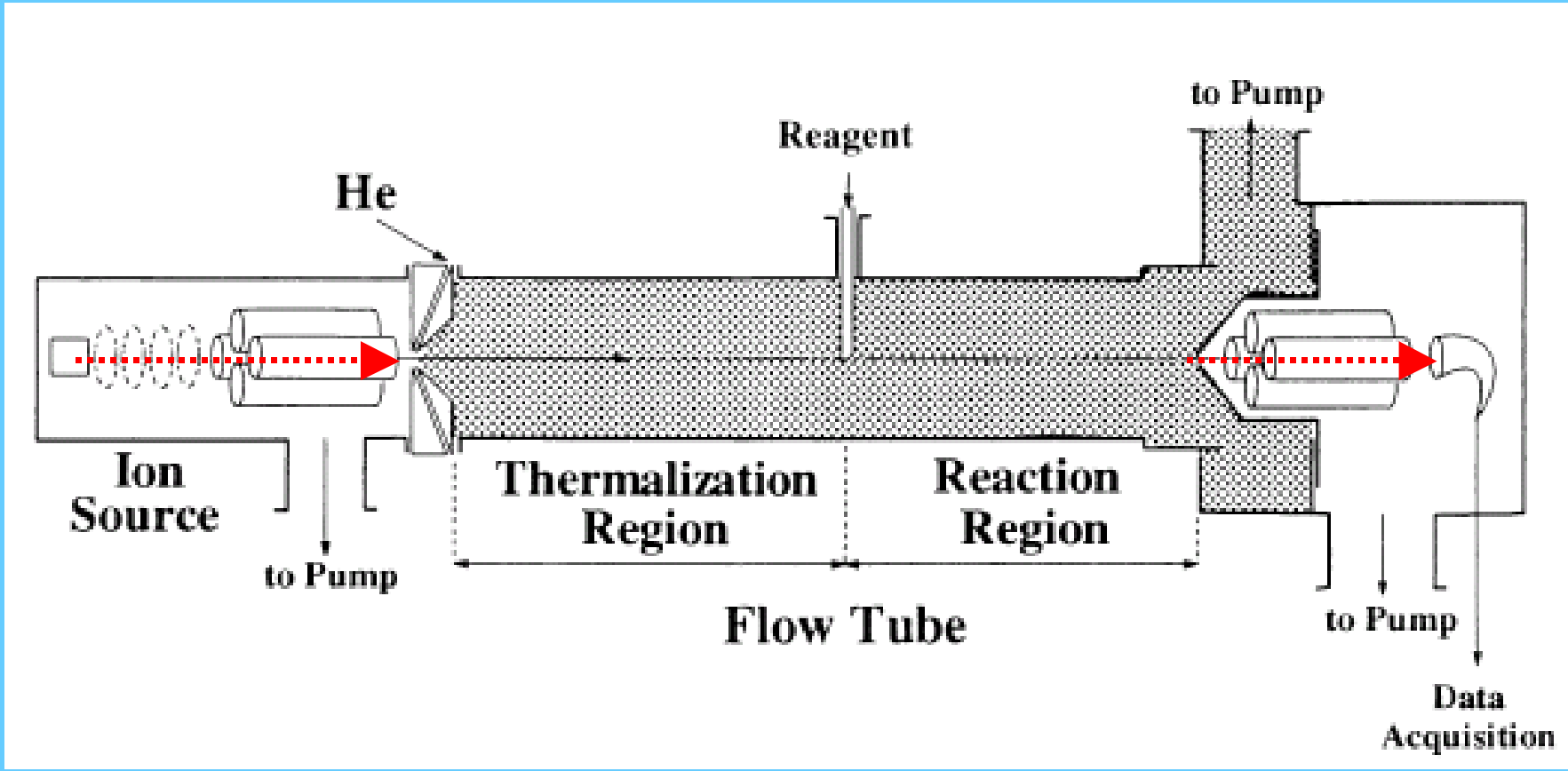

Ion-molecule reactions

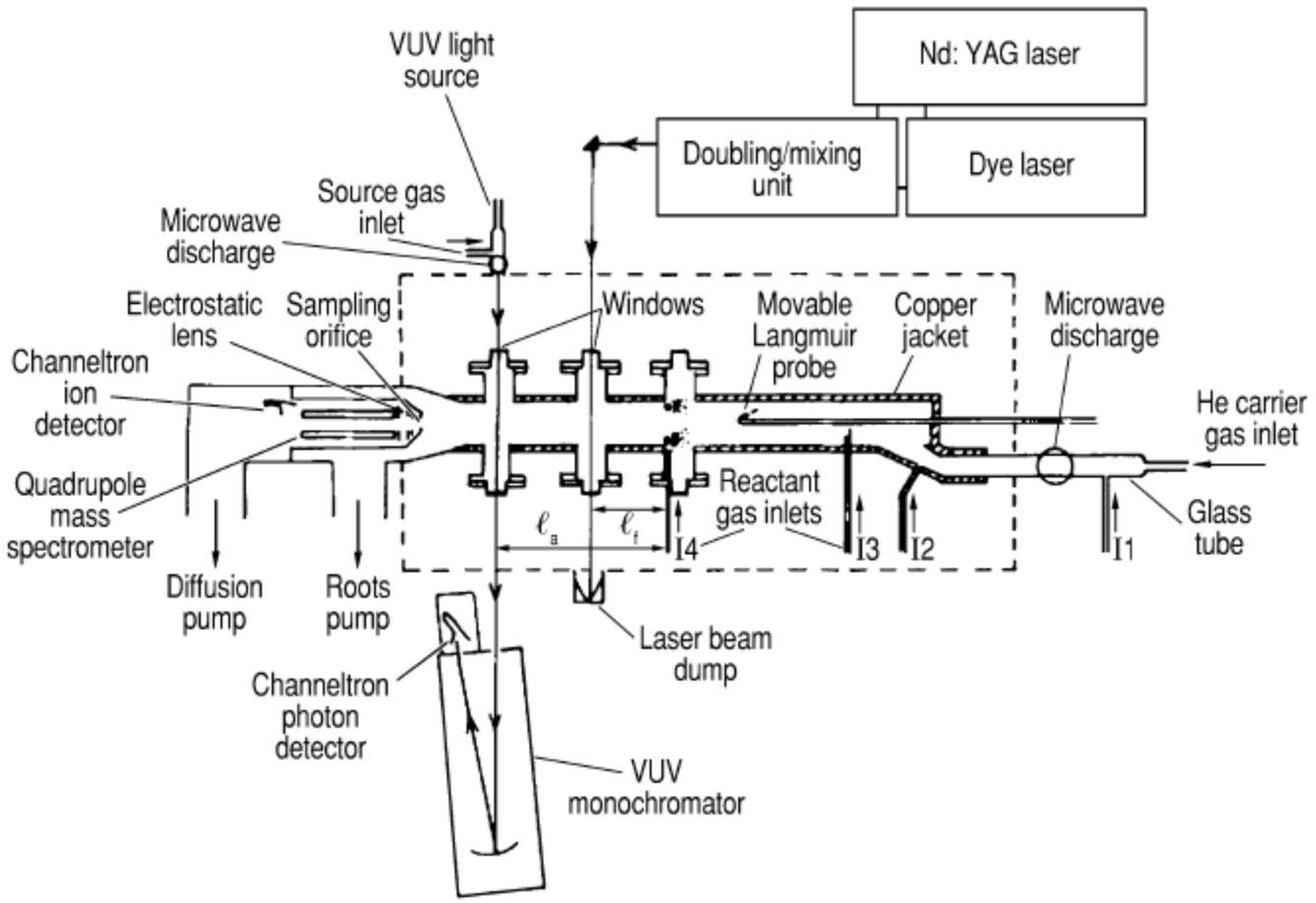

Fig. 13. Schematic diagram of the FALP-LIF/VUV apparatus used, in various configurations, since 1989 by Adams et al. [161] in their characterization of DR neutral products. The *dotted line* encasing the central flow tube represents a vacuum jacket facilitating operation at a broad range of temperatures

Diffusion and reaction

$$[A^+]_t = [A^+]_{t=0} \cdot e^{-k[B]L/v} e^{-constL/Q}$$

Measurements by mass spectrometer vat fixed position

$$H_3O^+ \quad + \quad CH_3COCH_3 \quad \rightarrow CH_3COCH_3H^+ + \quad H_2O$$

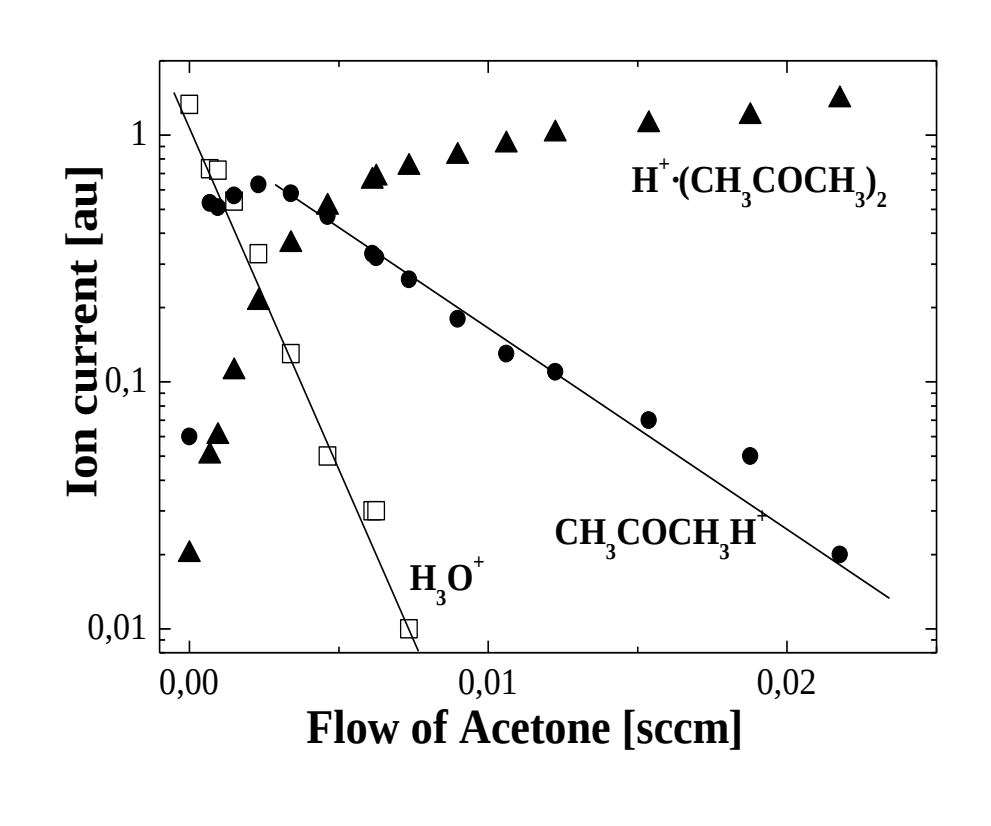

IMR thermal

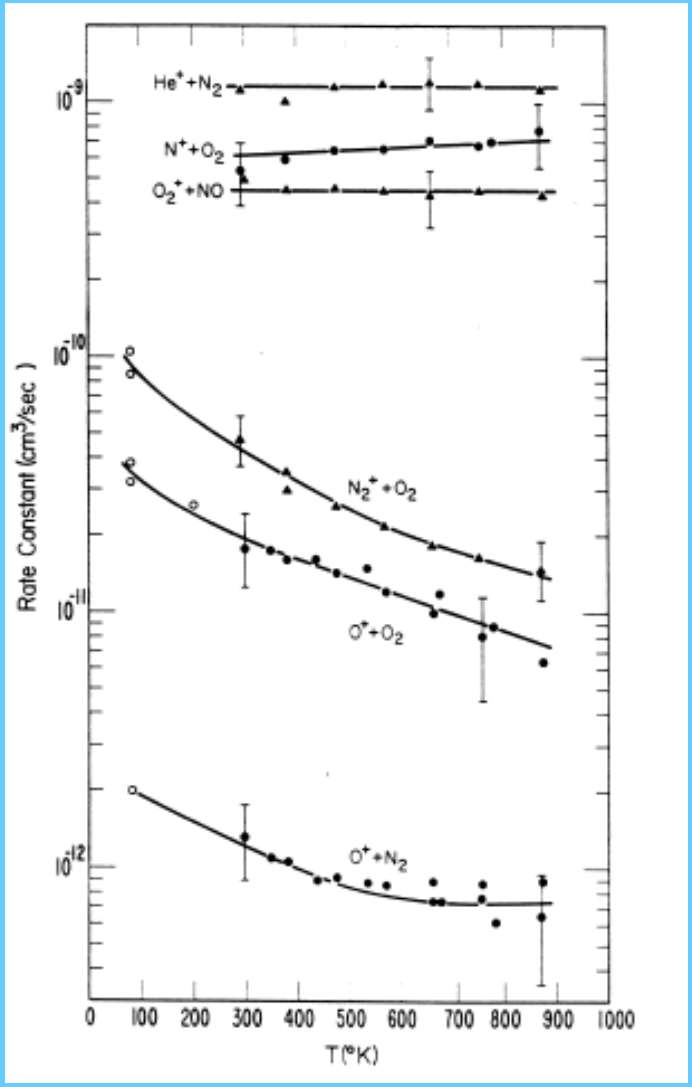

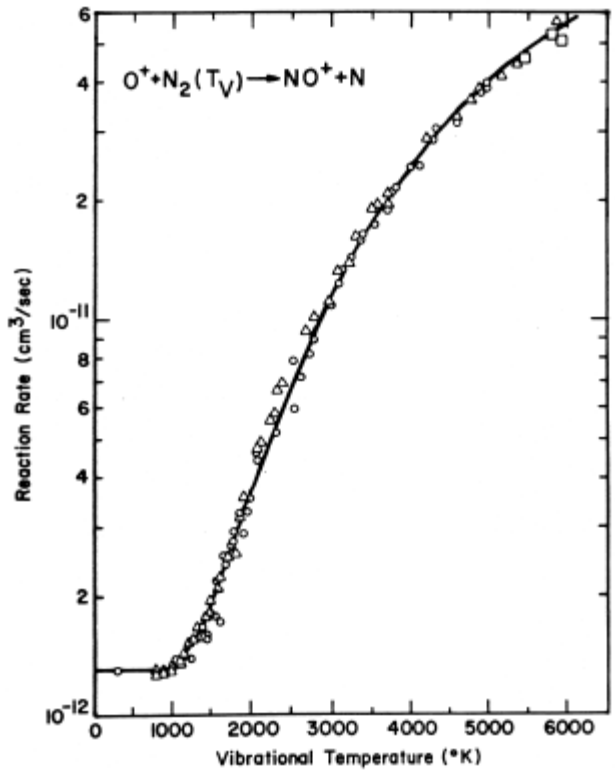

Fig. 12. Measurements of the variation of the rate coefficient for the reaction of $O^+ + N_2 \rightarrow NO^+ + N$ with the vibrational temperature of N_2 [16].

IMR C_{60}^+

$$[A^+]_t = [A^+]_{t=0} \cdot e^{-k[B]L/v} e^{-constL/Q}$$

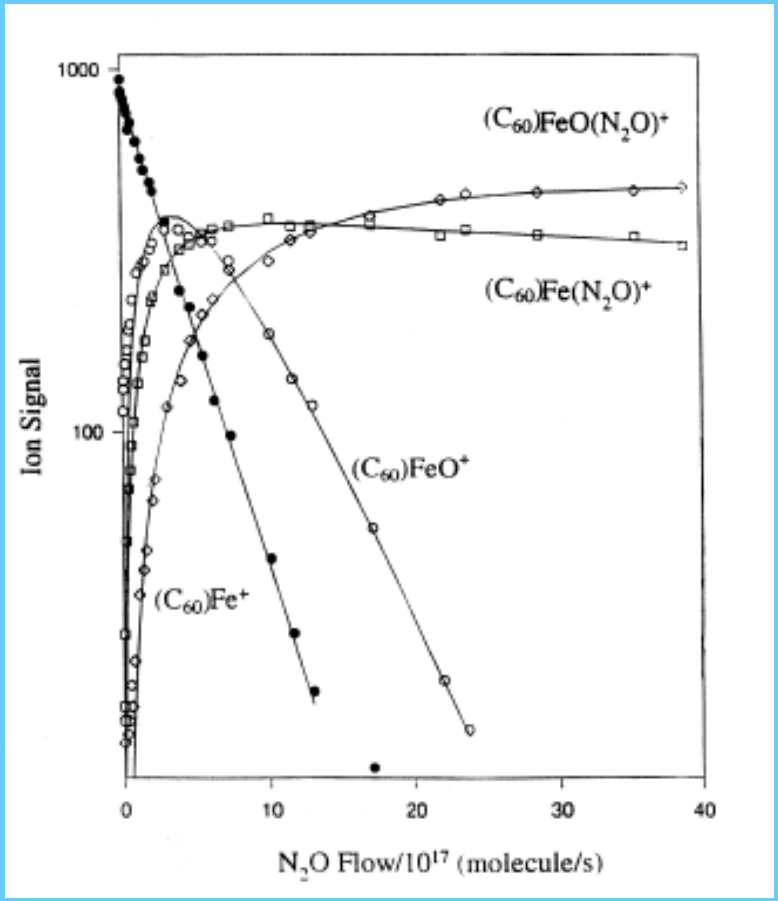

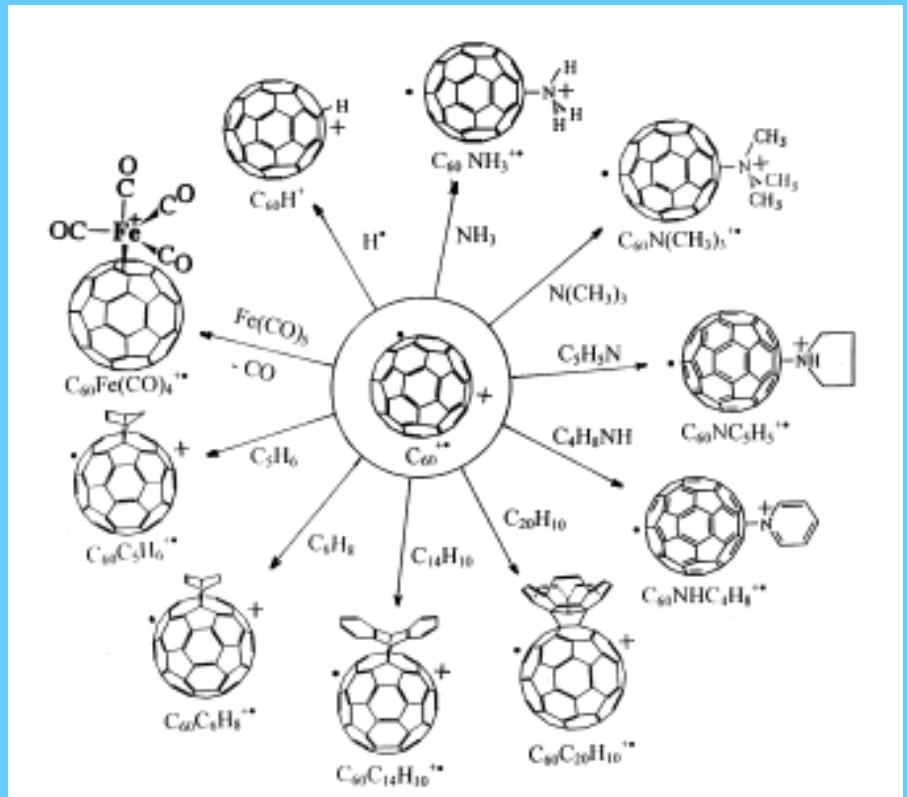

Fig. 31. An overview of derivatization reactions of C_{60}^+ observed with the York University SIFT apparatus at room temperature in helium buffer gas at 0.35 Torr. The assigned structures are speculative.

IMR – SIFT → Proton Transfer Mass Spectrometry

Spanel, Smith

$$[A^+]_t = [A^+]_{t=0} \cdot e^{-k[B]L/v} e^{-constL/Q}$$

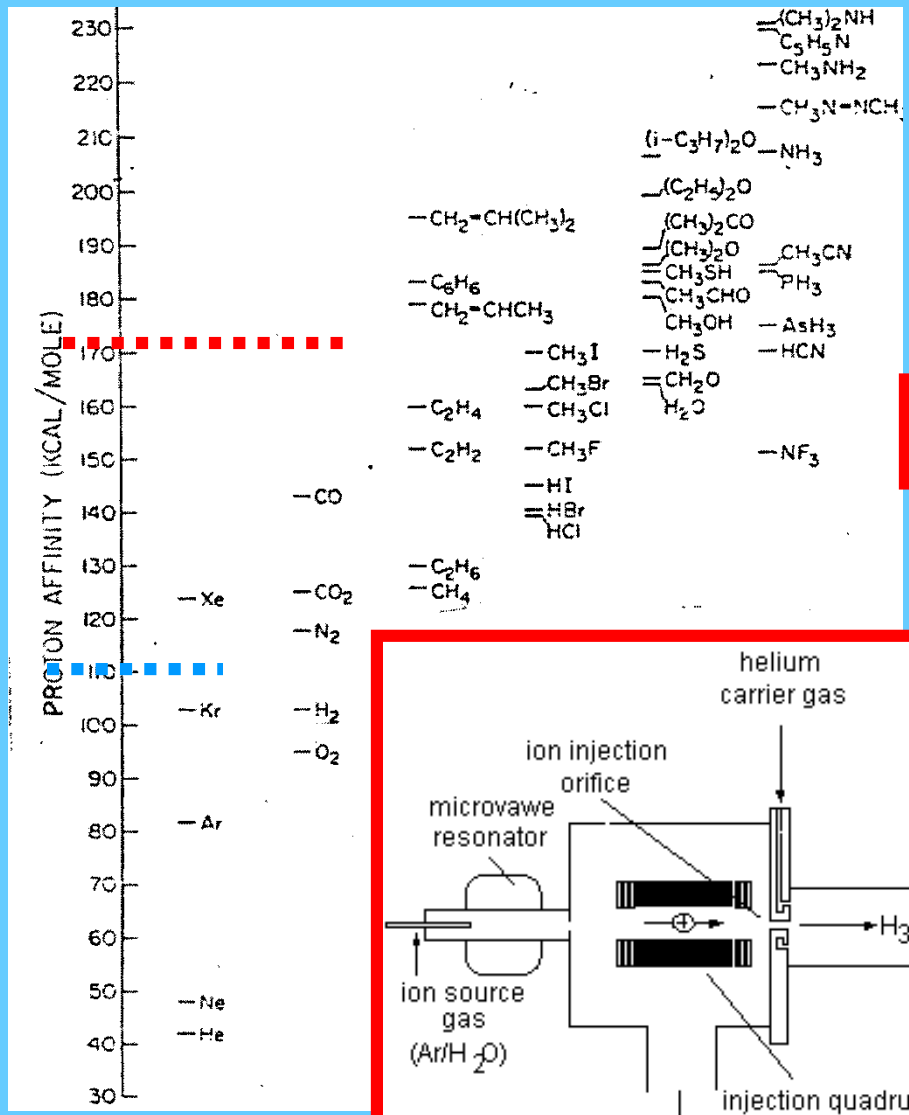

Primary ions

H_3O^+, O_2^+, NO^+

$$H_3O^+ + C_nH_m \rightarrow C_nH_{m+1}^+ + H_2O$$

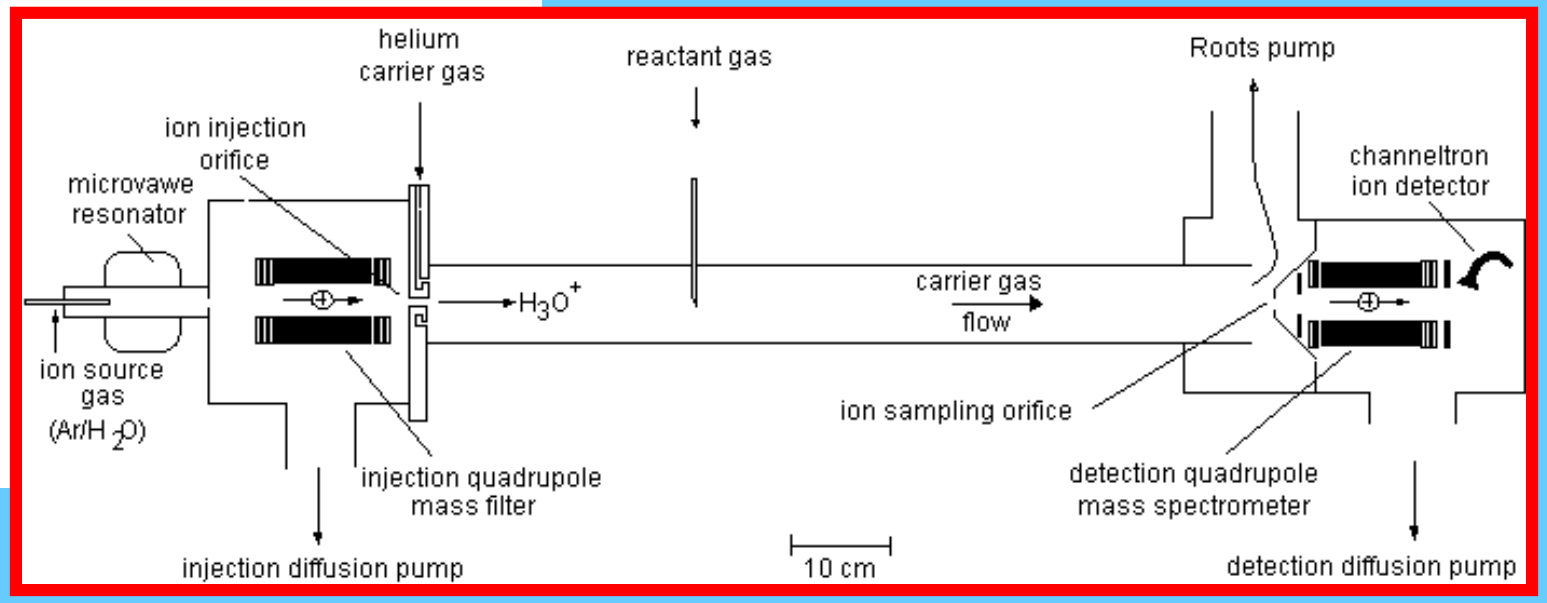

Selected Ion Flow Tube - SIFT

THE JOURNAL OF CHEMICAL PHYSICS VOLUME 59, NUMBER 12 15 DECEMBER 1973

Flow–drift technique for ion mobility and ion–molecule reaction rate constant measurements. I. Apparatus and mobility measurements

M. McFarland*, D. L. Albritton, F. C. Fehsenfeld, E. E. Ferguson*, and A. L. Schmeltekopf
Aeronomy Laboratory, NOAA Environmental Research Laboratories Boulder, Colorado 80302
(Received 24 September 1973)

The present paper describes the construction and operation of a new experimental device that combines the chemical versatility of a conventional flowing afterglow system with the energy variability of a drift tube. This allows the measurement of both positive and negative ion mobilities not previously measured. Ion mobility measurements offer a significant constraint upon the ion–neutral intermolecular potential and are therefore of value in testing either empirical or quantum mechanical theory. The mobilities of He^+, He_2^+, H^+, D^+, O^+, N^+, Ar^+, H_2^+, H_3^+, N_2^+, H^-, O^-, and OH^- in helium and H_3^+ in H_2 are presented in the present paper. The following papers describe positive ion–neutral and negative ion–neutral reaction rate constant measurements in the same device.

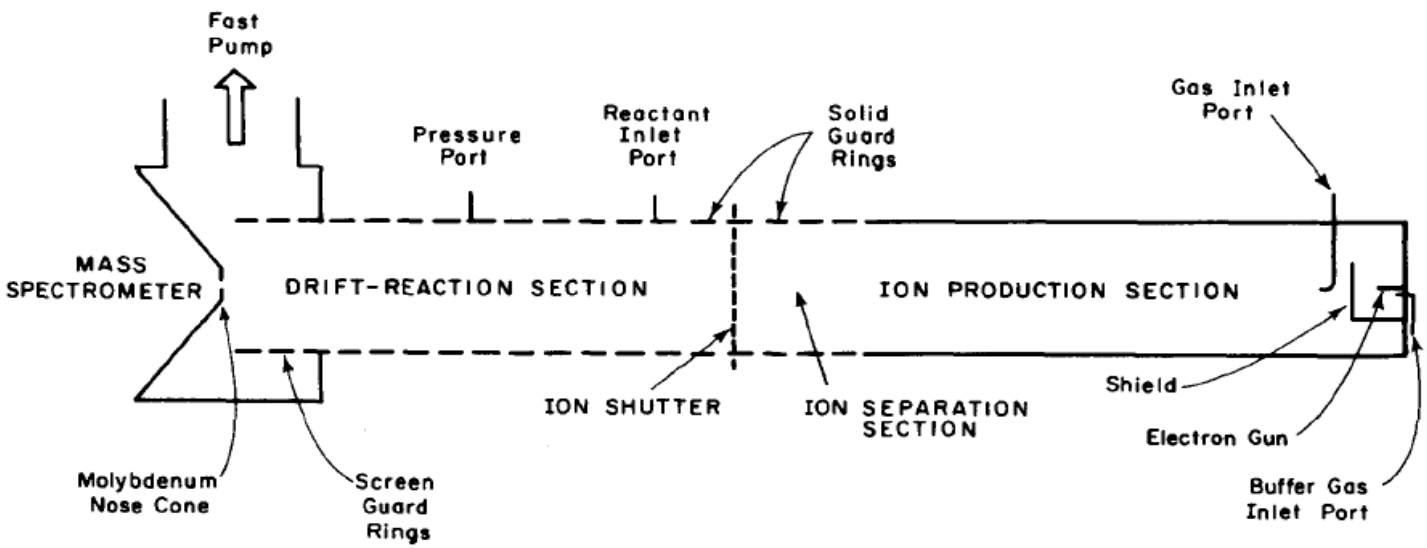

FIG. 1. Schematic drawing of the flow—drift tube.

SIFDT

100 K – 3eV

$$N_4^+ + He \rightarrow N_2^+ + N_2 + He$$

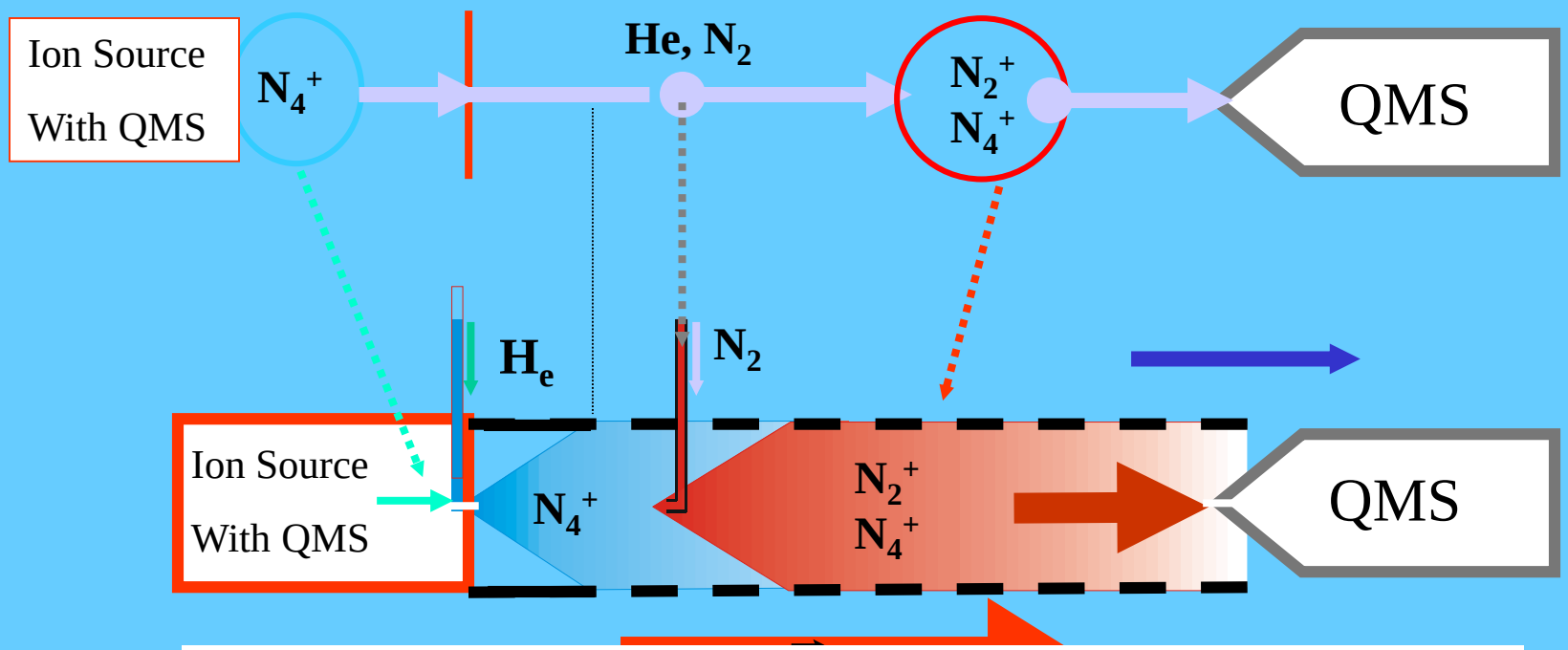

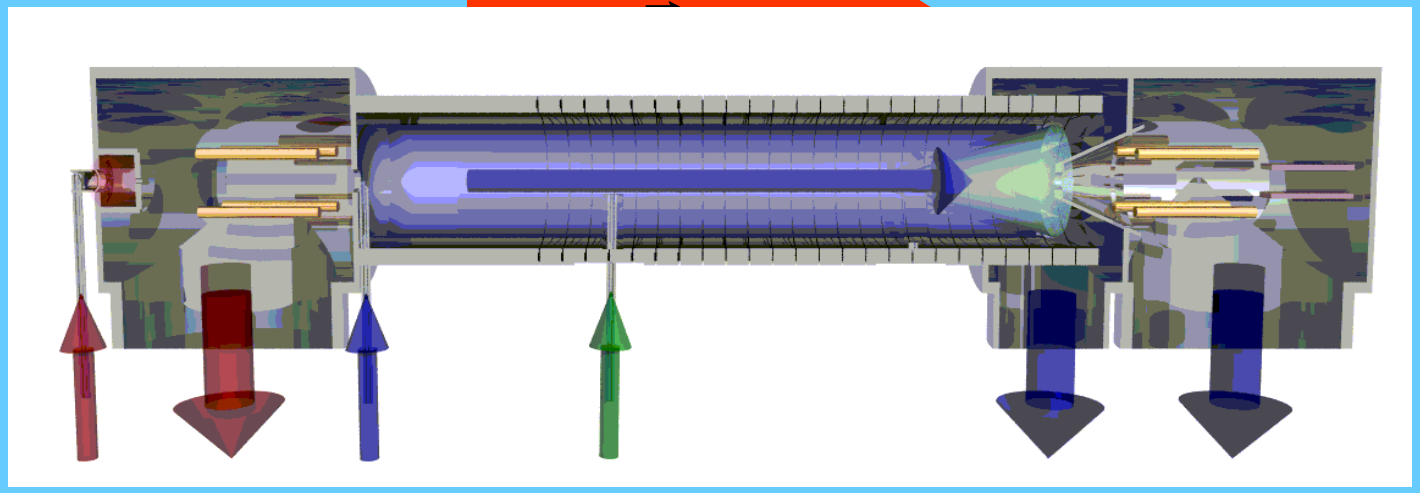

SIFDT experiment

Selected Ion Flow Drift Tube – SIFDT

$$v_d' = \mu \cdot E$$

$$\mu_0 = \mu \cdot \frac{p}{760} \cdot \frac{273}{T}$$

$$KE_{ion} = \frac{3}{2} k_b T_g + (m_c + m_i) \frac{v_d^2}{2}$$

$$KE_r = \frac{3}{2} k_b T_g + \frac{1}{2} m_r v_d^2 \left(\frac{m_i + m_c}{m_i + m_r}\right)$$

$$KE_c = \frac{3}{2} k_b T_g + \frac{1}{2} m_c v_d^2$$

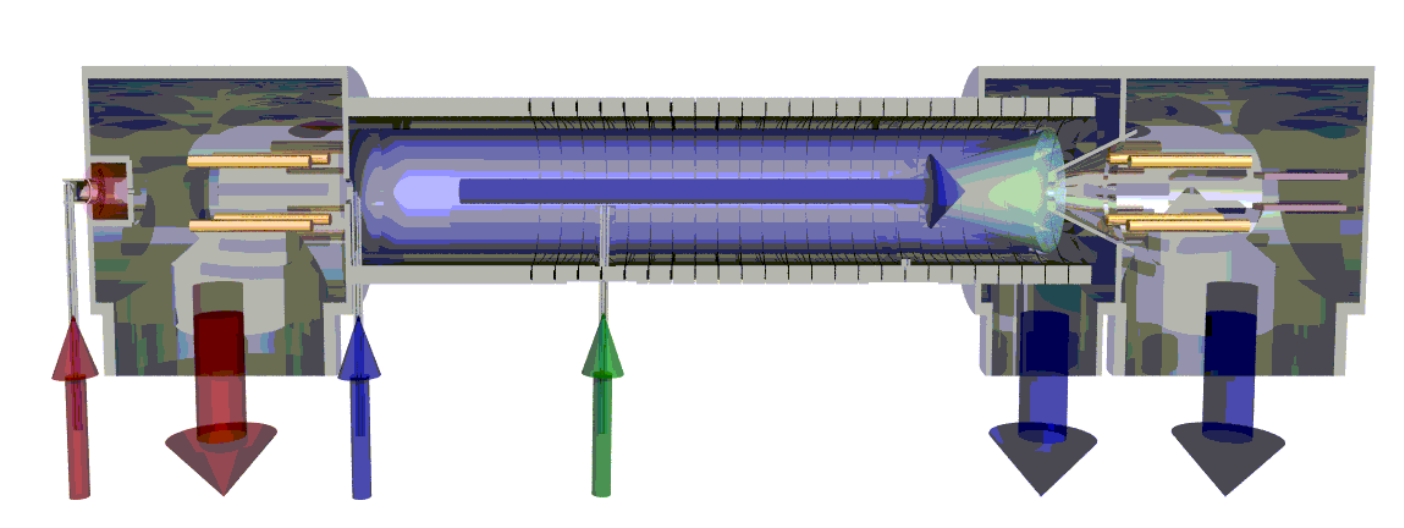

Proton transfer mass spectroscopy - Innsbruck

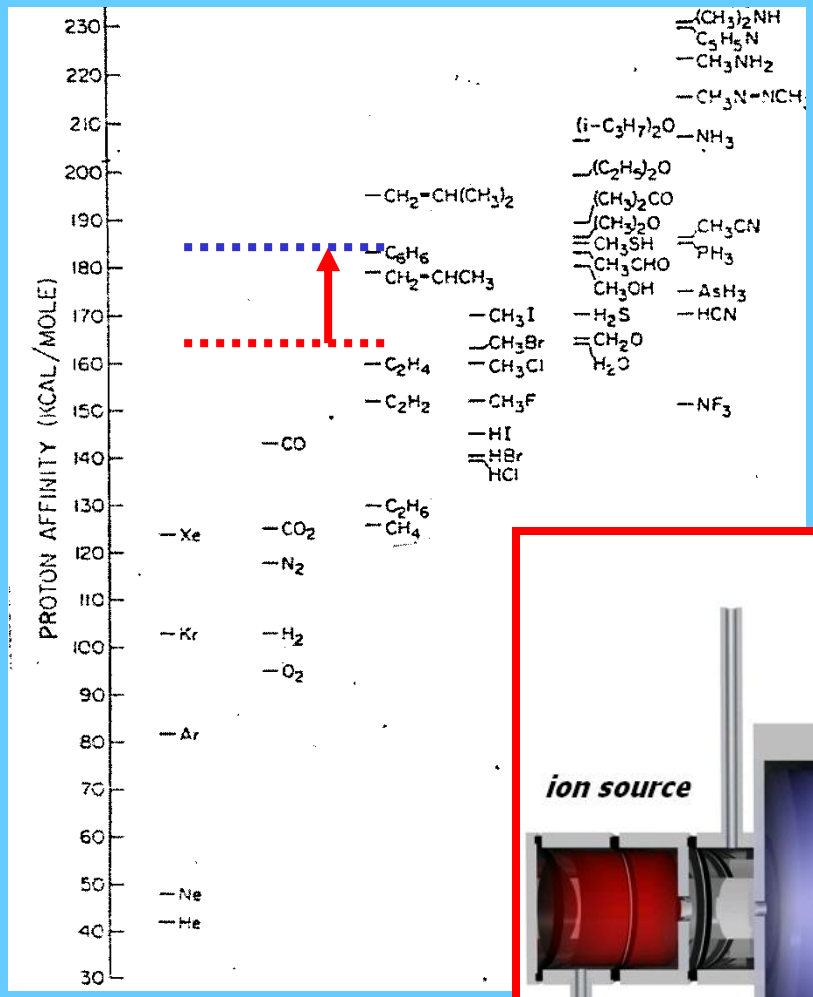

$$H_3O^+ + C_6H_6 \rightarrow C_6H_7^+ + H_2O$$

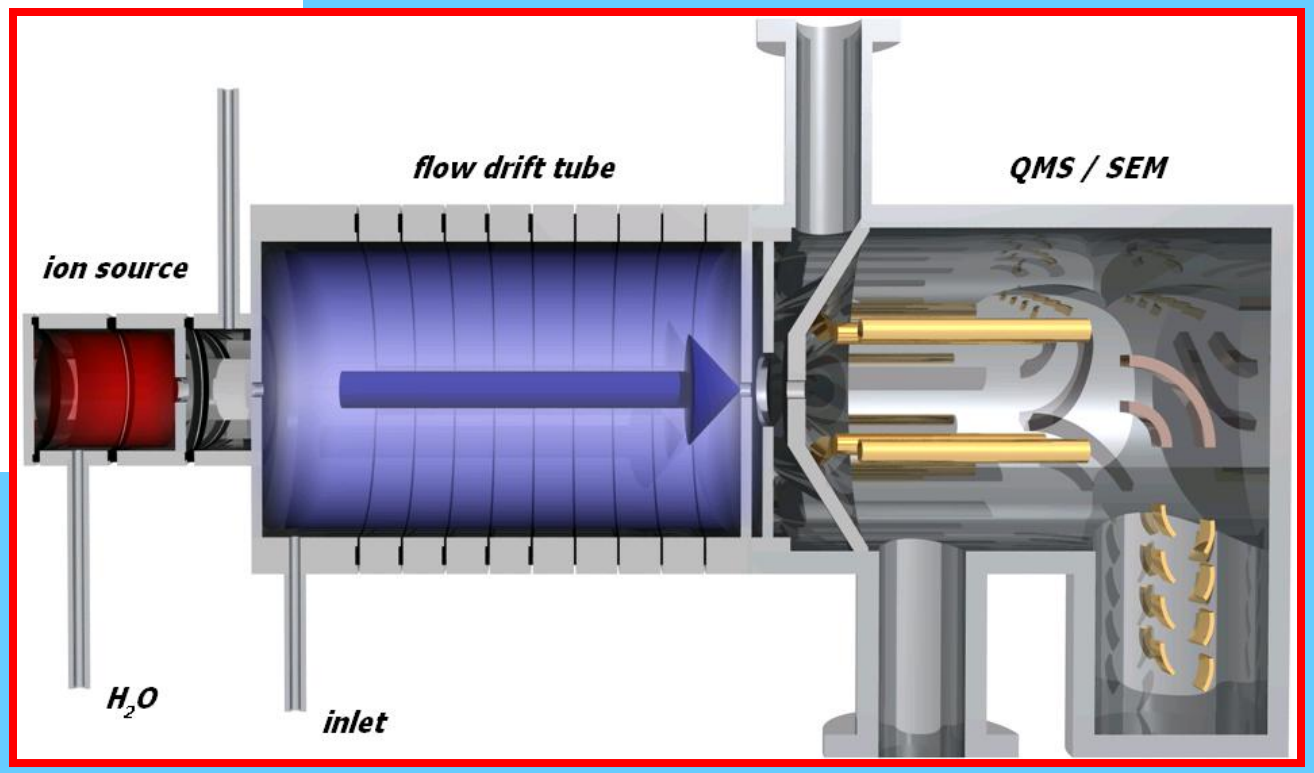

SIFDT time of flight

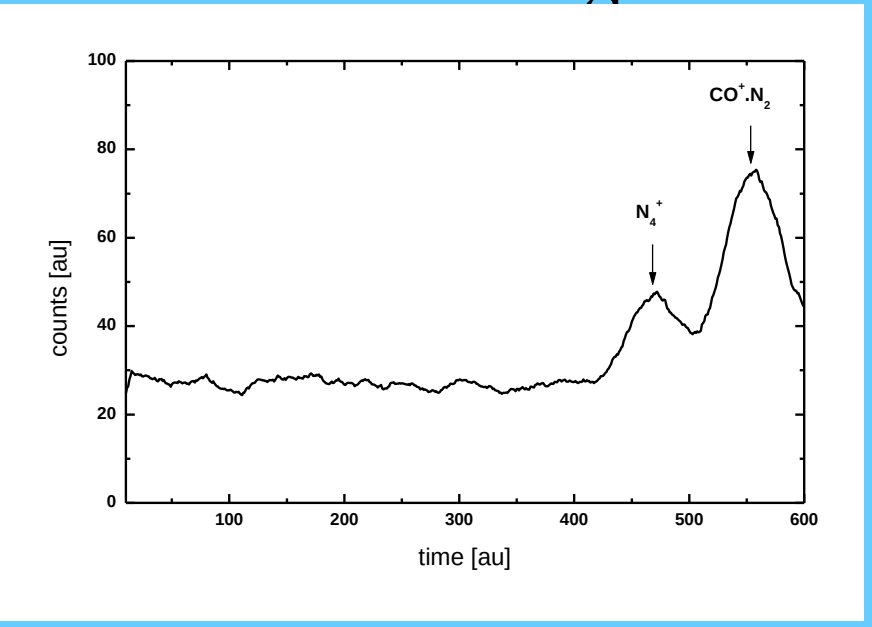

Time of flight“ spektrum iontů N_4^+ a $CO^+.N_2$ v dusíku a průběhy odpovídajících pohyblivostí.

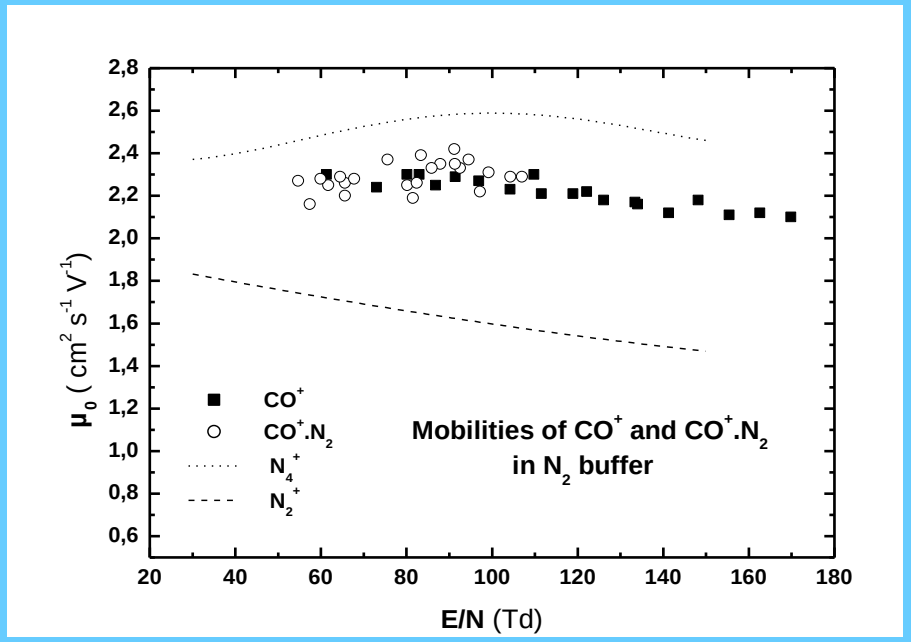

Ion mobilities

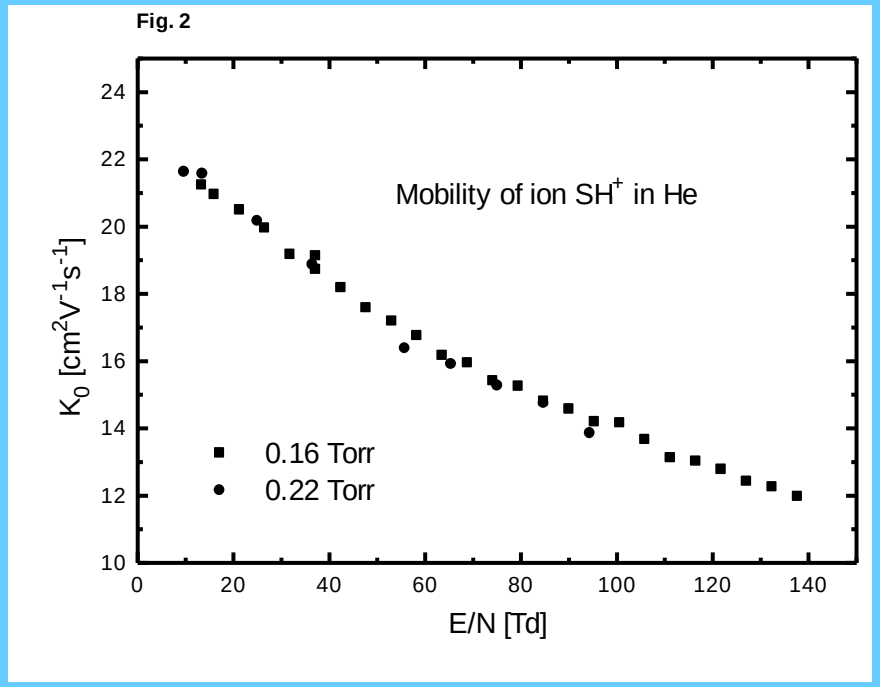

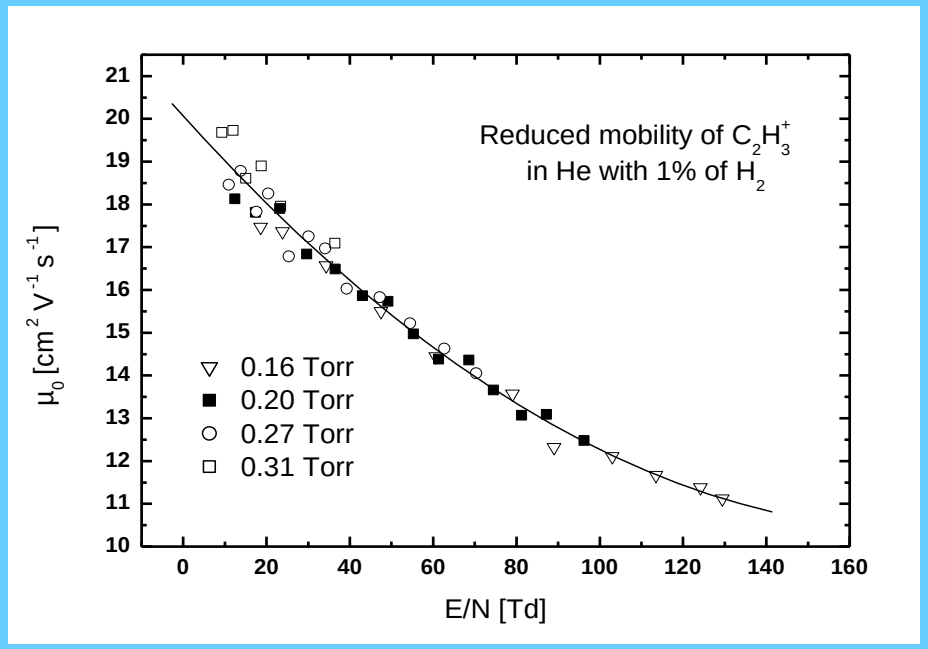

Reaction of Si^+ ions

$$Si^+ + C_6H_6 \rightarrow SiC_6H_5^+ + H$$
$$\rightarrow SiC_6H_6^+$$

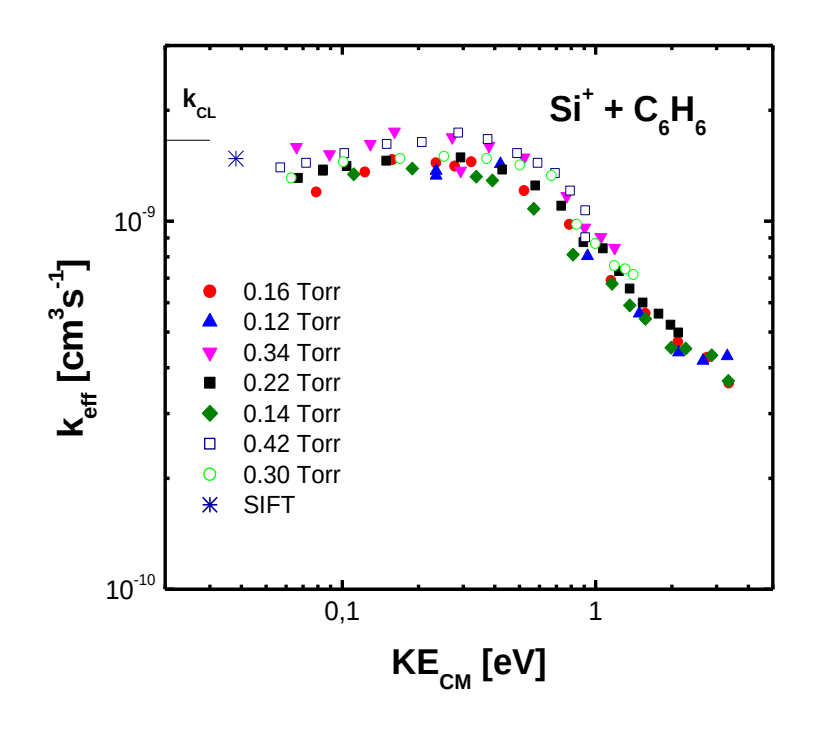

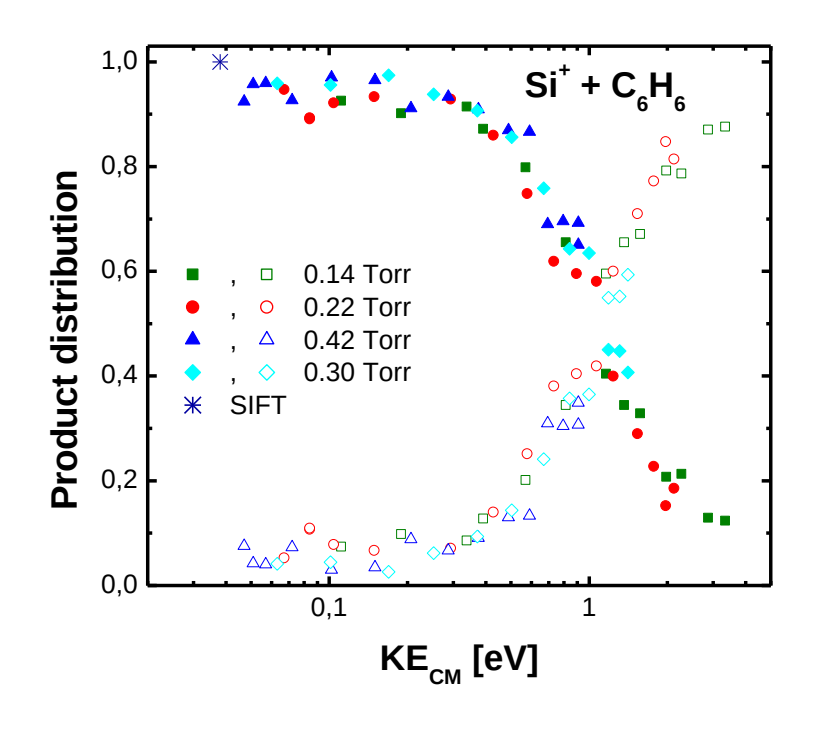

Reaction of Si^+ ions

$$Si^+ + C_6H_6 \rightarrow SiC_6H_5^+ + H$$
$$\rightarrow SiC_6H_6^+$$

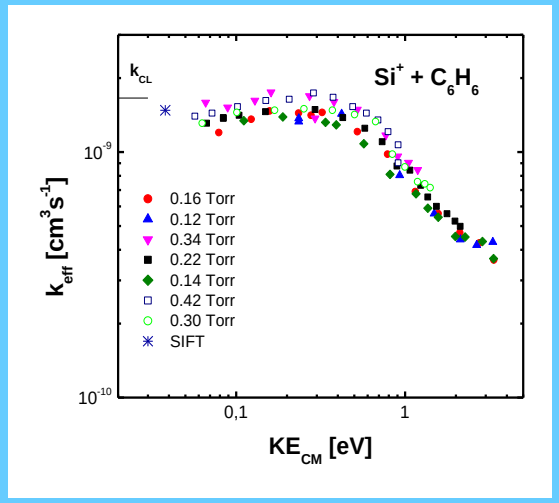

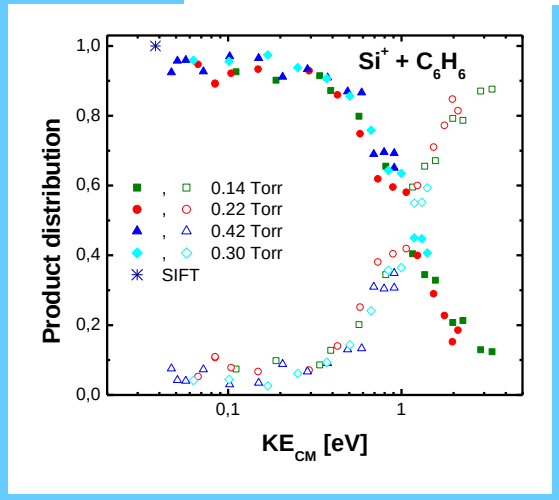

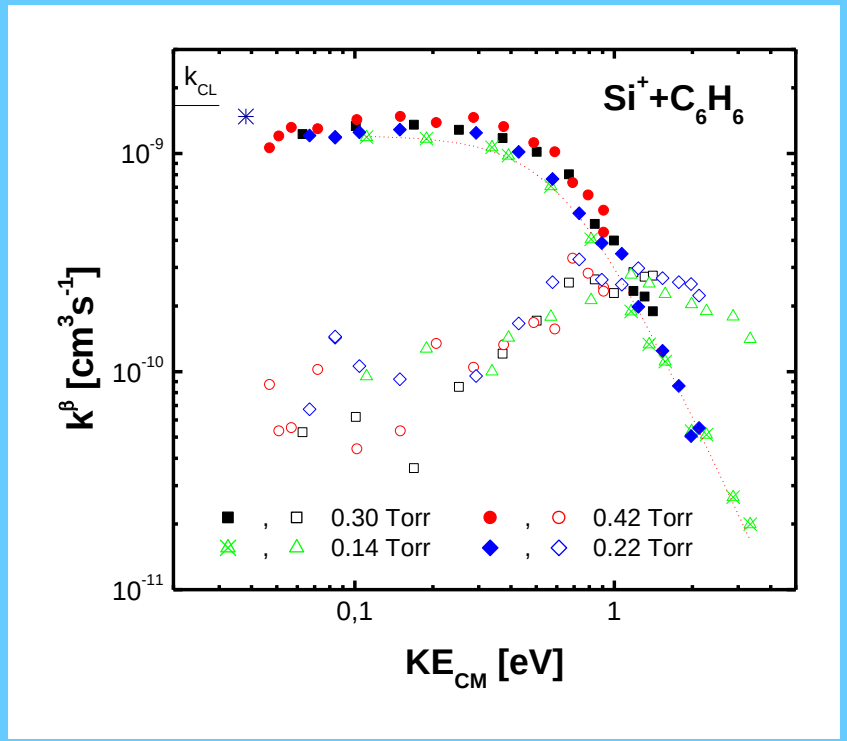

Kinetic energy dependence of IMR

eV range

$$
\begin{aligned}
Si^+ + C_2H_6 &\rightarrow SiCH_3^+ + CH_3 \\
&\rightarrow SiC_2H_4^+ + H_2 \\
&\rightarrow SiC_2H_5^+ + H \\
&\rightarrow SiC_2H_6^+
\end{aligned}
$$

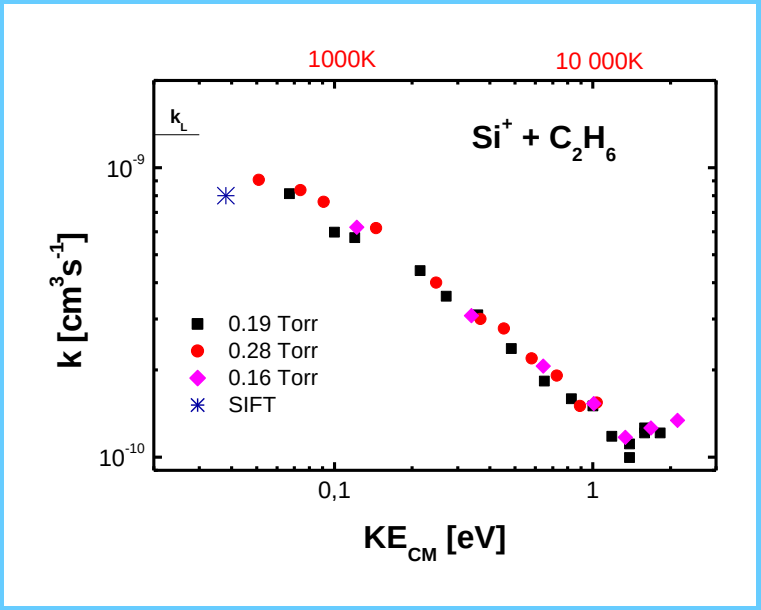

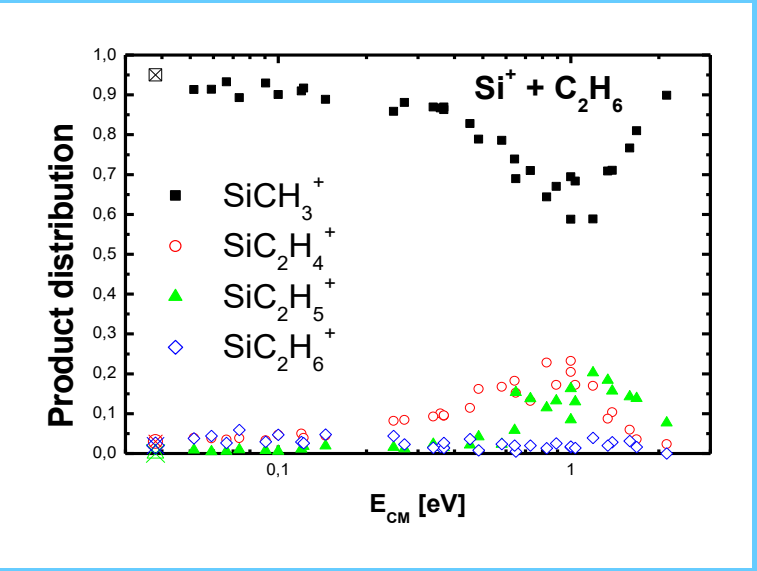

J. Glosík, P. Zakouril, W. Lindinger,
Experimental study of the reactions of $Si^+(^2P)$ ions with several small organic molecules at near thermal energies,
Czech. J. Physics, **47** (1998), pp. 29-44

SIFDT

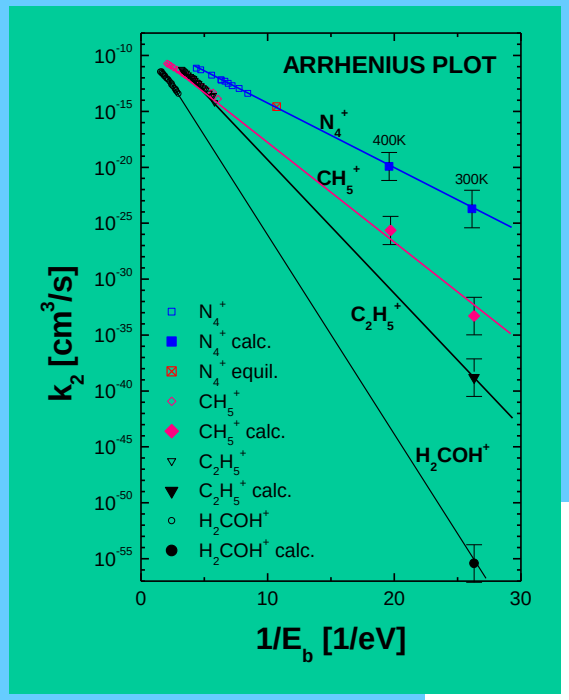

$$KE_{ion} = \frac{3}{2} k_b T_g + (m_c + m_i) \frac{v_d^2}{2}$$

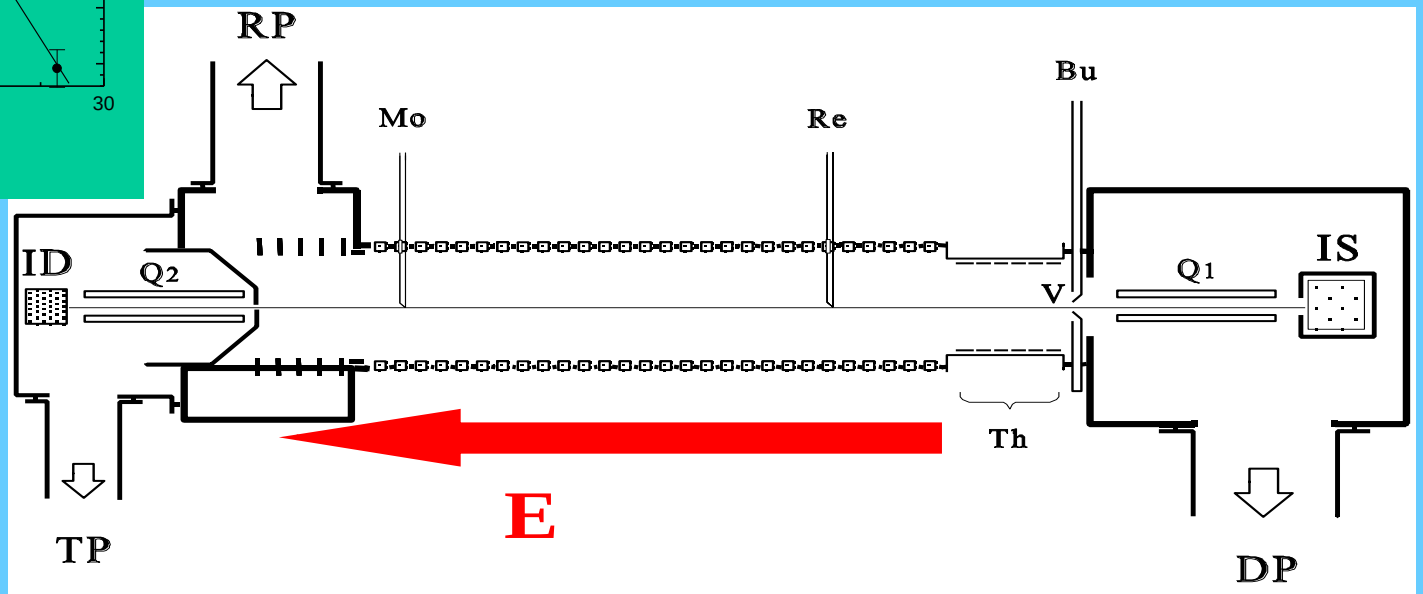

SIFDT - selected ion flow drift tube
Institut fr Ionenphysik, Universitt Innsbruck

Fig. 1

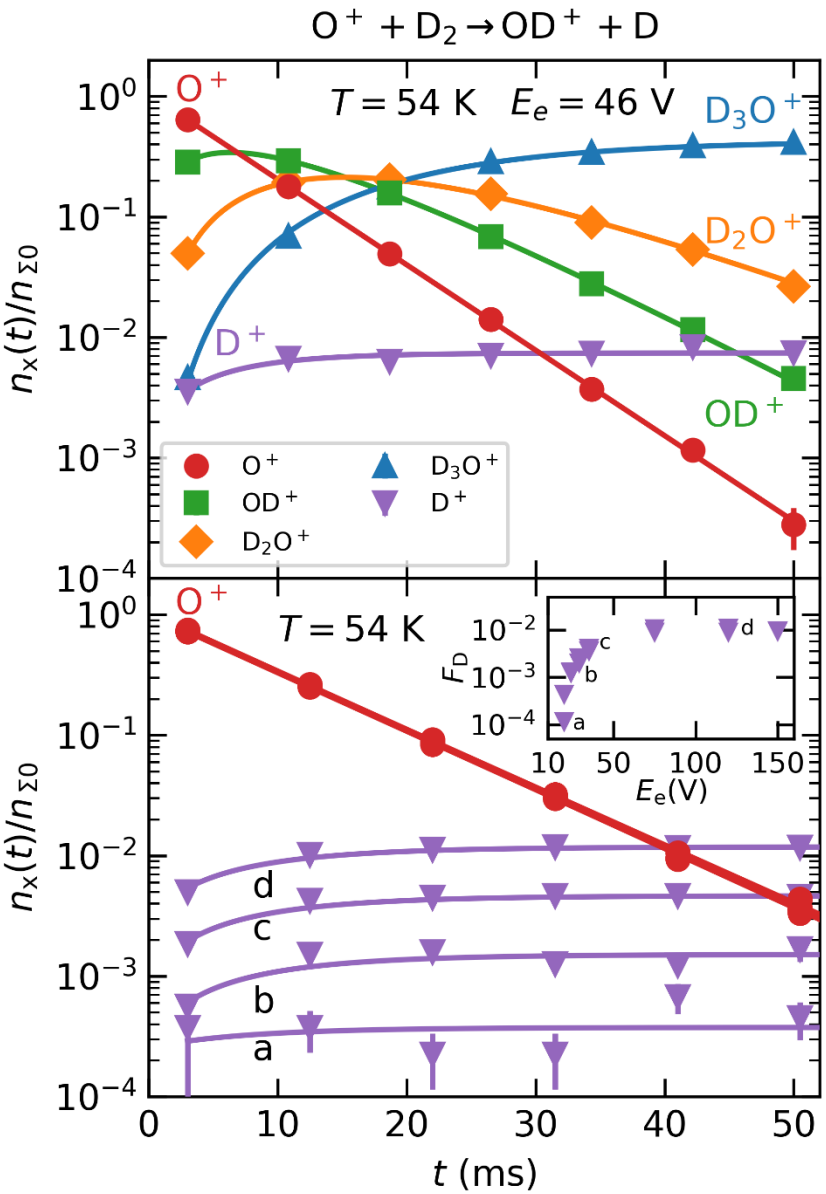

[He] = 2.39E13 cm-3

Fig. 2

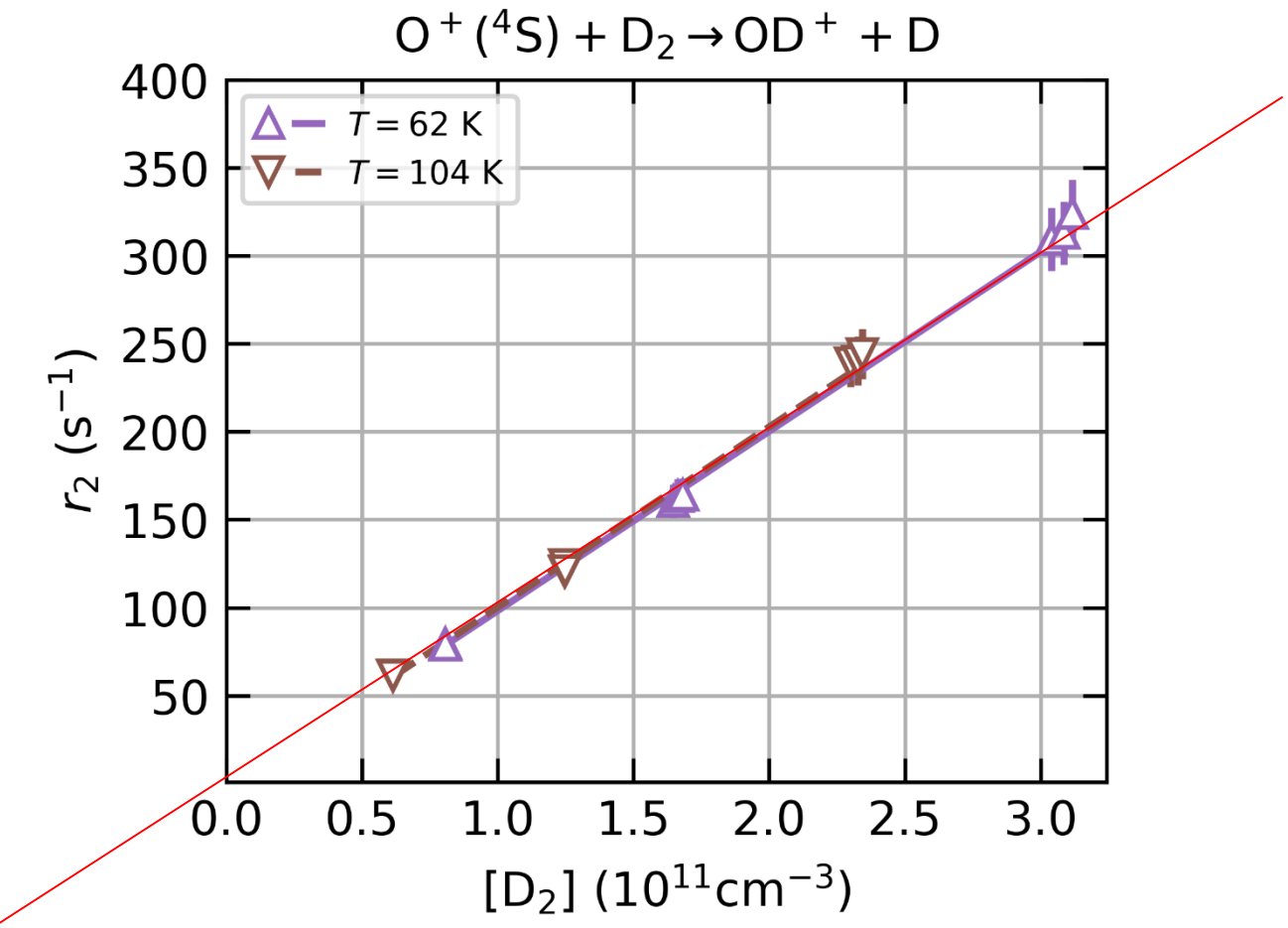

[He]_62K = 1.65E13 cm-3
[He]_104K = 2.15E13 cm-3

Fig. 3

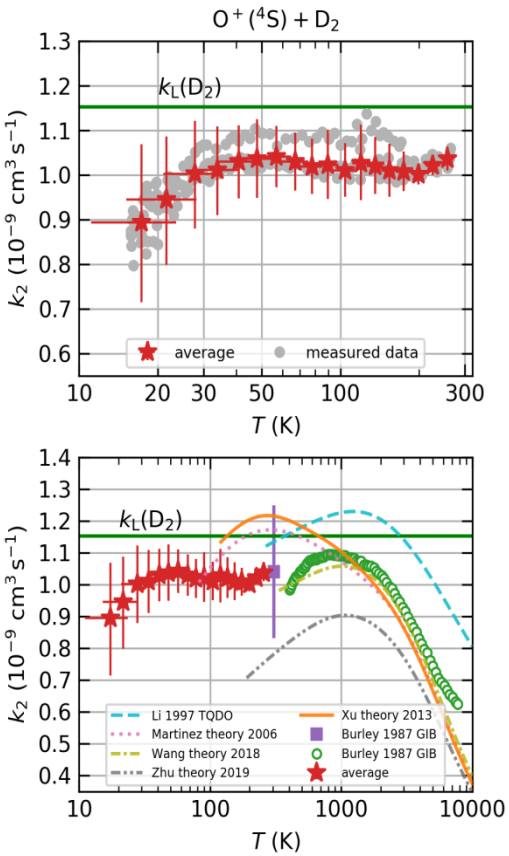
O + (4S) + D2
kL(D2)
k2 (10−9 cm3 s−1)
T (K)
average
measured data
Li 1997 TQDO
Martinez theory 2006
Wang theory 2018
Zhu theory 2019
Xu theory 2013
Burley 1987 GIB
Burley 1987 GIB
average

Fig. 4

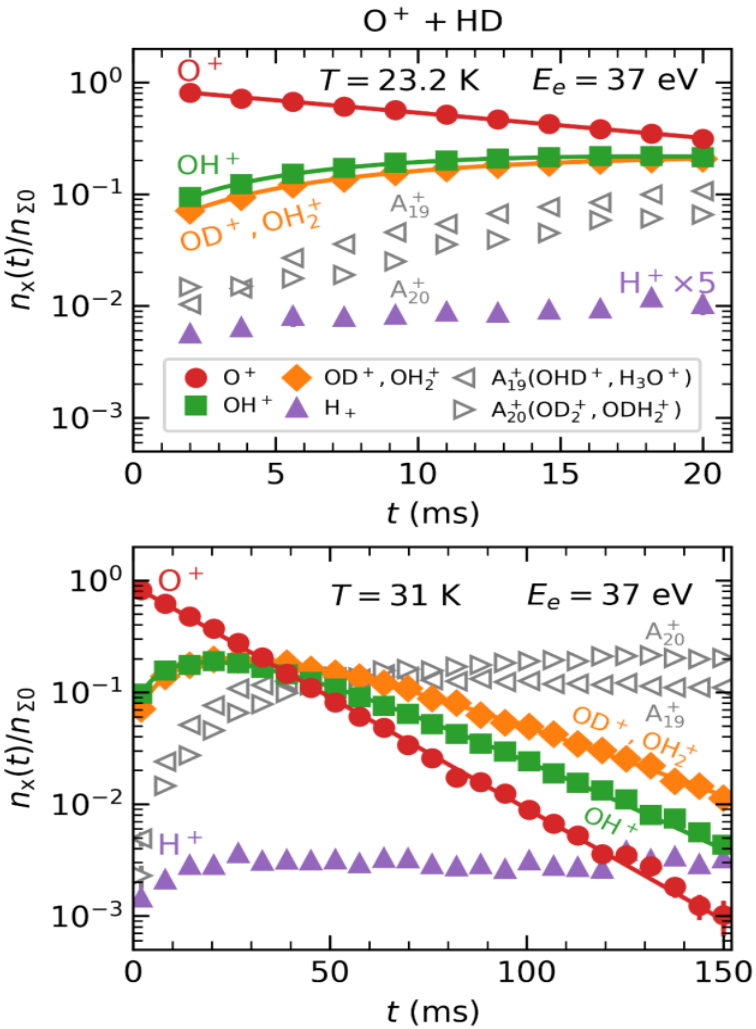
O⁺ + HD
T = 23.2 K
E_e = 37 eV
O⁺
OH⁺
OD⁺, OH₂⁺
A₁₉⁺
A₂₀⁺
H⁺ ×5
O⁺
OH⁺
OD⁺, OH₂⁺
H₊
A₁₉⁺(OHD⁺, H₃O⁺)
A₂₀⁺(OD₂⁺, ODH₂⁺)
n_x(t)/n_ΣO
t (ms)
T = 31 K
E_e = 37 eV
O⁺
A₂₀⁺
A₁₉⁺
OD⁺, OH₂⁺
OH⁺
H⁺
n_x(t)/n_ΣO
t (ms)

Fig. 6

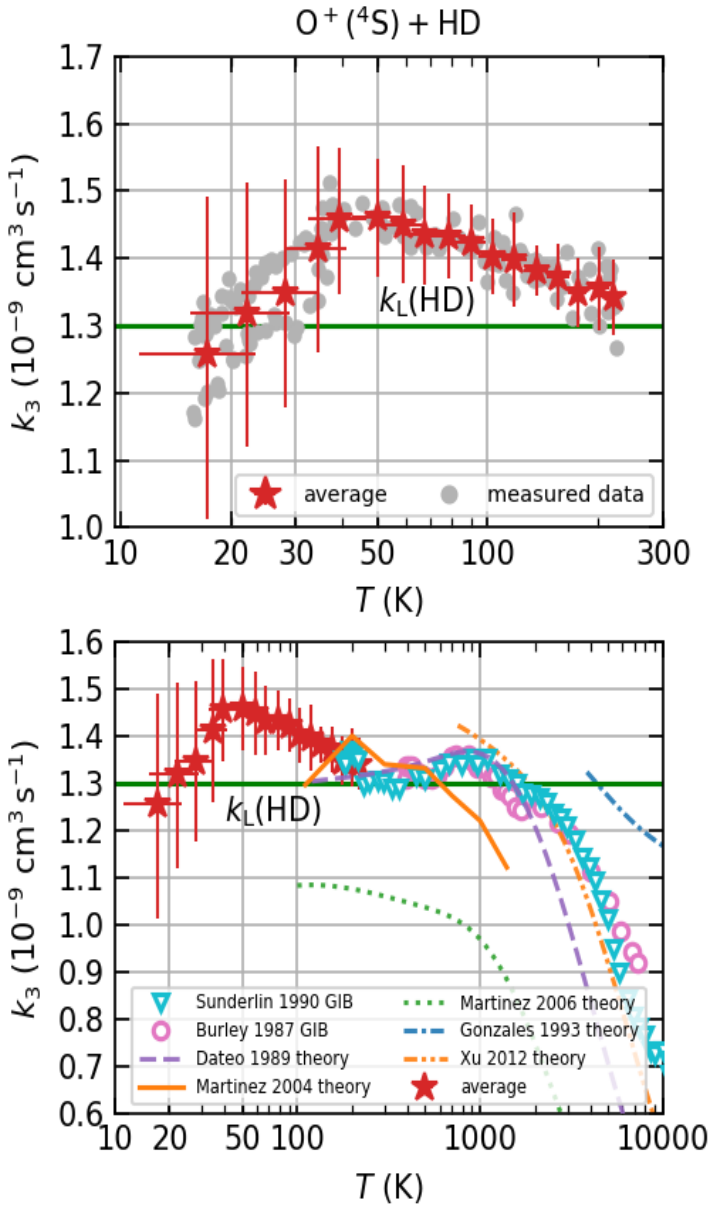
O+ (4S) + HD
k3 (10−9 cm3 s−1)
T (K)
kL(HD)
average
measured data
Sunderlin 1990 GIB
Burley 1987 GIB
Dateo 1989 theory
Martinez 2004 theory
Martinez 2006 theory
Gonzales 1993 theory
Xu 2012 theory
average

Fig. 7

09. 10. 2019, correction for 3% H2

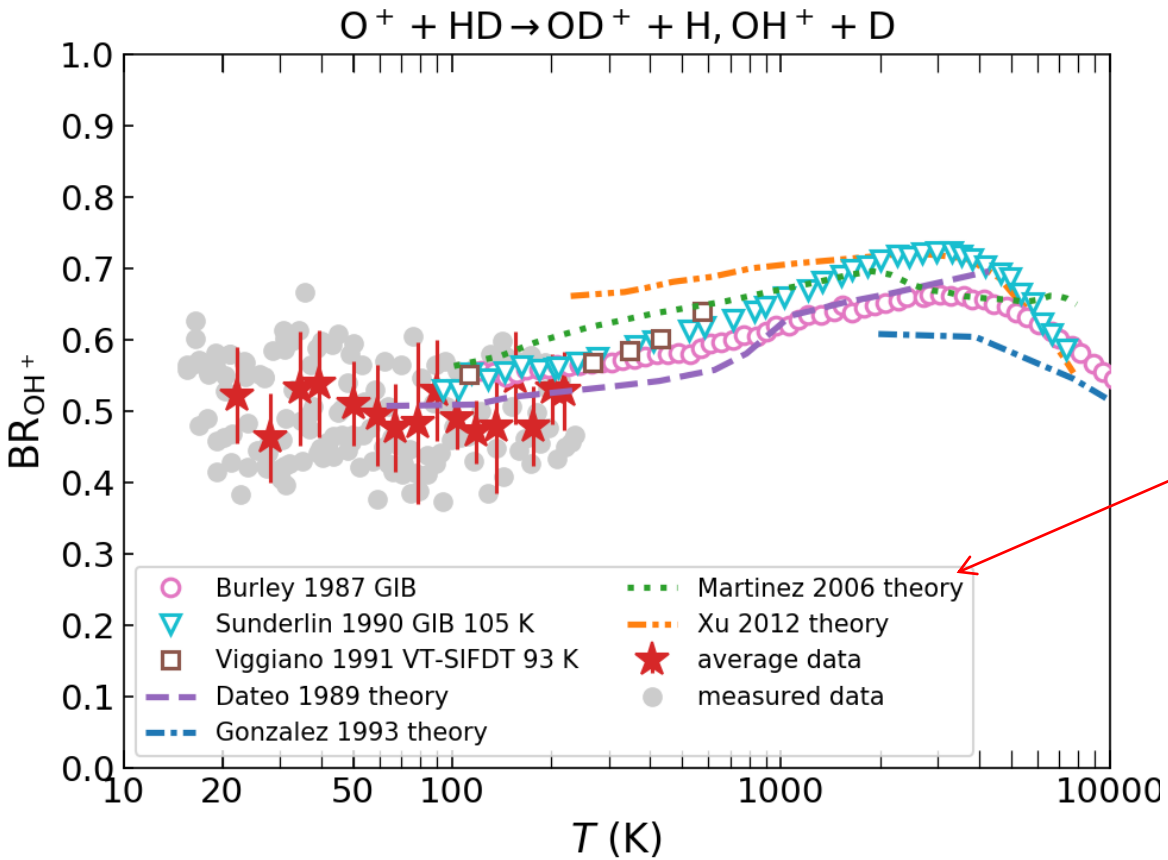

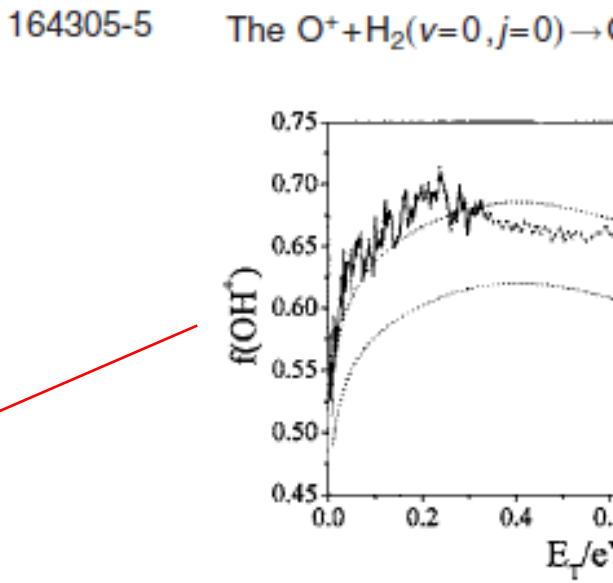

FIG. 5. HD-RWP intramolecular isotopic
action expressed in terms of the $f(OH^+)$ fr
for reaction $O^+ + HD(300\ K)$ are also repre
data, considering a 5% experimental error
$WP_2(HD)$, and (···) Expt.

Fig. 8

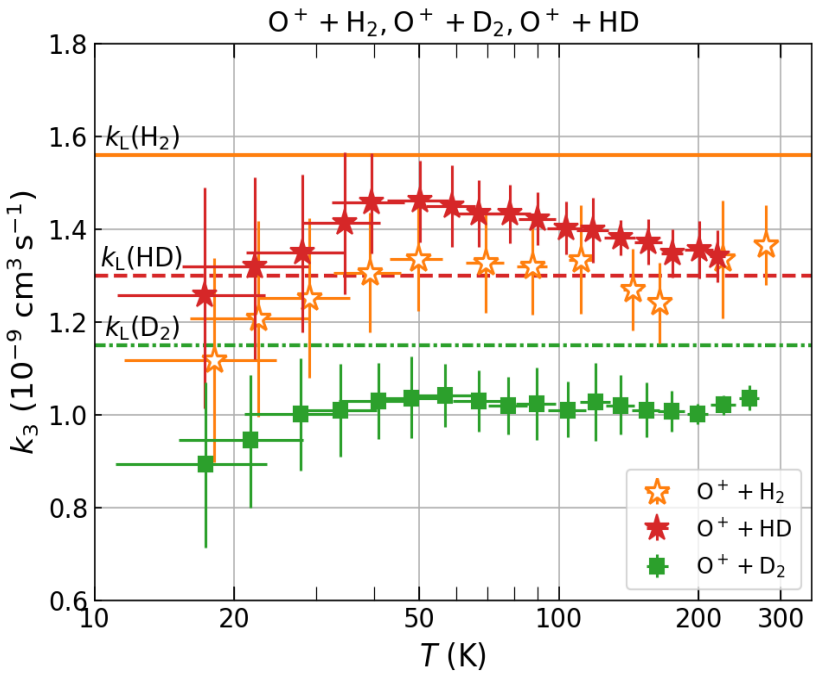
$O^+ + H_2, O^+ + D_2, O^+ + HD$
$k_L(H_2)$
$k_L(HD)$
$k_L(D_2)$
k_3 (10^{-9} cm^3 s^{-1})
T (K)
1.8
1.6
1.4
1.2
1.0
0.8
0.6
10
20
50
100
200
300
$O^+ + H_2$
$O^+ + HD$
$O^+ + D_2$

Reakce II.řádu

2 A ➔ P

$$-\int_{c_{A0}}^{c_A} \frac{dc_A}{c_A^2} = k\int_0^{\tau} dt$$

$$-\left[\frac{c_A^{-1}}{-1}\right]_{c_{A0}}^{c_A} = k\tau$$

$$\frac{1}{c_A} - \frac{1}{c_{A0}} = k\tau$$

$$c_A = \frac{c_{A0}}{1 + c_{A0}k\tau}$$

poločas reakce:

$$c_A = \frac{c_{A0}}{2}$$

$$\tau_{0,5} = \frac{1}{k}\left(\frac{2}{c_{A0}} - \frac{1}{c_{A0}}\right) = \frac{1}{k.c_{A0}}$$

Second-Order Reactions

$$\frac{1}{[A]} - \frac{1}{[A]_o} = k_A t \qquad (17.16)$$

$$\frac{1}{[A]} = \frac{1}{[A]_o} + k_A t$$

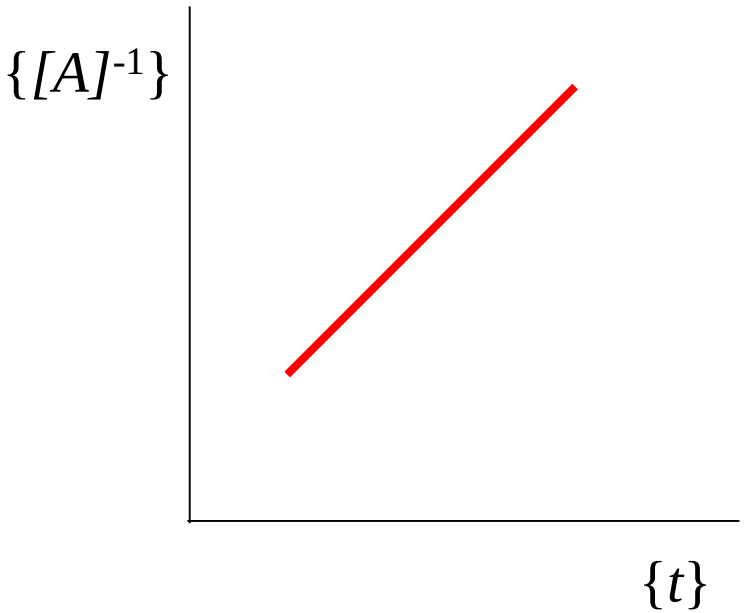

$$t_{1/2} = \frac{1}{[A]_o k_A}$$

Second-order reaction: *1/[A]* vs *t*

VT - AISA

2 Torr of He/Ar/H_2

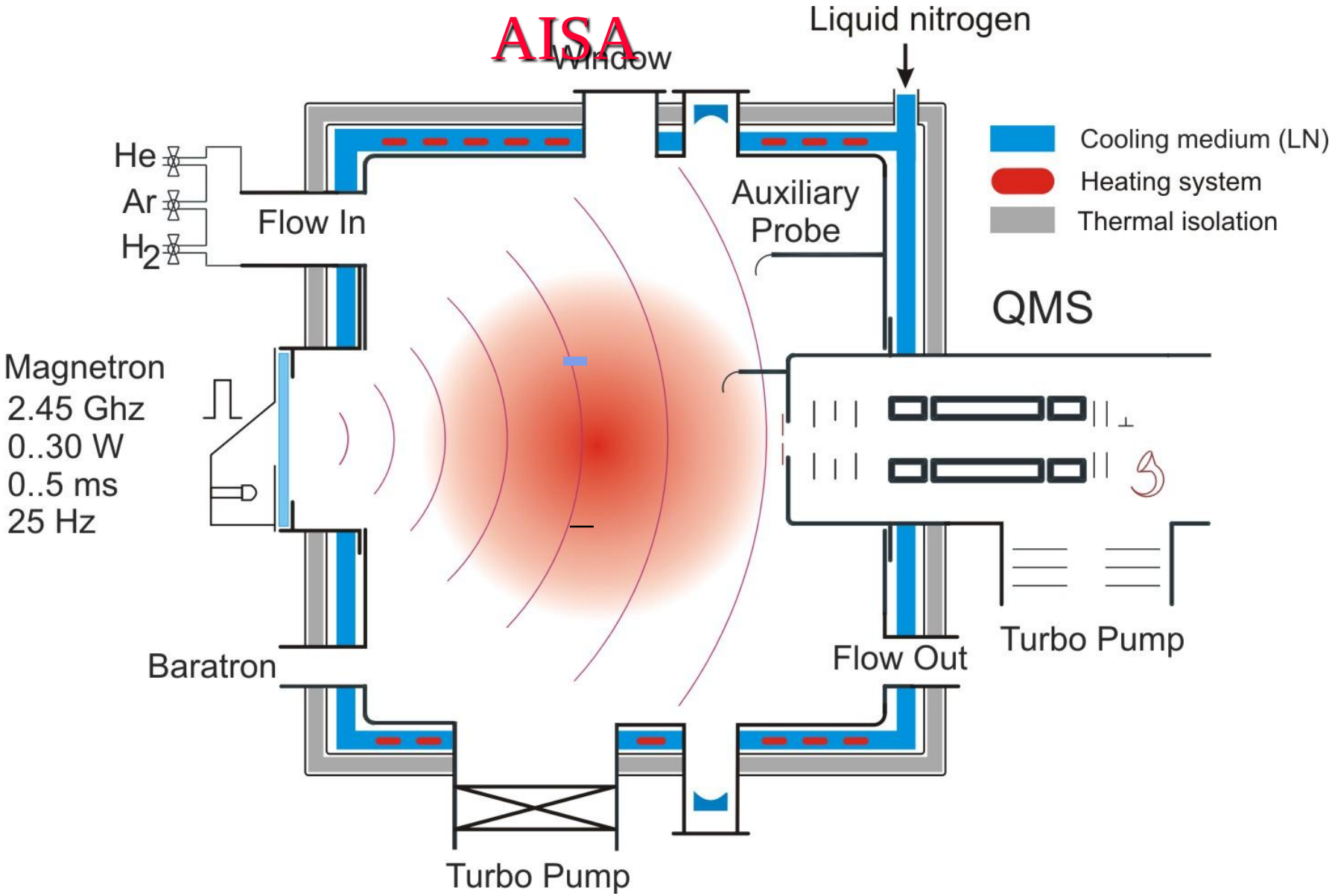

We measure effective – apparent binary recombination rate coefficient

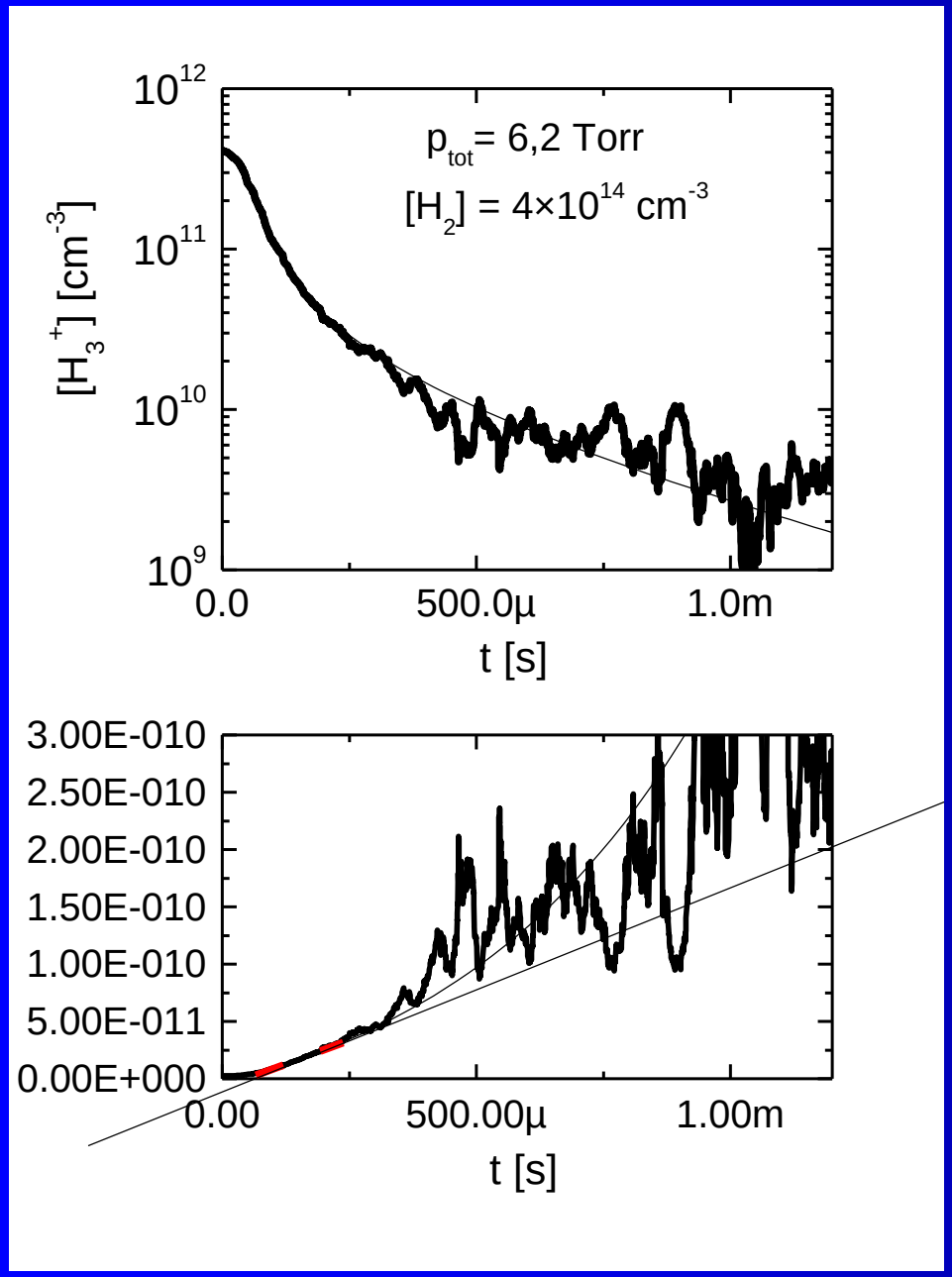

Quasineutral H_3^+ dominated plasma

$$\frac{\mathrm{d}n_\mathrm{e}}{\mathrm{d}t} = -\alpha_\mathrm{eff} n_\mathrm{e}^2 - \frac{n_\mathrm{e}}{\tau_\mathrm{L}}$$

$$\frac{1}{[H_3^+]} = \frac{1}{[H_3^+]_0} + \alpha t$$

We measure effective – apparent binary recombination rate coefficient

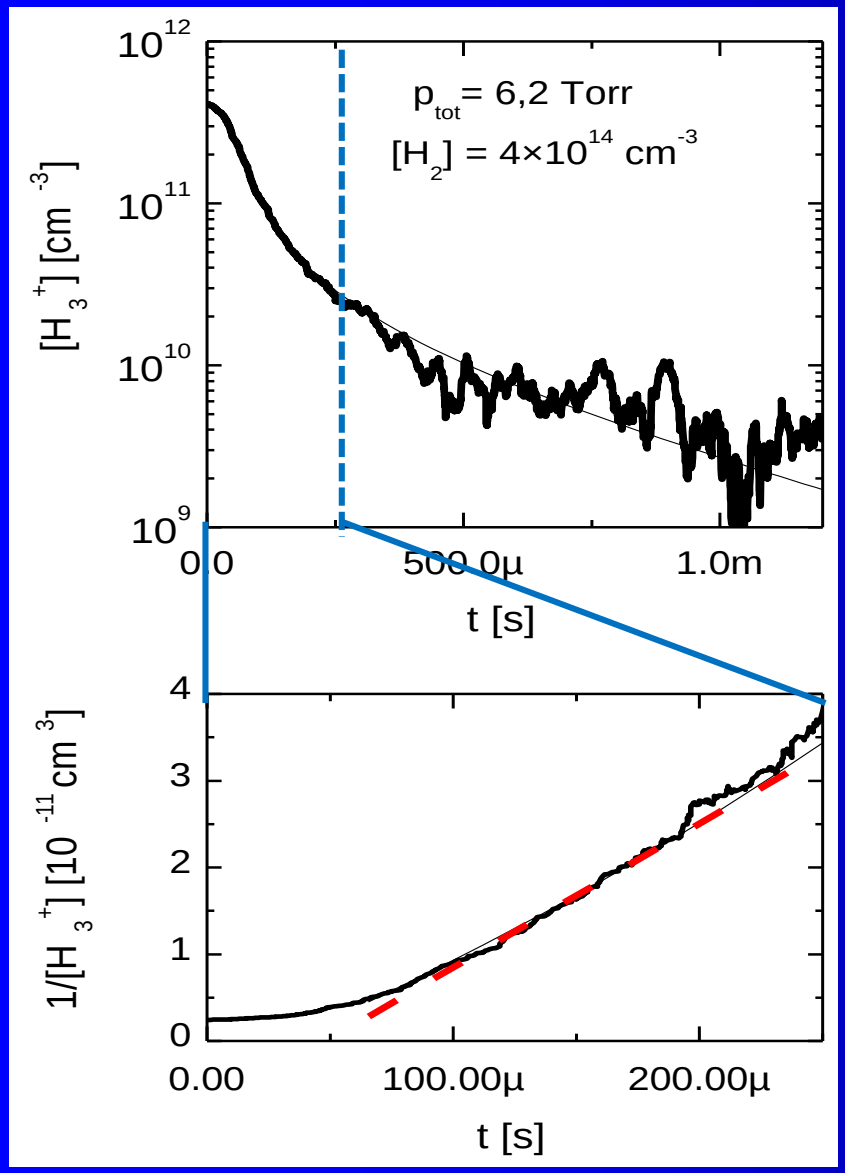

Quasineutral H_3^+ dominated plasma

$$\frac{\mathrm{d}n_\mathrm{e}}{\mathrm{d}t} = -\alpha_\mathrm{eff} n_\mathrm{e}^2 - \frac{n_\mathrm{e}}{\tau_\mathrm{L}}$$

$$\frac{1}{[H_3^+]} = \frac{1}{[H_3^+]_0} + \alpha t$$

Diffusion and recombination

$$\frac{dn_e}{dt} = -\alpha\, n_e^2 - \frac{D_a}{\Lambda^2} n_e$$

$$\frac{1}{n_e} = \alpha\, \frac{\exp(\nu t) - 1}{\nu} + \frac{1}{n_0} \exp(\nu t)$$

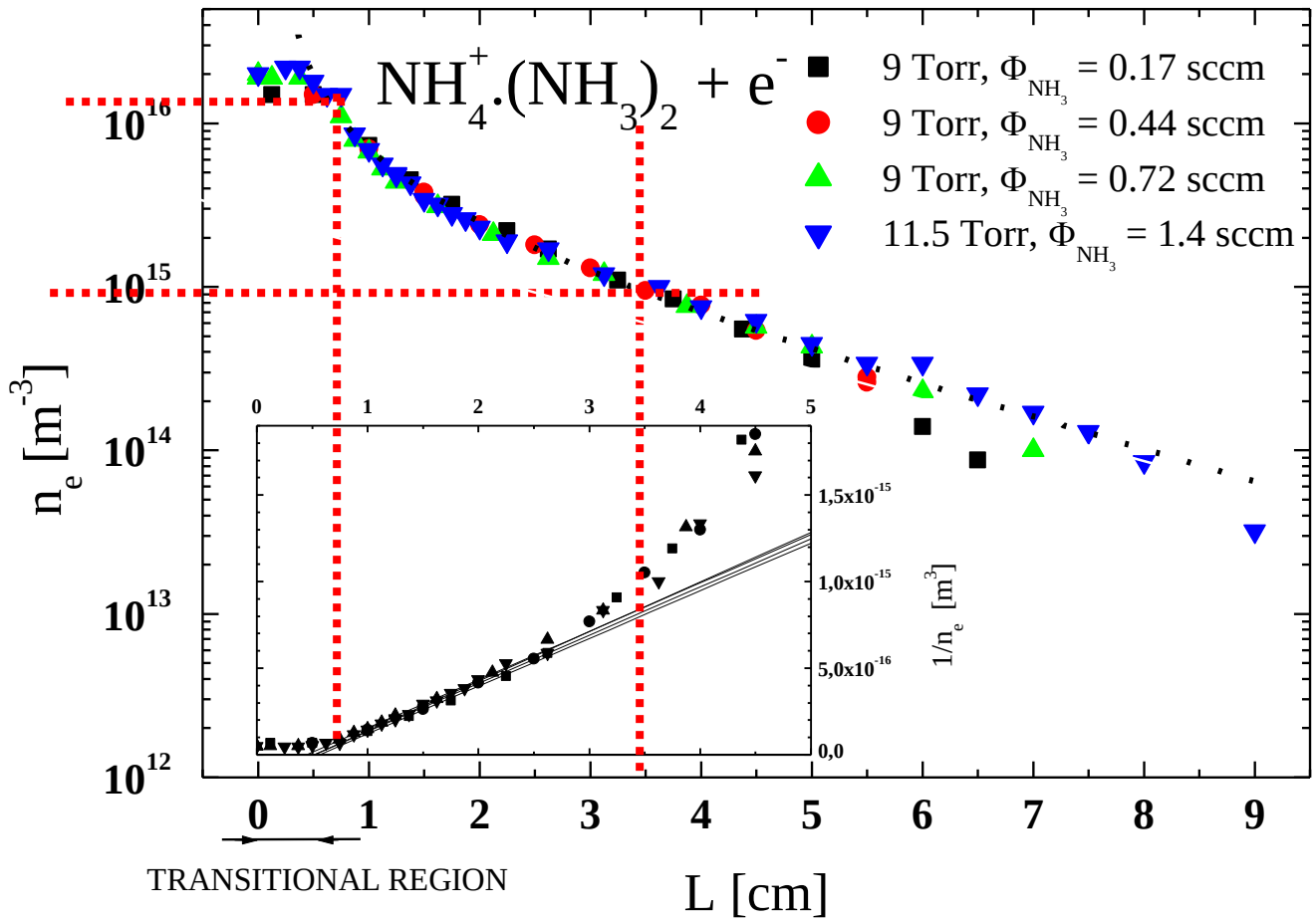

J. Glosík, G. Bánó, R. Plašil, A. Luca, P. Zakouril,
Study of the electron ion recombination in high pressure flowing afterglow. Recombination of $NH_4^+.(NH_3)_2$,
International J. Mass Spectrom., **189**, 103-113 (1999)

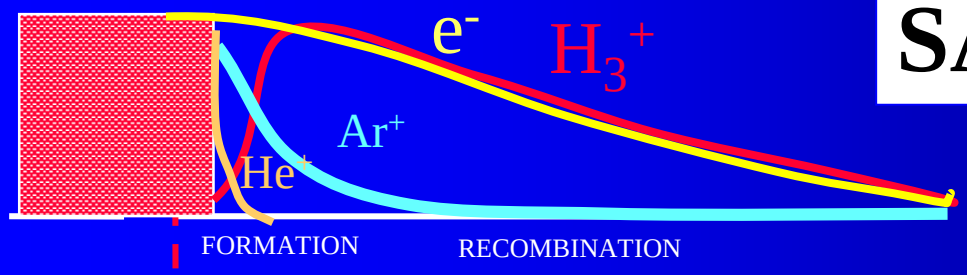

SA

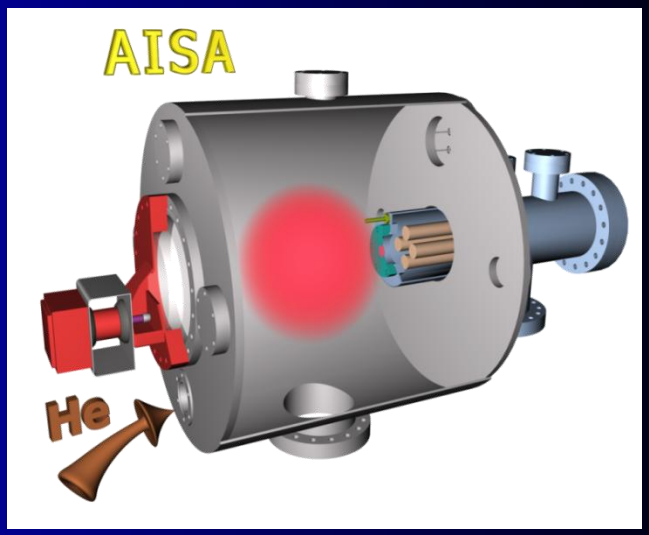

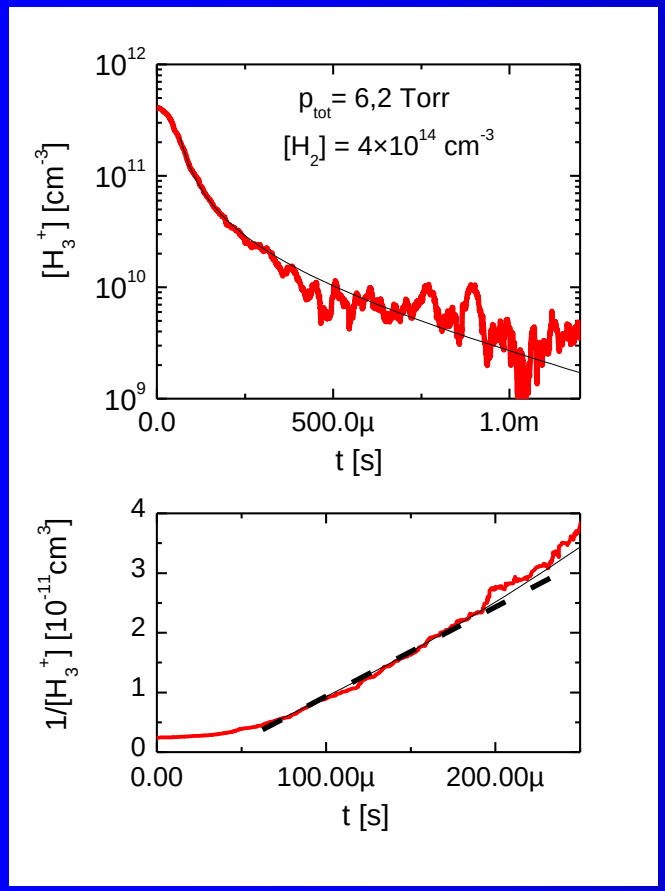

H_3^+/e^- plasma in $He/Ar/H_2$ gas mixture

$$\frac{dn_e}{dt} = -\alpha_{eff} n_e^2 - \frac{n_e}{\tau_L}$$

$$\frac{1}{[n_e]} = \frac{1}{[n_{e0}]} + \alpha_{eff} t$$

α_{eff}

effective (apparent) binary recombination rate coefficient

Emotional history of H_3^+ recombination

$$H_3^+ + e^- \Rightarrow H + H_2, 3H$$

α(T=300 K)

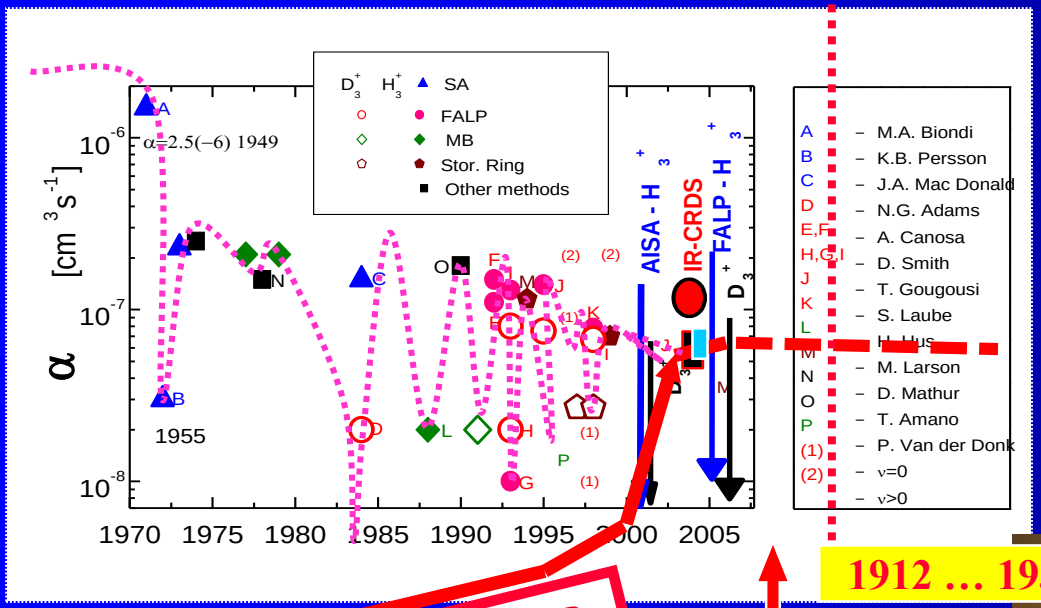

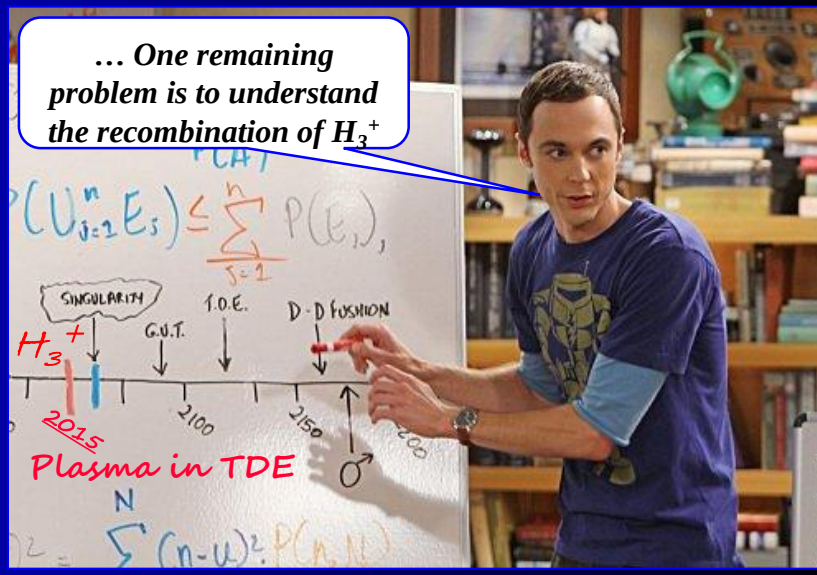

1912 … 1936 … 1949 … 1990 … 2003 …2008 …2011…

THEORY OF DR

Doubts 2011

Storage rings - state selected data:
"Presently no rate coefficient measurement with a confirmed temperature below 300 K exists".

Petrignani *et al.* Phys. Rev. A (2011)

and … history repeated itself .

M. Larsson et al, CP Letters (2008)

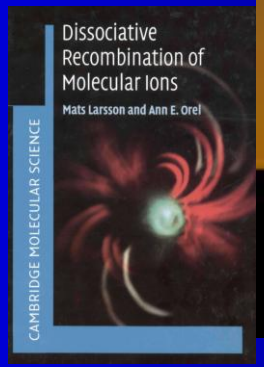

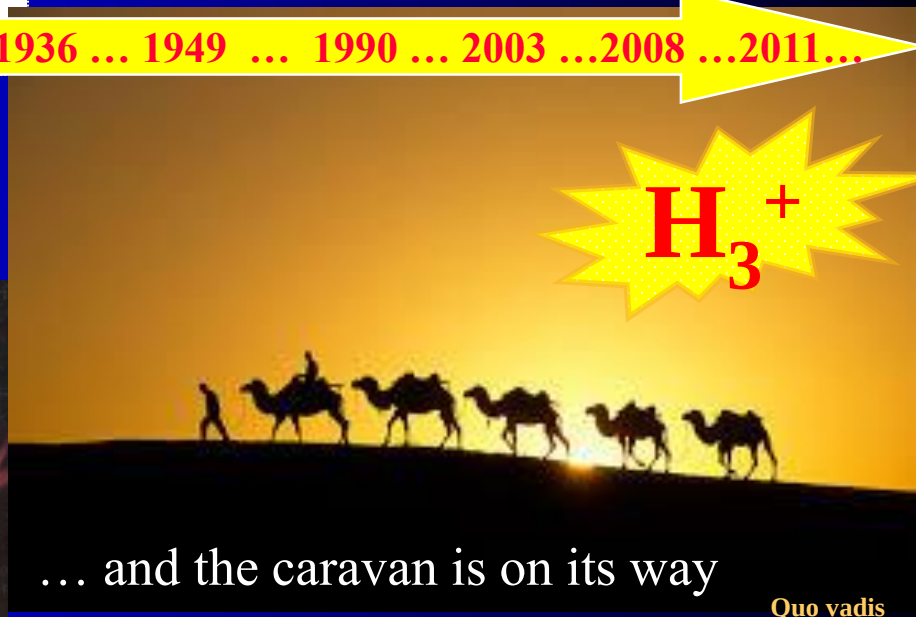

… and the caravan is on its way

Quo vadis

Stationary afterglow + Spectroscopic identification of recombining ions

SA-CRDS

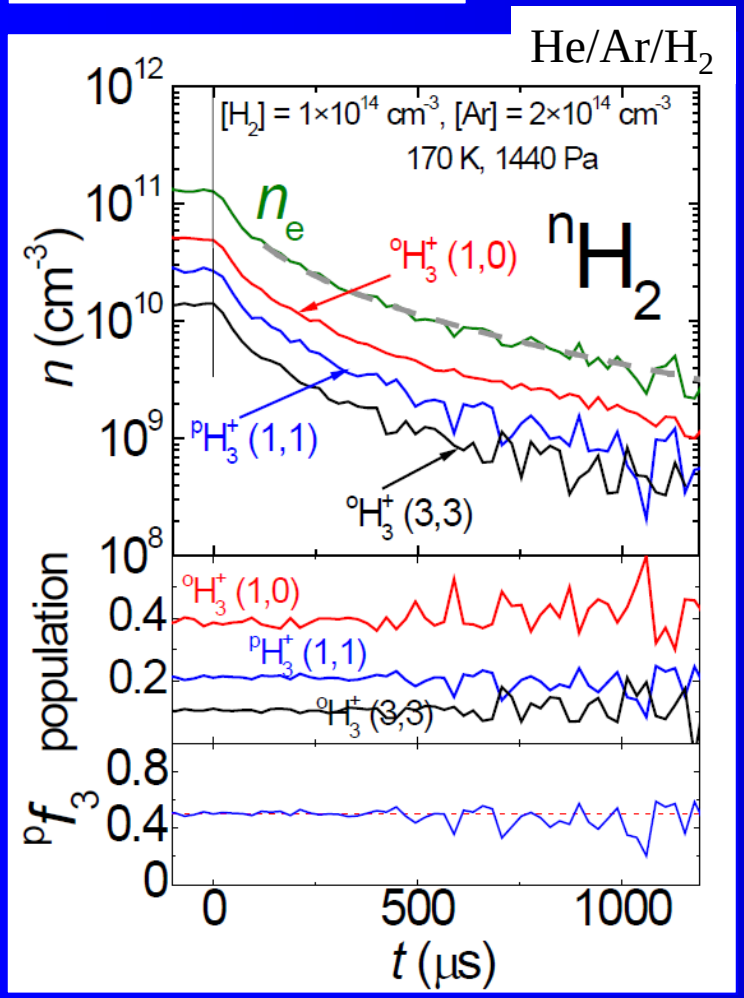

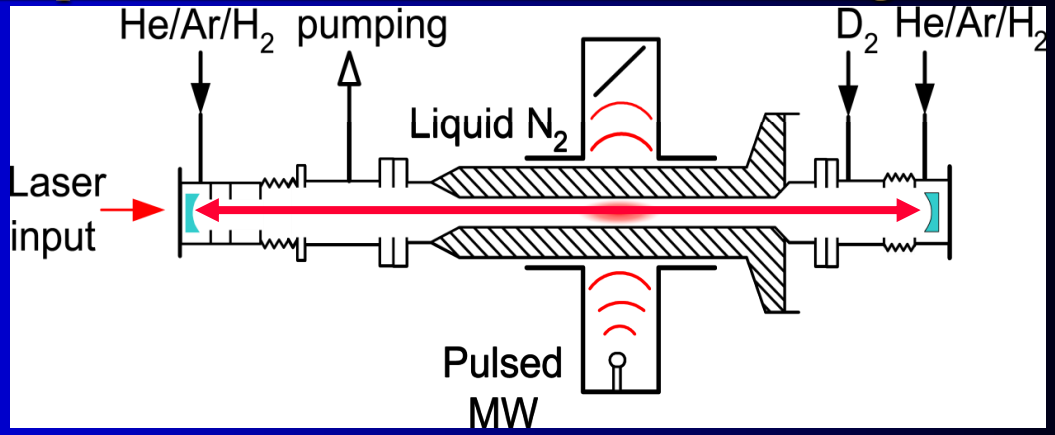

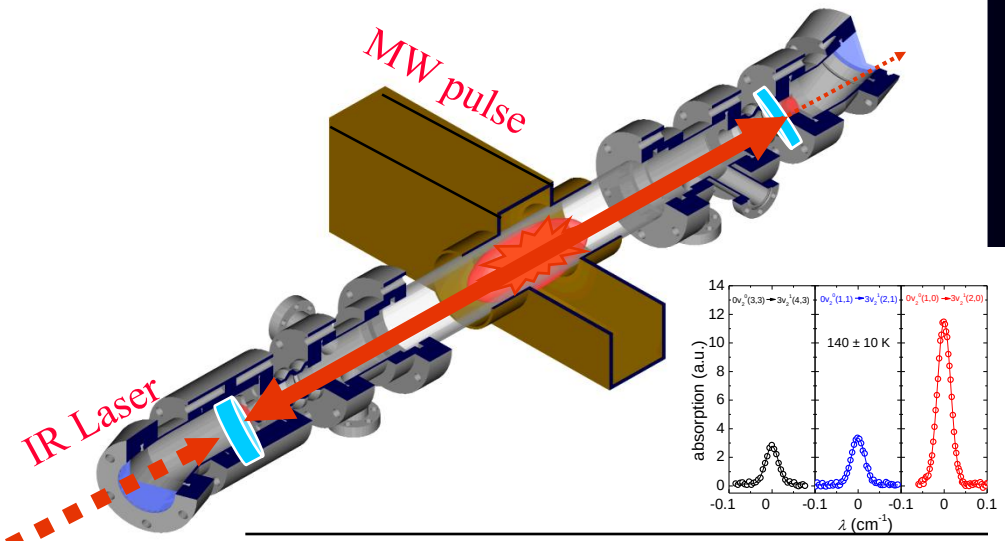

Wavenumber [cm^{-1}]	Spin	Transition
7234,957	o	$0\nu_2^0(3,3) \rightarrow 3\nu_2^1(4,3)$
7237,285	p	$0\nu_2^0(1,1) \rightarrow 3\nu_2^1(2,1)$
7241,245	o	$0\nu_2^0(1,0) \rightarrow 3\nu_2^1(2,0)$

$$\frac{d[H_3^+]}{dt} = -\alpha_{eff}[H_3^+]n_e = -\alpha_{eff}[H_3^+]^2$$

All experiments

Third-Order Reactions

$$\frac{d[A]}{dt} = -ak[A]^3 \quad \frac{d[A]}{dt} = -ak[A]^2[B] \quad \frac{d[A]}{dt} = -ak[A][B]^2 \quad \frac{d[A]}{dt} = -ak[A][B][C]$$

(Problems 17.17 and 17.24)

$$\frac{d[A]}{[A]^3} = -k_A dt \qquad \frac{1}{[A]^2} - \frac{1}{[A]_o^2} = 2k_A t$$

$$[A] = \frac{[A]_o}{\left(1 + 2kt[A]_o^2\right)^{1/2}} \qquad (17.24)$$

Reakce II.řádu

A + B ➔ P

y…….zreagované množství

$$c_A = c_{A0} - y$$

$$c_B = c_{B0} - y$$

$$-\frac{dc_A}{dt} = \frac{dy}{dt}$$

$$\frac{1}{c_{A0} - c_{B0}} . \ln \frac{c_{B0}(c_{A0} - y)}{c_{A0}(c_{B0} - y)} = k\tau$$

Závislost reakční rychlosti na teplotě

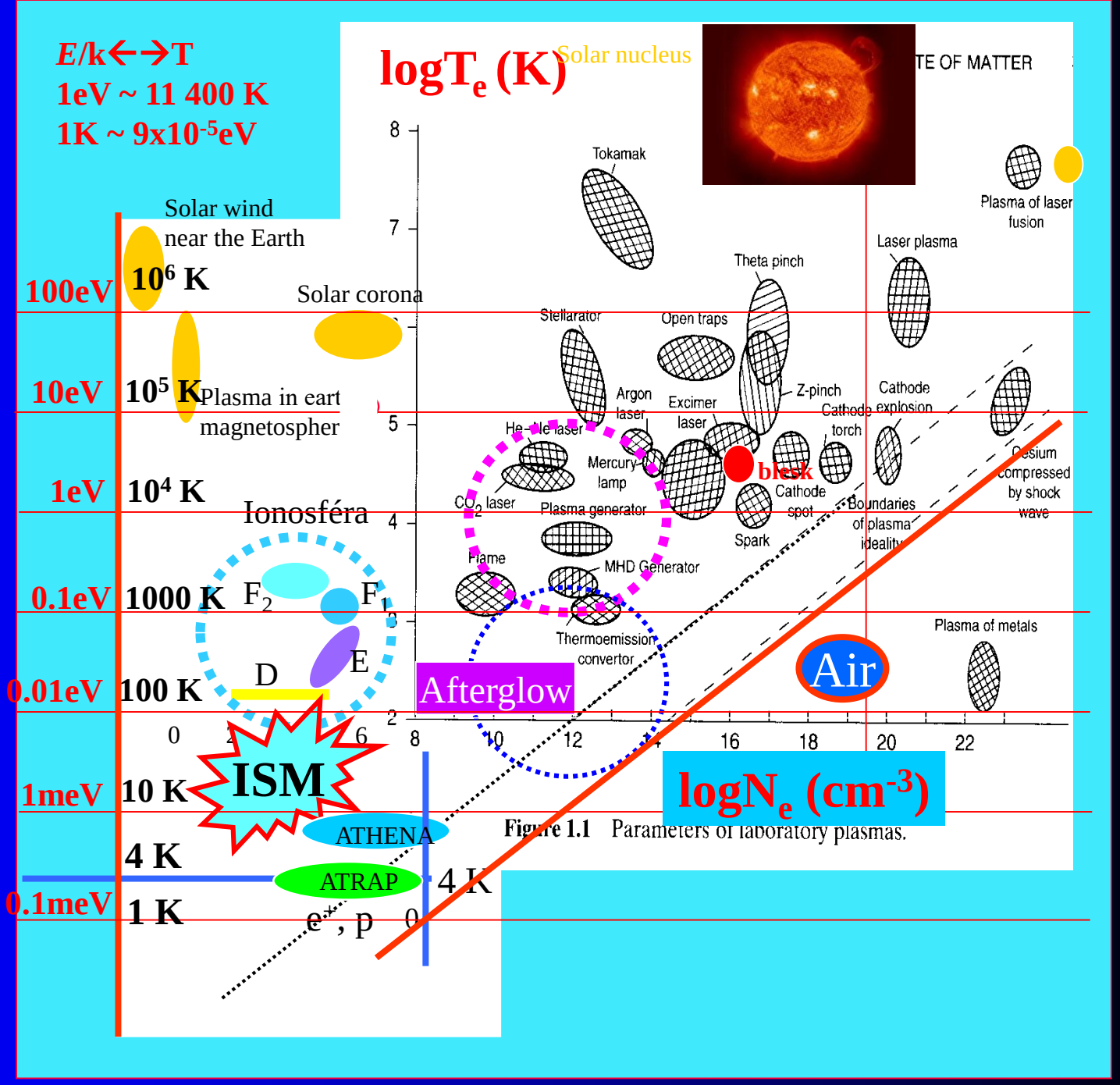
E/k←→T
1eV ~ 11 400 K
1K ~ 9x10-5eV
logTe (K)
Solar nucleus
TE OF MATTER
Solar wind
near the Earth
100eV
10^6 K
Solar corona
10eV
10^5 K
Plasma in eart
magnetospher
1eV
10^4 K
Ionosféra
0.1eV
1000 K
F2
F1
D
E
0.01eV
100 K
ISM
1meV
10 K
ATHENA
4 K
ATRAP
4 K
0.1meV
1 K
e+, p
Tokamak
Plasma of laser fusion
Laser plasma
Theta pinch
Stellarator
Open traps
Argon laser
Excimer laser
Z-pinch
Cathode explosion
Cathode torch
He-Ne laser
Mercury lamp
blesk
Cesium compressed by shock wave
CO2 laser
Plasma generator
Cathode spot
Boundaries of plasma ideality
Spark
Flame
MHD Generator
Thermoemission convertor
Plasma of metals
Afterglow
Air
logNe (cm-3)
Figure 1.1 Parameters of laboratory plasmas.

Temperature scale should be logarithmic

Temperature scale

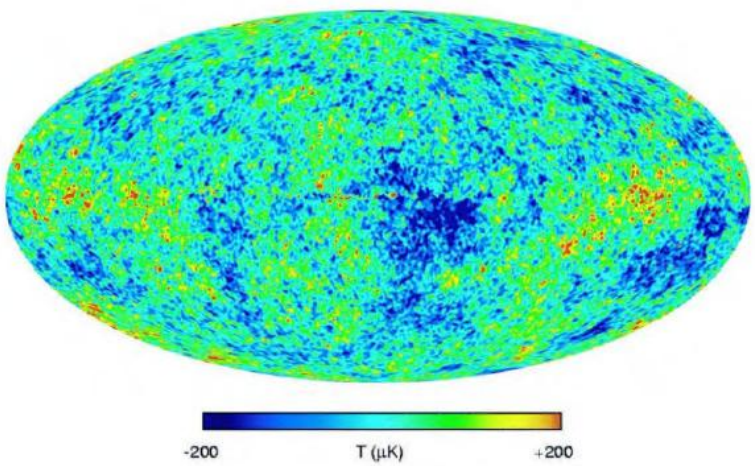

$T_{FIRAS} = T_0 = 2.730 \pm 0.001K$

$T = 2.717 \pm 0.003K$

monopole and dipole components

anisotropy 3.353±0.024 mK

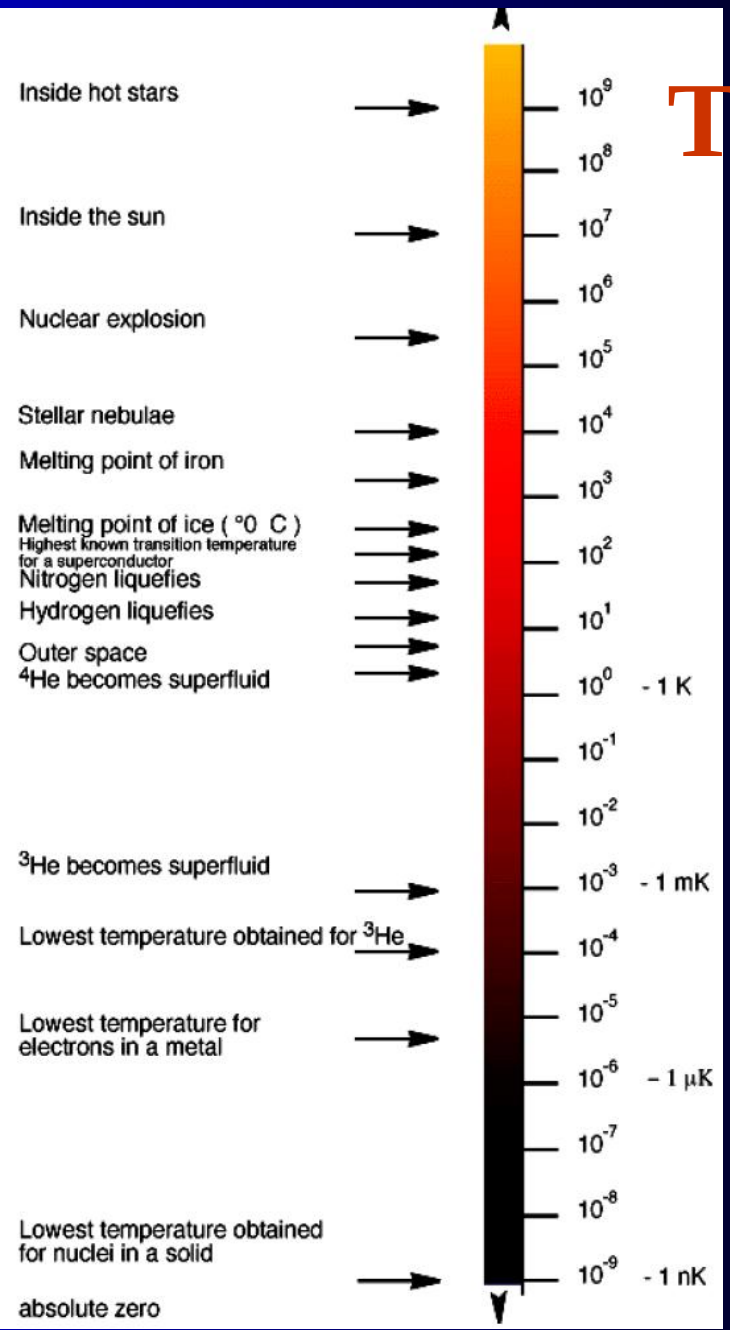

Reaction Rate of IMR relevant for ionosphere

k_{IMR}

$k_{coll} \sim 10^{-9} cm^3 s^{-1}$

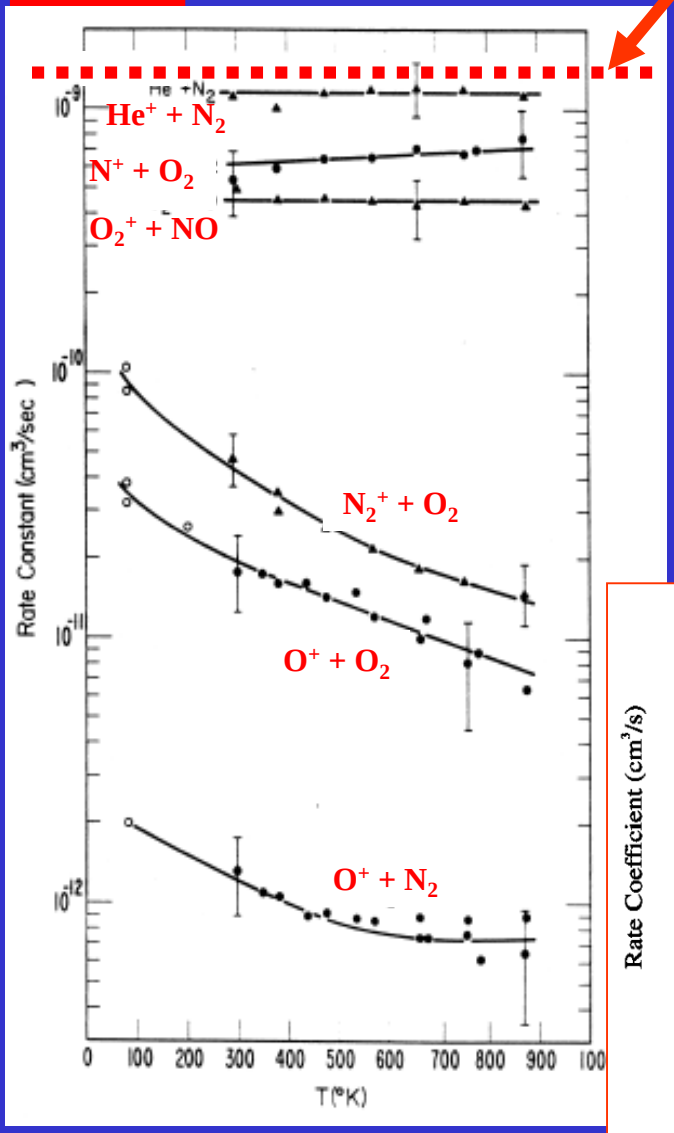

1975-90

1990-00

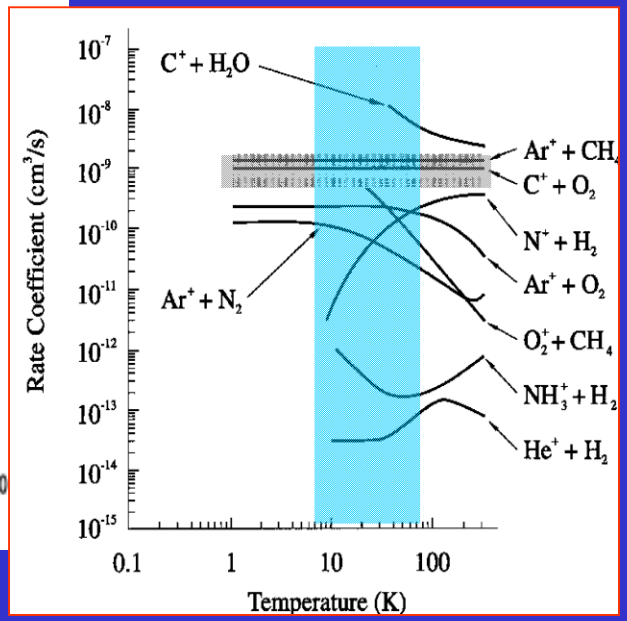

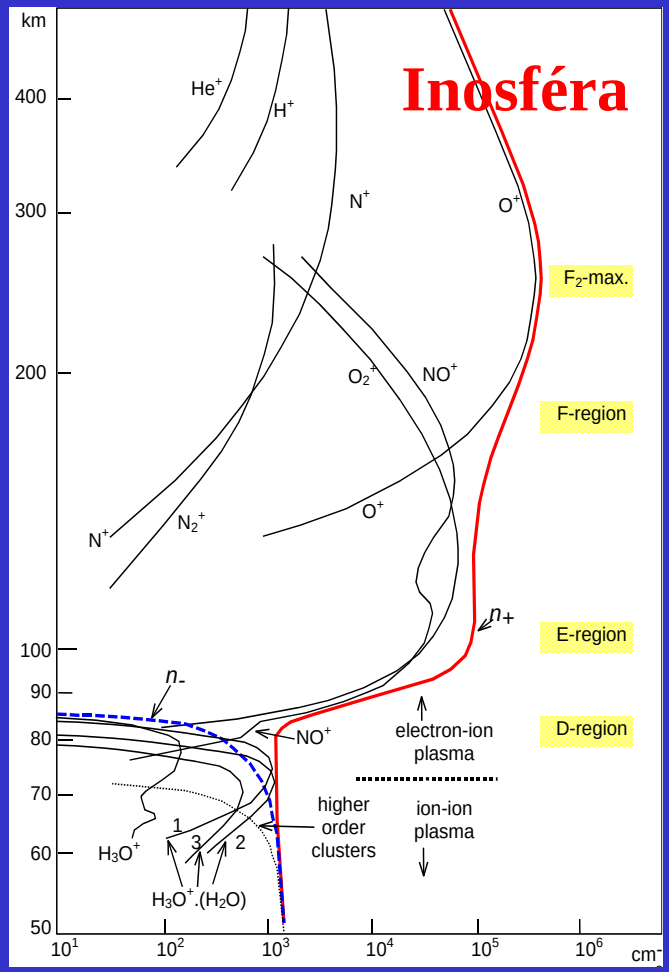

Závislost reakční rychlosti na teplotě

Arrheniův vztah

$$k = A.e^{-\frac{E_a}{RT}}$$

$$\ln k = \ln A - \frac{E_a}{RT}$$

A……frekvenční faktor

E_a……aktivační energie

T……teplota

Závislost reakční rychlosti na teplotě

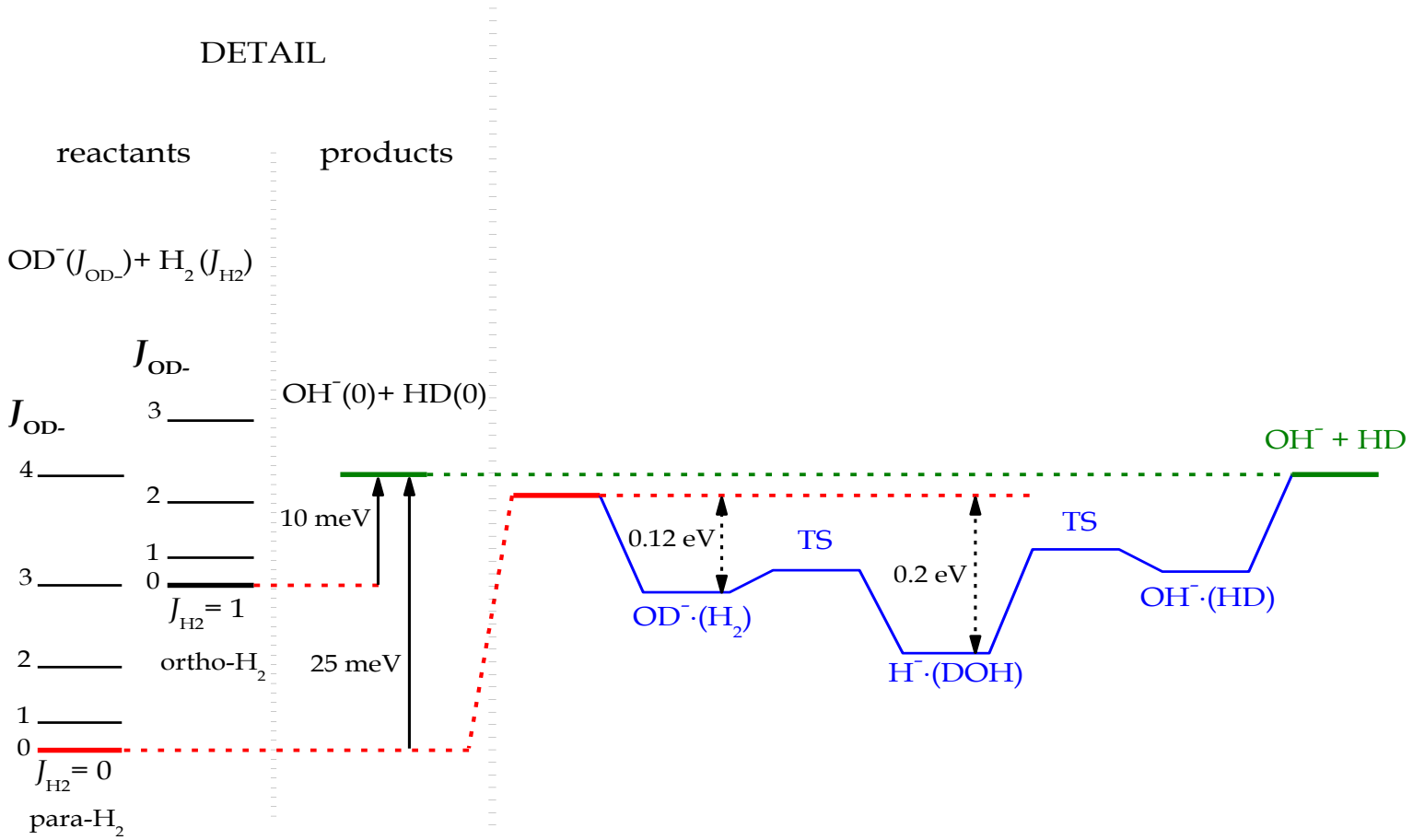

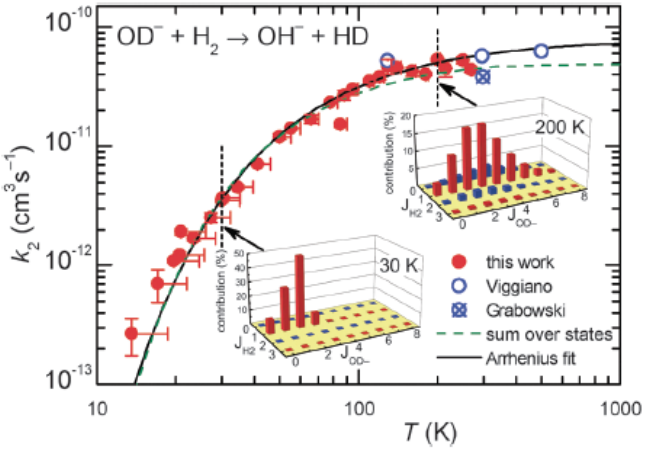

Fig. 7 Temperature dependence of the rate coefficient k_2 (filled circles) for the endothermic reaction (2). The vertical error bars of the two points at the lowest temperatures include the estimated error caused by the oscillations of temperature and pressure. At temperatures above 20 K, these effects are negligible and only statistical errors are shown. The results have been fitted using an Arrhenius temperature dependence (solid line). Previous FDT data of Viggiano and Morris[40] and SIFT data of Grabowski *et al.*[39] are also plotted. The dashed curve is a fit with function (7) (see the text for details). The insets indicate the $k_{J_{H_2}J_{OD^-}}/k_{2\Sigma}$ in percent (eqn (6) and (7)) at 30 K and 200 K.

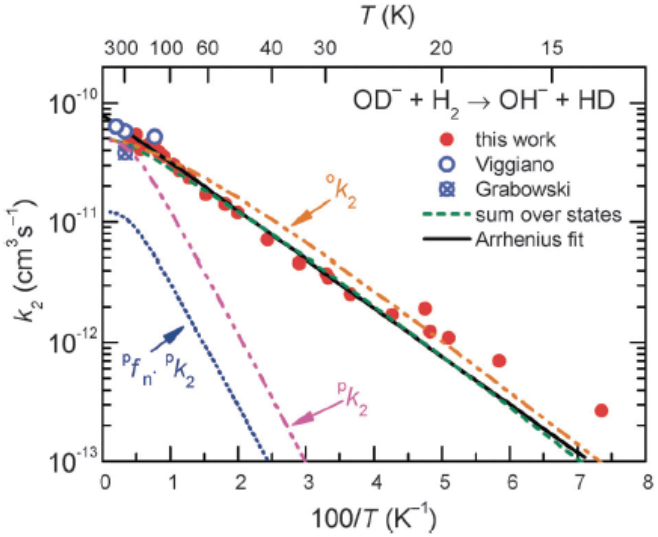

Fig. 8 Arrhenius plot of rate coefficient k_2 for reaction (2) measured with normal H_2. Shown are two almost identical fits, the two-parameter Arrhenius (solid line) and the sum over all relevant rotational states of the ion and of normal hydrogen (no *ortho–para* relaxation, dashed line). For details see the text. Previous FDT data of Viggiano and Morris[40] and SIFT data of Grabowski *et al.*[39] are also included in the plot. The plots marked with ${}^{o}k_2$ and ${}^{p}k_2$ are predictions for pure *ortho*- and *para*-hydrogen. In normal hydrogen, the contribution of *para*-hydrogen is only ${}^{p}f_n\,{}^{p}k_2 = \frac{1}{4}\,{}^{p}k_2$.

Dissociative Recombination of Molecular Ions

Mats Larsson, Ann E. Orel

Cambridge University Press 2008

Simultánní reakce

Vratné $A \Leftrightarrow B$

Paralelní $A \rightarrow B$

$A \rightarrow C$

Následné $A \rightarrow B \rightarrow C$

Vratné reakce

$$\mathbf{A} \underset{k_-}{\overset{k_+}{\Leftrightarrow}} \mathbf{B}$$

$$v_+ = k_+ [A]$$

$$v_- = k_- [B]$$

$$rovnováha \ldots\ldots\ldots\ldots v_+ = v_-$$

$$k_+ [A] = k_- [B]$$

$$\frac{k_+}{k_-} = \frac{[B]_r}{[A]_r} = K$$

K…..rovnovážná konstanta

Paralelní reakce

$$A \xrightarrow{k_1} B \qquad\qquad A \xrightarrow{k_2} C$$

Jsou-li obě reakce I. Řádu, pak platí:

$$v_1 = k_1[A]$$

$$v_2 = k_2[A]$$

$$v = v_1 + v_2$$

$$v = (k_1 + k_2)[A]$$

Následné reakce

$$A \xrightarrow{k_1} B \xrightarrow{k_2} C$$

$$-\frac{d[A]}{dt} = k_1[A]$$

$$\frac{d[B]}{dt} = (k_1 - k_2)[B]$$

$$\frac{d[C]}{dt} = k_2[B]$$

řetězové reakce = zvláštní typ následných reakcí

Chemická rovnováha

$$\mathbf{A + B} \underset{k_{-1}}{\overset{k_1}{\Leftrightarrow}} \mathbf{P + Q}$$

$$K = \frac{[P]_r [Q]_r}{[A]_r [B]_r}$$

$$K = \frac{k_1}{k_{-1}}$$

Guldberg-Waagův zákon

Vyjadřování rovnovážné konstanty

Předpokládáme reakci:

$b\,B + c\,C \rightarrow x\,X + y\,Y$

Stechiometrické koeficienty – obecně ν_i :

$\nu_B = -b \quad \nu_C = -c \quad \nu_X = x \quad \nu_Y = y$

Rovnici můžeme přepsat do tvaru:

$0 = x\,X + y\,Y - b\,B - c\,C$

Vyjadřování rovnovážné konstanty

Plynná reakční směs:

ΔG_r^0 …..standardní reakční Gibbsova energie (počítá se pomocí chemických potenciálů)

$$\Delta G_r^0 = -RT \ln K_p$$

$$K_p = \left[\frac{\left(\frac{p_X}{p^0}\right)^x \left(\frac{p_Y}{p^0}\right)^y}{\left(\frac{p_B}{p^0}\right)^b \left(\frac{p_C}{p^0}\right)^c} \right]_{rovn} = \left[\frac{p_X^x \, p_Y^y}{p_B^b \, p_C^c} \right]_{rovn} . \left(p^0\right)^{\sum_i \nu_i}$$

Ovlivňování chemických rovnováh

Henri Le Chatelier

Každá změna vnějších podmínek (akce) vyvolá v rovnovážné reakční směsi takové děje (reakce), které ve svých důsledcích působí proti zásahu zvenčí (akci), jímž byla chemická rovnováha narušena

Vliv tlaku na chemickou rovnováhu

- při reakcích v plynných směsích
- při reakcích, při kterých dochází ke změně molového čísla

Platí, že zvýšení tlaku (akce), vyvolá děje (reakce) vedoucí ke snížení tlaku v reakční směsi

Ternary processes

$$A^{+} + B + M \rightarrow C^{+} + D + M$$

Association reaction

$$A^{+} + B + M \rightarrow AB^{+} + M$$

Third-Order Reactions

$$\frac{d[A]}{dt} = -ak[A]^3 \quad \frac{d[A]}{dt} = -ak[A]^2[B] \quad \frac{d[A]}{dt} = -ak[A][B]^2 \quad \frac{d[A]}{dt} = -ak[A][B][C]$$

(Problems 17.17 and 17.24)

$$\frac{d[A]}{[A]^3} = -k_A dt \qquad \frac{1}{[A]^2} - \frac{1}{[A]_o^2} = 2k_A t$$

$$[A] = \frac{[A]_o}{\left(1 + 2kt[A]_o^2\right)^{1/2}} \qquad (17.24)$$

Deuteration is easy

$$D_3^+ + D_2 + D_2 \rightarrow D_5^+ + D_2$$

$$D_5^+ + D_2 + D_2 \rightarrow D_7^+ + D_2$$

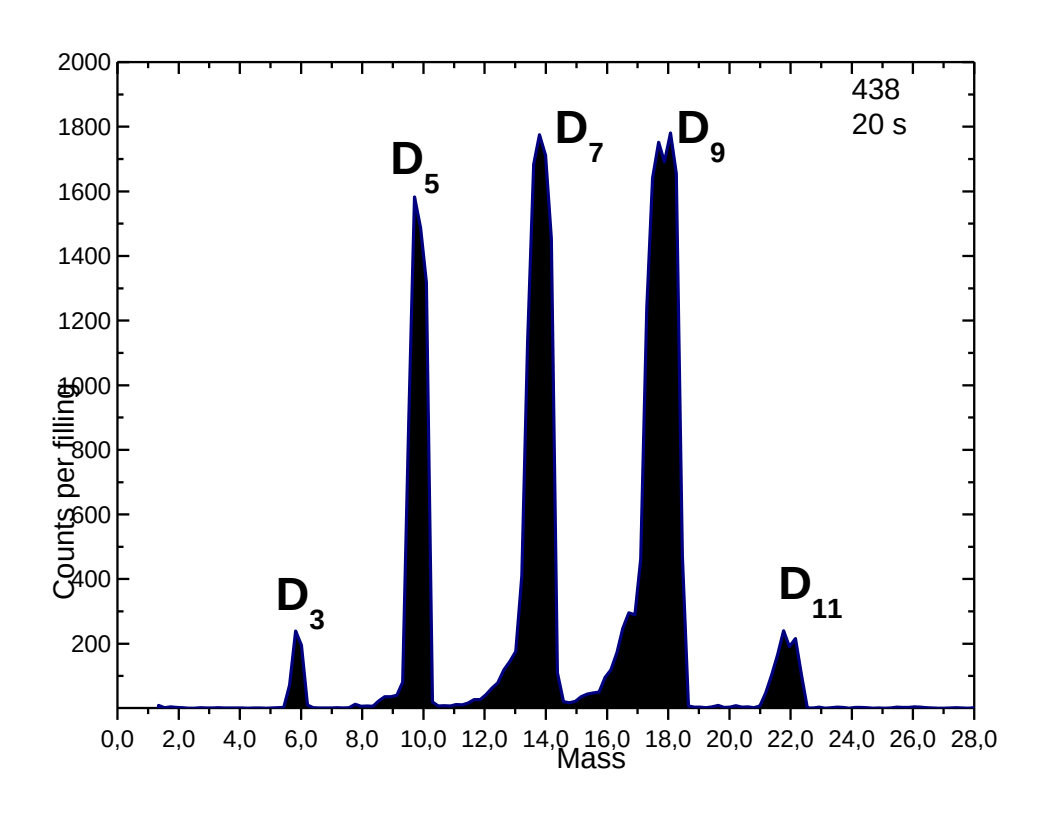

Deuteration was not so easy

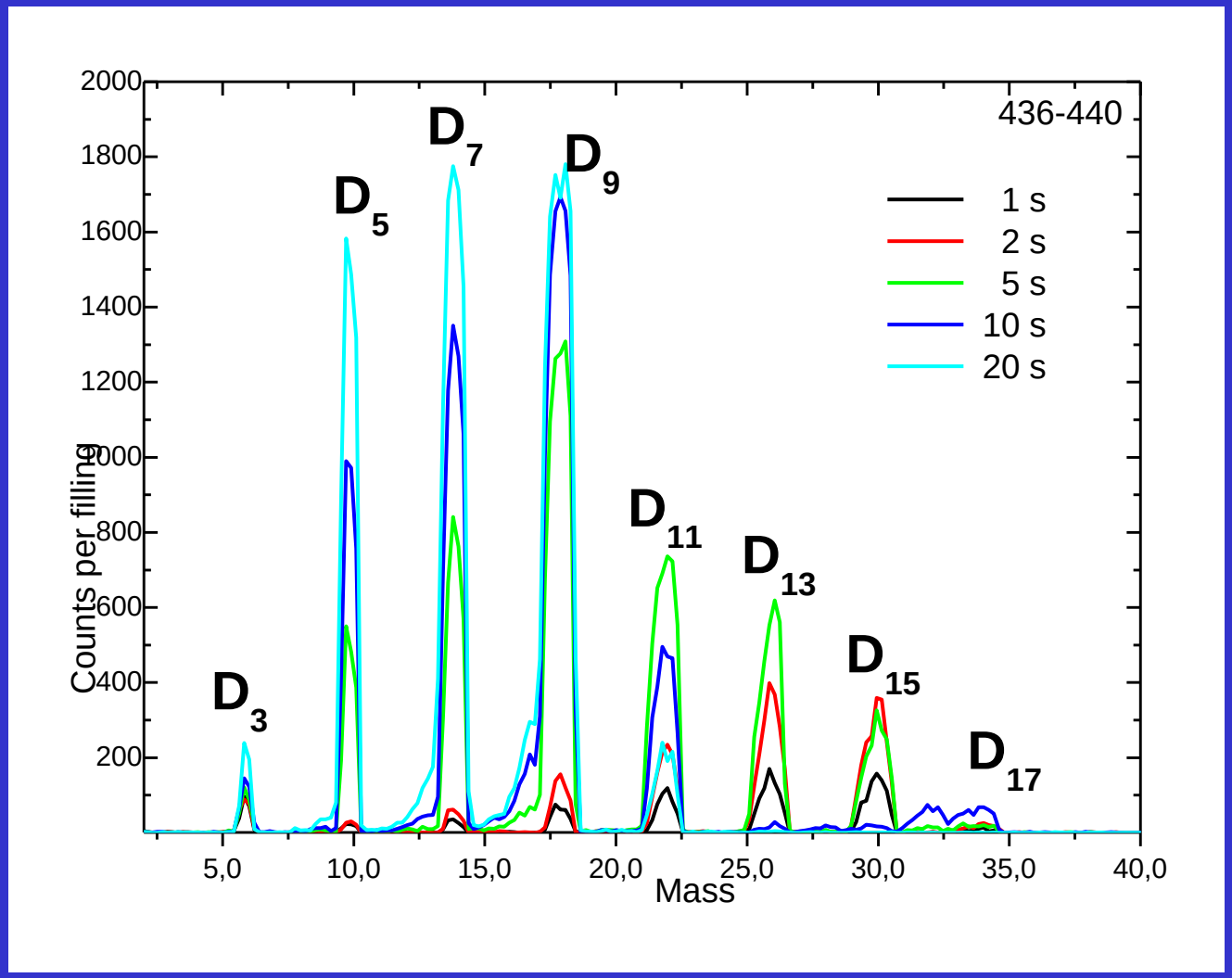

Association reactions

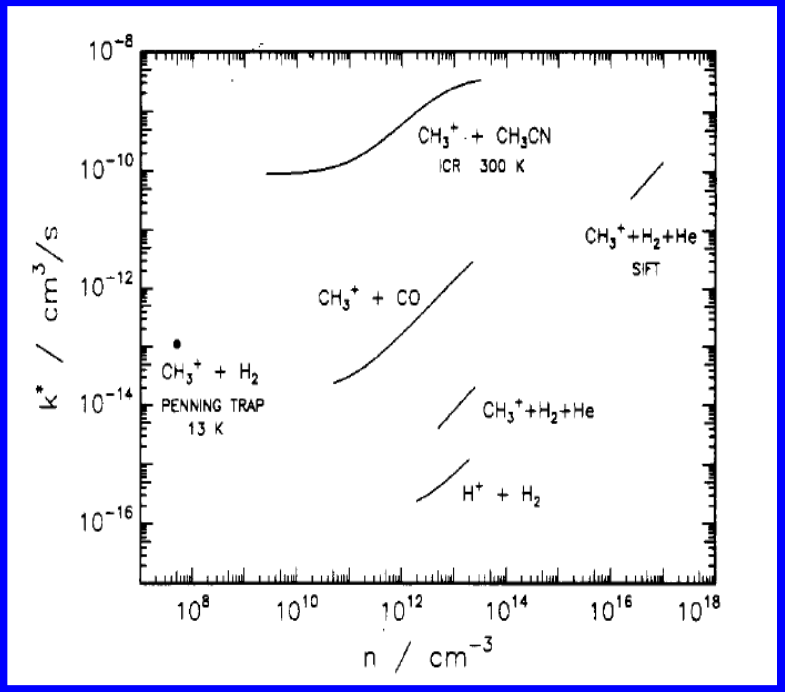

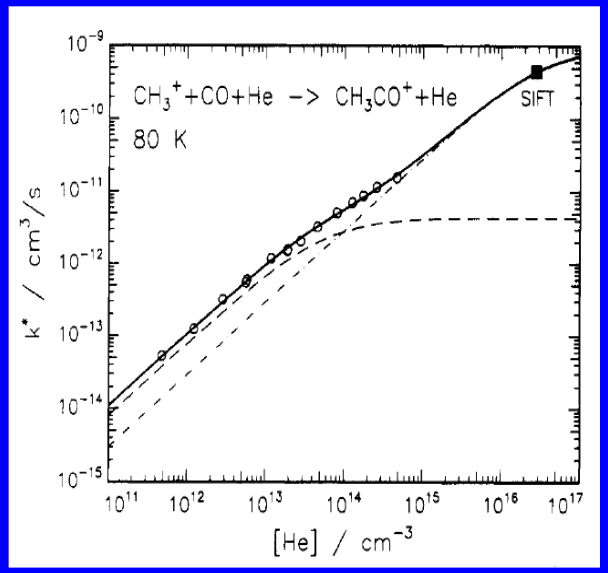

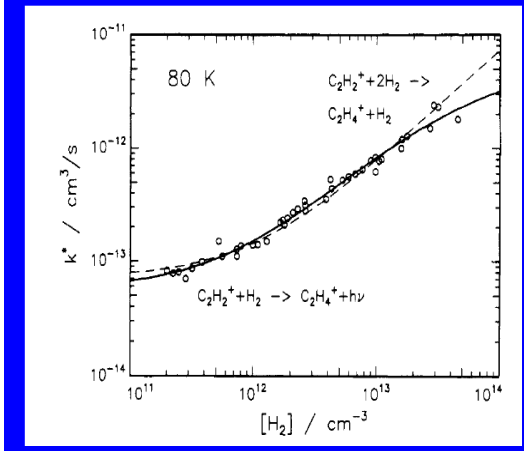

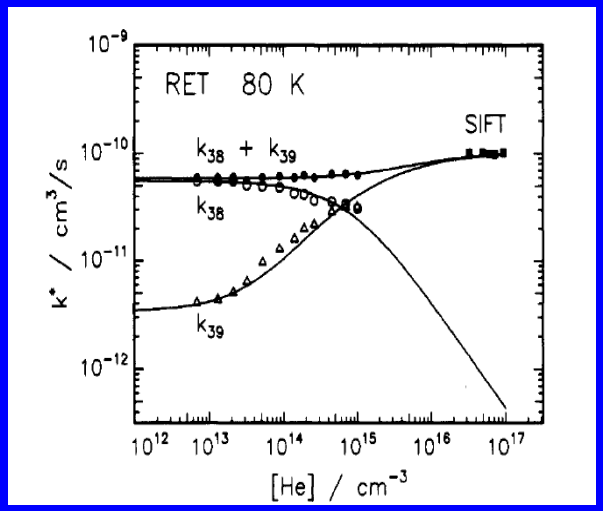

Rate Law

- **rate = $k[A]^x[B]^y$**
- **rate order = x + y**
- **knowledge of order can help control reaction**
- **rate must be experimentally determined**

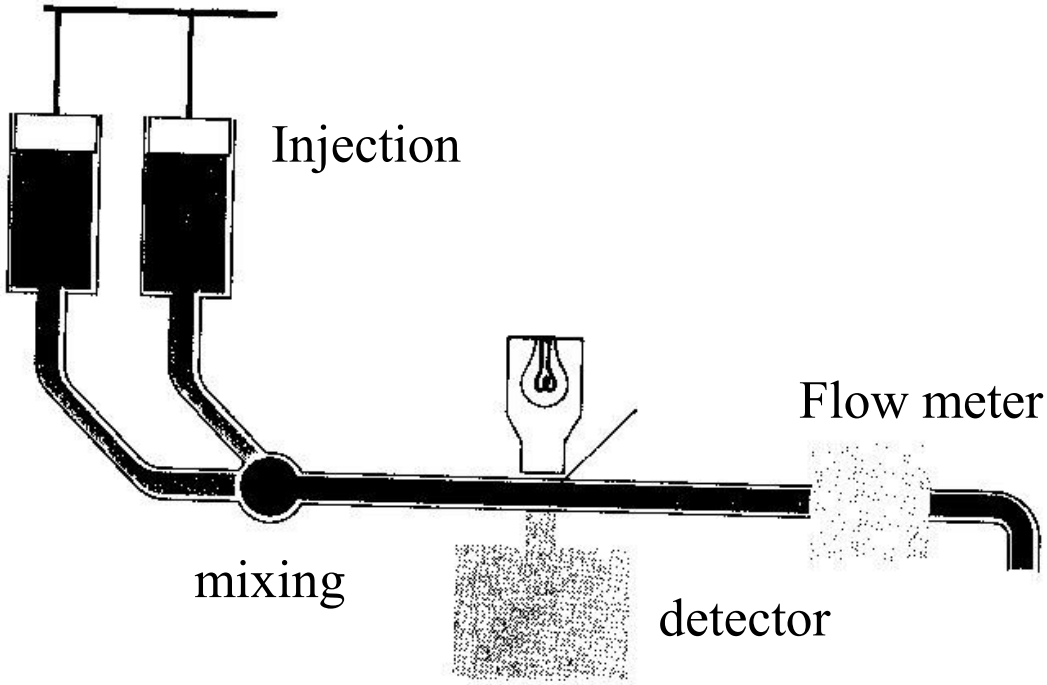

Classification of collisions

$$\mathbf{A}(E_{kin,0}, E_{int,0}) + \mathbf{B}(E_{kin,0}, E_{int,0}) \rightarrow \text{products}$$

Classification of collisions:

elastic

inelastic

Classification of collisions

$$\mathbf{A}(E_{kin,0},E_{int,0}) + \mathbf{B}(E_{kin,0},E_{int,0}) \rightarrow \text{products}$$

elastic

elastic: particles and their internal energy stays unchanged - only redistribution of kinetic energy and momentum → establishing of thermal equilibrium

$$\mathbf{A}(E_{kin,A,0},E_{int,A,0}) + \mathbf{B}(E_{kin,B,0},E_{int,B,0}) \rightarrow \mathbf{A}(E_{kin,A,1},E_{int,A,0}) + \mathbf{B}(E_{kin,B,1},E_{int,B,0})$$

$$E_{kin,A,0}+E_{kin,B,0} = E_{kin,A,1} + E_{kin,B,1}$$

- special case – superelastic collisions – kinetic energy increases in costs of internal energy

inelastic

inelastic: energy transfer from kinetic to internal energy: e.g. ionization, excitation, dissociation or chemical reaction

Always: $E_{tot} = \Sigma E_{i,before} = \Sigma E_{i,after} = \text{constant}$

$P_{tot} = \Sigma P_{i,before} = \Sigma P_{i,after} = \text{constant}$

Elementary processes:

Defined by:

cross section σ: most fundamental parameter, dimensions: area (usually in [cm^2])
describes the single collision,

e.g. hard sphere model:

$\sigma_{AB} = \pi(r_A + r_B)^2$

σ_{AB} depends in general on relative velocity of two colliding particles, can be orientation dependent
e.g. NO scattering on Ar

interaction frequency: $\nu_{AB} = v_A\, \sigma_{AB}(v_A)\, n_B$

Reaction rate coefficient: $k_{AB} = \langle \sigma(v) \cdot v \rangle$

JOURNAL OF CHEMICAL PHYSICS VOLUME 112, NUMBER 16 22 APRIL 2000

Guided ion beam studies of electron and isotope transfer in $^{14}N^{+}+^{15}N_2$ collisions

J. Glosik and A. Luca

$$^{14}N^{+}+^{15}N^{15}N \rightarrow ^{15}N^{+}+^{14}N^{15}N, \quad \text{(I)}$$

$$\rightarrow ^{15}N^{15}N^{+}+^{14}N, \quad \text{(II)}$$

$$\rightarrow ^{14}N^{15}N^{+}+^{15}N. \quad \text{(III)}$$

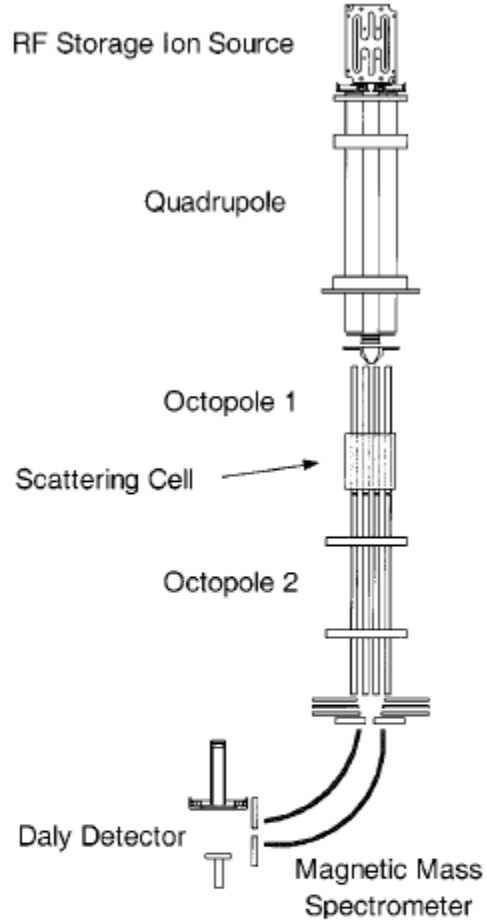

FIG. 1. Schematic view of the universal guided ion beam (GIB) apparatus. Ions are produced by electron impact in an rf storage ion source operating in a pulsed mode. In the quadrupole the ions are mass selected and also energy preselected by pulsing input and output lenses of the quadrupole. An einzel-lens focuses the ions onto the octopole injection electrode. The first octopole guides the ions through the 300 K scattering cell. The second, much longer, octopole guides primary and product ions toward the entrance slit of a 90° magnetic mass spectrometer. After mass selection the ions are detected with nearly 100% efficiency by a Daly detector. The second octopole is used also for time-of-flight analysis of the axial velocity of the primary and product ions.

Dynamic of IMR

$$N^+ + N_2 \rightarrow products$$

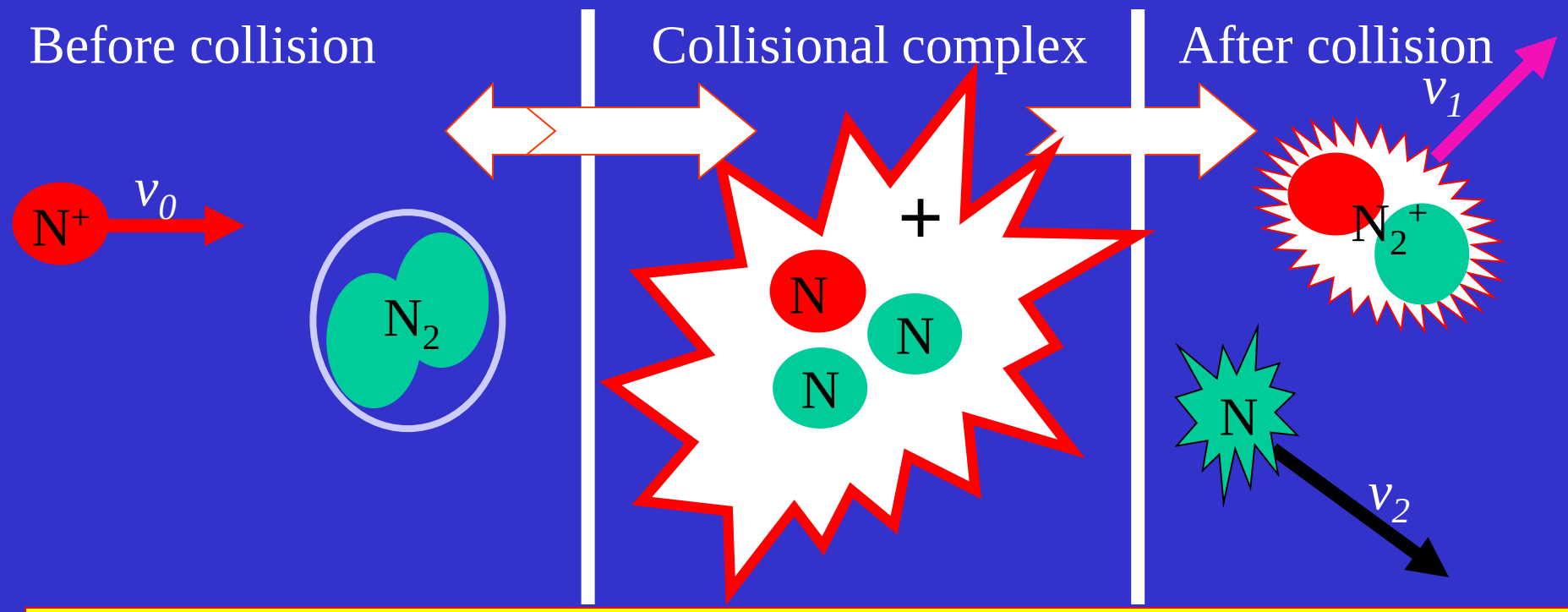

$$N^+ + N_2 \leftrightarrow (N_3)^{*+} \rightarrow N_2^+ + N$$

$$\sigma_{coll} = \pi\rho_0^2 = \frac{2\pi e}{v_0(4\pi\varepsilon_0)}\sqrt{\frac{\alpha}{\mu}}$$

Dynamic of IMR

$$N^+ + N_2 \leftarrow (N_3)^{*+} \rightarrow N_2^+ + N$$

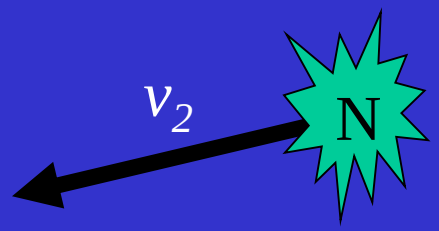

Collisional complex

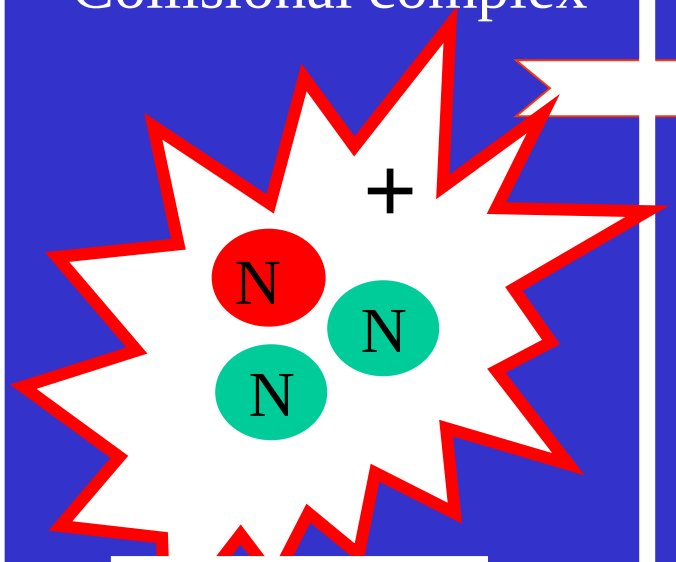

After collision

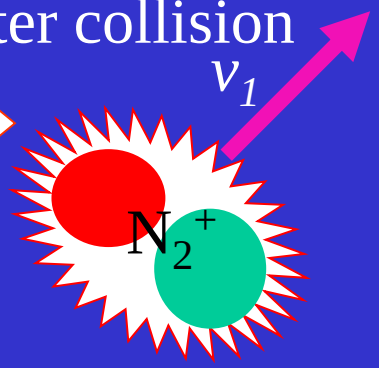

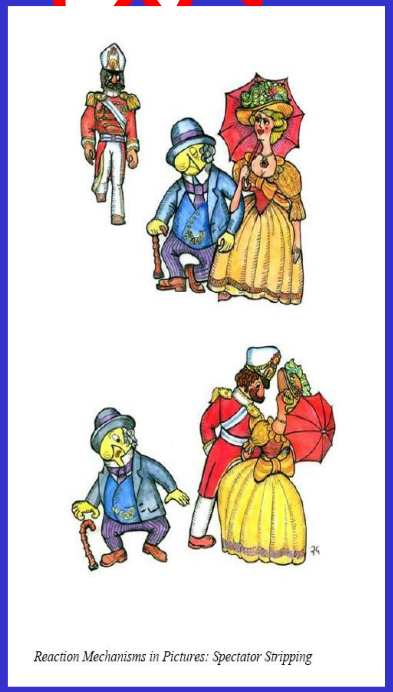

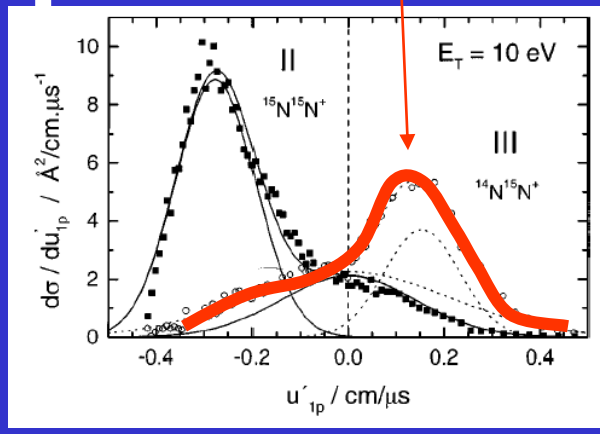

Dynamic of IMR

$$N^+ + N_2 \leftarrow (N_3)^{*+} \rightarrow N_2^+ + N$$

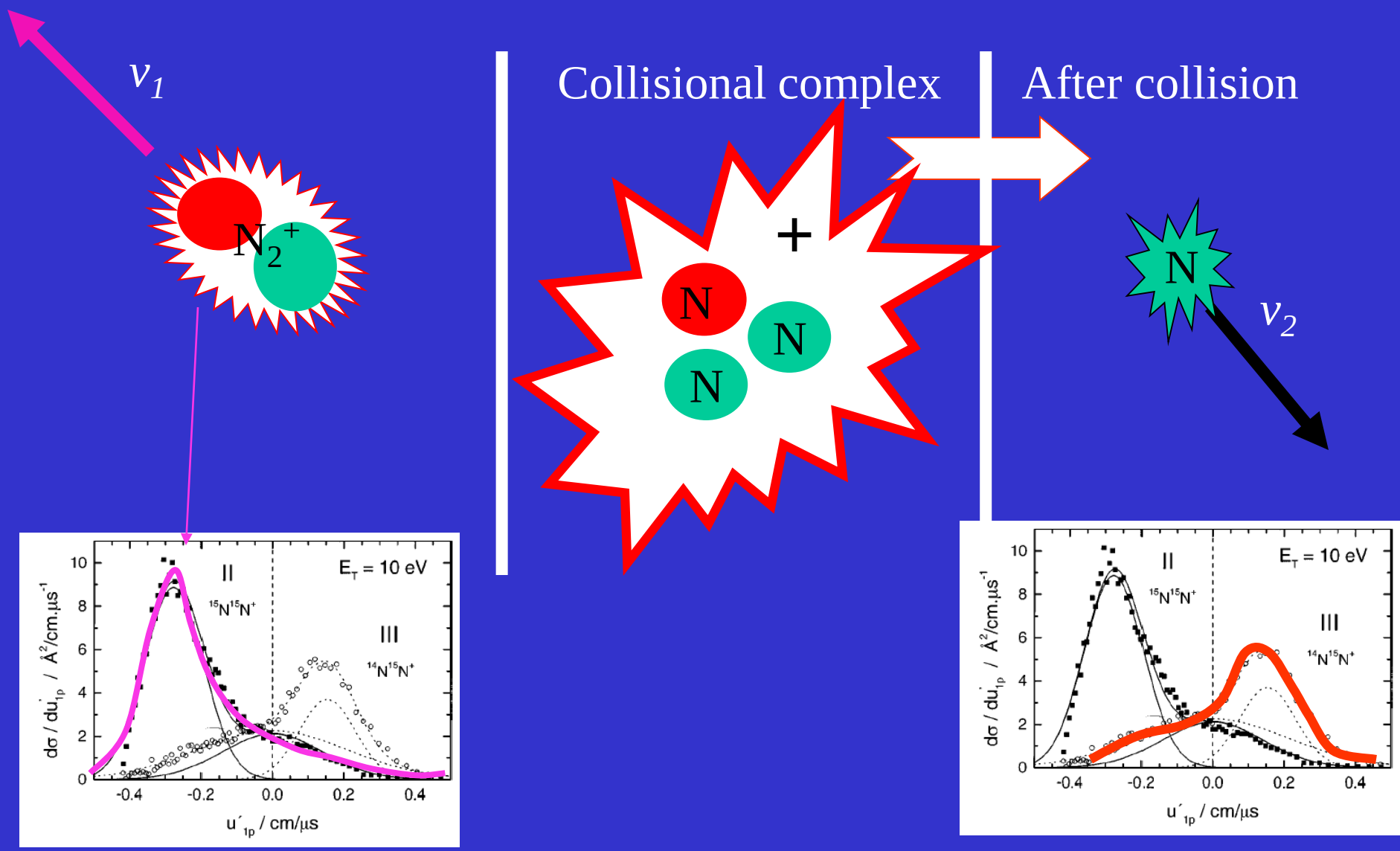

Dynamic of IMR

$$N^{+} + N_2 \leftarrow (N_3)^{*+} \rightarrow N_2^{+} + N$$

Collisional complex

After collision

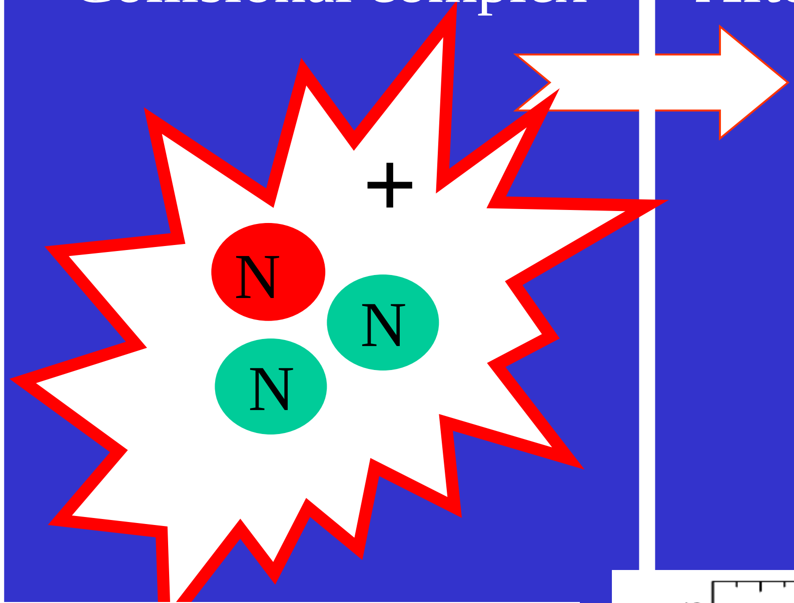

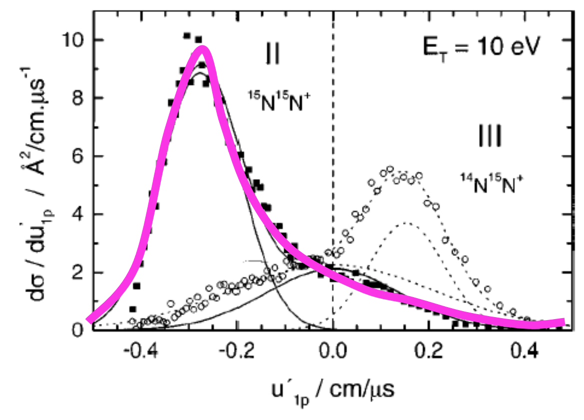

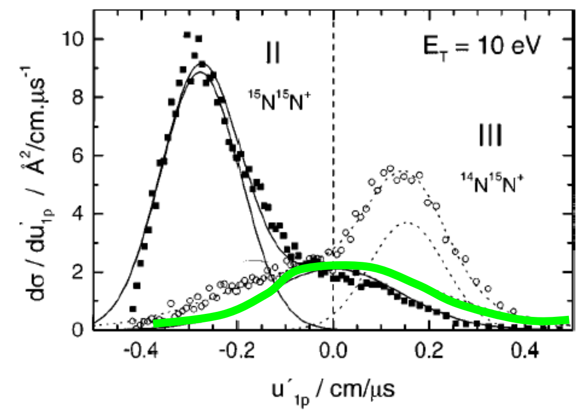

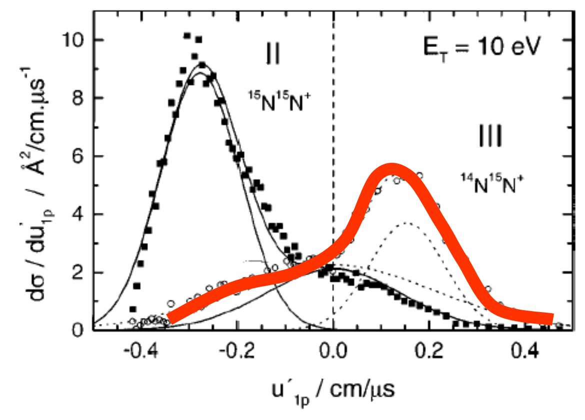

Koniec rosprávky 21 10 2019

Single collision

$$H_2^+ + Ar \Rightarrow ArH^+ + H$$

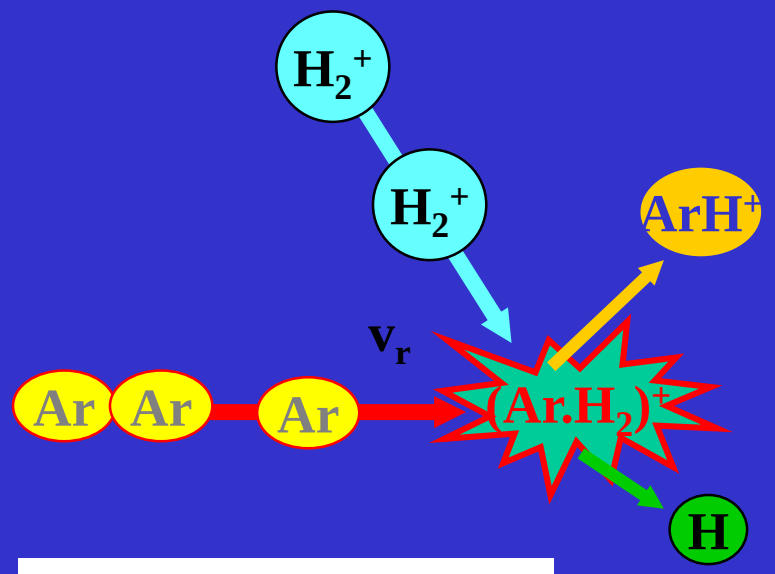

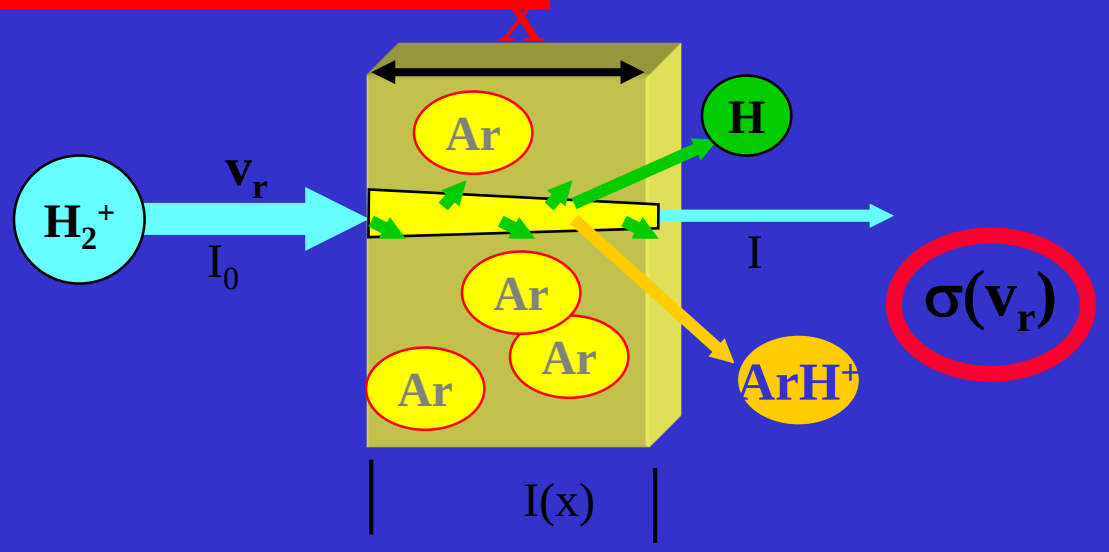

reaction cross section

$$I = I_0 \exp(-\sigma n_{Ar} x)$$

Single collision

$$H_2^+ + Ar \Rightarrow ArH^+ + H$$

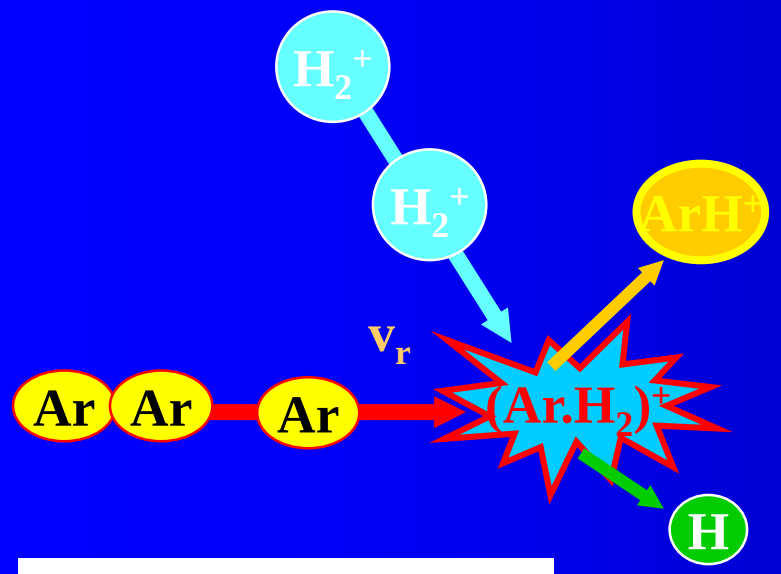

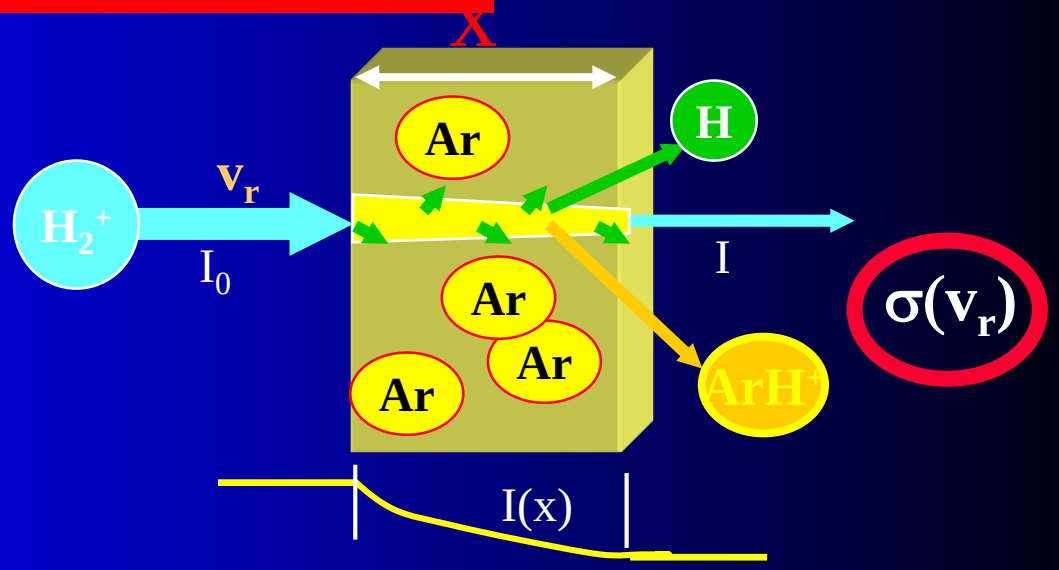

reaction cross section

$$I = I_0 \exp(-\sigma n_{Ar} x)$$

Proportionality factor

$$\frac{dI}{dx} \sim -IN$$

$$\frac{dI}{dx} = -\sigma IN$$

$$\frac{dI}{Idx} = \frac{d\ln(I)}{dx} = -\sigma N$$

$$I(x) = I_0 \exp(-\sigma N x)$$

polarizab

Single collision

$$H_2^+ + Ar \Rightarrow ArH^+ + H$$

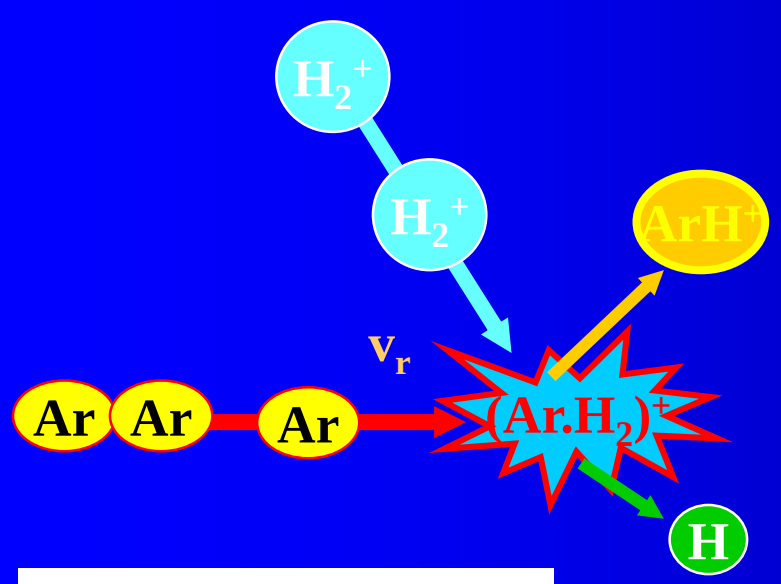

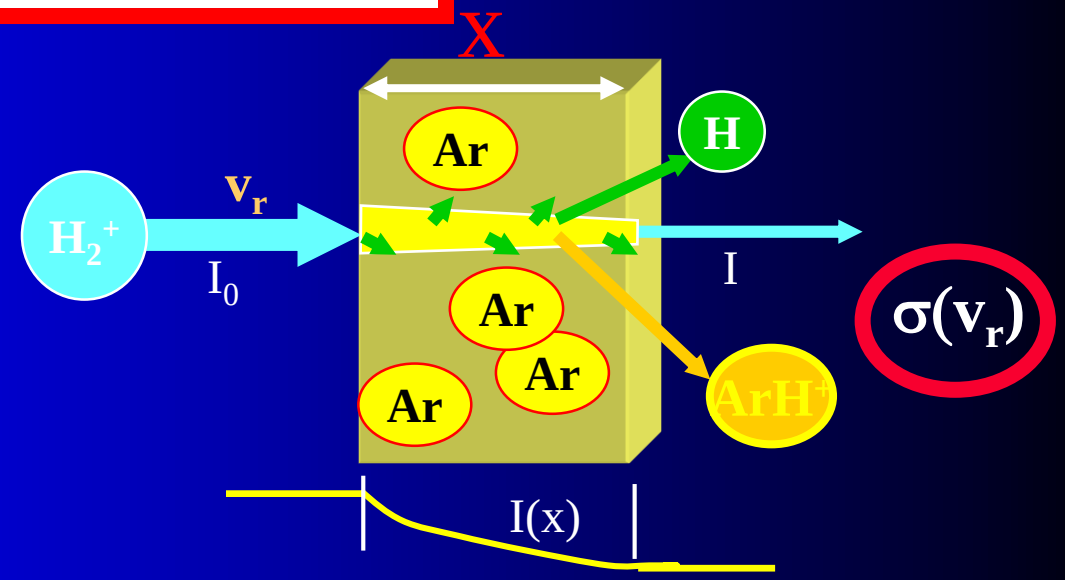

reaction cross section

$$I = I_0 \exp(-\sigma n_{Ar} x)$$

$$\nu_{coll} = -nV_{rel} = -n\nu S = -n\nu\pi\delta^2 = -n\nu\sigma$$

$$\frac{dI}{dt} = -\frac{I}{\tau_{coll}} = -I\nu_{coll}$$

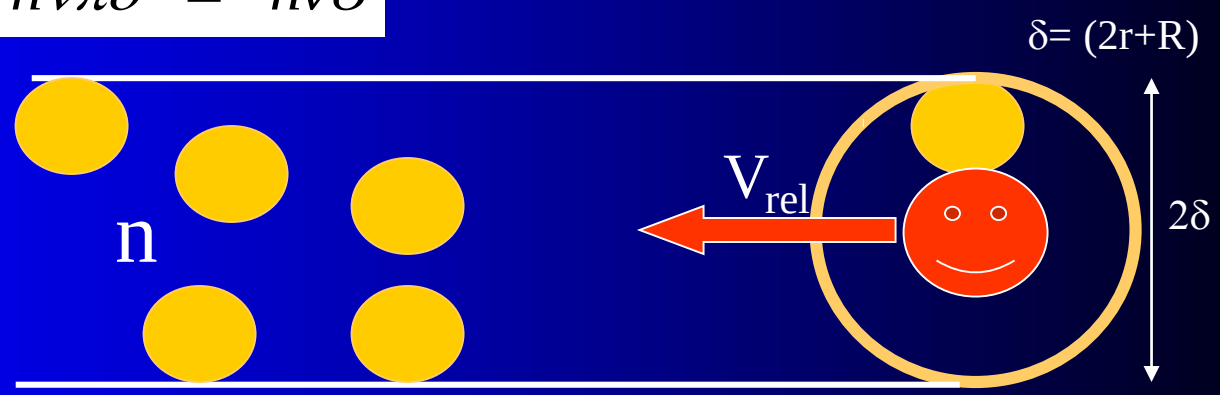

$$I(t) = I_0 \exp(-\nu_{coll} t) = I_0 \exp(-\sigma n \nu_{rel} t)$$

$$I = I_0 \exp(-\sigma n_{Ar} x)$$

Electron excitation cross-section

e.g.: Ar(1) + e → Ar(2) + e

Follows the model of Thomson with different integration boundaries

$$d\sigma_i(E) = \frac{1}{(4\pi\varepsilon_0)^2}\frac{\pi e^4}{E(\Delta E)^2}d(\Delta E)$$

$$\sigma_{e\_1}(E) = \int_{E_1}^{E} d\sigma_i \quad E < E_2$$

$$\sigma_{e\_1}(E) = \int_{E_1}^{E_2} d\sigma_i \quad E \geq E_2$$

or

$$\sigma_{e\_all}(E) = \int_{E_1}^{E} d\sigma_i \quad E < I$$

$$\sigma_{e\_all}(E) = \int_{E_1}^{I} d\sigma_i \quad E \geq I$$

Quantum mechanics → excitation to optically forbidden levels has lower cross-sections

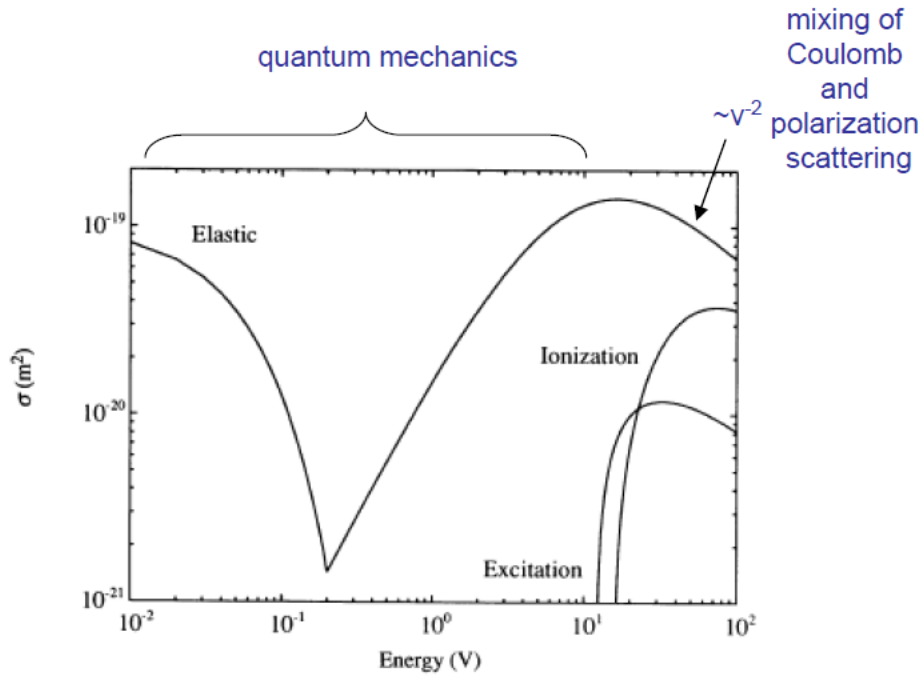

FIGURE 3.13. Ionization, excitation and elastic scattering cross sections for electrons in argon gas (compiled by Vahedi, 1993).

Lieberman&Lichtenberg

Collision frequency

$$A^+ + B \rightarrow C^+ + D$$

$$\frac{dA^+}{dt} = -k_{BIN} A^+ B$$

$$[k_{BIN}] = cm^3 s^{-1}$$

$1/\tau = k_{BIN}[B] = \ldots n v \rho \ldots = [B] v \rho \ldots . [B] \langle v \rho \rangle$

$$k_{BIN} = \langle v \rho \rangle$$

$$\nu_{coll} = -nV_{rel} = -n v S = -n v \pi \delta^2 = -n v \sigma$$

$$\frac{dI}{dt} = -\frac{I}{\tau_{coll}} = -I \nu_{coll}$$

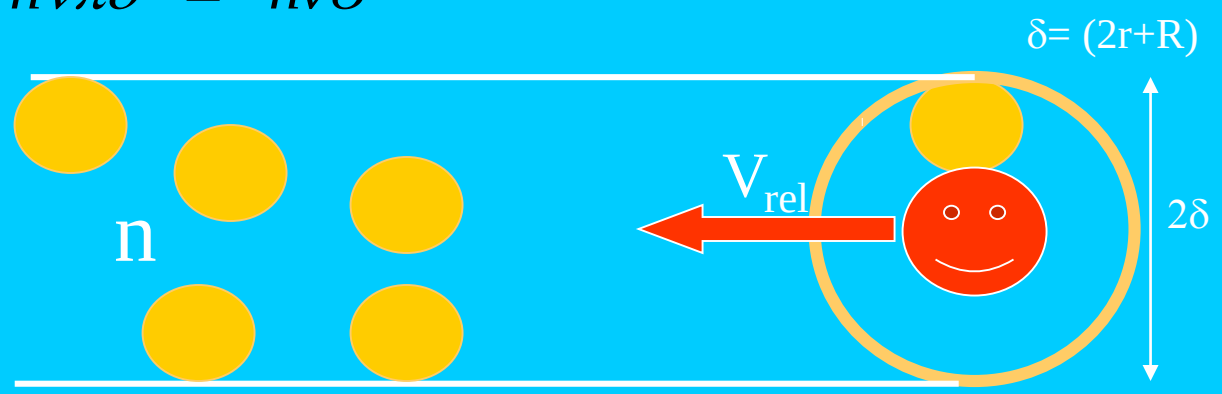

$$I(t) = I_0 \exp(-\nu_{coll} t) = I_0 \exp(-\sigma n v_{rel} t)$$

$$\mathbf{I = I_0 \exp(-\sigma n_{Ar} x)}$$

$$H_2^+ + Ar \Rightarrow ArH^+ + H$$

Single collision

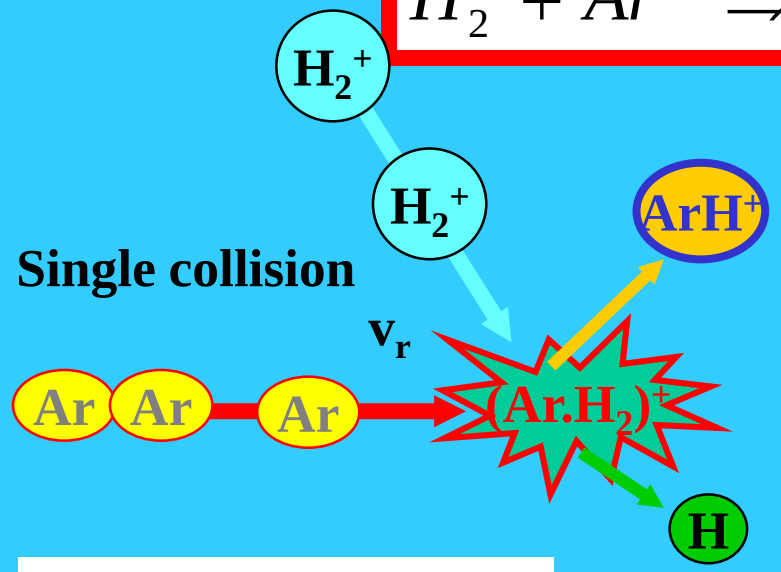

reaction cross section

$$I = I_0 \exp(-\sigma n_{Ar} x)$$

Multiple collision

@ T

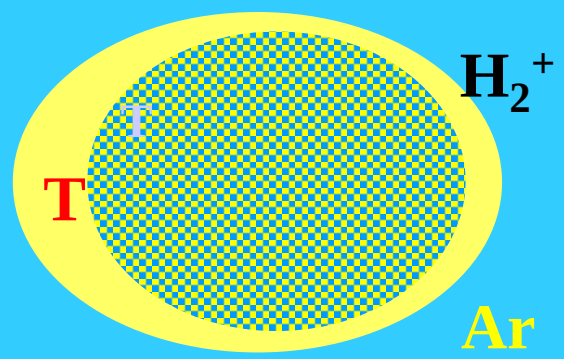

reaction rate coefficient

$$d(n_{H2^+})/dt = -k\, n_{H2^+} \cdot n_{Ar}$$

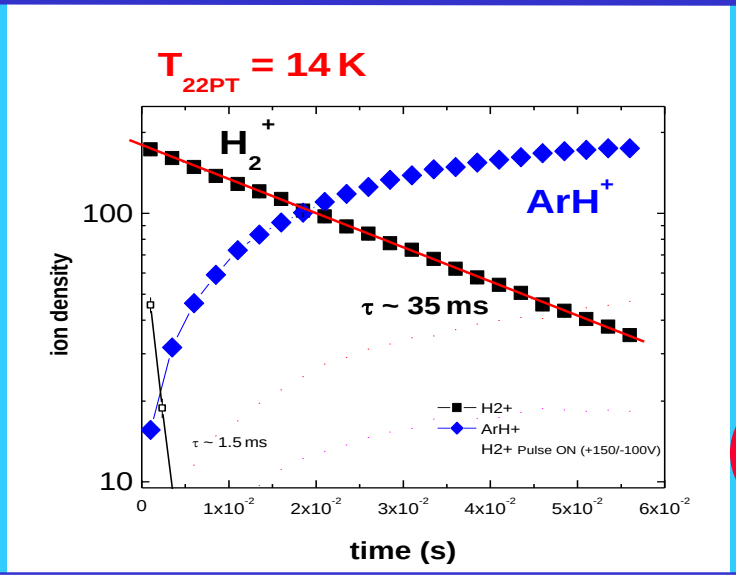

$$n_{H2^+} = (n_{H2^+})_0 \exp(-k n_{Ar} t)$$

$\sigma(v_r)$

$k(T) = \langle v\sigma \rangle$

$k(T)$

Electron scattering cross-section on Ar

Electrons – Boltzman distribution with T_e

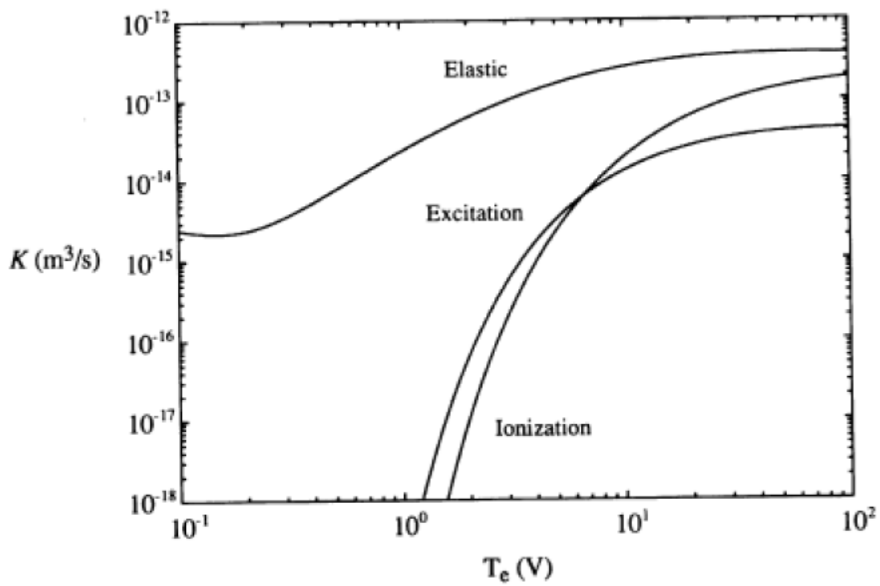

FIGURE 3.16. Electron collision rate constants K_{iz}, K_{ex} and K_m versus T_e in argon gas (compiled by Vahedi, 1993).

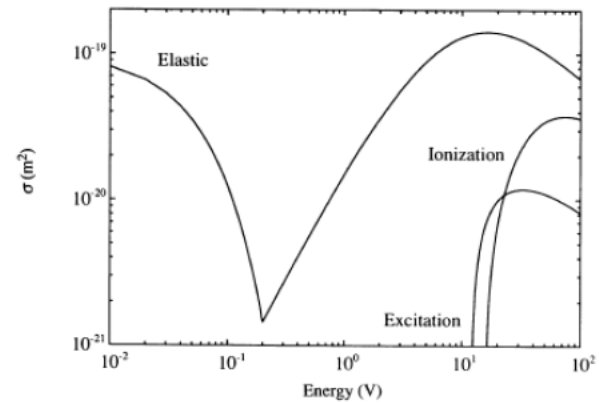

3. Ionization, excitation and elastic scattering cross sections for electrons in
piled by Vahedi, 1993).

What if we have metastables?

Lieberman&Lichtenberg

Collision Cross section of IMR

$$D_3^+ + H_2 \rightarrow H_2D^+ + D_2$$

Endothermic reaction

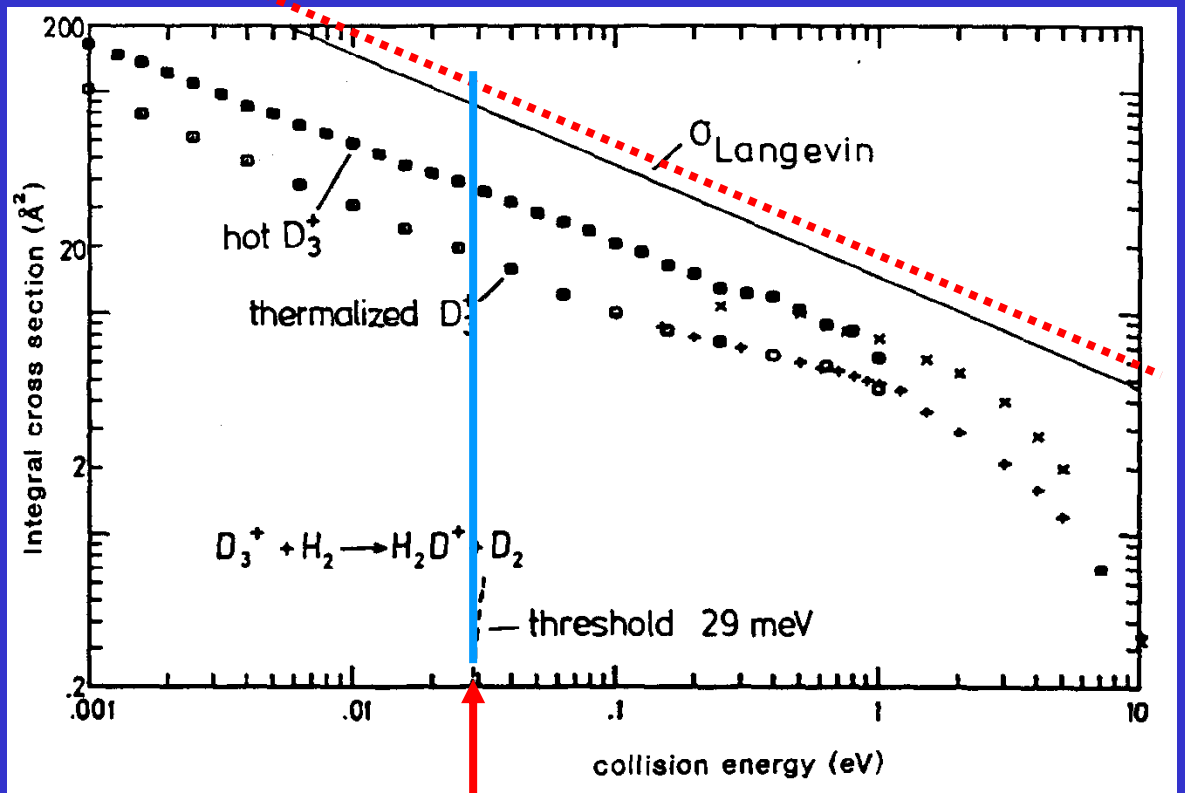

Figure 56. Integral cross sections for the 29 meV endothermic reaction $D_3^+ + H_2 \rightarrow H_2D^+ + D_2$ with hot D_3^+ (~2 eV internal energy) and ~350 K thermalized D_3^+. The merged beam results (●, ⊙) are, in the overlapping energy range, in good agreement with earlier guided ion-beam experiments (Piepke, 1980), recorded under similar storage ion source conditions (+, ×). The cross sections are significantly lower than the Langevin value.

Reactive Cross section of IMR

Collision rate coefficient

$$\sigma_0 = \pi\rho_0^2 = \frac{2\pi e}{v_0(4\pi\varepsilon_0)}\sqrt{\frac{\alpha}{\mu}} \sim \frac{1}{v_0}\sqrt{\frac{\alpha}{\mu}}$$

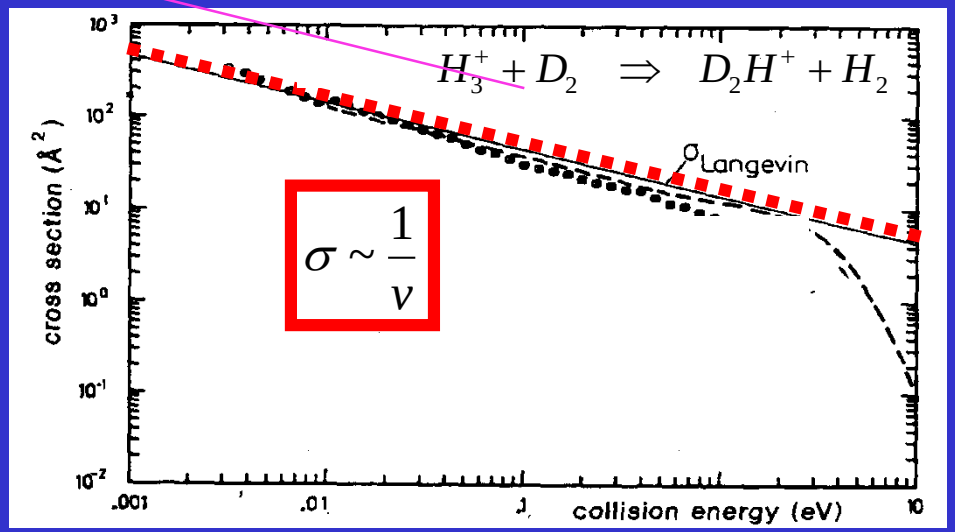

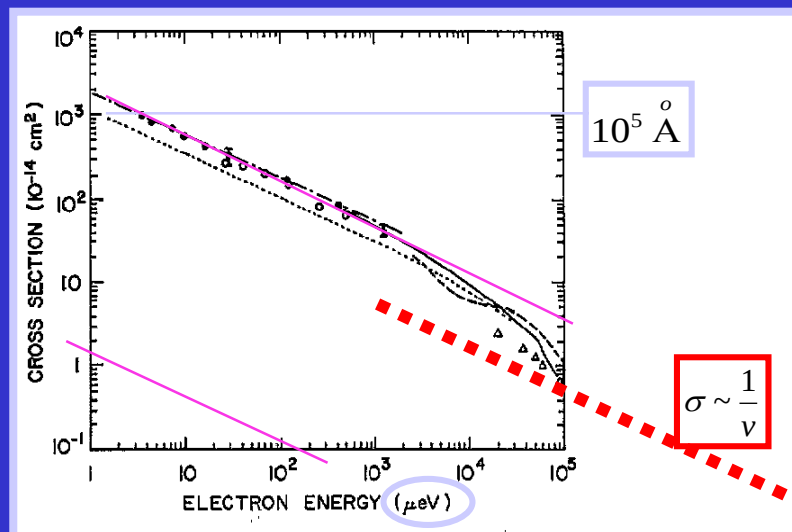

Figure 3. Cross sections for electron attachment to CCl_4. ●, $\bar{\sigma}_e$-K(np); —·—, $\sigma_e(v)$-K(np) (Frey *et al* 1994b); ○, $\bar{\sigma}_e$-K(np) (Ling *et al* 1992); ——, free electrons (Hotop 1994); - - -, free electrons (Orient *et al* 1989); △, free electrons (Christodoulides and Christophorou (1971); -----, theory (Kłots 1976).

k(T)=<vσ> ➡ $k = \int_{Max(T)} v\sigma(v)dv = k(T)$

k(T) reaction rate coefficient

k_{coll}(T) collision rate coefficient

k_{coll}(T)~collision frequency

Reaction rate coefficients

Typical values of at 300K (approximate values)

	reactants		products	rate coefficient
Electron atomic ion rec.	$A^+ + e^-$	➔	$A + h\nu$	$\sim 10^{-11} cm^3 s^{-1}$
Electron - ion recomb.	$O_2^+ + e^-$	➔	$O + O$	$2x10^{-7} cm^3 s^{-1}$
Electron – cluster ion recomb.	$H_5^+ + e^-$	➔	products	$3.5x10^{-6} cm^3 s^{-1}$
Ion – ion recombination	$Ar^+ + Cl^-$	➔	$Ar + Cl$	$2x10^{-8} cm^3 s^{-1}$
Ion – molecule reactions	$H_2^+ + H_2$,	➔	$H_3^+ + H$	$2x10^{-9} cm^3 s^{-1}$
	$H_3^+ + H_2 + He$	➔	$H_5^+ + He$	$k_{eff\ BIN} = k_3 x [He]$
				$k_3 < 2x10^{-29} cm^6 s^{-1}$
Attachment	$CCl_4 + e^-$		$Cl^- + CCl_3$	$\sim 10^{-7} cm^3 s^{-1}$
Penning ionization	$He^* + Ar$		$Ar^+ + e^- + He$	$7x10^{-11} c$.

JPL Publication 03-19

An Index of the Literature for Bimolecular Gas Phase Cation-Molecule Reaction Kinetics

Vincent G. Anicich

Rate coefficients

Introduction xi
Bimolecular Reactions xiii
Comments on Termolecular Reactions xiv
Notes on the Table xv
Methods Used in Citation xvi
Journals Cited xvii
Publications by Journal xix
The Authors of the articles in this bibliography xx
References for Introduction xxii
The Table of Ion-Molecule Reactions with Reference Numbers 1

H_n^+ 1
HeH_n^+ 29
LiH_n^+ 49
$As_mH_n^+$ 592
$Se_mH_n^+$ 594
$Br_mH_n^+$ 594

National Aeronautics and Space Administration

Jet Propulsion Laboratory
California Institute of Technology
Pasadena, California

November 2003

A^+		B		products			%	k[cm^3s^{-1}]	T		
C^+	+	C_2H_6	→	Products					300	MS	6406
C^+	+	CH_2CCH_2	→	$C_4H_2^+$	+	H_2	0.40	1.40×10^{-9} ±20	300	SIFT	8207
				$C_3H_3^+$	+	CH	0.25				
				$C_2H_2^+$	+	C_2H_2	0.20				
				$C_3H_4^+$	+	C	0.15				
C^+	+	CH_3CCH	→	$C_4H_2^+$	+	H_2	0.30	1.90×10^{-9} ±25	300	SIFT	8207
				$C_3H_4^+$	+	C	0.30				
				$C_3H_3^+$	+	CH	0.20				
				$C_2H_2^+$	+	C_2H_2	0.10				
				$C_2H_3^+$	+	CCH	0.10				
C^+	+	CH_3CHCH_2	→	$C_2H_3^+$	+	$CHCH_2$	0.30	2.00×10^{-9} ±25	300	SIFT	8207
				$C_3H_3^+$	+	CH	0.20				
				$C_3H_3^+$	+	CH_3	0.15				
				$C_2H_2^+$	+	C_2H_4	0.15				
				$C_3H_6^+$	+	C	0.10				
				$C_4H_3^+$	+	H_2 + H	0.10				

Reaction Rate of IMR relevant for ionosphere

k_{IMR}

$k_{coll} \sim 10^{-9} cm^3 s^{-1}$

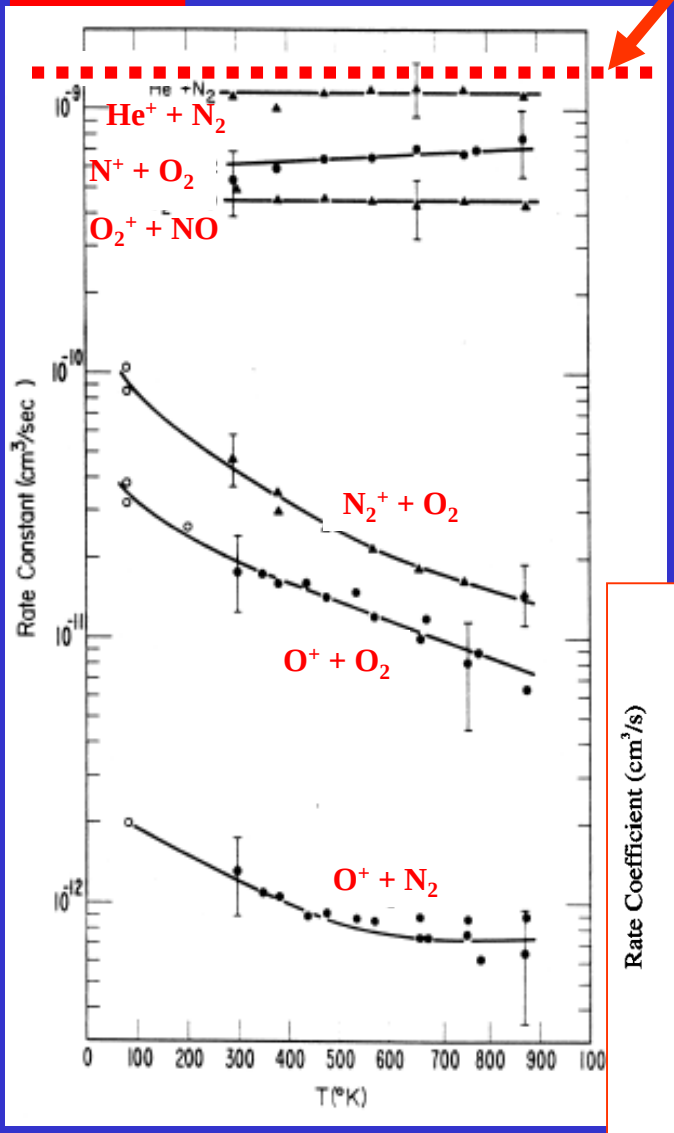

1975-90

1990-00

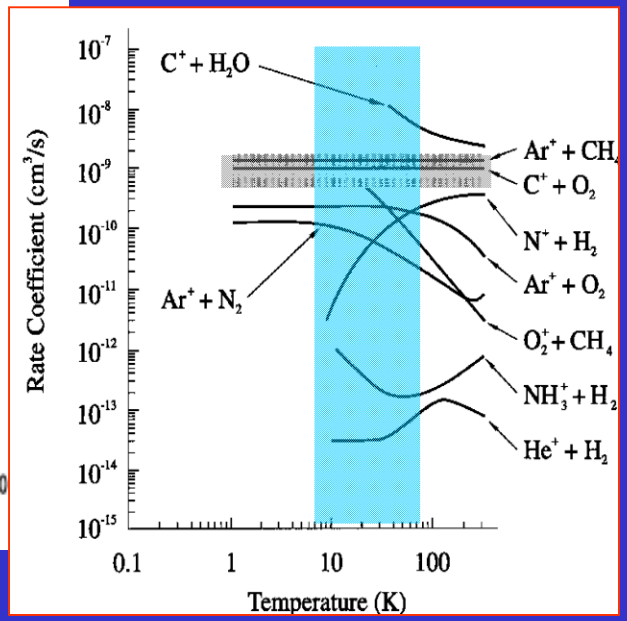

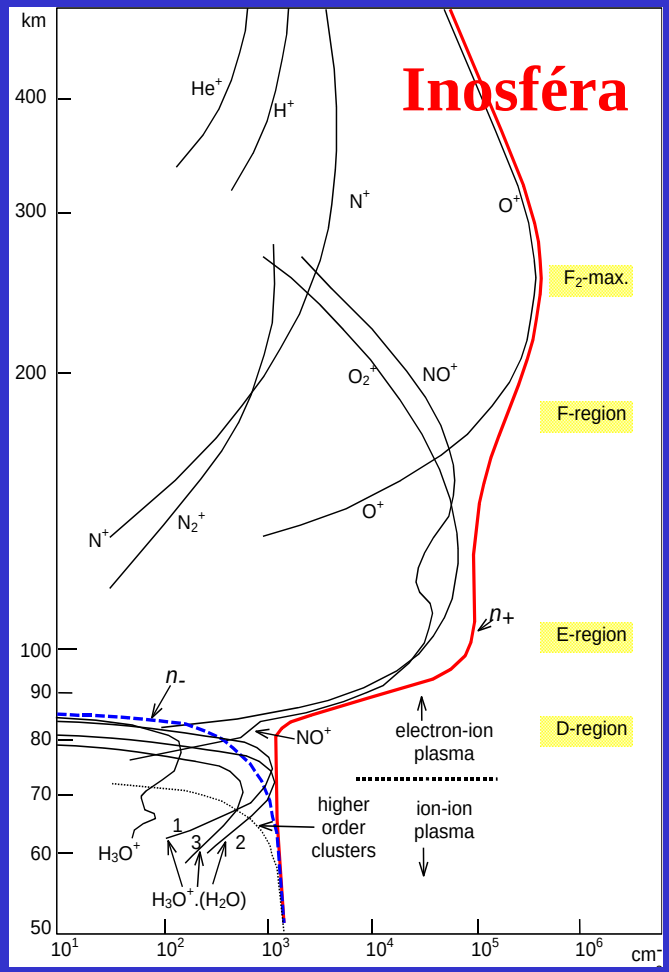

The initial reactions and radiative association in dense interstellar clouds

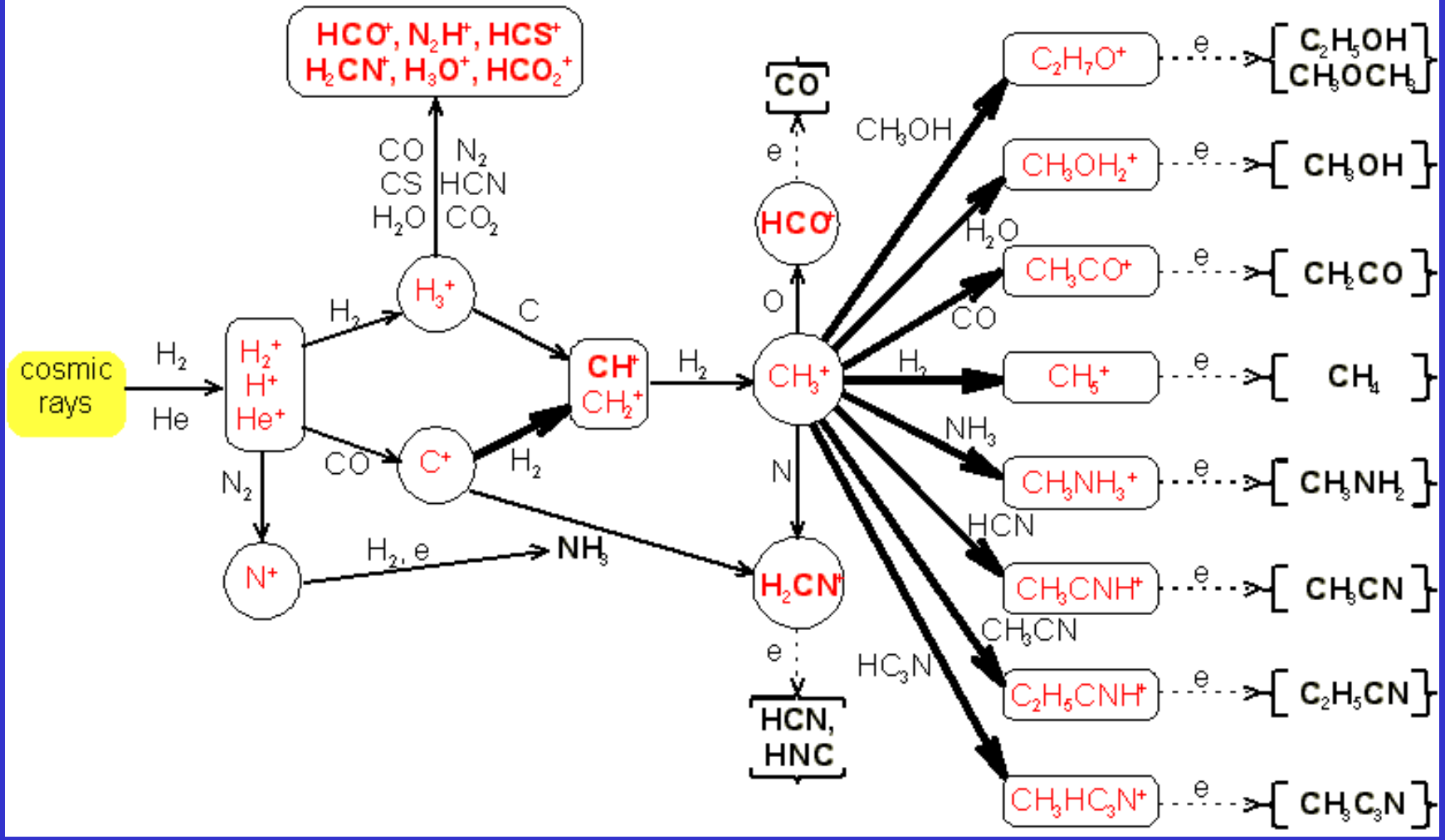

H_3^+ in interstellar space

$$H_2 \xrightarrow{\text{cosmicray}} H_2^+ + e^-$$

$$H_2 + H_2^+ \rightarrow H_3^+ + H$$

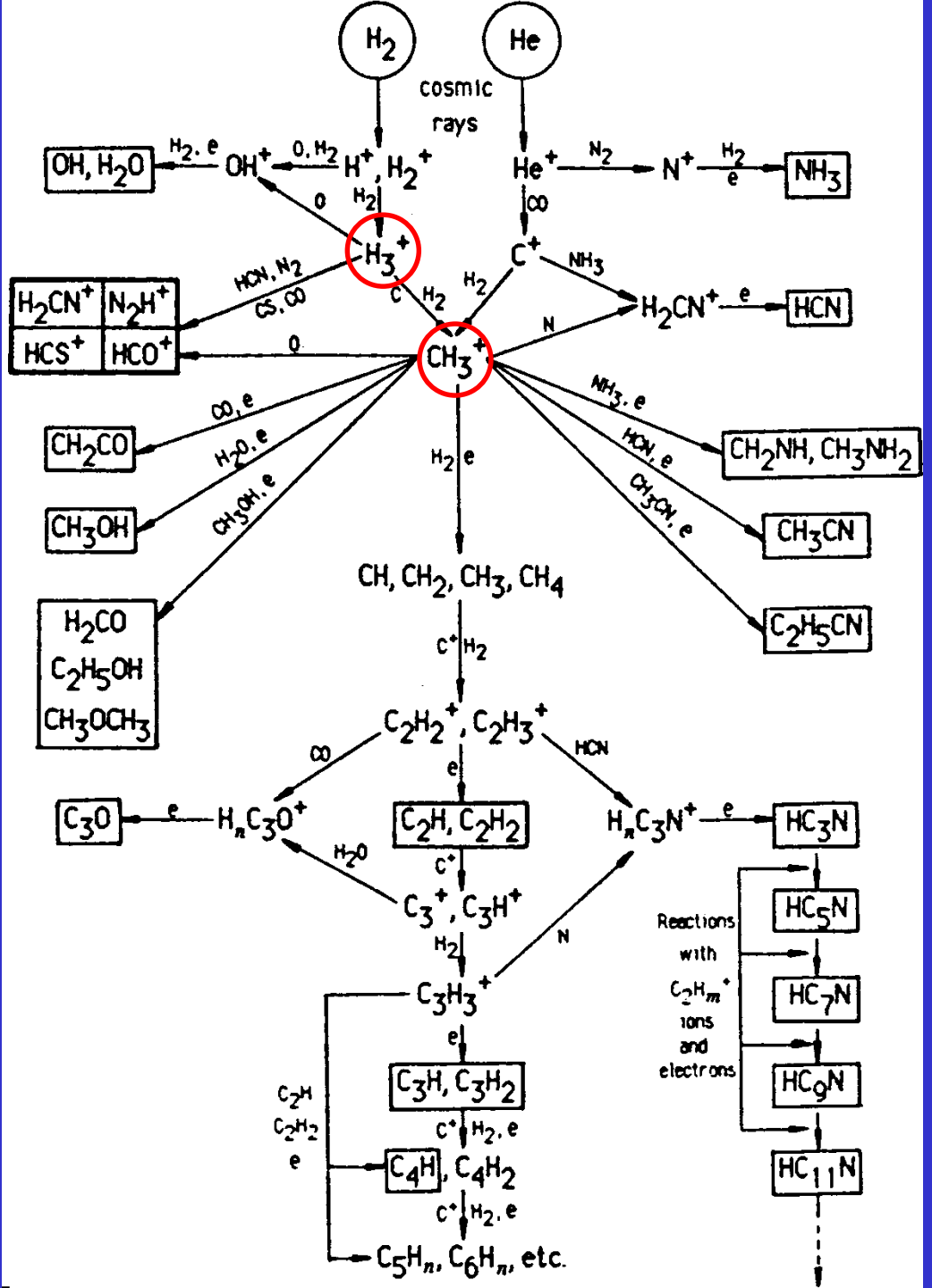

Very low collision energies

TOPICAL REVIEW

Electron–molecule collisions at very low electron energies

F B Dunning

Department of Physics and the Rice Quantum Institute, Rice University, PO Box 1892, Houston, TX 77251, USA

J. Phys. B: At. Mol. Opt. Phys. 28 (1995) 1645–1672. Printed in the UK

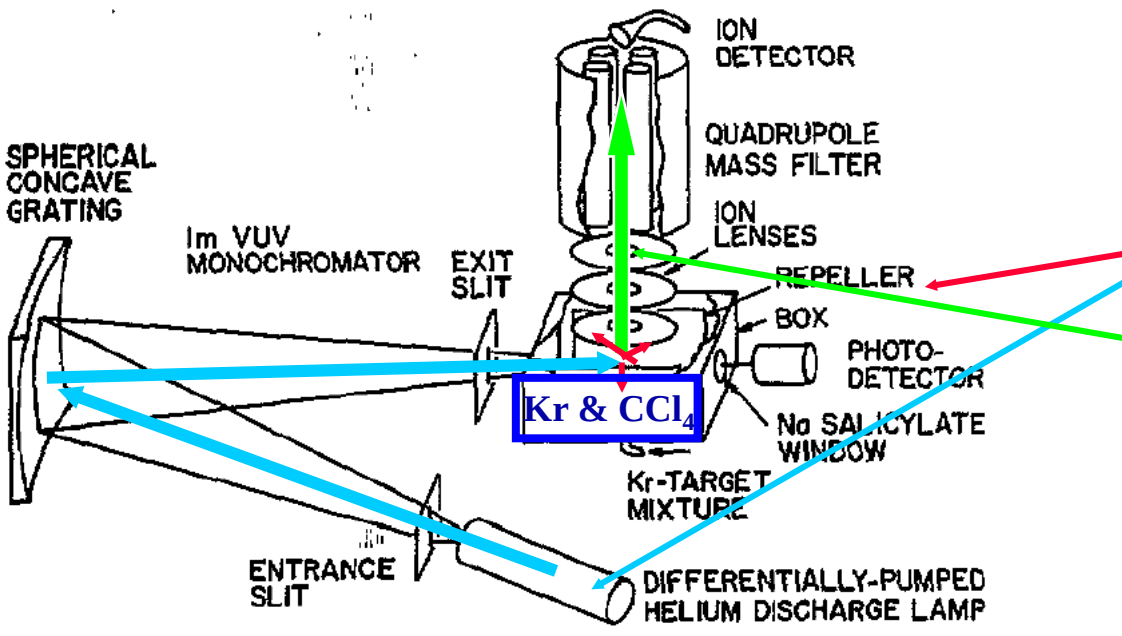

Figure 1. Schematic diagram of the VUV photoionization apparatus used for attachment studies (Chutjian and Alajajian 1985a, b).

$$Kr(^1S_0) + \hbar\omega \rightarrow Kr^+(^2P_{1/2}) + e^-(\varepsilon)$$

$$e^- + CCl_4 \rightarrow CCl_4^{-*} \rightarrow CCl_3 + Cl^-$$

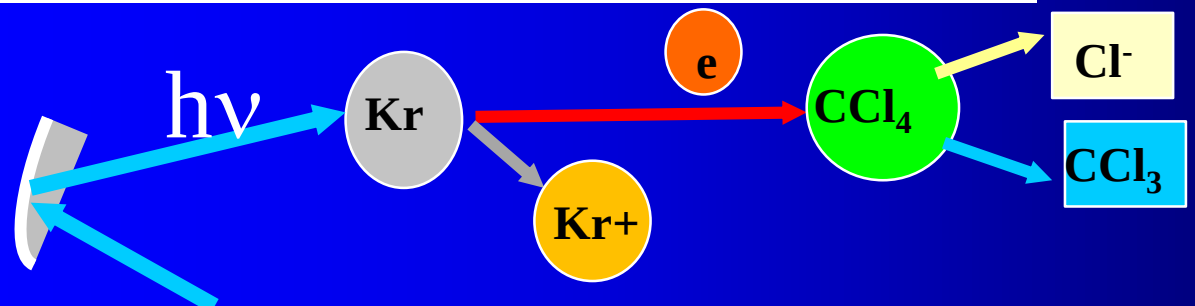

Electron attachment at very low electron energies

10^5 Å

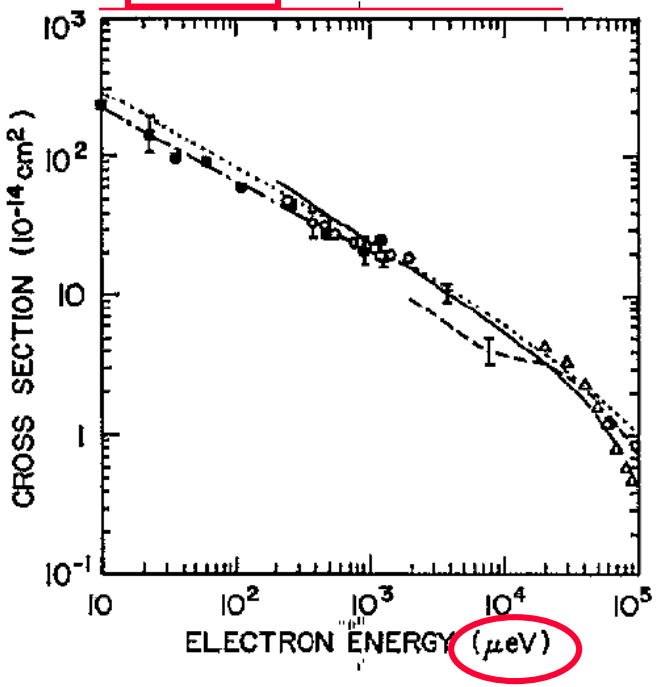

Figure 2. Cross section for electron attachment to SF_6. ■, $\bar{\sigma}_e$-K(np); —·—, $\sigma_e(v)$-K(np) (Ling *et al* 1992). ○, $\bar{\sigma}_e$-Rb(ns) (Zollars *et al* 1985); ——, free electrons (Klar *et al* 1992a, b); – – –, free electrons (Chutjian and Alajajian 1985); Δ, free electrons (Pai *et al* 1979, Chutjian and Alajajian 1985a); -----, theory (Klots 1976).

10^5 Å

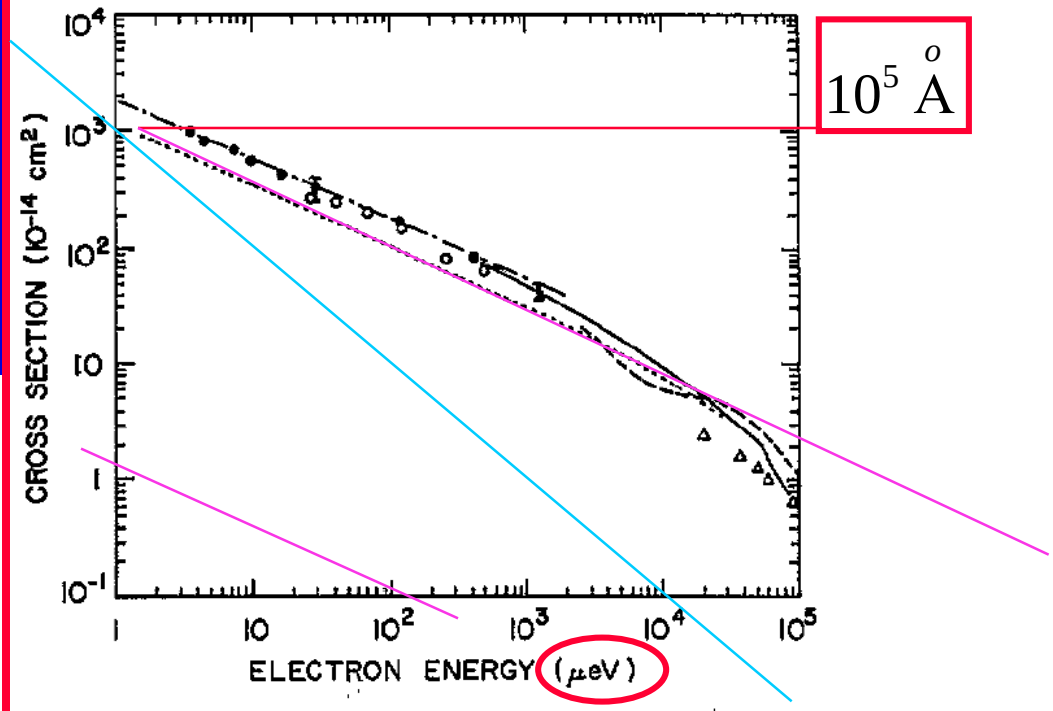

Figure 3. Cross sections for electron attachment to CCl_4. ●, $\bar{\sigma}_e$-K(np); —·—, $\sigma_e(v)$-K(np) (Frey *et al* 1994b); ○, $\bar{\sigma}_e$-K(np) (Ling *et al* 1992); ——, free electrons (Hotop 1994); – – –, free electrons (Orient *et al* 1989); Δ, free electrons (Christodoulides and Christophorou (1971); -----, theory (Klots 1976).

Details of Ramsauer effect

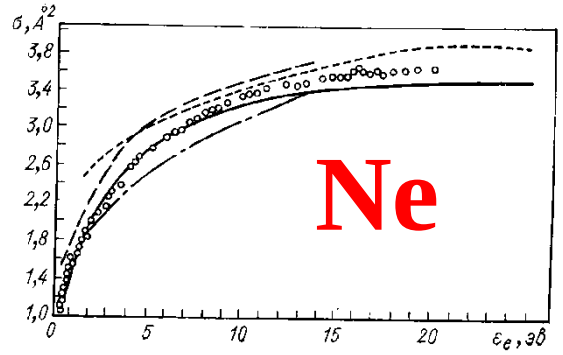

Рис. 5.8. Полное сечение рассеяния электрона на атоме неона.

Эксперимент (метод Рамзауэра): ○ — [101]; ——— — [29]; ····· — [92]; —— · —— — [95]. Теория: — — — [109].

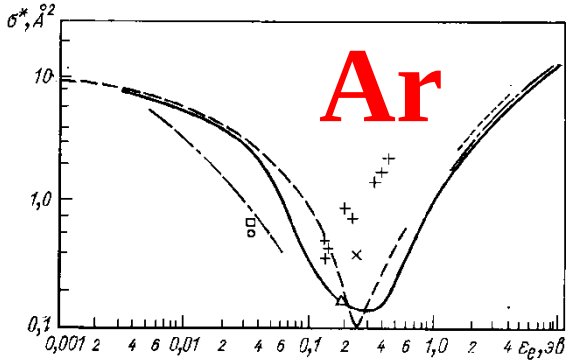

Рис. 5.9. Диффузионное сечение столкновения электрона с атомом аргона.

Эксперимент (подвижность электронов при малых полях и температурах): ····· — [21]; ——— — [47]; × — [60]; ○ — [91]; □ — [112]; △ — [44]; —— · —— — [16]; · · · · — — [108]; + — [43]. Теория: — — — [87].

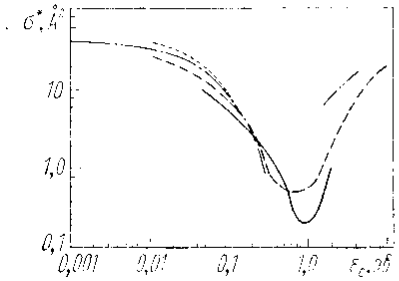

Рис. 5.12. Диффузионное сечение столкновения электрона с атомом криптона.

Эксперимент (подвижность электронов при малых полях и температурах): ····· — [34]; —— · · —— — [21]; — — — — [47]; ——— — [63]. Теория: —— · —— — [87].

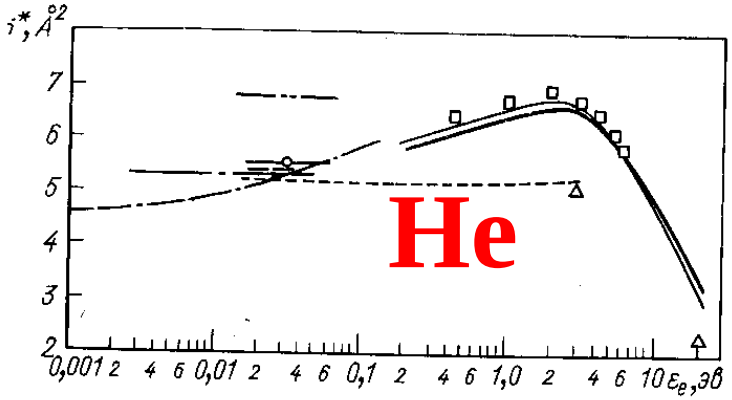

Рис. 5.3. Диффузионное сечение столкновения электрона с атомом гелия.

Эксперимент (подвижность электронов при малых полях и температурах): □ — [39]; △ — [73]; —— · —— — [88]; — — — — [91]; ····· — [58]; —— ····· —— — [13]; —○— — [62]. Теория: ——— — [75]; ——— — [32]; — — · — — расчет по формуле (5.37).

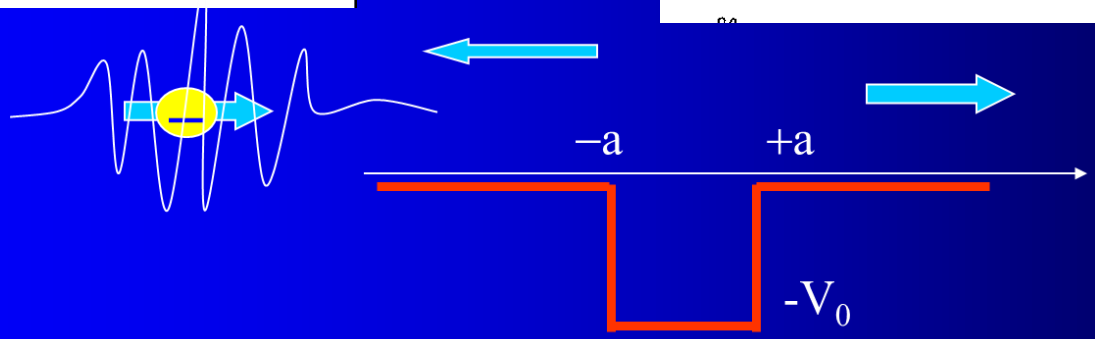

Total collision and reactive cross sections comparison

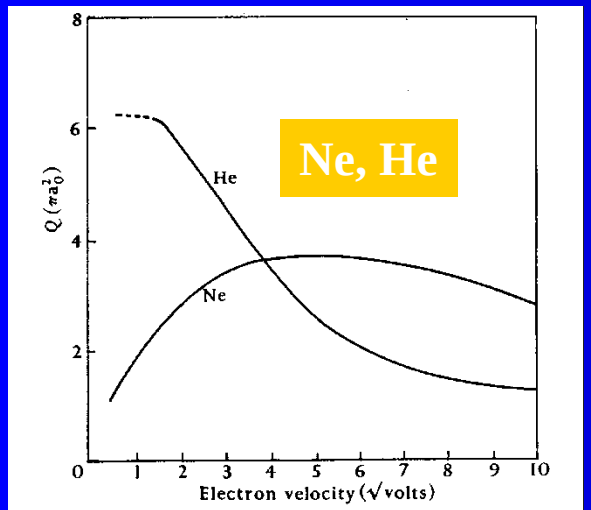

FIG. 1.10. Observed total collision cross-sections of He and Ne.

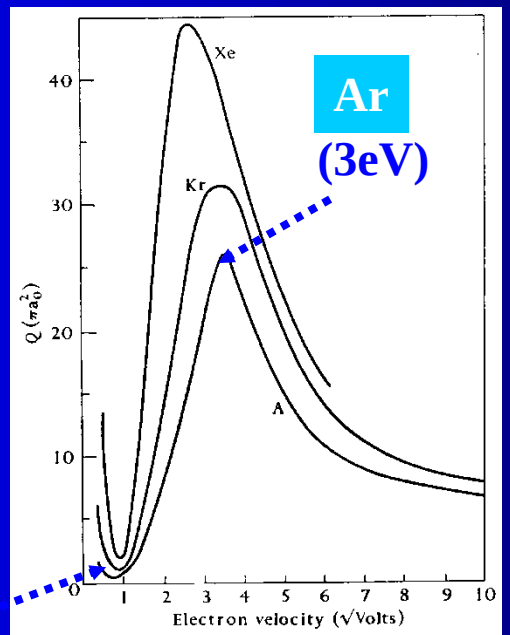

FIG. 1.9. Observed total collision cross-sections of A, Kr, and Xe.

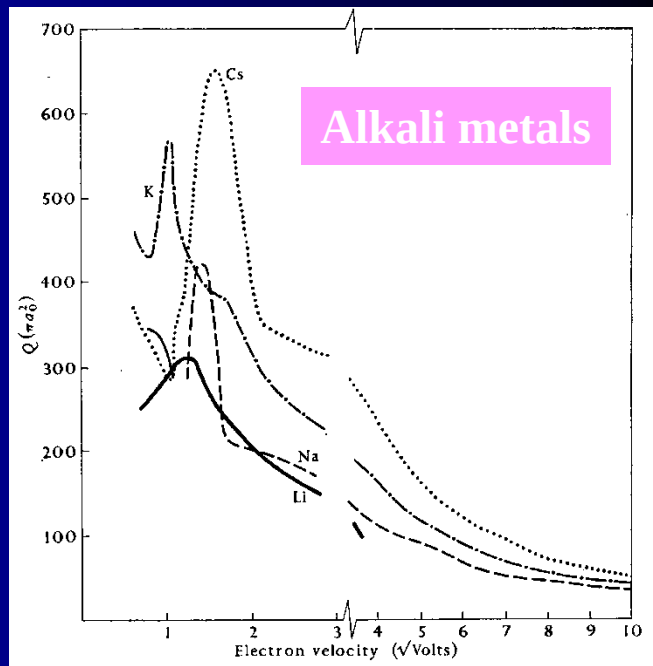

FIG. 1.16. Observed total collision cross-sections of Li, Na, K, and Cs.

(0,3eV)

σ(v)

e^-(v)

Ar

(3eV)

Ne

Ar

(0.3eV)

500A

Cs

(2eV)

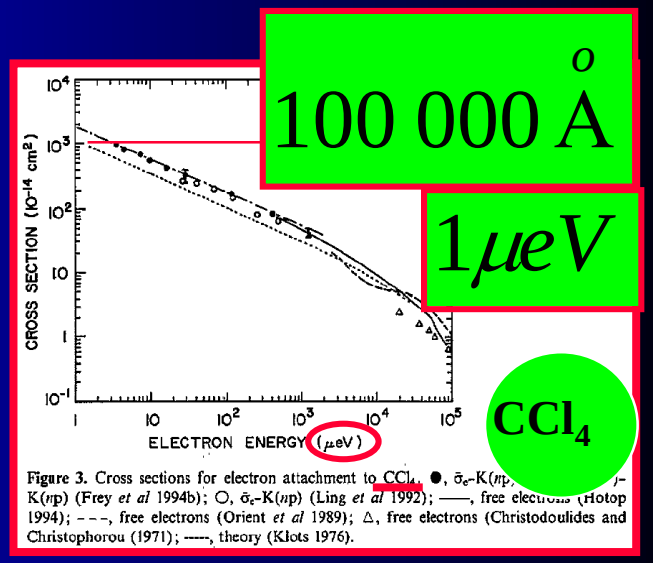

Figure 3. Cross sections for electron attachment to CCl_4. ●, $\bar{\sigma}_e$-K(np, ...)-K(np) (Frey *et al* 1994b); ○, $\bar{\sigma}_e$-K(np) (Ling *et al* 1992); ——, free electrons (Hotop 1994); – – –, free electrons (Orient *et al* 1989); △, free electrons (Christodoulides and Christophorou (1971); -----, theory (Klots 1976).

Reakční rychlost

Značí se **v** nebo **r**

$$v = \frac{1}{\nu_i} \frac{dn_i}{dt}$$

Předpokládáme reakci:

b B + c C ➔ x X + y Y

Stechiometrické koeficienty – obecně ν_i :

Řád chemické reakce

$$v = k.c_A^{w_A}.c_B^{w_B}.....c_R^{w_R}$$

$w_A, w_B.....w_R$ se určují experimentálně = reakční řády vzhledem k jednotlivým složkám

Celkový řád chemické reakce

$$n = \sum_i w_i$$

Celkový řád reakce a molekularita mají stejnou hodnotu pouze u elementárních reakcí

Závislost reakční rychlosti na teplotě

Závislost reakční rychlosti na teplotě